Navigating Challenges in mRNA Lipid Nanoparticle Therapeutics for Metastatic Epithelial Cancers

By

Tetiana Korzun

A DISSERTATION

Presented to the Department of Biomedical Engineering
and the Oregon Health & Science University
School of Medicine

in partial fulfillment of
the requirements for the degree of

Doctor of Philosophy

April 2024

School of Medicine
Oregon Health & Science University

CERTIFICATE OF APPROVAL

This is to certify that the PhD dissertation of
Tetiana Korzun

has been approved:

_____
Oleh Taratula, PhD
Mentor,
Oregon State University

_____
Sanjay Malhotra, PhD
Committee Chair,
Oregon Health and Science University

_____
Thuy Ngo, PhD
Member,
Oregon Health and Science University

_____
Jonathan Brody, PhD
Member,
Oregon Health and Science University

_____
Gaurav Sahay, PhD
Member,
Oregon State University

_____
Monica Hinds, PhD
Member,
Oregon Health and Science University

Table of Contents

To Maverick, who knows the chapters I left unsaid.

What do women hold?

The home and the family.
And the children and the food.
The friendships.
The work.
The work of the world.
And the work of being human.
The memories.
And the troubles.
And the sorrows and the triumphs.
And the love.

Men do as well,
but not quite in the same way.

Maira Kalman

Acknowledgments

If this dissertation is a success, it is a testament to the collective support from many.

Are you the mentor who guided me with patience and wisdom? Your insights were invaluable. You taught me to be kind more than to be smart and successful.

Are you my dissertation advisors? You constantly refined my focus and taught me the art of doing less while accomplishing more, shaping my approach to both research and life.

Are you the dedicated team that shared the hands-on work, turning theories into reality? Your commitment has been the engine behind our discoveries.

Are you family or friends who offered unwavering support? Your love was my strength.

Are you the love of my life? Your belief in me, even in my moments of doubt, has been the light guiding me through the darkest days.

Are you the scientist who balances the role of parenting? You've shown me that being a dedicated scholar and a loving parent is entirely possible. Your example has given me the courage.

Are you my little dog, whose spirit was as ferocious as any giant? You taught me that courage comes not from size but from the heart.

Are you my lab mates, whose hearts were in this journey of discovery and challenge? Our now lifelong friendship, collaboration, laughter, and shared late-afternoon coffee runs have not just made this work possible, but joyful.

Are you the one who kept our spaces clean and welcoming in the lab? Your smile in the late hours reminded me that kindness can be found in the smallest of gestures.

Are you the mice who silently contributed to every experiment? Your involvement is a profound testament to the progress of science and medicine.

If this dissertation is not a success, it is dedicated to significant challenges.

Are you the war that tested our resilience and unity? Your harsh lessons taught me strength beyond my understanding.

Are you the virus that brought the world to its knees, yet showed us the power of community and adaptability? Your challenge was a call to innovation, pushing us towards solutions we never thought necessary.

Are you the chance deviation, a moment’s choice, that overturns everything? You teach a lesson in the impermanence of what we deem immutable, safe, and steady.

To all the named and unnamed - this journey bears your mark. My deepest gratitude for every lesson, every word of encouragement, and every act of kindness.

Abstract

Cachexia and cancer, when intertwined, precipitate severe adverse outcomes for patients, underscoring the urgent need for innovative therapeutic strategies. This dissertation addresses a significant gap in current treatments for metastatic epithelial cancers that overexpress activin A, a therapeutic target implicated in the propagation of tumorigenesis, metastatic spread, and cancer-associated cachexia. Activin A overexpression is a common denominator in various epithelial malignancies, including prostate, pancreatic, colorectal, lung, head and neck, liver cancers, and, notably, epithelial ovarian carcinoma - the focal point of this dissertation. At the heart of this research is developing and optimizing a novel lipid nanoparticle-based formulation for delivering *follistatin* mRNA aimed at neutralizing activin A by sequestering it in an inactive state. To decrease the reactogenicity of the developed formulation, we integrate an ionizable lipid with the lowest reactogenic potential and employ the Nobel Prize-recognized method of pseudouridine-substituted mRNA in *follistatin* mRNA lipid nanoparticles. Importantly, we also identify the crucial roles of toll-like receptor 4 and the MyD88 adaptor protein in eliciting sickness behaviors in mice as a result of the reactogenic characteristics of lipid nanoparticles and propose strategies to counteract these effects. The optimized *follistatin* mRNA lipid nanoparticles lead to a marked decrease in tumor growth, metastasis reduction, and cachexia alleviation, evidenced by the preservation of muscle mass and fat stores in cancer-bearing mice. This therapeutic approach meets the critical need in managing metastatic epithelial cancers and cancer-associated cachexia, paving the way for novel mRNA treatments that aim to markedly improve patient outcomes.

Table of Figures

Index of Tables

Abbreviations

ActA: Activin A
ActRI: Activin Type I Receptors
ActRII: Activin Type II Receptors
ALK4: Activin Receptor-Like Kinase 4
ALK5: Activin Receptor-Like Kinase 5
ALP: Alkaline phosphatase
ALT: Alanine transaminase
ANOVA: Analysis of variance
BMP: Bone Morphogenic Protein
BUN: Blood urea nitrogen
C57BL/6: A strain of laboratory mouse
CAC: Cancer-associated cachexia
CAR: Chimeric Antigen Receptor
CBC: Complete blood cell count
CCL12: Chemokine (C-C motif) Ligand 12
CCL2: Chemokine (C-C motif) Ligand 2
CCL3: Chemokine (C-C motif) Ligand 3
CCL4: Chemokine (C-C motif) Ligand 4
CCL7: Chemokine (C-C motif) Ligand 7
CD68: Cluster of Differentiation 68
CDC: Centers for disease control and prevention
CDDP: Cisplatin
CDH1: Cadherin-1 (E-cadherin)
CXCL1: Chemokine (C-X-C motif) Ligand 1
CXCL2: Chemokine (C-X-C motif) Ligand 2
DAMPs: Damage-Associated Molecular Patterns
ECM: Extracellular Matrix
ELISA: Enzyme-Linked Immunosorbent Assay
eLNP: Empty lipid nanoparticles
EMT: Epithelial-mesenchymal transition
EOC: Epithelial ovarian carcinoma
FACS: Fluorescence-activated cell sorting
FDA: Food and drug administration
Foxo1: Forkhead Box O1
FST: Follistatin
GFP: Green Fluorescent Protein
HNSCC: Head and neck squamous cell carcinoma
HPV: Human papillomavirus
IL1B: Interleukin-1 Beta
IFN: Interferon
IL: Interleukin
IP: Intraperitoneal
LNP: Lipid nanoparticle
Luc: Luciferase
MAPK: Mitogen-Activated Protein Kinase
MCH: Mean corpuscular hemoglobin
MCHC: Mean corpuscular hemoglobin concentration
MET: Mesenchymal-epithelial transition
mRNA: Messenger ribonucleic acid
MyD88: Myeloid Differentiation Primary Response 88
NF-κB: Nuclear Factor-kappa B
NTA: Nanoparticle tracking analysis
ORF: Open reading frame
PBS: Phosphate-buffered saline
PCR: Polymerase chain reaction
PDI: Polydispersity index
Pen-Strep: Penicillin-streptomycin
qRT-PCR: Quantitative reverse transcription polymerase chain reaction
RFS: Relapse-free survival
RIG: Retinoic Acid-Inducible Gene
RNAi: RNA interference
ROS: Reactive oxygen species
SEM: Standard error of the mean
SMAD: Small Mother Against Decapentaplegic
SQ/SubQ: Subcutaneous
TGF-β: Transforming Growth Factor Beta
TLR: Toll-Like Receptor
TNF-α: Tumor Necrosis Factor-alpha
TNF: Tumor Necrosis Factor
TOP2A: DNA Topoisomerase II Alpha
TPM: Transcripts per Million
TRIF: TIR-domain-containing adapter-inducing interferon-β
USC: Uterine serous carcinoma
WT: Wild type

Chapter 1: Introduction

1.1 Dissertation overview

In this dissertation, I introduce novel nucleic acid formulations for the targeted treatment of metastatic epithelial ovarian carcinoma (EOC) and cancer-associated cachexia (CAC). These formulations signify a substantial development in addressing the dual challenges of cancer and its associated comorbidity of CAC, which is marked by decreased appetite, accelerated loss of fat and lean body mass, and persistent fatigue. In *Chapter 1* of my dissertation, I address the fundamental question of *why* I undertook the specific work outlined in my research. I present an introductory section that provides valuable insights into the landscape of gynecological cancers. In exploring effective management and novel therapeutics for gynecological cancers, I examine the historical context of nucleic acid therapeutics and underscore their essential synergy with lipid nanoparticles (LNPs), a key factor in advancing this field. In Chapter 2, I provide a detailed background for gynecological cancers, covering definitions, causes, associated health challenges, current treatment approaches, and their limitations. I then expand the theme of limited treatments and emphasize the significance of advancing nucleic acid therapeutics through a comprehensive review of their application in the context of

gynecological malignancies. This review in Chapter 3 encompasses a detailed analysis of various nucleic acid-based approaches, including small interfering RNA (siRNA), messenger RNA (mRNA), and microRNA (miRNA) therapies. In Chapter 4, which is a pivotal section of my dissertation, I propose an LNP-based formulation for delivering *follistatin* mRNA to treat EOC and CAC in nude mice. Further, because my studies directed my attention to the reactogenicity of LNPs, in Chapter 5, I examine the molecular and cellular mechanisms behind side effects that I witnessed following LNP administrations in wild-type mice. In Chapter 6, I share my findings on the involvement of toll-like receptors and their associated adaptor proteins in this intricate process. I delve into molecular foundations of reactogenic cascades that manifest in the behavioral responses elicited by the LNP formulations. After I identify LNP formulations with favorable safety profiles, in Chapter 7, I introduce the improved *follistatin* mRNA LNP formulation as a proof-of-concept to address metastatic epithelial carcinoma, laying the groundwork for further developments in EOC therapeutics. Finally, I outline future prospects for nucleic acid therapeutics in gynecological oncology, which serves as a conclusion to my dissertation work in Chapter 8.

1.2 Setting the stage: An Introduction to the challenge of ovarian cancer in gynecological malignancies

Gynecological malignancies represent a significant and complex health challenge for patients with female reproductive organs, and encompass a range of cancers, including vaginal, vulvar, cervical, endometrial, and ovarian neoplasms. [1] While advances in early detection and treatment have improved survival rates and quality of life for individuals with gynecological cancers, these cancers continue to pose

substantial health risks. These challenges underscore the ongoing need for comprehensive approaches to address the complexity of gynecological cancers. [2, 3] One particular gynecological malignancy that commands attention is ovarian cancer. Its high mortality rate and a five-year survival of under 30% for cases with distant metastases emphasizes the crucial need for changes in our strategy to address this disease. [4, 5] Ovarian cancer, predominantly epithelial ovarian carcinoma (EOC) in over 95% of cases, poses a distinct challenge as it is frequently diagnosed at an advanced stage, with metastases already disseminated within the abdominal cavity. [6] Advanced disease restricts therapeutic options, which are already limited for ovarian cancer, to a combination of primary surgical debulking with adjuvant platinum- and taxane-based chemotherapy. [7] While most patients with advanced-stage ovarian cancer respond to first-line chemotherapy, these responses are not durable, and a large proportion of patients ultimately develop and succumb to chemo-resistant disease. [8] These intricacies of ovarian cancer in both clinical and research domains inspired my dedication to advancing more effective treatments amid the limitations of conventional approaches. Moreover, the complex web of health challenges surrounding ovarian cancer, including CAC, further stirred my commitment to developing therapies that holistically address this disease.

As I explored the complexities of advanced EOC, witnessed firsthand in clinical settings and bolstered by insights from the literature, it became evident to me that patients with ovarian cancer often contend with malnutrition and CAC, resulting in substantial health implications. [9] Indeed, in CAC, many patients are in a state of nutritional bankruptcy and chronic wasting, which renders them poor or suboptimal

candidates for primary therapeutic interventions including surgery and chemotherapy. [10] Of note, while remaining the frontline treatment for metastatic ovarian cancer, chemotherapy itself carries an inevitable iatrogenic burden [11], leading to loss of muscle mass, depletion of fat stores, fatigue, and propagation of systemic inflammation proportional to the aggressiveness of disease management. [12] Consequently, I realized that the relationship between cancer and CAC is highly complex when factoring in the treatment. It was clear to me that while cancer serves as the catalyst for CAC, the interventions, particularly chemotherapy, significantly amplify and worsen the manifestations of CAC throughout the course of active antineoplastic interventions. This realization emphasizes the complexity of addressing both the disease itself and the iatrogenic consequences, presenting a challenge as I consider the comprehensive care required for patients dealing with these interconnected issues. Therefore, I aimed to identify new therapeutic targets and appropriate drug combinations that could improve both efficacy and tolerability of chemotherapy for EOC treatment and beyond. As further outlined in Chapter 4, follistatin mRNA was selected as our therapeutic option due to its capacity to disrupt detrimental mechanisms involved in both CAC and cancer progression.

1.3 Nucleic acid therapeutics for gynecological cancers: Promising prospects in the post-SARS-CoV-2 vaccine landscape

Compared to traditional small molecule drugs, chemotherapeutics, biologics, and other conventional cancer therapies, nucleic acid therapeutics are a significant and promising therapeutic option offering distinct benefits. [13] I found myself captivated by the versatility and customizability inherent in nucleic acid therapeutics. Starting my

dissertation work, I promptly recognized their vast potential in overcoming drug resistance mechanisms, as well as their ability to modify underlying processes driving cancer progression, disrupting key signaling pathways, altering the tumor microenvironment, and inducing immune responses for long-term disease control. [14] My fascination with nucleic acid therapeutics further stemmed from the potential to create personalized treatment strategies, including tailored nucleic acid vaccines designed for individual patients or specific cancer subtypes. [15] In the context of developing these therapeutics, I recognized that the progress in this field relied significantly on the effective design and utilization of delivery systems such as LNPs. Therefore, I envisioned LNPs as optimal vehicles for targeted nucleic acid delivery to cancer cells, due to their ability to offer enhanced efficacy while minimizing off-target effects. [16-18]

To emphasize the progressive evolution of nucleic acid therapeutics and LNP delivery systems and the synergy that has emerged between them, I summarize the historical integration of LNP-guided therapies, which also includes nanoparticle-based gynecological chemotherapeutics and the first nucleic acid therapies (**Figure 1**). The integration of lipid nanoparticles into therapeutic approaches for gynecological oncology unfolds as a captivating historical narrative. In the mid-20th century, the emergence of doxorubicin, cisplatin, and paclitaxel significantly reshaped chemotherapy practices. The 1960s introduced liposomal structures, paving the way for targeted liposomes in the 1980s. Progressing into the 1990s-2000s, liposomal formulations for anti-cancer drugs not only gained prominence but also became integral to daily clinical practice. Currently, liposomal formulations for chemotherapy drug delivery in gynecological oncology stand

as a pivotal advancement, providing a path towards enhanced drug delivery precision, reduced systemic toxicity, and ultimately, improved therapeutic efficacy.

For nucleic acid therapeutics, currently still in their early stages as potential therapies for gynecological cancers, a pivotal moment occurred in 1989 when cationic liposomes successfully delivered the first mRNA. In 2018, Onpattro, the inaugural FDA-approved liposomal siRNA formulation for amyloidosis treatment, marked a transformative milestone. Transitioning into the early 2020s, the initiation of clinical trials for the first mRNA-LNP therapies anticipated the global release of mRNA vaccines in 2022.

Each era in this progression (**Figure 1**) underscores the significant evolution of nanoparticle integration, contributing to the ongoing scientific progress in nucleic acid therapeutics and their incorporation to gynecological oncology. However, the synergy between LNPs and nucleic acid-based treatments has never been more apparent than in the post-SARS-CoV-2 vaccines landscape. The rapid development and successful deployment of mRNA SARS-CoV-2 vaccines showcased the potential of LNPs as a versatile and effective delivery system. [19] This milestone in vaccinology advanced the field of nucleic acid therapeutics, providing a robust foundation for their application in diverse therapeutic domains, including my own endeavors in developing mRNA LNP therapy for the treatment of EOC.

Inspired by the unfolding potential in cancer therapeutics, I contributed to the advancement of EOC management, by developing mRNA LNP therapy, beginning with the identification of therapeutic targets and concluding with the optimization of the formulation improving its safety profile. The synergy between technological progress

and scientific inquiry within my research endeavors seeks not only to expand our arsenal for addressing the complexities of cancer and its associated syndromes but also highlights the need for advancements in the field of gynecological oncology. Particularly crucial is the improvement of therapies for EOC, where the potential impact of nucleic acid therapies opens new horizons. Therefore, recognizing these transformative possibilities, I will now outline the specific aims and objectives of my dissertation.

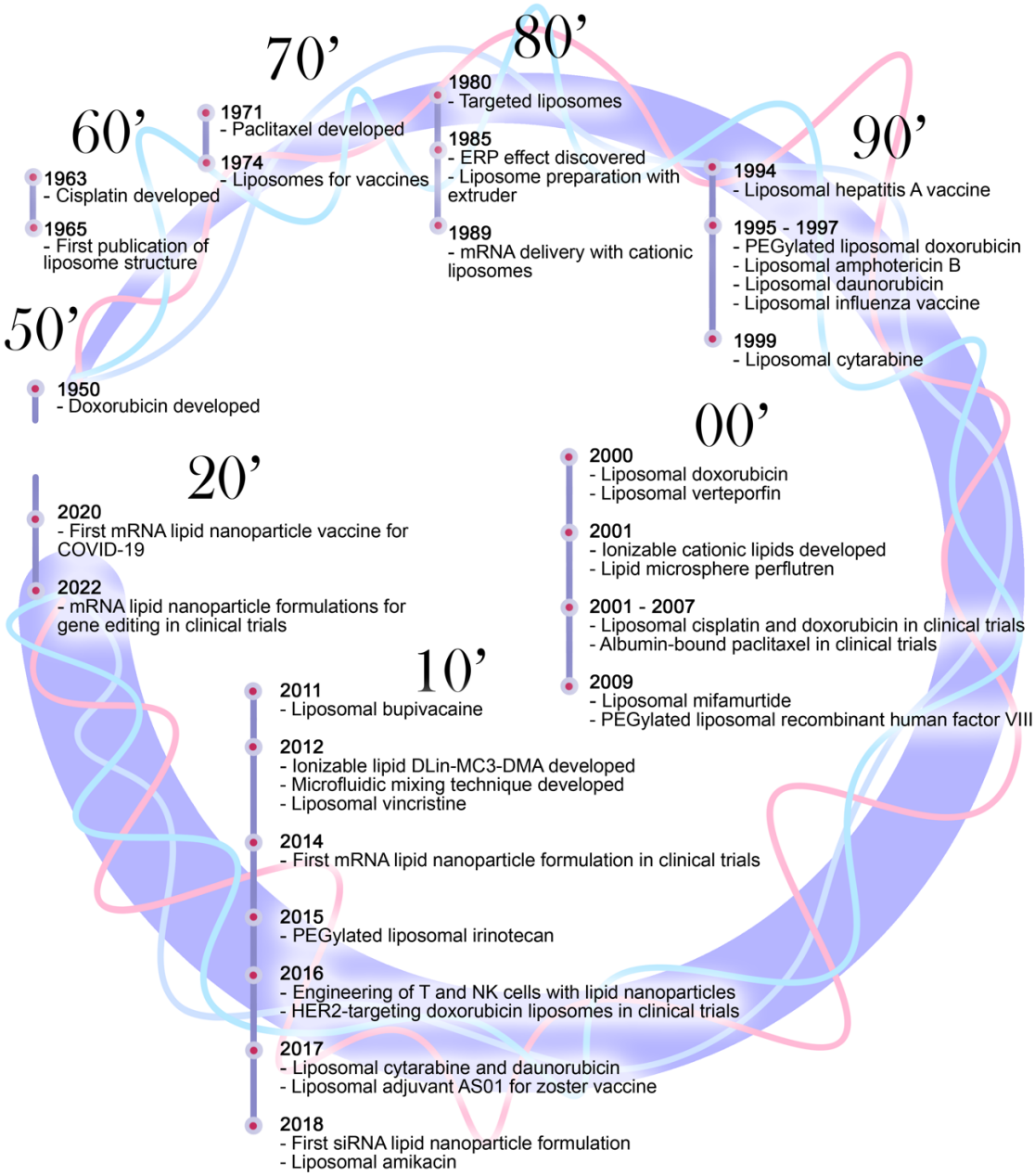

Figure 1. Nucleic acid therapies and lipid nanoparticles: A shared timeline: Since the initial characterization of liposome structure in 1965, the field of lipid nanoparticles (LNPs) has seen significant advancements. By 1974, liposomes were utilized for vaccine delivery, followed by the development of targeted liposomes in 1980. In a mere nine years, mRNA delivery was achieved using cationic liposomes. Concurrently, notable antineoplastic agents such as cisplatin and paclitaxel were discovered, with their encapsulation into liposomal formulations, including daunorubicin, cytarabine, and doxorubicin, alongside non-cancer-related drugs like amphotericin B and verteporfin, observed in the early 1990s and 2000s. This era also marked the advent of liposomal antiviral vaccines in 1990. Progress continued through the 2010s with the discovery of novel ionizable lipids and improved LNP formulations, culminating in the approval of the first siRNA therapy for amyloidosis, Onpattro, by the FDA in 2018. Notably, in the 2020s, the world witnessed the debut of mRNA vaccines encapsulated in LNPs. Given the classification of mRNA drugs as a third-generation therapeutic modality following small molecules and biologics, a new wave of these therapeutics is anticipated, including their potential application as antineoplastic agents.

1.4 Research goals in focus: Aims and objectives

My dissertation aims to deepen knowledge of nucleic acid therapeutics and their application, specifically in the context of gynecological cancers. Existing gaps in this field revolve around the restricted therapeutic options available for effectively combating metastatic EOC and the CAC. However, as demonstrated by the remarkable success of nucleic acid formulations in controlling infectious diseases with the SARS-CoV-2 vaccines, I see the development of robust nucleic acid formulations for cancer therapeutics emerging as an important objective. Therefore, a central and critical objective of my dissertation is *to address and bridge the therapeutic gap by developing and evaluating a novel LNP-based formulation for delivering therapeutic* mRNA *as a potential intervention for ovarian cancer*.

Three major aims of my dissertation and associated objectives are listed below (**Figure 2**).

Specific Aim 1: To develop and evaluate a novel lipid nanoparticle-based formulation for delivering follistatin mRNA as a therapeutic intervention for EOC.

Objective 1.1: Provide a complete overview of gynecological malignancies and distinctly define ovarian cancer in the context of these malignancies.

Objective 1.2 Conduct a comprehensive review of existing research on lipid nanoparticle formulations and their potential in the delivery of nucleic acids for gynecological cancer therapy.

Objective 1.3: Formulate and optimize a lipid nanoparticle-based delivery system for follistatin mRNA.

Objective 1.4: Assess the efficacy of the formulated lipid nanoparticles in delivering follistatin mRNA and its impact on EOC treatment and CAC management in a relevant preclinical murine model.

Specific Aim 2: To investigate the mechanisms and reactogenicity associated with the administration of lipid nanoparticles, focusing on the involvement of toll-like receptor 4 (TLR4) and its adaptor proteins Myeloid Differentiation Primary Response 88 (MyD88) and TIR Domain-Containing Adapter-Inducing Interferon-β (TRIF).

Objective 2.1: Review the published literature to investigate how toll-like receptors and their associated adaptor proteins are involved in the recognition and subsequent response to lipid nanoparticles.

Objective 2.2: Study the behavioral and reactogenic responses of mice to lipid nanoparticles.

Objective 2.3: Understand how these mechanisms influence the administration and effects of lipid nanoparticles in vivo.

Specific Aim 3: To identify the improved mRNA lipid nanoparticle formulation as a proof of concept in treating metastatic epithelial carcinoma and lay the foundation for future ovarian cancer therapeutics.

Objective 3.1: Develop and optimize an improved mRNA lipid nanoparticle formulation.

Objective 3.2: Investigate the therapeutic efficacy of the improved mRNA lipid nanoparticles in a metastatic epithelial carcinoma model.

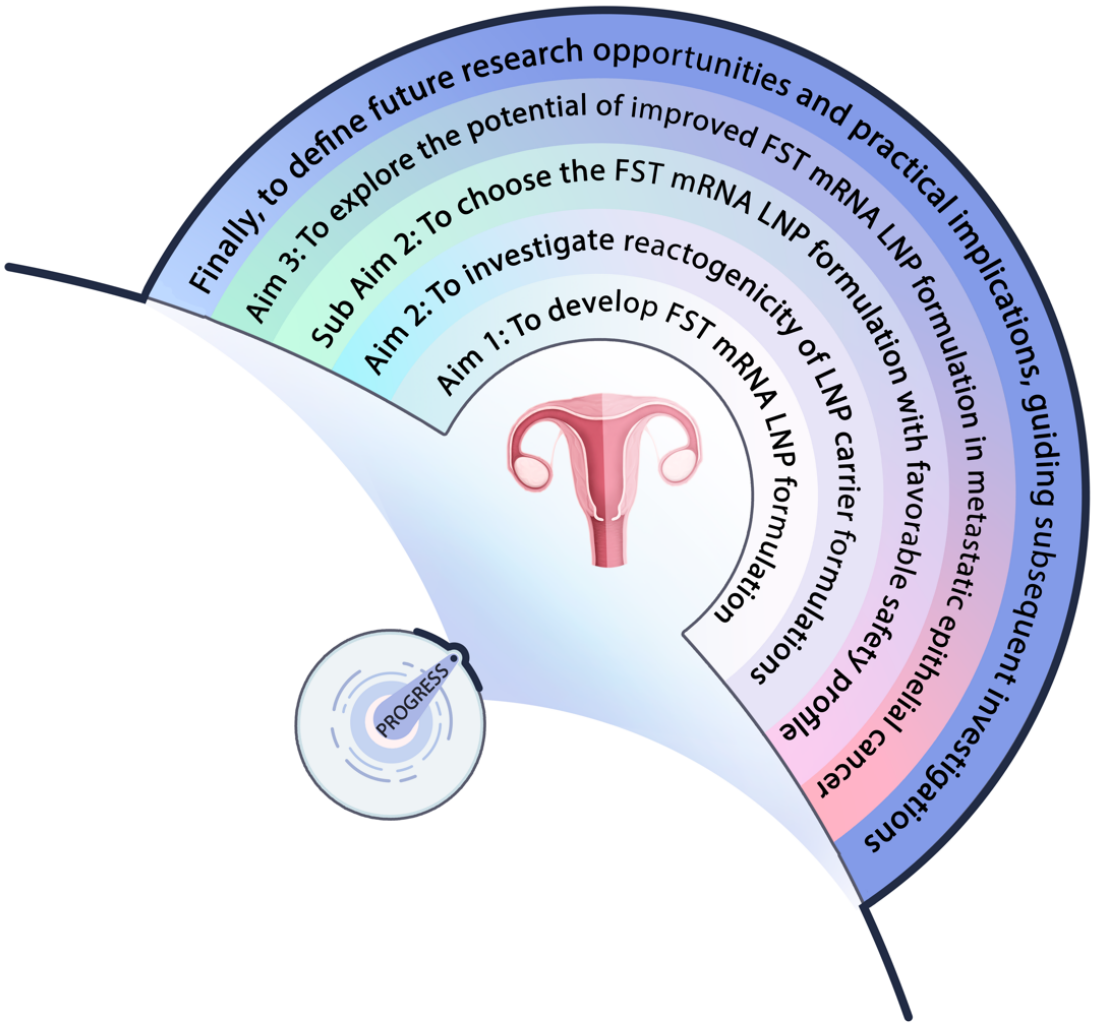

Figure 2. Visual representation of dissertation aims: The aims of this dissertation encompassed several key objectives in the development and application of *Fst* mRNA LNP formulations for the treatment of ovarian cancer and CAC. Aim 1 focused on developing tailored *Fst* mRNA LNP formulations to enhance therapeutic efficacy against both ovarian cancer and CAC. Aim 2 involved a detailed investigation into the reactogenicity of LNP carrier formulations, particularly crucial during the transition to wild-type murine models, aiming to address reactogenic manifestations that hindered translation to immunocompetent animals. Sub-aim 2 aimed at selecting the *Fst* mRNA LNP formulation with the most favorable safety profile to support a chronic injection regimen. Aim 3 aimed to explore the potential of improved *Fst* mRNA LNPs specifically in the context of metastatic epithelial cancer in wild-type mice. Lastly, the dissertation concluded with a comprehensive delineation of future research and development prospects for *Fst* mRNA therapeutics, thereby providing a roadmap for advancing the clinical translation of this promising therapeutic approach.

Through a comprehensive exploration of this research focus, my dissertation seeks to provide valuable insights and solutions that can help address the challenges and drive progress in the treatment of gynecological cancers.

1.5 Chapter summary

This chapter introduces the context and motivation for my dissertation's research goals, which revolve around addressing therapeutic gaps in treating gynecological cancers, with the emphasis on metastatic EOC, and surrounding health challenges, including CAC. It offers essential background information and the rationale for exploring novel nucleic acid formulations, setting the stage for the next two chapters providing comprehensive review of gynecological cancers and nucleic acid therapeutics for their treatment.

.

Chapter 2: Gynecological cancers and conventional therapies: Uncovering therapeutic gaps and challenges

Chapter published in: Korzun, T., et al., Development and Perspectives: Multifunctional Nucleic Acid Nanomedicines for Treatment of Gynecological Cancers. *Small*, 2023: p. e2301776.

2.1 Gynecological cancers: Overview

Gynecological malignancies are significant contributors to morbidity and mortality among individuals with female reproductive organs. [1] Vaginal, vulvar, cervical, endometrial, and ovarian neoplasms are the five most common types of gynecologic cancer. [1]

2.1.1 Vaginal and vulvar neoplasms

Squamous cell carcinoma (SCC) of the vagina, often resulting from cervical SCC, vaginal clear cell adenocarcinoma (ADC), linked to diethylstilbestrol (DES) exposure in utero, and vaginal sarcomas are the most common vaginal tumors. [20] SCC is the most common cancer among older patients with vaginal and vulvar malignancies. The mean age of diagnosis for vaginal SCC is 60 years or older. Furthermore, up to 20% of

patients are found to be asymptomatic at the time of diagnosis. [21, 22] Vaginal ADC is the most frequent malignancy in patients 20 years and younger, with most patients presenting with stage 1 disease resulting in a favorable prognosis. [21] Leiomyosarcomas, endometrial stromal sarcomas, malignant mixed Müllerian tumors, and rhabdomyosarcomas are the most frequent primary vaginal sarcomas. [23] The vast majority of vaginal malignancies are spread by direct invasion of the pelvic soft tissues via lymphatic and hematogenous dissemination. [24] In comparison, vulvar cancers affect any part of the external genitalia but exhibit limited cancer spread to the regional lymph nodes, with distant metastasis rarely formed. [24]

2.1.2 Cervical cancer

Cervical cancers are the third most prevalent gynecological malignancy and the fourth most common malignancy overall in patients with female reproductive organs. [25] SCC and ADC are the most common types of cervical cancer with SCC accounting for 85% of all cervical cancer cases. [26] Importantly, the occurrence of both SCC and ADC in younger patients has recently dramatically increased. [27, 28] Human papillomavirus (HPV) is a well-documented causative agent of all cervical cancer cases. [25] Approximately 90% of cervical cancer–related deaths occur in low- and middle-income countries (LMIC), making cervical cancer the third leading cause of death in the developing world. [29] This disproportionate burden of disease in LMIC is at least in part due to limited access to preventive measures (especially HPV vaccines and effective screening programs), as well as the contribution of increased burden of HIV disease, which increases the risk of cervical cancer. Importantly, up to 60% of cervical cancer patients suffer a disease recurrence with distant metastases. [29] Despite

advancements in screening programs and existing treatment modalities, cervical cancer remains one of the leading causes of death in the developing world. [30] In the context of LMIC, the availability of conventional cancer therapies including those for cervical cancer is often limited. [31] However, it is crucial to emphasize the importance of accessing novel therapies in this setting, as these innovative approaches have the potential to revolutionize treatment outcomes. Thus, limited access to these therapies in resource-constrained settings necessitates a comprehensive examination of the barriers and potential strategies to enhance their availability, ensuring equitable access and addressing the disparities in cervical cancer outcomes globally.

2.1.3 Endometrial cancer

Endometrial carcinoma is the most prevalent form of endometrial cancer, affecting up to 3% of adult patients with uteri in the United States, with the incidence rising between the ages of 55 and 64. [32] Type I endometrial tumors are endometrioid in origin and include histological grades 1 and 2. [33] Type II endometrial tumors are endometrioid tumors of grade 3 or tumors of non-endometrioid origin that include serous, clear cell, mucinous, squamous, transitional cell, mesonephric, and undifferentiated histological types. [34] Compared to uterine endometrioid malignancies, uterine serous carcinoma (USC) and uterine clear cell carcinoma (UCCC) have a worse prognosis due to a greater tendency for lymphovascular invasion, intraperitoneal, and extra-abdominal metastasis. Patients with USC and UCCC often present with extrauterine cancer dissemination in the later stages of the disease. [35, 36]

2.1.4 Ovarian cancer

The most pervasive malignant neoplasms are ovarian germ cell tumors (GCTs), mixed germ cell tumors, granulosa cell tumors, and epithelial ovarian carcinomas (EOC). Although genetic factors, i.e., BRCA mutations, are the most significant drivers of EOC risk, such as BRCA mutations, other factors, including hormonal, reproductive, environmental, racial, and ethnic factors also have a significant impact. [37, 38] EOCs account for 90% of all ovarian malignancies, with the most common types being high- and low-grade serous carcinomas (HGSC and LGSC), endometrioid carcinoma, clear cell carcinoma, and mucinous carcinoma. [38] Close to 75% of patients with EOC exhibit advanced disease at a presentation that has either spread throughout the peritoneal cavity, to lymph nodes (Stage III), or to more distal sites (Stage IV). [38] Approximately 80% of all malignant ovarian neoplasms are HGSCs. [39, 40] Most HGSCs are diagnosed at an advanced stage, with extraovarian development and rapid metastasis. [6, 41] Immature teratomas, tumors of the yolk sac, and dysgerminomas, which are GCTs, are primarily seen in young patients (10-30 years old) and form up to 5% of malignant neoplasms of the ovary. [42, 43] Granulosa cell tumors are the most prevalent sex cord-stromal tumors (SCSTs) of the ovary, 90% of which are malignant. [44]

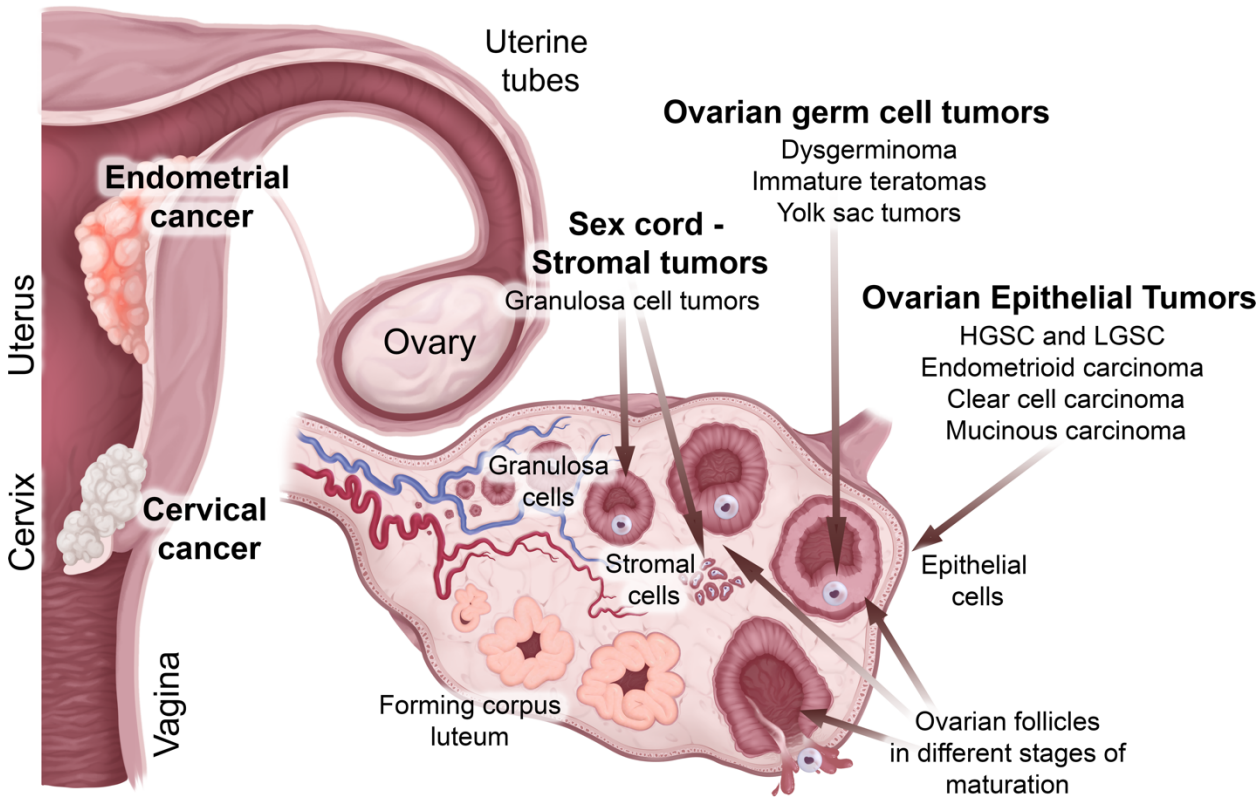

Figure 3. **Overview of gynecological malignant tumor types in the female reproductive system:** Vaginal and vulvar cancers primarily affect the vaginal and vulvar regions, respectively. Cervical cancer is in the cervix, while endometrial cancer originates in the endometrium, the inner lining of the uterus, and encompasses various histological types. Ovarian cancer includes sex cord stromal tumors, ovarian germ cell tumors, and ovarian epithelial tumors, with the latter comprising the highest percentage of all ovarian malignancies.

2.2 Conventional treatment approaches for the management of gynecological malignancies

Gynecological cancer management is highly entrained to the cancer type and degree of malignant dissemination. Although therapies for benign gynecological diseases hold significance in health management, the urgency and complexity surrounding gynecological malignancies require a targeted discussion regarding their distinctive challenges, treatment options, and advancements. Hence, the focus of this

section on conventional therapeutics is oriented specifically towards therapies for malignant gynecological tumors.

Vulvar tumors, as well as lesions in the lower third of the vagina, currently require vulvovaginectomy or alternative chemoradiation and assessment of inguinofemoral lymph nodes. [45-47] In malignant vaginal tumors, Stage I patients are candidates for radiation with or without surgical resection. [45] For Stage II-IV, external beam radiation therapy, brachytherapy, and combined chemotherapy with radiation therapy are the preferred approaches. [45] At present, neoadjuvant chemotherapy administered prior to surgery is considered an experimental therapeutic strategy in the current stage of developing treatment modalities. This approach involves the administration of chemotherapy before the surgical removal of a tumor to reduce its size and facilitate resection, potentially improving patient outcomes. [48-50]

The most common approach for early-stage cervical tumors is surgical resection (preferred over radiation), including conization and simple or radical hysterectomy. [28] Locally advanced and early-stage disease patients with medical comorbidities or poor functional status receive primary radiation therapy. [51] Management of metastatic cervical cancer depends on the extent of the disease at presentation. Local resection, chemotherapy, or radiation can manage disease isolated to the lymph nodes or presenting with limited metastases. Metastatic disease is often treated with platinum chemotherapy (platinum-based with or without taxane) in combination with the angiogenesis inhibitor bevacizumab as a first-line treatment. [52-54] Chemotherapy-naïve patients are also recommended to undergo treatment incorporating pembrolizumab, a monoclonal anti-PD-1 antibody. [55]

Surgery alone or in combination with adjuvant therapy is usually curative for endometrial uterine cancers. Extrafascial hysterectomy with bilateral salpingo-oophorectomy is the standard of care for uterine malignancies. [56] Metastatic endometrial cancer often requires cytoreduction intervention with extended field radiation. [57] Based on the stage, grade, and stratification according to tumor size, adjuvant therapy can include chemotherapy with or without radiation therapy. [58]

In spite of excellent initial treatment responses in about 70% of women with EOC, the majority of patients experience disease recurrence within three years after the first treatment. [59] For patients with early-stage EOC exhibiting high-risk features, the evidence supports the use of adjuvant chemotherapy in addition to primary surgical debulking. [60] The most common adjuvant chemotherapy for EOC is a platinum-based combinatorial treatment (i.e., paclitaxel and carboplatin). [60] Chemotherapy can be delivered by intravenous (IV) or intraperitoneal (IP) routes, with the latter showing increased progression-free survival (PFS) and OS relative to systemic delivery. [61, 62] Management of advanced EOC includes primary surgical cytoreduction in combination with chemotherapy that usually includes platinum chemotherapeutics and taxane. However, patients who are unable to undergo surgery, because of disease progression, may be considered for neoadjuvant chemotherapy with subsequent delay of primary surgery. [59] Dose-dense therapy characterized by shorter intervals between chemotherapy administrations has enhanced or similar efficacy to a conventional dose regimen, although this typically leads to higher toxicities. [63-68]

Management of EOC also requires maintenance therapy, which could include poly(ADP-ribose) polymerase (PARP) inhibitors (i.e., olaparib, niraparib) and inhibitors

of angiogenesis. [69-72] PARP inhibitors are recommended for maintenance therapy after first-line chemotherapy, especially for patients with breast cancer susceptibility gene 1/2 (BRACA1/2) mutations. In patients with high risks of recurrence, angiogenesis inhibitors such as bevacizumab were shown to increase PFS and OS, especially in patients with ascites and stage IV disease. [73-76] Tyrosine kinase inhibitors directed against the VEGF, platelet-derived growth factor (PDGF), and c-KIT receptors (i.e., pazopanib), also showed an increase in PFS, but not OS, when used as maintenance therapy. [77] Patient groups with platinum-sensitive disease are recommended to undergo secondary cytoreduction or receive an additional round of chemotherapy with or without bevacizumab. [78] Vascular endothelial growth factor receptor (VEGFR1-3) inhibitors (i.e., cediranib) and PARP inhibitors (i.e., niraparib, olaparib, and rucaparib) showed efficacy in maintenance therapy of patients with platinum-sensitive disease. [79-82]

Other malignant ovarian neoplasms are managed similarly to EOC. For ovarian GCT treatment, a total extra fascial hysterectomy with bilateral salpingo-oophorectomy and pelvic and para-aortic lymph node dissection is required. Although cytoreductive surgery is essential for advanced disease management, fertility-sparing options should be considered for young patients who wish to preserve their fertility. [83] Management of malignant SCSTs depends on staging and can range from a radical hysterectomy with bilateral salpingo-oophorectomy to conservative unilateral oophorectomy for fertility preservation with or without adjuvant chemotherapy. [84]

2.3 Gaps in treatment modalities

Although many gynecological cancer patients achieve complete clinical remission with first-line treatment, the majority of malignancies (such as EOC) recur. [85] The clinical trials of maintenance or consolidation therapy for advanced gynecological cancers demonstrated an increase in the percentage of patients who remain relapse-free for extended time. [85-89] However, recent evidence suggests that maintenance chemotherapy administered after first-line therapy does not improve survival outcomes. [90-92]

The course of the illness determines the feasibility of secondary, tertiary, or quaternary cytoreduction surgery in these advanced cases, as well as the surgical strategy of choice (i.e., open, laparoscopic, or robotic). Pathological variables such as extrapelvic involvement, carcinomatosis, and extent of disease progression determine complete cytoreduction. [93, 94] For instance, multifocal EOC dissemination indicates a poor prognosis, a higher frequency of morbidity, and an increased disease burden. [95, 96] However, complete cytoreduction decreases these adverse indicators. [97-99]

Although only 70-80% of patients with recurrent gynecological malignancies receive additional debulking treatments, the occurrence of post-operative adverse events renders them frail and disqualified for subsequent therapies, leading to a mere 23% of patients surviving beyond 5 years. [100] Adhesions resulting from cancer-related inflammation and surgery, as well as carcinomatosis, may aggravate intestinal obstruction to the point where it becomes a medical emergency. Surgical decompression and excision of obstructive carcinomatosis and bowel obstructions are

palliative treatments with high post-operative mortality rates, demonstrating a need to improve therapy and slow intraperitoneal cancer progression. [101-104]

The newest clinical therapies aiming to decrease the recurrence of malignant gynecological cancers include the development of therapeutic vaccines, dose-dense cycle approaches, as well as intraperitoneal therapy administered alone or in combination with IV therapy. [62, 105, 106] The field of therapeutic vaccine development for gynecological cancers has witnessed significant advancements, representing a promising frontier in improving treatment modalities for these malignancies. [107, 108] These innovative vaccines are designed to activate and enhance the patient's immune response against specific antigens expressed by gynecological cancer cells. [108] For instance, ongoing clinical trials are actively investigating the potential of DNA vaccines encoding neoantigens as a promising therapeutic approach for the treatment of cervical cancer. These vaccines utilize customized DNA sequences to express unique neoantigens specific to individual patients, aiming to stimulate a robust and targeted immune response against cervical cancer. By leveraging the immune system's natural ability to identify and target cancer cells, therapeutic vaccines hold the potential to provide personalized and precise treatment approaches, augmenting the arsenal of available therapeutic options for patients with gynecological cancers. [108] Furthermore, dose-dense cycle approaches have emerged as a significant advancement in the treatment of gynecological cancers. [109] These strategies involve administering chemotherapy at shorter intervals or with higher drug doses, aiming to maximize the therapeutic effect and improve treatment outcomes. By reducing the interval between cycles, dose-dense regimens aim to exploit the tumor's vulnerability and potentially

enhance the efficacy of chemotherapy while minimizing the opportunity for cancer relapse. Despite these advancements, at the current stage of therapeutic development, randomized clinical trials assessing therapeutic vaccines and dose-dense cycle approaches have shown contradictory outcomes in either relapse-free survival (RFS) or overall survival (OS) compared to placebo or standard treatment regimens. [90, 107, 110-112] In this regard, nanomedicine is emerging as a promising approach to enable the clinical translation of novel oncological medications.

2.4 Chapter Summary

In fulfillment of **Objective 1.1**, in Chapter 2, I provide an overview of gynecological cancers, their treatment methods, and the existing gaps in addressing these malignancies, setting the stage for the exploration of nucleic acid therapeutics in the subsequent chapter. The primary theses of this chapter encompass several key aspects:

1) Gynecological malignancies are a significant health concern among individuals with female reproductive organs, including vaginal, vulvar, cervical, endometrial, and ovarian cancers.
2) The management of gynecological malignancies varies based on cancer type and stage, involving surgical resection, radiation therapy, and chemotherapy.
3) Despite advancements, most gynecological cancers, such as EOC, recur, and post-operative complications impact secondary treatments.

Chapter 3: Nucleic acids therapeutics for gynecological cancers

Chapter published in: Korzun, T., et al., From Bench to Bedside: Implications of Lipid Nanoparticle Carrier Reactogenicity for Advancing Nucleic Acid Therapeutics. *Pharmaceuticals* (Basel), 2023. 16(8).

3.1 FDA-approved nanoparticle-based treatment for gynecological malignancies

Over the years, several types of nanoparticles were investigated for their potential applications in gynecological cancer treatment, and some of these formulations received regulatory approval from the U.S. Food and Drug Administration (FDA). One notable class of nanoparticles utilized in FDA-approved therapeutics for gynecological cancers is liposomes. Liposomes are spherical vesicles composed of lipids that can encapsulate hydrophobic and hydrophilic drugs, providing protection against degradation and improving their bioavailability. For instance, liposomal formulations of chemotherapeutic agents such as doxorubicin are approved for the treatment of ovarian cancer, offering improved efficacy, and reduced systemic toxicity compared to conventional drug formulations. [113]

In addition to liposomes, polymeric nanoparticles demonstrated significant potential for gynecological cancer therapy. These nanoparticles are composed of biocompatible and biodegradable polymers that can encapsulate drugs or nucleic acids, allowing for controlled release and targeted delivery to cancer cells. [114] Polymeric nanoparticles are utilized in FDA-approved therapeutics for gynecological cancers, particularly in the context of sustained release of chemotherapeutic agents, such as paclitaxel, for the treatment of ovarian cancer. [115-117]

Furthermore, inorganic nanoparticles, such as gold nanoparticles and iron oxide nanoparticles, show promise in gynecological cancer treatment. Gold nanoparticles possess unique optical properties, making them suitable for imaging and photothermal therapy. [118] Iron oxide nanoparticles, on the other hand, have magnetic properties that enable their use in magnetic resonance imaging (MRI) and magnetic hyperthermia. [119-121] Although FDA-approved therapeutics specifically utilizing these inorganic nanoparticles for gynecological cancers are currently limited, their potential applications in diagnostics and combination therapies are being actively investigated. It is worth noting that the FDA-approved nanoparticles for gynecological cancers represent a subset of the wide range of nanoparticle formulations being developed and studied. Other nanocarriers, such as micelles, dendrimers, and carbon- and silica-based nanoparticles, hold great promise and are under active investigation for their potential in gynecological cancer therapy.

Nanomedical approaches for treating gynecological malignancies have tremendous potential as new treatment modalities, especially as a means to decrease the iatrogenic burden of historically toxic or invasive treatments. For instance, high

cardiotoxicity and myelosuppression of doxorubicin preclude its aggressive use for gynecological cancers. However, liposomal doxorubicin formulation decreased adverse toxicological effects, and is now a part of everyday practice in gynecological cancer management. [122-124] Preparation of the liposomal formulation of doxorubicin and other hydrophobic drugs, such as paclitaxel, produced an increase in circulation half-life while simultaneously decreasing drug toxicity and increasing allowable loading and cumulative doses. Coating with polyethylene-glycol (PEG) and the addition of structural lipids such as sphingomyelin and choline to increase liposomal stability further increased circulation time and prevented activation of the reticuloendothelial system. [125] Therefore, pegylated liposomal doxorubicin (PLD) became a viable therapeutic option for EOC patients whose disease progressed with first-line platinum chemotherapy or who became non-candidates for platinum chemotherapies. [113, 126]

The list of nanomedicines for gynecological malignancies that are approved by the FDA or are currently undergoing investigation in various stages of clinical trials has been expanding since the 1990s (**Table 1**). Doxil and Caelyx are the two PEGylated doxorubicin formulations approved by the FDA in 1995 and 1996. [127-129] PLD is administered in doses of 50 mg m^{-2} every four weeks, compared to topotecan administered in 1.5 mg m^{-2} daily doses for five days every three weeks, yielding similar OS, overall response rate, and similar time to progression, but with reduced myelotoxicity in EOC patients who previously received platinum chemotherapy or who were platinum-refractory. [130, 131] In 2005, the FDA approved the use of nanoparticle albumin-bound paclitaxel, also known as Abraxane. Subsequent studies demonstrated that Abraxane, when compared to conventional paclitaxel, is associated with

significantly fewer instances of neuropathy, anemia, pain, diarrhea, and hypersensitivity reactions. [132-135] Abraxane exhibits encouraging efficacy in multiple studies as a single agent or in combination with other drugs, including total remission in recurrent ovarian cancer. [136-138]

Table 1: Nanoparticle formulations for gynecological cancer treatments

Name	Active Drug	Nanoparticle	Targeting	Approval status or Trial Start	Indications
Doxil/Caelyx [139-141]	Doxorubicin	Liposome	Passive	FDA approved since November 1995	Ovarian cancer
Liposomal topotecan [142]	Topotecan	Liposome	Passive	Phase I trial, August 2019	Advanced solid tumors, including ovarian cancer
Liposomal paclitaxel, LEP-ETU [143]	Paclitaxel	Liposome	Passive	Phase I/II trials, April 2004	Advanced cancers, including ovarian cancer
Liposomal lurtotecan [144]	Lurtotecan	Liposome	Passive	Phase I/II trial, October 2022	Relapsed epithelial ovarian cancer
siRNA-EphA2 [145-147]	siRNA-EphA2	Liposome	Passive	Phase I trial, May 2012	Advanced solid tumors, including ovarian cancer
Abraxane [137, 148-150]	Paclitaxel	Albumin-bound NP	Passive	FDA approved since January 2005	Ovarian cancer
Paclitaxel polyglutamate [115-117]	Paclitaxel	Polymeric NP	Passive	Phase II trial, April 2005.	Ovarian cancer
Genexol PM [151, 152]	Paclitaxel	Polymeric micelle	Passive	Phase II trial, January 2011	Ovarian cancer
CriPec Docetaxel [153]	Docetaxel	Polymeric micelle	Passive	Phase II trial, November 2018	Ovarian cancer
ALN-VSP02 [154]	VEGF and KSP siRNA	Lipid NP	Passive	Phase I trial, July 2010	Solid tumors, including ovarian cancer

Note: Only the nanoparticle formulations that are FDA-approved or currently undergoing trials are listed.

In addition, the FDA approved the antibody-drug conjugate (ADC) Trastuzumab emtansine (Kadcyla) for HER2-positive metastatic breast cancer that previously was treated with trastuzumab and a taxane chemotherapy. Kadcyla combines the cytotoxic drug DM1 with a monoclonal antibody targeting the HER2 receptor (Trastuzumab). HER2 receptor overexpression is common in multiple types of gynecological cancers, indicating potential benefits of drugs targeting this receptor. [155, 156] Although ADC linker chemistry is not a direct branch of nanomedicine, ADC techniques are used to conjugate antibodies and other peptides to nanoparticles for targeting purposes.

Examples of nanoparticle-based medications currently used in clinical practice, such as Abraxane, liposomal Doxil, and the antibody-drug conjugate Kadcyla, demonstrate the potential of nanomedicine in treating gynecological cancers. However, while ovarian cancer is the focus of the vast majority of nanomedicine-based treatments in clinical use or undergoing various phases of clinical trials, other gynecological malignancies have received less attention in terms of therapy advancements. Therefore, there is an immediate need to expedite the transfer of numerous nanoparticle formulations undergoing pre-clinical investigations to clinical trials, in preparation for their potential clinical use in treating other gynecological malignancies. Importantly, harnessing the potential of nucleic acid therapeutics, with their ability to target specific molecular pathways and exhibit synergistic effects with existing treatments, holds great promise for improving patient outcomes and addressing the unmet medical needs in gynecological malignancies.

3.2 The advantages of nanocarriers in nucleic acid delivery

In the field of nucleic acid therapeutics, the use of nanoparticles as carriers offers distinct advantages, addressing the challenges associated with efficient delivery and intracellular uptake of nucleic acids as drugs. One of the main challenges in nucleic acid delivery is their susceptibility to enzymatic degradation by nucleases present in bodily fluids and cells. [13, 157] Nanoparticle carriers can shield the nucleic acid cargo from enzymatic degradation, thereby increasing their stability and prolonging their circulation time in the body. This protective barrier also enables controlled release of nucleic acids at the tumor site, maximizing their local concentration and therapeutic effect. [158] Furthermore, nanoparticle carriers can be engineered to possess surface modifications, such as PEG coating, which prolong their circulation time, evade immune recognition, and enhance accumulation within the tumor microenvironment. [125] Additionally, nucleic acids have difficulty crossing cellular membranes due to their large size, negative charge, and hydrophilic nature. [159, 160] Delivery systems can facilitate cellular uptake by promoting endocytosis or by facilitating active transport of the nucleic acid payload across the cell membrane. [158] Through the incorporation of ligands, targeting moieties, cell-penetrating and fusogenic peptides, nanoparticles can selectively recognize and bind to receptors overexpressed on cancer cells, facilitating their internalization via receptor-mediated endocytosis and aiding penetration of plasma membranes and organelles. [161, 162] Moreover, the co-delivery of nucleic acids and other therapeutic agents, such as chemotherapeutic drugs or immunomodulators, within the same nanoparticle system allows for synergistic combination therapies. [18, 163] This approach exploits the complementary mechanisms of action of different

therapeutics, leading to enhanced treatment efficacy and the potential to overcome drug resistance commonly observed in gynecological malignancies.

The selection of a nucleic acid therapy delivery system is a crucial decision influenced by various factors, including therapeutic objectives, target cells or tissues, safety considerations, and delivery efficiency. In the realm of nanoparticle-based nucleic acid therapy, a diverse array of materials and preparations exists for their assembly. Lipid-based nanoparticles, such as liposomes, represent a widely employed approach for nucleic acid delivery. [164] These nanoparticles can encapsulate nucleic acid payloads through electrostatic interactions between positively charged ionizable lipids and negatively charged phosphates of the nucleic acid. [165] Additionally, polymer-based nanoparticles, including polymeric micelles and polyplexes, have demonstrated their utility in nucleic acid delivery. [166, 167] These nanoparticles can protect nucleic acids from degradation by encapsulating them through electrostatic binding to positively charged polymers. [167] Moreover, beyond these conventional nanoparticle carriers, other innovative carriers employing cationic lipids, dendrimers, and inorganic materials such as silica have also found application in pre-clinical and clinical studies for nucleic acid delivery. [168] The diverse range of nanoparticle carriers available offers researchers and clinicians multiple options to tailor their nucleic acid therapies to specific requirements, enhancing the potential for successful therapeutic outcomes.

Nanoparticle carriers represent only a subset of nucleic acid therapy options that find application in pre-clinical and clinical investigations, as well as FDA-approved therapeutics. However, it is essential to acknowledge that several other nucleic acid therapy modalities are extensively employed in the field. These include various

technologies and approaches to facilitate efficient delivery of nucleic acids. Among the notable alternatives are viral vectors, which are genetically modified viruses engineered to deliver nucleic acids into target cells. [169] Viral vectors, including adenoviruses, lentiviruses, and adeno-associated viruses, offer high transduction efficiency and are frequently utilized in gene therapy applications. [169, 170] Another prominent approach involves electroporation devices, which apply brief electric pulses to cells, inducing transient pores in their membranes for the uptake of nucleic acids. [171] Electroporation serves as a versatile technique for delivering nucleic acids in a wide range of research and therapeutic settings. Furthermore, microbubbles, small gas-filled microspheres, can be utilized in conjunction with ultrasound to enhance nucleic acid delivery through a process known as sonoporation. [172, 173] Each nucleic acid therapy modality possesses unique attributes, advantages, and considerations, and their selection is contingent upon the specific therapeutic objectives and target cells or tissues under investigation.

3.3 Nucleic acid-based therapeutics for gynecological malignancies

Nucleic acid therapeutics, including mRNA, siRNA, and miRNA, have emerged as promising new approaches for treating gynecological cancers. These innovative therapies are based on manipulating specific genes or gene products in the cancer cells, providing a targeted approach to treating cancer without the toxic effects of traditional chemotherapy drugs. By specifically silencing or expressing specific genes involved in cancer growth and progression, nucleic acid therapeutics have a strong potential to improve the outcomes for patients with gynecological cancers. RNA therapeutics possess the capability to surmount multidrug resistance, enhance the

therapeutic efficacy of first-line treatments, increase the vigilance of the immune system to cancer cells by expressing exogenous therapeutic antibodies or chimeric antigen receptors on the immune cells, prevent the metastatic spread of cancer, and treat cancer-associated syndromes.

3.3.1 mRNA therapies

With the advent of nucleic acid-based therapies, such as mRNA lipid nanoparticles (LNPs) for SARS-CoV-2 vaccines, the nanomedicine industry gained momentum toward advancing mRNA-based therapeutics beyond infectious disease management and prevention. Despite their potential, mRNA therapies for gynecological cancers are still in their early stages of research and development and have limited data available. In fact, only a couple of articles describe mRNA therapeutics for gynecological malignancies. This limited body of work underscores the need for further exploration in this area.

One proposed mRNA LNP therapeutic was described as an efficacious modality for *ex vivo* transfection utilized in chimeric antigen receptor (CAR) cell therapy. [174] CARs expressed in T cells facilitate eradication of tumor cells by equipping T cells with a single-chain variable fragment (scFv) recognition domain, allowing them to bind target cell surface antigens and initiate cell killing. [175] Therefore, Hung *et al.* proposed a therapeutic approach based on mRNA transfection of peripheral blood lymphocytes (PBLs) for ovarian cancer treatment. [176] Mesothelin was used as a target protein due to its common overexpression in solid tumors, including ovarian cancers. The developed therapy consisted of mRNA-guided transient expression of CARs in T cells that specifically targeted mesothelin as tumor-associated antigen. Cells were

supplemented with CAR mRNA using a commercially available electroporation system, yielding 30-35% transfection efficiency with minimal toxicity to the transfected cells. Importantly, mRNA-mediated transient CAR transfection of PBLs, including T cells, is known to mitigate target-specific off-tumor toxicity effects as previously described by other researchers. [177, 178]

In addition to mRNA-based CAR T therapies, an alternative strategy involves the expression of mRNA-encoded antigens that resemble tumor-associated antigens, leveraging the immune system's capabilities to generate a potent response against cancer cells by producing cancer-specific antibodies. [179] Following administration of mRNA therapy, the encoded tumor-associated antigens are processed and presented by antigen-presenting cells, triggering the activation of specific immune cells, such as B cells, which then undergo a process of antibody production and maturation, leading to the generation of high-affinity antibodies against the targeted tumor-associated antigens. An example of innovative treatment in the context of ovarian cancer involves autologous dendritic cells (DCs) transfected with mRNA encoding tumor-associated antigens. This approach harnesses the potential of personalized immunotherapy by utilizing patient-specific DCs to present tumor-specific antigens, thereby enhancing the immune response against ovarian cancer cells. [180, 181]

The transfection of mRNA into antigen-presenting cells, specifically dendritic cells, has garnered interest in the research and development of mRNA vaccines. Presently, there are no therapeutic mRNA vaccines that the FDA has approved. However, a significant number of mRNA vaccines for cancer treatment are currently undergoing pre-clinical studies and clinical trials, including those intended to target

gynecological cancers. Two clinical trials currently in Phase 1 aim to deliver proprietary ovarian cancer tumor-associated antigens using mRNA and the intracellular domain of HER2 using DNA constructs for the treatment of ovarian cancer. [182]

3.3.2 siRNA therapies

For the application of non-coding RNA in the treatment of gynecological cancers, there is greater availability of data on siRNA-based nanomedicines that utilize an RNA interference (RNAi) approach. RNA interference (RNAi) reduces the expression of proteins crucial to cancer development by silencing a specific mRNA. The delivered siRNA binds to argonaute proteins, which are the components of the RNA-induced silencing complex (RISC) that, in turn, splits double-stranded siRNA into two strands. The guide strand acts as a probe, attaching RISC to mRNA targets in order to promote mRNA cleavage and subsequently inhibit mRNA translation. [183] Lipid, polymeric, dendritic, and other nanoparticle platforms are used for siRNA delivery, shielding siRNA molecules from endogenous nucleases and facilitating the transport of negatively charged siRNA through the plasma membrane. [184] Nanoparticle-based siRNA therapeutics function to decrease multidrug resistance in gynecological cancers, potentiate chemotherapy treatments, as well as function as single-agent therapeutics with promising antitumoral effects. While ovarian cancer has been a primary focus of siRNA therapeutics, ongoing research in this field has expanded to encompass other gynecological cancers, including cervical and endometrial malignancies (**Table 2**).

Table 2: Pre-clinical siRNA therapeutics for gynecological malignancies

Reference	Target	Nanocarrier	Targeting	Cancer Type	Model
[185]	*E6*	Antibody/Peptide/ Lipid Complex	Targeted	Cervical	*In vitro*: CaSki, SiHa, and HeLa cells
[186]	*E6, E7*	Chitosan NP	Targeted	Cervical	*In vitro*: SiHa cells
[187, 188]	HPV18 *E6*	Gold NP	Targeted	Cervical	*In vitro*: HeLa cells; *in vivo*: nude mice with HeLa tumors
[189]	HPV16 *E7*	Lipid NP	Passive	Cervical	*In vitro*: TC-1 cells; in vivo using obese and non-obese C57Bl/6 mice with TC-1 tumors
[190]	*Cdk4*	Lipid NP	Passive	Cervical	*In vitro*: HeLa cells
[191]	HPV16: *E6, E7*	Liposomes	Passive	Cervical	*In vitro*: CaSki and TC-1 cells, in vivo using C57Bl/6 mice with TC-1 tumors
[192]	HPV16 *E6*	Liposomes	Passive	Cervical	*In vitro*: CaSki cells, in vivo using nude mice bearing CaSki tumors
[193]	HPV16 *E6*	Liposomes	Passive	Cervical	*In vitro*: CaSki cells
[194]	HPV16 *E6, E7*	Polymeric Micelles	Passive	Cervical	*In vitro*: SiHa and HeLa cells
[195]	*Egfp*	Polymeric NP	Passive	Cervical	*In vitro*: HeLa cells
[196]	*Tert*	Polymeric NP	Passive	Cervical	In vitro using Hela cells
[197]	*Derlin1*	Selenium NP	Passive	Cervical	*In vitro*: HeLa and HUVEC cells; *in vivo*: nude mice with Hela tumors
[198]	*Ezh2*	Chitozan NP	Passive	Endometrial and Ovarian	I *In vitro*: Ishikawa, Hec-1A, KLE, and SK-OV-3-ip1 cells; *in vivo:* nude mice bearing Ishikawa and Hec-1A tumors
[199]	*Axl*	Peptide NP	Passive	Endometrial, Ovarian	*In vitro*: ARK1 and OVCAR-8 cells; *in vivo*: NOD SCID or NU/FOX mice bearing ARK1 and OVCAR-8 tumors
[200]	*Egfr*	Carbon NP	Passive	Ovarian	*In vitro*: HeyA8-F8 cells
[201]	*Hif-1α*	Chitosan Lactate NP	Targeted	Ovarian	*In vitro*: OVK18 cells
[202]	*Postn, Fak, Dlxdc1*	Chitosan NP	Targeted	Ovarian	*In vitro*: SK-OV-3-ip1, HeyA8, and A2780 cells; in vivo using A2780 tumor-bearing nude mice

[203]	*Plxdc1*	Chitosan NP	Passive	Ovarian	*In vitro*: HUVEC, MOEC, SK-OV-3, A2780 and HeyA8 cells; *in vivo*: nude mice with A2780 and HeyA8 tumors
[204]	*Src* and *Fgr*	Chitosan NP	Passive	Ovarian	*In vitro*: SK-OV-3-ip1 and HeyA8 cells; *in vivo*: nude mice with SK-OV-3-ip1 and HeyA8 tumors
[205]	*Jagged1*	Chitosan NP	Passive	Ovarian	*In vitro*: SK-OV-3-Trip2 cells; *in vivo*: nude mice with SK-OV-3-Trip2 tumors
[206]	*P70-S6*	Dendrimer NP	Passive	Ovarian	*In vitro*: SK-OV-3 cells; *in vivo*: nude mice with SK-OV-3 tumors
[207]	*Akt*	Dendrimer NP	Passive	Ovarian	*In vitro*: SK-OV-3 cells; *in vivo*: nude mice with SK-OV-3 tumors
[208]	*Cd44*	Dendrimer NP	Targeted	Ovarian	*In vitro* and *in vivo* using PDX in nude mice
[209]	*Dj-1*	Dendrimer NP	Passive	Ovarian	*In vitro*: HUVEC, ES2 and A2780/AD cells; *in vivo*: nude mice bearing ES2 and A2780/AD tumors
[210]	*Erbb2*	Gold NP	Passive	Ovarian	*In vitro*: SK-OV-3 cells; *in vivo*: nude mice with SK-OV-3 tumors
[211]	*Micu1*	Gold NP	Passive	Ovarian	*In vitro*: OVCAR5, OV167, OV202, A2780, SKOV3-ip, OSE cells
[212]	*Mdr1*	Hyaluronic acid NP	Passive	Ovarian	*In vivo*: nude mice with SK-OV-3-TR, OVCAR-8-TR tumors
[213]	*Fak*	Hyaluronic NP	Passive	Ovarian	*In vivo:* nude mice with HeyA8-MDR, SK-OV-3-TR cells and PDX
[214]	*Egfr*	Hydrogel	Passive	Ovarian	*In vitro*: Hey and SK-OV-3 cells
[215]	*Plk1*	Lipid NP	Passive	Ovarian	*In vitro*: SK-OV-3 cells; *in vivo:* SCID mice bearing SK-OV-3 tumors
[216]	*Hmcp1*	Lipid NP	Passive	Ovarian	*In vitro*: SK-OV-3-ip1 cells; *in vivo* nude mice bearing SK-OV-3-ip1 tumors
[217]	*Claudin-3*	Lipidoid NP	Passive	Ovarian	*In vivo*: MISIIR/TAg transgenic mice, mice with ID8 tumors, and nude mice with OVCAR-3 tumors
[218]	*Parp1*	Lipidoid NP	Passive	Ovarian	*In vivo*: nude mice bearing mT2K tumors

[219]	No target	Lipoprotein NP	Passive	Ovarian	*In vitro*: multiple cell lines, including ovarian cancer cell lines OVCAR-3, OVCAR-4, OVCAR-5, OVCAR-8, Caov-3, HeyA8, Monty-1, and SK-OV-3-ip1; *in vivo:* NSG mice with HeyA8 tumors
[220]	*Notch1*	Liposome	Passive	Ovarian	*In vitro*: SK-OV-3
[221]	*Ksp*	Liposomes	Passive	Ovarian	*In vivo*: nude mice with SK-OV-3 tumors
[222]	*Epha2*	Mesoporous silicon NP	Passive	Ovarian	*In vitro*: SK-OV-3 cells; *in vivo*: nude mice bearing SK-OV-3 tumors
[223]	*Survivin*	Polymeric micelles	Passive	Ovarian	*In vitro*: A2780, SK-OV-3 and multi-drug resistant SK-OV-3-TR cells
[224]	*Ezh2*	Polymeric NP	Passive	Ovarian	*In vitro*: SK-OV-3-ip1 and HeyA8 cells; *in vivo*: nude mice with SK-HeyA8-luciferase tumors
[225]	*Tlr4*	Polymeric NP	Passive	Ovarian	*In vitro*: SK-OV-3/LUC cells
[226, 227]	*Vegf*	Polymeric NP	US-assisted	Ovarian	*In vitro*: A2780 cells
[228]	*Pd-l1*	Polymeric NP	Targeted	Ovarian	*In vitro*: SK-OV-3-Luc cells
[229]	*Gro-alpha*	Polymeric NP	Targeted	Ovarian	*In vitro*: ES-2 cells
[230]	*Gapd*	Polymeric NP	Targeted	Ovarian	*In vitro*: SK-OV-3 cells
[231]	*Snai1*	Mesoporous Silica NP	Passive	Ovarian	*In vivo*: nude murine model with ovarian PDX
[232]	*P62*	Chitosan polymeric NP	Passive	Ovarian	*In vitro*: 2008/C13 cells
[233]	*Bcl-2*	Polymeric micelles	Targeted	Ovarian	*In vitro*: SK-OV-3 cells
[234]	*Notch3*	Gold NP	Passive	Ovarian	*In vitro*: SK-OV-3-DPP cells
[235]	*Twist*	Dendrimer NP and Mesoporous Silica NP	Passive	Ovarian	*In vitro*: A2780R and OVCAR8 cells; *in vivo:* nude mice with OVCAR8 tumors
[236]	*Pkm-2 and Mdr-1*	Hyaluronic NP	Targeted	Ovarian	*In vitro*: SK-OV-3 cells; *in vivo*: nude mice with SK-OV-3 tumors
[237]	*Survivin, Bcl-2, P-gp*	Polymeric NP	Passive	Ovarian	*In vitro*: ES-2, OVCAR-3, and SK-OV-3 cells, *in vivo:* nude mice with KV-OV-3 tumors

Abbreviations: NP – nanoparticles; PDX – patient-derived xerograph; US - ultrasound.

In the treatment of ovarian cancer, multidrug resistance (MDR) represents a significant obstacle. [238] MDR arises when cancer cells gain resistance to multiple chemotherapy drugs, making it challenging to manage the disease effectively. [239] Multidrug-resistant cancer patients may benefit from siRNA nanoparticle-based therapeutics. [240] The mechanism of action of siRNA nanoparticle treatment includes the transport of siRNA molecules to the cancer cell cytosol, where they can target mRNA transcribed from the genes associated with drug resistance. The siRNA inhibits the normal function of the targeted genes, which may increase the sensitivity of cancer cells to chemotherapy, therefore improving its efficacy. [241] The list of MDR-associated genes in ovarian cancer constantly expands, but some of the most cited are *per2*, *itga6*, *lrp*, *mdr1, birc5*, *ptk2, and park7*. [242-245] P-glycoprotein (*mdr1*) is an MDR marker responsible for ATP-dependent clearance of compounds, including antineoplastic drugs used for cancer treatment. [246] Liposomal formulations complexing paclitaxel with anti-*mdr1* siRNA not only allowed a downregulation of resistance-associated proteins, but also decreased paclitaxel toxicity, increased its cellular penetrability, and, therefore, increased overall therapeutic efficacy of the combinatorial treatment in the ovarian cancer xenograft model using nude mice. [247] Another MDR marker survivin (*birc5*), a member of the inhibitors of apoptosis protein (IAP) family, was shown to be significantly upregulated in various human malignancies, such as breast and ovarian cancer, although its expression was low in normal tissues. [248, 249] Silencing of survivin and associated focal adhesion kinase, FAK (*ptk2*), produced a decrease in paclitaxel resistance and potentiated therapeutic efficacy of paclitaxel chemotherapy in mice. [213, 223] siRNA-mediated knockdown of epidermal growth factor receptor (EGFR) was

also successfully employed to decrease taxane and doxorubicin chemoresistance. [195, 214] Yet another MDR marker DJ-1, expressed from the *park7* gene, is implicated in various stages of cancer progression, including proliferation, metastases, as well as chemotherapy resistance. [250] The study by Schumann *et al*. found that the combination of siRNA-mediated suppression of DJ-1 protein and low-dose cisplatin was effective in reducing the growth of ovarian cancer cells *in vitro* and *in vivo* (**Figure 4**). [251] Furthermore, DJ-1 siRNA in combination with targeted photodynamic therapy, incorporating a photosensitizing agent phthalocyanine, allowed complete eradication of ovarian cancer cells in the intraperitoneal model of ovarian cancer in nude mice. [209] These two research papers indicate that the targeting of DJ-1 constitutes a potentially valuable strategy for addressing ovarian cancer progression and chemotherapy resistance. Therefore, the downregulation of DJ-1 demonstrated promising outcomes in pre-clinical investigations and may offer novel therapeutic alternatives for individuals who have ovarian cancer.

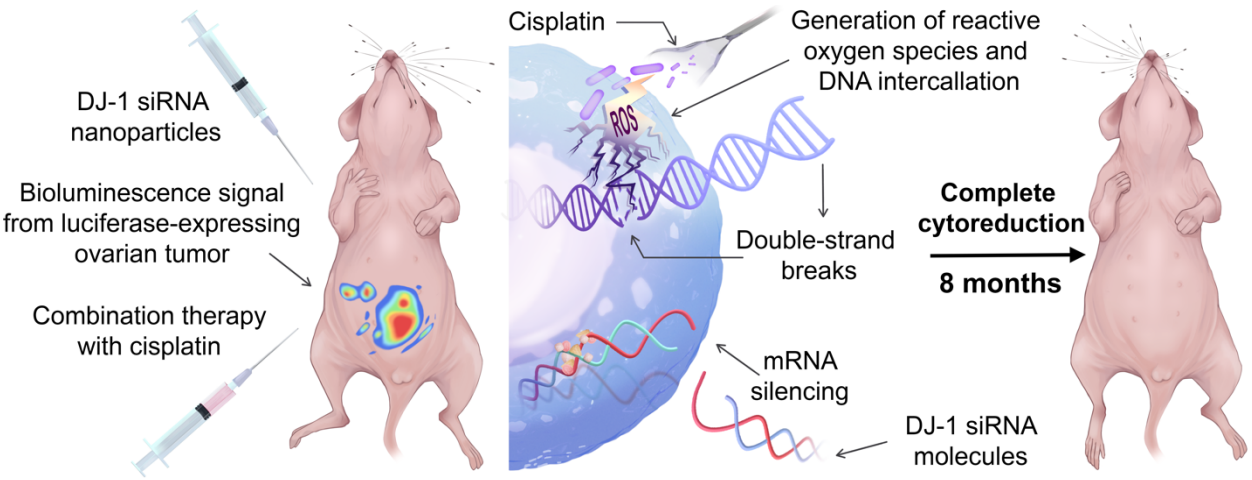

Figure 4. A nanoparticle-based siRNA therapy combined with cisplatin effectively suppresses DJ-1 protein to treat metastatic ovarian cancer: The siRNA-mediated suppression of DJ-1 protein, combined with low-dose cisplatin, effectively inhibited ovarian cancer cell growth in nude mice. While cisplatin is known to induce DNA double-strand breaks (DSBs) and generate reactive oxygen species (ROS), the siRNA approach targeting DJ-1 mRNA translation potentially resulted in a decreased ability of cancer cells to counteract ROS action, leading to a reduction in DJ-1-dependent enhancement of cell survival. Therefore, the therapeutic approach as the one described in [251] could serve as antineoplastic therapy sensitizer.

In addition to combinatorial siRNA-chemotherapeutic treatments, siRNA therapeutics were successfully combined with hyperthermia for the potentiation of cytotoxic responses in gynecological cancers. For instance, inhibition of genes associated with heat shock protein 70, Hsp70, encoded by *hspa6*, was employed to sensitize ovarian cancer to magnetic fluid hyperthermia (MFH). [252] siRNA-mediated inhibition of another heat shock protein Hsp26, encoded by *hspb1* gene, sensitized ovarian cancer cells to hyperthermic intraperitoneal chemotherapy (HIPEC). Furthermore, yet another target, connective tissue growth factor (CTGF), is involved in glycolytic activity rescue after hyperthermic shock; therefore, silencing of CTGF halts cellular ability to recover, leading to cell death. [253] Therefore, *ctgf* downregulation using nanoparticle-based technology delivering anti-*ctgf* siRNA led to increased

apoptosis of ovarian and uterine cancer cell lines and tumors in the ovarian orthotopic mouse model subjected to hyperthermia treatment. [253]

Stand-alone siRNA nanoparticle therapies provide promising results in treating gynecological cancers. siRNAs have been employed to decrease the expression of cancer-related genes since siRNA may rapidly degrade target mRNA without requiring nuclear entry. [254] This therapeutic modality is especially relevant to genes once considered "undruggable." For instance, human papillomavirus (HPV) oncoproteins E6 and E7 are well-characterized as causative agents for cervical cancer. [255] E6 promotes the degradation of p53 preventing infected cell cycle arrest and apoptosis, while E7 binds to the retinoblastoma protein (pRb) and prevents pRb complex formation with transcription factor E2F leading to the absence of transcriptional repression and proliferation dysregulation. [256] Importantly, siRNA-mediated E6 and E7 knockdown suppressed cervical tumor growth and increased cancer cell apoptosis in both *in vitro* and *in vivo* mouse models of HPV-positive cervical cancer. [185-189, 191-194] In ovarian cancer models, multiple genes were targeted to reduce tumor growth, angiogenesis, and metastatic potential proving siRNA as a promising single-drug therapeutic modality. For instance, dysregulation of the Notch-VEGF axis was implicated in cancer angiogenesis and associated with decreased survival in ovarian cancer patients. [257] Targeting and downregulation of Notch and its ligands lead to reduced proliferation and increased apoptosis of ovarian cancer cells. [205, 220, 234] Direct targeting of vascular endothelial growth factor (VEGF) *in vivo* gave promising results of decelerated tumor growth and decreased tumor size in a nude mouse model of ovarian cancer. [227] Furthermore, VEGF was successfully silenced in combination

with kinesin spindle protein (KSP) knockdown. [258] Liposomal formulation aiming to deliver anti-*ksp* siRNA allowed substantial growth suppression of ovarian cancer tumors, mirroring a successful silencing of VEGF/ksp in hepatocellular carcinoma that reached human trials. [221]

The success of single-agent siRNA therapeutics is not surprising, since siRNA nanoparticle therapy has several advantages over traditional chemotherapy. Utilizing nanoparticles for siRNA administration enables a regulated and prolonged release of siRNA molecules and assists in reducing off-target effects, which may be a substantial impediment in cancer treatment. [259]

3.3.3 miRNA therapies

Another non-coding RNA therapy approach utilizes microRNA (miRNA) for cancer therapeutics. miRNAs are a form of short non-coding RNAs that are a potential therapeutic target for gynecological cancers. These small molecules play an important role in gene expression regulation and are altered in a variety of gynecological malignancies, including ovarian, cervical, and endometrial cancers. miRNAs for cancer therapies entail either suppressing the expression of oncogenic miRNAs or increasing the expression of tumor suppressor miRNAs, resulting in a novel and targeted method for treating malignancies. For instance, plasmid encoding microRNA miR-let-7c-5p, characterized by tumor suppressive properties, was functionalized using biodegradable silica nanoparticles for delivery to HeLa cells. [260] The treatment developed by Shao *et al.* showed promising results in inhibiting the growth of cancer cells, not through traditional cytotoxic effects, making it a potential candidate for a systemic treatment approach. Similarly, miR-499a-5p encapsulated in exosomes decreased endometrial

cancer proliferation *in vitro* using human endometrial cancer cell lines, including Ishikawa, HEC1A, and AN3CA, and *in vivo* using nude mice bearing Ishikawa cell xenografts. [261] Since exosomes are endogenous liposome-like structures that share chemical and physical properties with liposomes, miR-499a-5p technology could benefit from a liposomal modality for delivery to cancer cells. [262] Gandham *et al.* proposed Let7b miRNA hyaluronic acid nanoparticle therapy for treating relapsed and multidrug-resistant epithelial ovarian cancer. [263] Let7b miRNA intraperitoneal co-delivery with paclitaxel was tested in the ID8-VEGF murine ovarian cancer model. ID8-VEGF cells overexpressing VEGF were utilized for tumor burden assessment and evaluation of Let7b miRNA therapeutic efficacy. This combinatorial treatment with paclitaxel decreased VEGF levels in the peritoneal fluid compared to monotherapy indicating decreased ID8-VEGF cellular proliferation. Some miRNAs have an oncogenic effect and require silencing using an anti-miRNA approach. For instance, Ysrafil *et al.* developed anti-miRNA-324-5p therapy functionalized by chitosan nanoparticles to decrease the proliferation of SK-OV-3 cells. [264]

Both anti-oncogenic and pro-tumor suppressive miRNA therapies show promising results in pre-clinical studies and hold the potential to become an effective treatment option for various types of cancers. Moreover, miRNA and siRNA combinatorial therapies can advance innovative gene silencing methods. For instance, combining the upstream tumor suppressive miRNA and anti-oncogenic siRNA both targeting the EphA2 receptor resulted in superior silencing outcomes decreasing tumor growth in ovarian cancer. [265] Given the similarities of siRNA and miRNA therapeutic modalities, using miRNA as cancer therapeutics offers several benefits, including

selective targeting, reduced side effects, potential for combinatorial therapy, and therapeutic entrainment of cancer pathways, making it a promising therapeutic option for treating gynecological cancers.

3.4 Nucleic acid therapies for management of malignant ascites in advanced gynecological cancers

Gynecological malignant ascites refers to the accumulation of fluid in the abdominal cavity. The presence of ascites is often indicative of the advancement of disease to malignancy with peritoneal involvement and the formation of extrapelvic metastases. [266] The fluid buildup is caused by the spread of cancer cells into the peritoneal cavity, which contains both adherent and non-adherent cancer cell clusters. [267] Malignant ascites can cause significant discomfort and impair the quality of life for the affected patients. [268, 269]

Treating malignant ascites in gynecological cancers has several challenges. Malignant ascites can be difficult to diagnose due to the related non-specific symptoms, which can mimic other conditions. [270] Difficulty in diagnostics can lead to a delay in treatment and progression of the disease. Malignant ascites is often hard to treat with surgical intervention due to the wide dissemination of cancer clusters. Furthermore, gynecological cancers, such as ovarian and endometrial cancers, are often associated with ascites resistant to chemotherapy. Chemotherapy resistance makes it difficult to decrease cancer progression and can result in a poorer prognosis for the patient. [269] Moreover, malignant ascites can rapidly progress, leading to an uncontrolled deterioration of the patient's condition. [268, 269]

Currently, treatment options for malignant ascites are limited, and those that are available often have low efficacy. For example, diuretics can help remove excess fluid, but they do not address the underlying malignant cells in the suspension of the accumulating fluid and therefore are contraindicated. [271] The implications of these challenges are significant, as malignant ascites can cause significant morbidity and impact the quality of life of patients with gynecological cancers. In addition, ascites can reduce the effectiveness of other treatments and limit the options available to the patient. Therefore, it is essential to develop new and effective therapies for malignant ascites in gynecological cancers, as well as provide early diagnosis to improve patient outcomes. In the realm of cancer therapy, cutting-edge nucleic acid-based therapeutics have emerged as a strategy for selectively targeting genes that drive cancer growth and contribute to the spread of malignant ascites. However, the existing research on nucleic acid therapeutics aimed at treating malignant ascites in gynecological cancers is limited.

The development of malignant ascites is often linked to the process of epithelial-mesenchymal transition (EMT), in which cancer cells lose their epithelial characteristics and acquire mesenchymal features, such as enhanced mobility and invasiveness. These mesenchymal cells can then detach from the primary tumor and disseminate into the peritoneal cavity, developing malignant ascites. Conversely, during mesenchymal-epithelial transition (MET), mesenchymal cells regain their epithelial properties, including cell-cell adhesion and polarity. Nucleic acid therapeutics can target malignant ascites by reversing the cancer cell phenotype from mesenchymal to epithelial. This reversal is achieved by manipulating specific genes and pathways involved in the EMT process and inhibiting their expression or activity.

For instance, miRNAs can target specific mRNAs that are involved in EMT, leading to their degradation and the suppression of EMT-related gene expression. In a recent study, anti-Let7b miRNA therapy not only decreased the tumor burden of multi-drug resistant cancer, but also led to the absence of ascitic fluid in the peritoneum of treated mice. [263] Research demonstrated that heightened levels of vascular endothelial growth factor (VEGF) are implicated in the peritoneal spread of ovarian cancer, which can ultimately lead to the proliferation of tumors within the peritoneal cavity and the subsequent formation of malignant ascites. [272] Anti-Let7b miRNA monotherapy therapy led to 2.2-fold decrease in VEGF levels in ascites and, consequently, decreased ascites in the peritoneal cavity. [263] Furthermore, a downregulation of E-cadherin and an upregulation of vimentin and N-cadherin are well-known hallmarks of EMT. [273] In orthotopic murine ovarian cancer models, liposome-mediated administration of miR-506 induced E-cadherin and inhibited tumor growth. [274] This finding was corroborated in the study using liposome-mediated delivery of miR-506 to an EOC murine model resulting in decreased EOC dissemination, as well as shifting EOC from a more aggressive metastatic mesenchymal phenotype to an epithelial phenotype. [275] It was evidenced by increased expression of E-cadherin and decreased expression of vimentin and N-cadherin induced by miR-506 treatment.

Additionally, mRNA therapies can induce the overexpression of genes that promote the shift toward MET. My own studies detailed in Chapter 4 highlight nanoparticle-based follistatin mRNA therapy to stimulate the shift from EMT to MET in metastatic ovarian cancer cells. We demonstrated that follistatin, a protein that regulates activin and myostatin signaling, can effectively inhibit EMT by suppressing

TGF-β-related signaling pathways, which are known to promote EMT. The induced shift from EMT to MET phenotype was associated with a reduction in tumor size and an increase in survival in a mouse model of ovarian cancer. These results demonstrate the potential of this therapy as a strategy for treating metastatic ovarian cancer and other cancers that undergo EMT.

Furthermore, it is worth noting that siRNA therapy has the potential to target genes that promote fluid accumulation, including highly-cited genes such as VEGF, leptin, and IL-10, among others. [276-278] There is a scarcity of literature on the use of siRNA-based single-agent therapeutics for treating gynecological cancers characterized by ascites. A few articles reported the utilization of single-agent siRNA therapeutics for hindering metastasis-driving processes in ovarian and uterine cancers. For instance, siRNA therapy decreased mesothelial interaction, migration, and invasion in ovarian cancer stem cells. This outcome was achieved by downregulating p70S6 kinase using siRNA dendriplex nanoparticles. [206] P70S6 kinase induces stem cell-like properties in cancer cells and acts as a downstream regulator of mTOR. siRNA-mediated downregulation of P70S6 kinase gave promising outcomes in *in vitro* and *in vivo* experiments. Another target, AXL receptor tyrosine kinase, is involved in the metastasis and propagation of both ovarian and uterine cancers. AXL downregulation using the P5RHH siRNA delivery platform yielded a decrease in metastases and invasion in ovarian and uterine cancer xenograft mouse models. [199] siRNA-mediated downregulation of claudin-3 not only decreased tumor burden, but also decreased malignant ascites in the murine model of epithelial ovarian cancer. [217]

3.5 Chapter summary

In this chapter, I provide a comprehensive review of FDA-approved nanoparticle-based antineoplastic treatments for gynecological malignancies and outline the advantages of nanocarriers in delivering other types of therapeutics, laying the foundation for further investigation of nucleic acid nanoparticle formulations in subsequent chapters. Furthermore, I explore nucleic acid therapies at various stages of development, from early research to clinical trials, and highlight their potential to improve the outcomes for patients with gynecological malignancies. The primary theses of this chapter encompass several key aspects:

1) Liposomes, polymeric nanoparticles, and inorganic nanoparticles have received FDA approval for specific gynecological cancer therapies.
2) Nanoparticle carriers can shield nucleic acids from degradation, enhance their stability, control their release at the tumor site, and improve their accumulation within the tumor microenvironment.
3) Nanoparticles can facilitate cellular uptake and provide a platform for co-delivery of nucleic acids and other therapeutic agents, enabling combination therapies.
4) Nanoparticle-based therapeutics utilize various forms of nucleic acids, including mRNA, siRNA, and miRNA, to overexpress proteins or manipulate gene products within cancer cells for stabilization or degradation.

Collectively, Chapter 3 of my dissertation fulfils the **Objective 1.2**, as I conduct a comprehensive review of existing research on lipid nanoparticle formulations and their potential in the delivery of nucleic acids for gynecological cancer therapy.

Vol. 18 • No. 44 • November 3 • 2022

www.small-journal.com

NANO · MICRO small

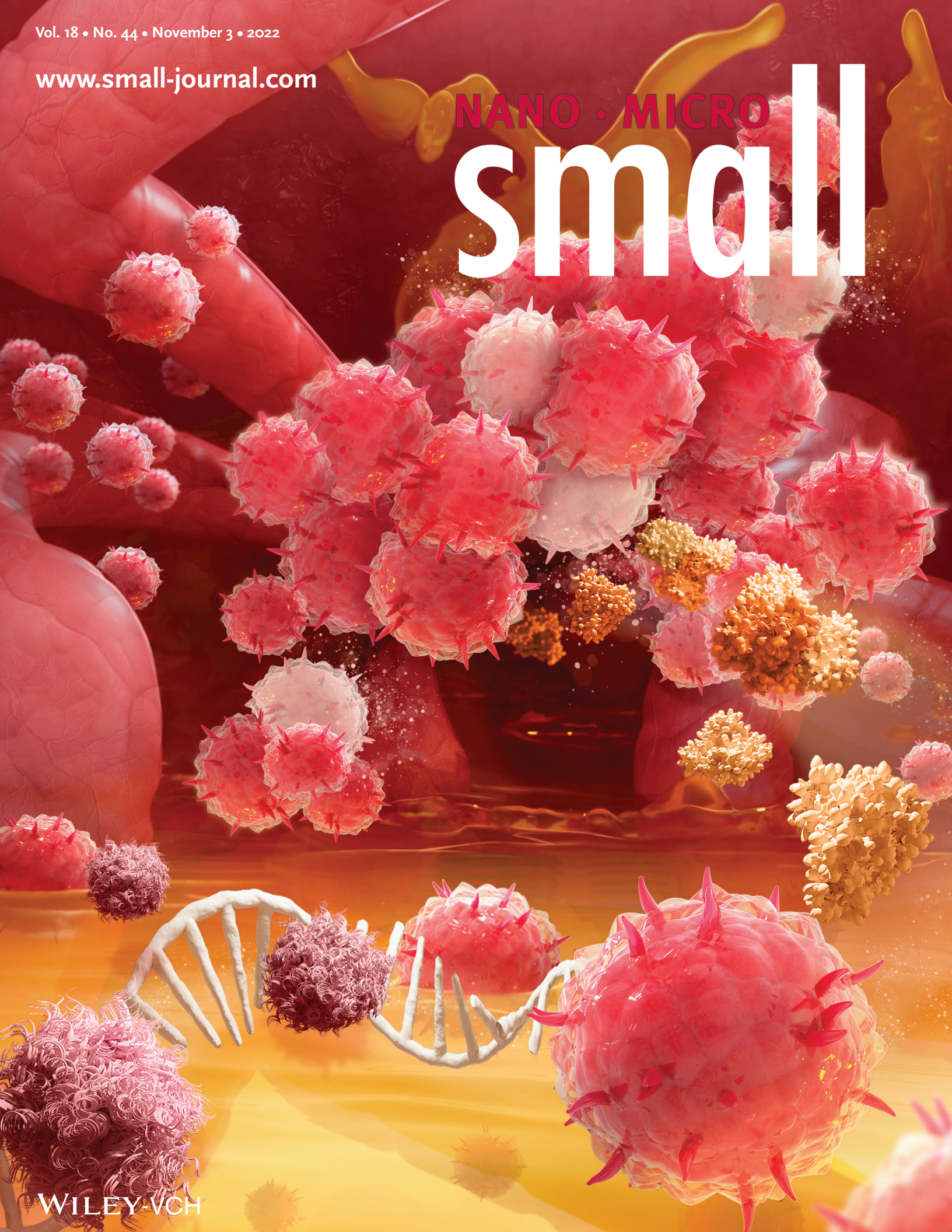

WILEY-VCH

Chapter 4: Follistatin mRNA LNP therapy for advanced ovarian cancer and cancer associated-cachexia

Chapter published in: Korzun, T., et al., Nanoparticle-Based Follistatin Messenger RNA Therapy for Reprogramming Metastatic Ovarian Cancer and Ameliorating Cancer-Associated Cachexia. *Small*, 2022. 18(44): p. e2204436.

4.1 The Dynamic duo: Follistatin and activin A in the context of ovarian cancer and cancer-associated cachexia

The success of mRNA-loaded LNPs in developing SARS-CoV-2 vaccines proved them to be the most efficient modalities for transient protein expression. [165] Although therapeutic applications of mRNA are still in their infancy, they offer promising clinical

potential outside the vaccine field and the management of infectious diseases. And so, the advances in mRNA therapeutics can fuel the development of novel cancer treatment strategies, including cancer vaccines and intratumoral therapies that require frequent dosage. In this Chapter, I will describe the first *multi-dose* protein-coding mRNA therapy aimed at treating metastatic EOC and CAC by overexpressing follistatin (FST) protein for effective neutralization of activin A (ActA).

Cytokines from the transforming growth factor β (TGF-β) family are well-known for exerting adverse modifying actions on cancer behavior. The established literature extensively documents the role of TGF-β ligands in inducing metastasis, invasion, and proliferation. [279] These ligands, including ActA, myostatin, bone morphogenetic protein 7 (BMP7), and other secreted proteins, signal through downstream mediators called Smads. ActA, discovered as a signaling molecule that induces the release of follicle-stimulating hormone (FSH), has a wide arsenal of actions that range from wound healing to muscle wasting in cancer patients. [280] Its physiological role in forming primordial follicular tissue can take an abnormal developmental trajectory leading to neoplasia. Indeed, ActA levels are pathologically elevated in patients with gynecological malignancies. [281, 282] Overexpressed ActA predominantly stimulates proliferation, migration, and invasion of ovarian cancer cells contributing to ovarian tumor metastasis and aggressiveness in later stages. [283, 284] In addition, elevated serum levels of ActA correlate with persistent and recurrent disease and cancer-associated comorbidities, including CAC. [285, 286]

Tumor-derived ActA and myostatin contribute to muscle wasting which, together with the depletion of fat stores and fatigue, plays an essential role in the progression of

CAC. [287, 288] However, unlike myostatin, ActA has a more prominent role in negatively regulating muscle mass in primates. [289] Recent studies in pre-clinical animal models and human subjects show that ActA inhibition by ligand traps results in increased muscle mass, lean body weight, and higher endurance. [290-292] For these reasons, ActA represents an attractive therapeutic target for both cancer therapy and the treatment of cancer-associated muscle wasting.

FST, a circulating glycoprotein, functions as an endogenous regulator for several members of the TGF-β family, including ActA. [293] FST inhibits these proteins by direct binding, sequestering them in an inactive complex and preventing their interactions with the Activin receptor type-2B (ActRIIB). [294, 295] Its high target affinity and nearly irreversible binding kinetics result in complete neutralization of circulating targets. [283, 294, 296] *In vitro* work highlights the ability of recombinant FST to attenuate the stimulatory effect of ActA on the proliferation and migration of ovarian cancer cell lines. [283, 297-299] Additionally, by specifically inhibiting ActA, FST leads to an increase in muscle size and strength, and the regenerative capabilities of muscles in different species. [289, 294] For these reasons, FST-based treatments are promising agents for targeted inhibition of ActA.

Our studies in a murine model of metastatic ovarian cancer show that treatment with *Fst* mRNA encapsulated in LNPs substantially increases systemic and local peritoneal levels of FST protein exerting *in situ* and abscopal therapeutic actions. Production of FST in an autocrine/paracrine fashion and its increase in systemic circulation provides survival benefits similar to cisplatin, a platinum-based chemotherapy drug used as a standard of care in ovarian cancer treatments. Our data

also reveal that systemic FST-mediated inhibition of ActA counteracts muscle loss and in combination with cisplatin provides a synergistic anticancer effect (**Figure 5**). The proposed *Fst* mRNA LNP therapy is a highly translatable platform that outperforms recombinant protein supplementation and limits cancer progression while simultaneously enhancing resilience during an aggressive chemotherapeutic regimen.

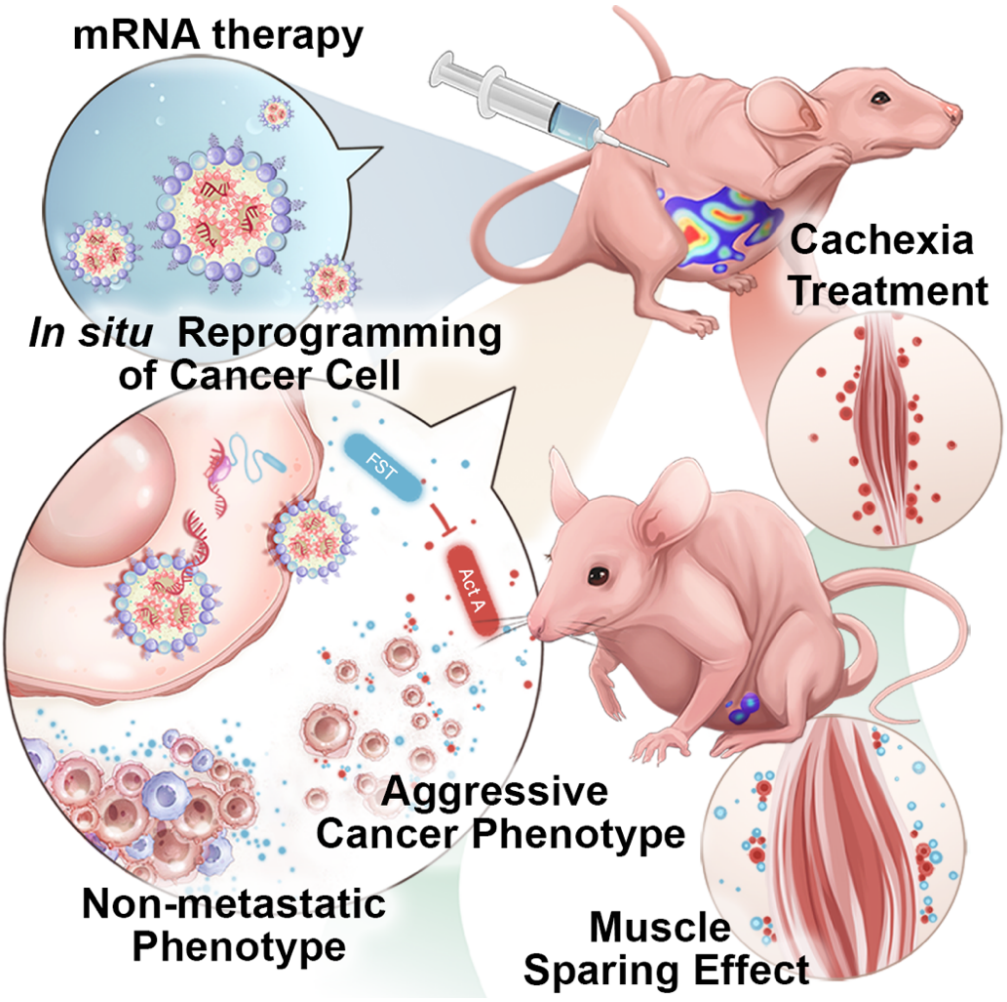

Figure 5. **Mechanisms of activin A and follistatin proteins: Shaping cancer cell phenotype and promoting muscle recovery:** LNPs deliver *Fst* mRNA into cancer cells, leading to its translation into a secretory protein. Secreted FST binds ActA, sequestering it from the pool of bioactive ActA and reducing its activation of ActRIIB receptors. This molecular shift decreases the aggressiveness of EOC and mitigates muscle loss associated with CAC that are dependent on ActRIIB activation.

4.2 Preparation, characterization, and biodistribution of mRNA-LNPs in sham and cancer-bearing mice

The purpose of this work was to develop and test the efficacy of adjuvant LNP-based mRNA therapy to supplement FST protein for the treatment of metastatic ovarian cancer and CAC. This approach allows for transient and highly localized protein over-expression while avoiding permanent genomic changes, the immunogenicity of exogenous proteins, and dose-related toxicity. Indeed, for non-genetic conditions where gene editing may not be the optimal approach, utilizing mRNA for protein overexpression offers significant advantages. This approach allows for precise control over the production of specific proteins, circumventing the need to manipulate the genome directly. Moreover, the transient nature of transcription of *exogenous* mRNA delivered to the targeted cells ensures a temporally controlled and customizable expression profile, enhancing safety and flexibility. This transient nature is attributed to post-transcriptional repressive control mechanisms in the cytoplasm, allowing tight regulation of protein expression levels. [300] Additionally, the expression of mRNA to produce endogenous proteins offers the advantage of avoiding the reactogenicity and immunogenicity associated with direct peptide delivery. This is because the mRNA is translated within the targeted organism, ensuring the incorporation of organism-specific post-translational modifications that are essential for proper protein function and immunological tolerance. [167] Therefore, we used LNP technology to realize the full potential of the mRNA-based therapeutics for FST supplementation in both the immediate tumor environment and systemically.

The LNPs, loaded with different mRNA transcripts (i.e., *FST*, Enhanced Green Fluorescence Protein (*Egfp)*, and firefly luciferase (*Luc)* mRNA), were assembled following the microfluidic mixing procedure **(Figure 6 A)**. [301] LNPs were synthesized in the ratios 50:38.5:10:1.5 of the ionizable lipid DLin-MC3-DMA, cholesterol, DSPC, and DMG-PEG-2k. An N:P ratio of 5.67 was maintained between ionizable lipids and nucleic acids to synthesize nanoparticles. The prepared *Fst* mRNA LNPs had a spherical shape (**Figure 6 B)**, an average hydrodynamic size of 84.5 nm (**Table 3**) with a polydispersity index (PDI) of 0.065, ζ potential of –8 mV, and were characterized by >90% mRNA encapsulation efficiency.

Table 3: Dynamic Light Scattering Properties of Assembled mRNA LNP platforms

LNP	Dynamic Light Scattering		
	d (nm)	*PDI*	*ζ (mV)*
Luc mRNA LNP	84.15	0.148	9.07
Egfp mRNA LNP	102.00	0.207	-2.38
Fst mRNA LNP	84.57	0.065	-7.78
EgfpFst mRNA LNP	86.55	0.217	3.04
Empty LNP	72.22	0.116	1.55

To evaluate mRNA delivery efficiency of the prepared LNPs and therapeutic efficacy of the expressed proteins, we used a murine model of metastatic ovarian cancer (**Figure 6 C-F**), in which nude mice (Nu/Nu) received intraperitoneal (IP) injections of either wild type (ES-2-WT) or luciferase-producing (ES-2-Luc) ES-2 ovarian clear cell carcinoma cells. Ovarian clear cell carcinoma (OCCC) is a subtype of EOC characterized by the presence of clear cells within the tumor tissue. These clear cells have a distinct appearance under the microscope, with clear cytoplasm due to the accumulation of glycogen or lipid vacuoles. OCCC is considered a rare subtype of ovarian cancer, ranging from 5 to 23% of all EOC cases. [302, 303] It tends to have a

poorer prognosis compared to other types of ovarian cancer, may exhibit resistance to certain chemotherapy regimens and is characterized by high metastatic potential. Although OCCC is a rare cancer in humans, this human model of EOC proved effective in nude athymic mice. The model replicated the rapid progression of the disease within the peritoneal cavity, and also led to cachexia manifestations such as muscle mass loss and depletion of fat stores. Injected cancer cells proliferated in the peritoneal cavity, resulting in malignant ascites with a suspension of cancer clusters (**Figure 6 E, F**).

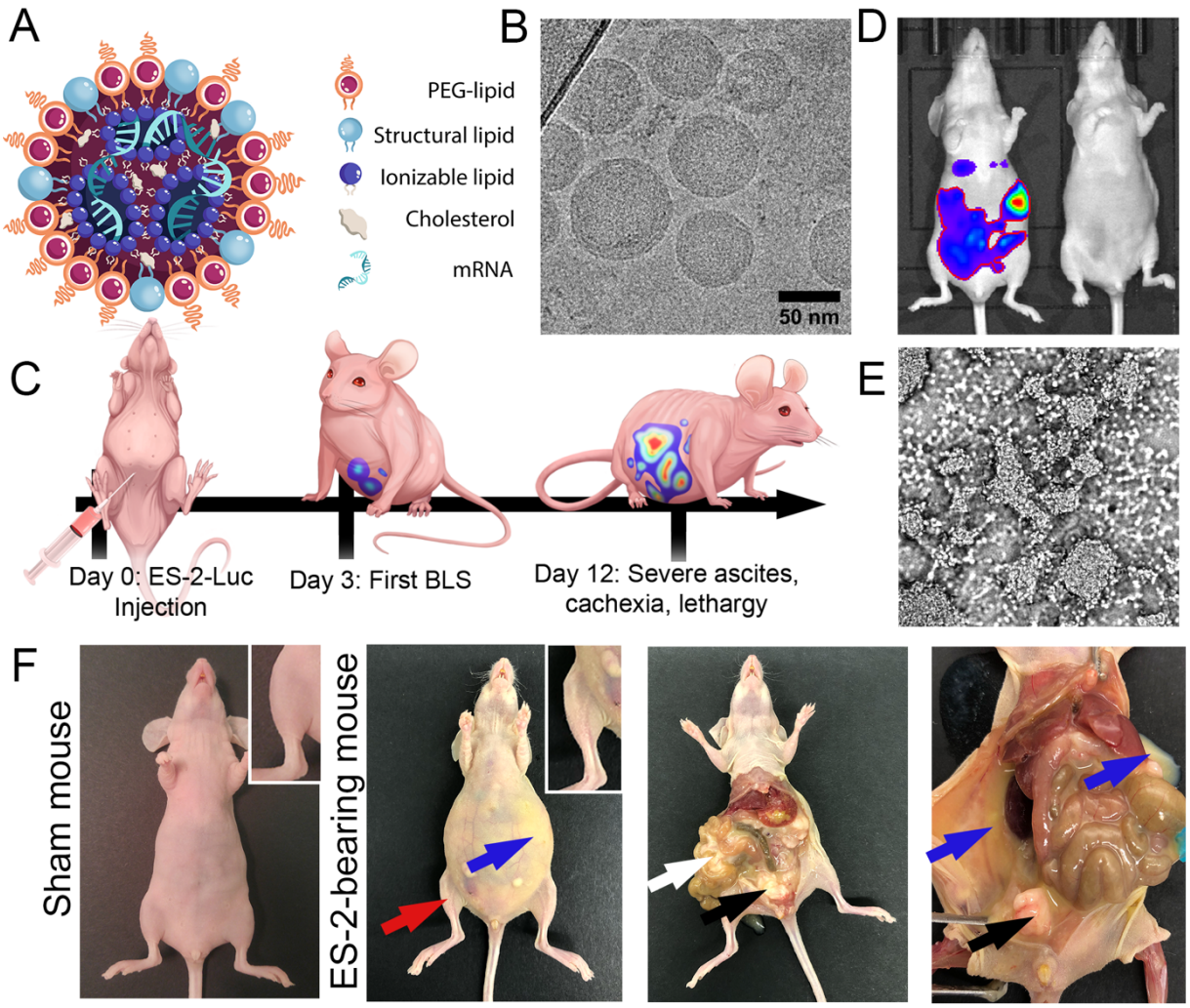

Figure 6. Description of mRNA LNP platform and murine model of metastatic ovarian cancer. (A) Visual representation of the mRNA LNP structure. **(B)** A representative cryo-transmission electron microscopy (TEM) image shows the spherical shape and size distribution of LNPs. **(C)** Illustration of the experimental design used to create the ES-2-Luc mouse model of metastatic ovarian cancer. **(D)** Representative BLS images of ES-2-Luc bearing mouse (left) and sham mouse (right) 15 min after D-luciferin injection. (**E**) Light micrograph of a thin smear of ascites containing ES-2 clusters on a glass slide. Ascitic fluid was collected from ES-2-Luc mice. (**F)** Post-mortem photographs of a sham mouse and ES-2-Luc-bearing mice at the primary humane endpoint (~ day 12) showed distended abdomen due to accumulation of malignant ascites (blue arrows), decreased muscle bulk (red arrows and inset), metastases formed on omentum and mesentery (white arrows), and ovaries and gonadal fat pads (black arrows).

In recent decades, intraperitoneal metastases and malignant ascites were targeted by regional IP therapies exploiting enhanced endocytic characteristics of cancer cells. Multiple malignancies, including ovarian cancer, upregulate endocytic activity to enhance tumorigenesis and metastasis and to aid cancer cell metabolism. [304] We show that ES-2 cancer cells in suspension demonstrate increased *in vivo* capacity for LNP-mediated transfection, presumably due to upregulated endocytosis as a consequence of increased metabolic activity in comparison to normal cells. We evaluated mRNA LNP formulations transfection efficiency by mRNA quantification, and bioluminescent and fluorescent imaging. To determine the biodistribution profiles of mRNA-LNPs and efficiency of delivered mRNA translation to bioactive proteins, we established two experimental groups, including mice bearing ES-2-WT tumors and sham mice (**Figure 7 A**). Mice injected with ES-2-Luc cells served as positive controls; ES-2-WT-bearing mice and sham mice injected with PBS served as negative controls. Mice received single intraperitoneal (IP) injections of LNPs loaded with firefly luciferase mRNA (*Luc* mRNA LNPs) with a dose equivalent to 10 μg mRNA per mouse. Four hours after administration of *Luc* mRNA LNPs, a bioluminescence signal (BLS) generated by luciferase was detected in both sham and ES-2-WT mice injected with D-luciferin (**Figure 7 B**). The results suggest that the luciferase enzyme was translated from the *Luc* mRNA delivered by the LNP platform to various tissues. Importantly, BLS was significantly higher in cancer-bearing mice than in sham animals. Bioluminescence imaging validated that strong BLS generated by the produced luciferase enzyme was predominantly observed in ascitic fluid and other tissues (e.g., gonadal fat pads) containing ES-2 cancer cells infiltrations (**Figure 7 C, D**). Similar BLS distribution was

confirmed by imaging the positive control mice inoculated with ES-2 cells stably transfected with *Luc* gene (ES-2-Luc). In contrast to cancer-bearing mice, relatively weak BLS was detected in the liver, spleen, and IP fluid of sham mice injected with *Luc* mRNA LNPs (**Figure 7 C, D**). This observation supports our hypothesis that the cancer cells are the dominant cell type internalizing LNPs and translating delivered mRNA when administered intraperitoneally.

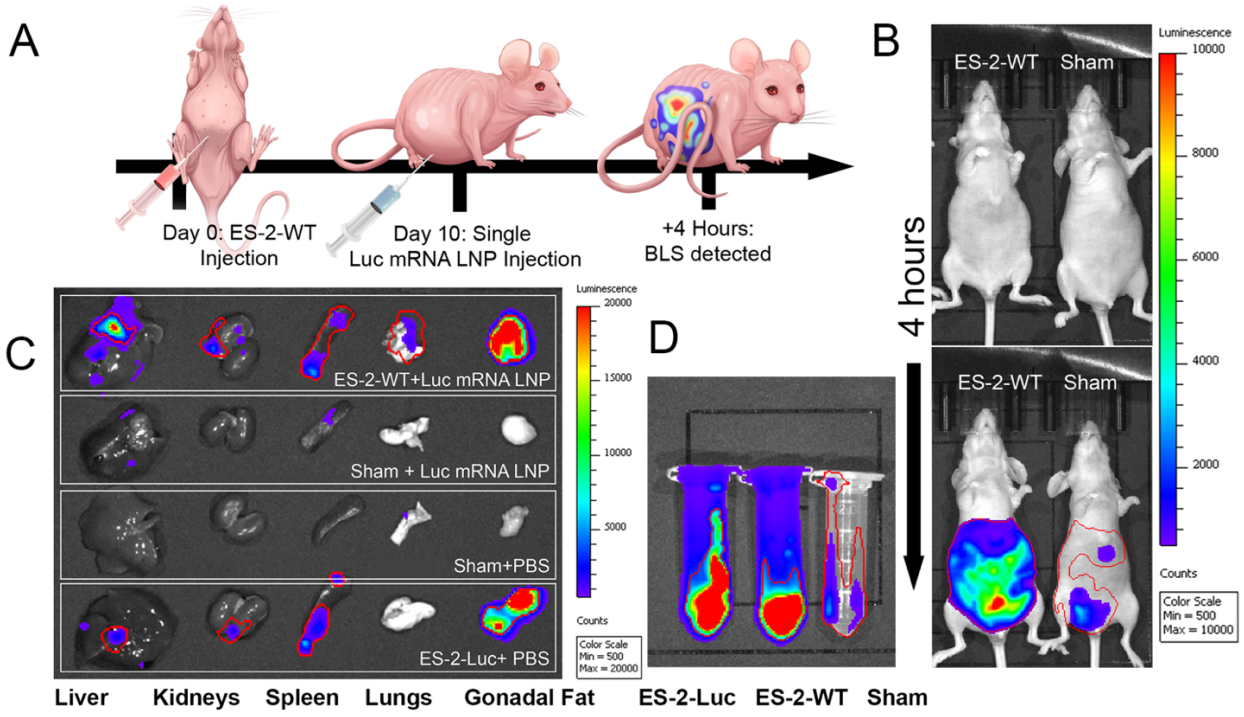

Figure 7. ES-2 clusters demonstrate increased *in vivo* capacity for LNP uptake compared to normal tissues. (A) Experimental design depicting a biodistribution study with ES-2-WT-bearing mice and sham age-matched controls (not shown) administered *Luc* mRNA LNPs. **(B)** BLS images of ES-2-WT and sham mice before (top) and 4 h after (bottom) treatment with *Luc* mRNA LNPs. **(C)** Representative BLS images of tissues collected from ES-2-WT-bearing (ES-2-WT + Luc mRNA LNP) and sham (sham + Luc mRNA LNP) mice at 4 h-post injection with *Luc* mRNA LNP in comparison to negative (sham + PBS) and positive controls (ES-2-Luc-bearing mice + PBS). Organs are (left to right): liver, kidneys, spleen, lungs, gonadal fat pads. **(D)** BLS images of ascitic and physiological peritoneal fluids from ES-2-WT-bearing mice (middle) and sham mice (right), producing an active luciferase enzyme after *Luc* mRNA LNP treatment in comparison to a positive control (ascites of ES-2-Luc-bearing mice, left, treated with PBS).

After investigating biodistribution properties of the LNP formulation, we assessed toxicological and reactogenic profile of the developed mRNA LNPs. Histopathological examination of murine livers that had received chronic mRNA LNP injections was used to assess the safety and tolerability of mRNA LNPs in nude mice. Systemic toxicity and formulation reactogenicity were further assessed by analyzing complete blood counts with differential, blood chemistry, pancreatic and hepatic inflammation panels, and hepatic cytokines associated with inflammation. We observed no changes among treatment and control groups in gross pathology and histopathology of livers resulting from three daily injections of mRNA LNPs (**Figure 8**) in doses equivalent to 10 μg mRNA per mouse. Although we detected some instances of cell death in a small number of cells in the liver in LNP-treated mice, there were no gross changes in tissue morphology, nor infiltration of innate immune cells.

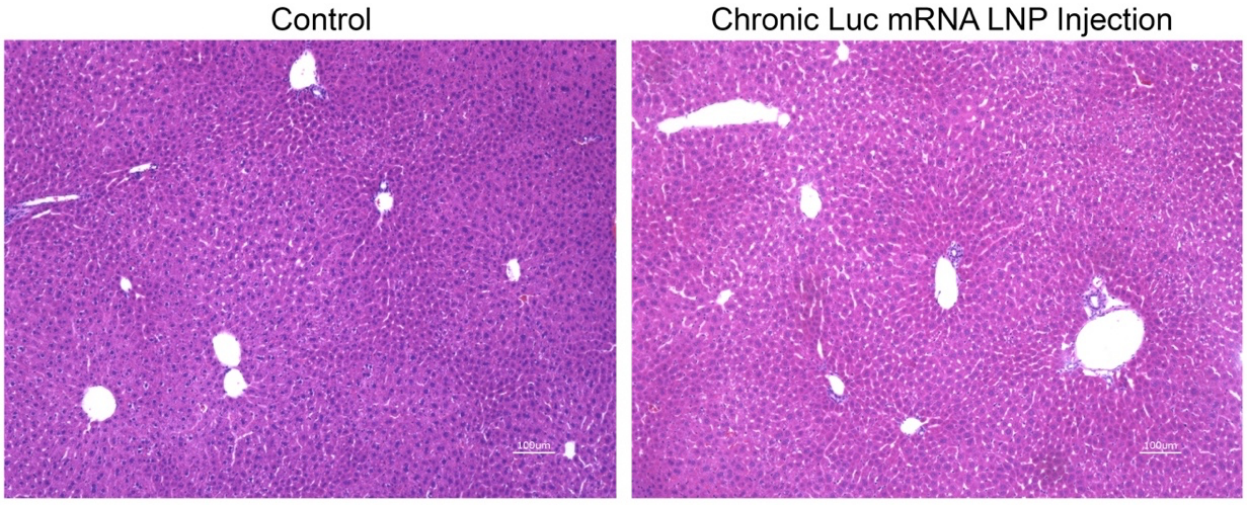

Figure 8. Representative histopathological examination of murine liver sections after chronic injection of Luc mRNA LNPs: H&E histology of liver tissue showing no significant differences between treatment and control groups following three daily injections of mRNA LNPs. Despite the observation of sporadic cell death in a small subset of hepatocytes in LNP-treated mice, there were no apparent alterations in tissue morphology or infiltration of innate immune cells.

Furthermore, hepatic gene expression studies confirmed mRNA LNP formulation to be safe for chronic administration regiments in nude mice (**Figure 9**). The selection of interleukin-6 (IL-6), interleukin-1 beta (IL-1β), and tumor necrosis factor (TNF) as hepatic inflammation markers in this study was justified by wide recognition of these effector molecules as key mediators of the inflammatory response in the liver. [305] IL-6, for example, plays a central role in initiating the acute phase response, while IL-1β is a potent proinflammatory cytokine involved in the regulation of immune and inflammatory reactions. [306, 307] TNF, similarly, is a crucial cytokine known for its involvement in the promotion of inflammation. [308]

Monitoring the gene expression levels of these markers allowed for a comprehensive assessment of the liver's inflammatory state, providing valuable insights into the safety and potential hepatic effects of the mRNA LNP formulation during chronic administration regimens in the animal model. Consequently, the results demonstrating no change in *Il6* and *Tnf* levels, as well as the downregulation of *Il1β* following three daily injections of LNPs (**Figure 9**), characterized the formulation as having a favorable safety profile for nude mice. However, it's important to note that these findings may not be generalizable to other animal models and require further testing for translation.

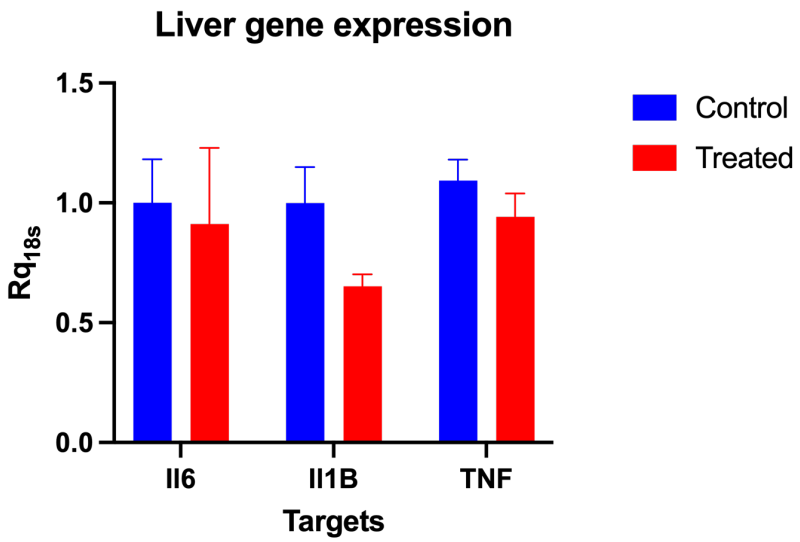

Figure 9. Expression of hepatic inflammatory phase reactants in mice for Luc mRNA LNP formulation safety profiling. Expression of *Il6*, *Il1B* and *Tnf* were assessed in healthy nude mice injected with PBS (control grou) and *Luc* mRNA LNP (treated group). Expressed as mean ± SEM, *n*=5, analyzed by one-way ANOVA, followed by Bonferroni's *post hoc* test.

Additionally, complete blood counts with differentials (**Figure 10 A, B**) and complete metabolic panels (**Figure 10 C**) were unremarkable for mRNA LNP-treated mice. The exception was decreased albumin level in treated mice, which could be due to albumin being consumed as part of protein corona surrounding lipid nanoparticles.

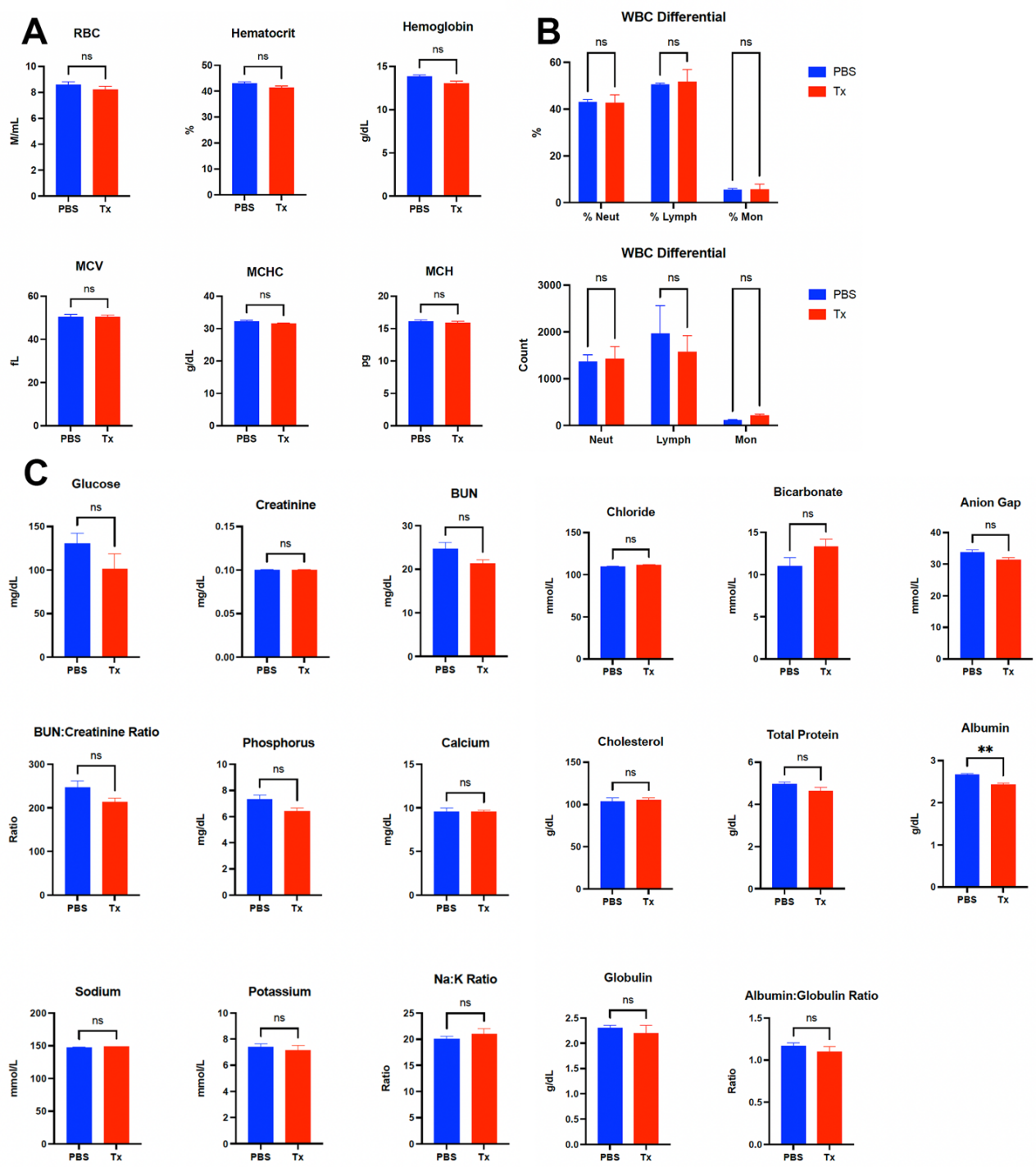

Figure 10. Blood analysis for evaluation of systemic toxicity of chronically injected Luc mRNA LNPs: Healthy nude mice were injected with three daily injections of Luc mRNA LNP formulation in a dose equivalent to 10μg mRNA. (A) erythrocytes and (B) leukocytes; (C) blood chemistry were evaluated as part of safety profiling for the proposed therapeutic. Expressed as mean ± SEM, *n*=5, analyzed by t-test.

Finally, enzymes signifying hepatic (aminotransferases AST, ALT) and pancreatic (amylase and lipase) function were unremarkable with the exception of alkaline phosphatase (ALP) (**Figure 11 A, B**) in mRNA LNP-treated nude mice. Increased ALP could signify some levels of acute hepatic toxicity with following downregulation of ALP that we observe in the mice treated with Luc mRNA LNPs. Creatinine kinase as a marker of skeletal and cardiac muscle function had no change in treatment group (**Figure 11 C**).

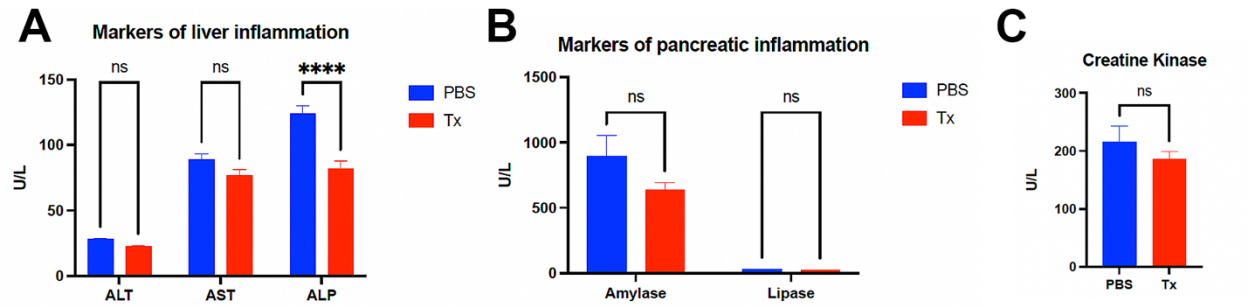

Figure 11. **Toxicity studies: Effects on liver, pancreas, and muscle function.** Healthy nude mice were injected with three daily injections of Luc mRNA LNP formulation in a dose equivalent to 10μg mRNA. Blood markers of liver (A) and (B) pancreatic function, as well as (C) Creatine kinase, the marker of skeletal and cardiac muscle function was assessed as part of safety profiling of the proposed therapeutic.

4.3 Regional mRNA LNP therapy administration targets cancer cell clusters in the peritoneal cavity

To evaluate the therapeutic efficacy of the developed FST therapy, we employed mice inoculated with ES-2 cells stably expressing luciferase enzyme (ES-2-Luc). The luciferase reporter was chosen in order to monitor cancer progression and therapeutic response in cancer-bearing mice using non-invasive bioluminescence imaging. Therefore, in the next step, we validated that ES-2-Luc cells, similar to the ES-2-WT cells, can efficiently internalize LNP-encapsulated mRNA and translate it into bioactive proteins (**Figure 12 A**). We took this additional step to ensure that ES-2-Luc cells were

able to internalize LNPs and express exogenous mRNA to a degree consistent with ES-2-WT cells. This validation was crucial to establish that the luciferase-expressing cells were functionally equivalent to wild-type ES-2 (ES-2-WT) cells in terms of their molecular response to LNP-encapsulated mRNA.

ES-2-Luc-bearing mice received a single IP injection of LNPs encapsulating Cy5-tagged *Egfp* mRNA. The fluorescence signal generated by Cy5 allowed us to confirm mRNA LNP internalization into ES-2-Luc cancer cells, while the EGFP signal validated translation of the encapsulated mRNA into the functional encoded protein. We also used *Egfp* mRNA without the Cy5 tag to control for possible tag interference with cellular uptake and translation of released mRNA (**Figure 12 B**). Four hours after injection, we collected peritoneal cavity fluid containing ES-2-Luc clusters. Fluorescence imaging and qRT-PCR analysis revealed that LNPs successfully delivered Cy5-*Egfp* and *Egfp* mRNAs to ES-2-Luc cells in the IP fluid, and both mRNAs were efficiently translated to EGFP (**Figure 12 B, C**). The green fluorescent signal was not produced when *Egfp* mRNA was replaced with *Fst* mRNA in LNPs, and the signal was observed again, when *Egfp* and *Fst* mRNAs were combined in a single LNP formulation with 1:1 mRNA molar ratio (**Figure 12 B**). qRT-PCR results displayed a concentration-dependent increase in *Egfp* mRNA detected in the ascites treated with *Fst*, *Egfp/Fst*, and *Egfp* mRNA LNP formulations. Therefore, we observed 3- and 3.5-fold increase in normalized *Egfp* mRNA transcript counts on the log scale (**Figure 12 C**) compared to PBS and *Fst* mRNA LNP-treated mice.

Next, we evaluated if ES-2-Luc clusters can internalize *Fst* mRNA LNPs and efficiently produce bioactive FST protein. Two formulations of LNPs loaded with different

Fst mRNA amounts (10 and 5 μg in FST_H mRNA LNP and FST_L mRNA LNP formulations, respectively) were administered into ES-2-Luc cancer-bearing mice. The IP fluid collected at 4 hours-post single injection was analyzed with qRT-PCR (**Figure 12 D**). qRT-PCR results demonstrate that treatment with two LNP formulations containing high (10 μg) and low (5 μg) amounts of *Fst* mRNA increased *Fst* mRNA by ~250- and ~90-fold, respectively, in ES-2-Luc clusters compared to negative controls. The controls receiving *Egfp* mRNA LNPs did not display a non-specific increase in endogenous *Fst* mRNA transcription (**Figure 12 D**).

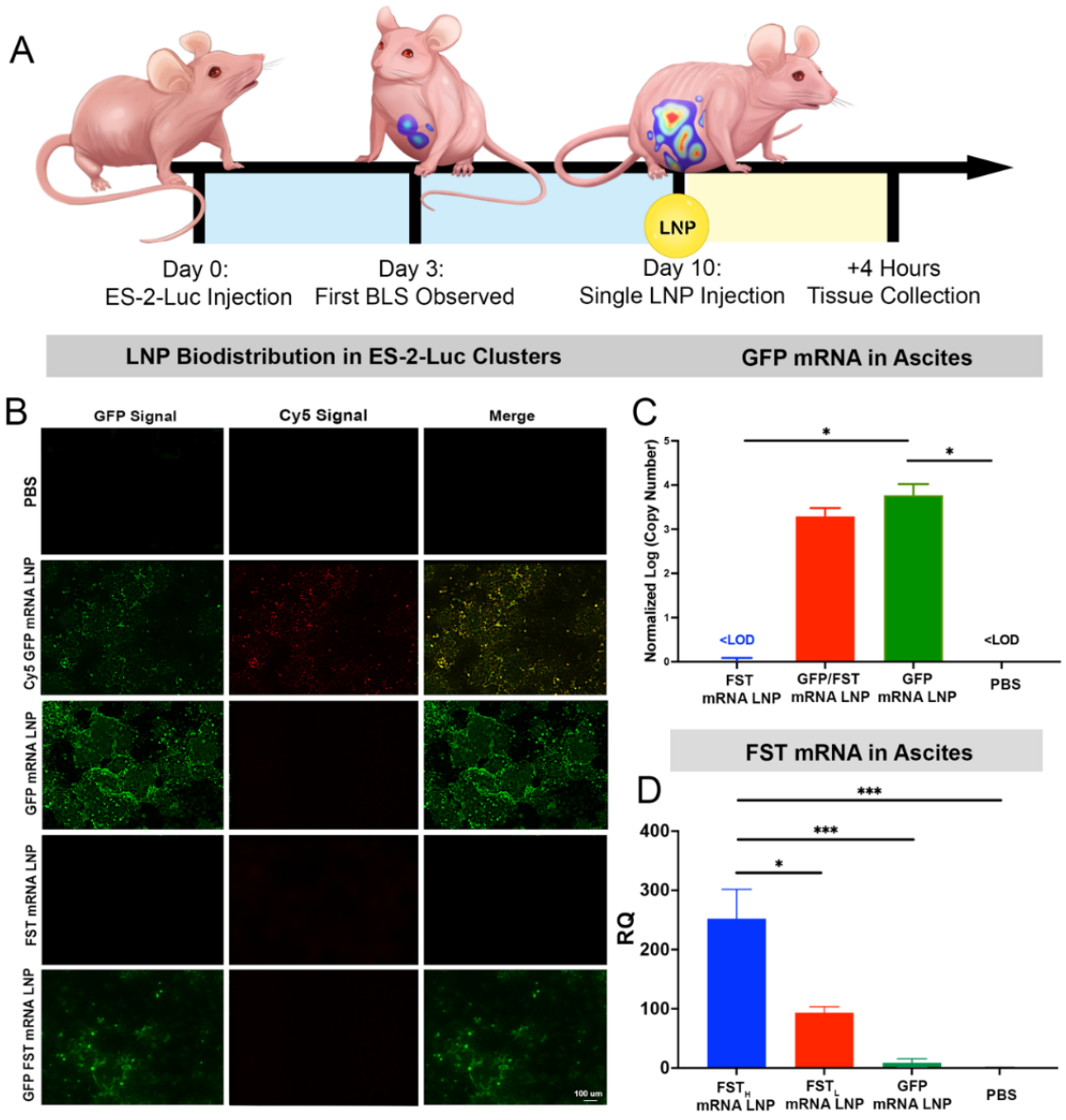

Figure 12. Efficiency of LNP-mediated delivery of *Fst* mRNA was evaluated by transfection investigations in ES-2 ascites. (A) Experimental design illustrating ES-2-Luc bearing mice receiving a single mRNA LNP dose (*Egfp* mRNA, Cy5-*Gfp* mRNA, *Gfp/Fst* mRNA, and *Fst* mRNA, 10 µg total mRNA equivalents per dose per mouse). Four hours after IP injection, sera and ascitic fluid were collected for analysis. **(B)** Fluorescence images of ES-2-Luc clusters 4 h after a single injection with the LNPs loaded with the indicated mRNAs. **(C)** Absolute qRT-PCR quantification of *Egfp* mRNAs in ES-2-Luc clusters 4 h after IP injection of PBS and LNPs loaded with 0 µg Egfp mRNA (*Fst* mRNA LNP), 5 µg *Egfp* mRNA (*Gfp*/*Fst* mRNA LNP), and 10 µg *Egfp* mRNA (*Egfp* mRNA LNP). **(D)** Relative qRT-PCR quantification of *Fst* mRNAs in ES-2-Luc clusters 4 h after IP injection of PBS and LNPs loaded with 10 µg *Fst* mRNA (FST_H mRNA LNP), 5 µg *Fst* mRNA (FST_L mRNA LNP), or 0 µg *Fst* mRNA (*Gfp* mRNA LNP). Expressed as mean ± SEM, n=5, *p<0.05, ***p<0.001, ****p<0.0001 analyzed by one-way ANOVA followed by Bonferroni's *post hoc* test.

To further confirm our hypothesis that mRNA LNP formulation is predominantly internalized by cancer clusters, we performed *in vitro* and *in vivo* flow cytometry studies, where ES-2-WT cells were either co-cultured with RAW 264.7 murine macrophages or injected to IP cavities of nude mice and allowed to proliferate for 10 days (**Figure 13**). Following treatment with *Egfp* mRNA LNPs, IP cavity fluid and cocultured ES-2-WT/RAW 264.7 cells were analyzed by flow cytometry. In both experiments, only HLA-ABC positive cells (ES-2-WT human cell line) were EGFP-positive, confirming the predominant LNP uptake by ES-2 cancer cells (**Figure 13**).

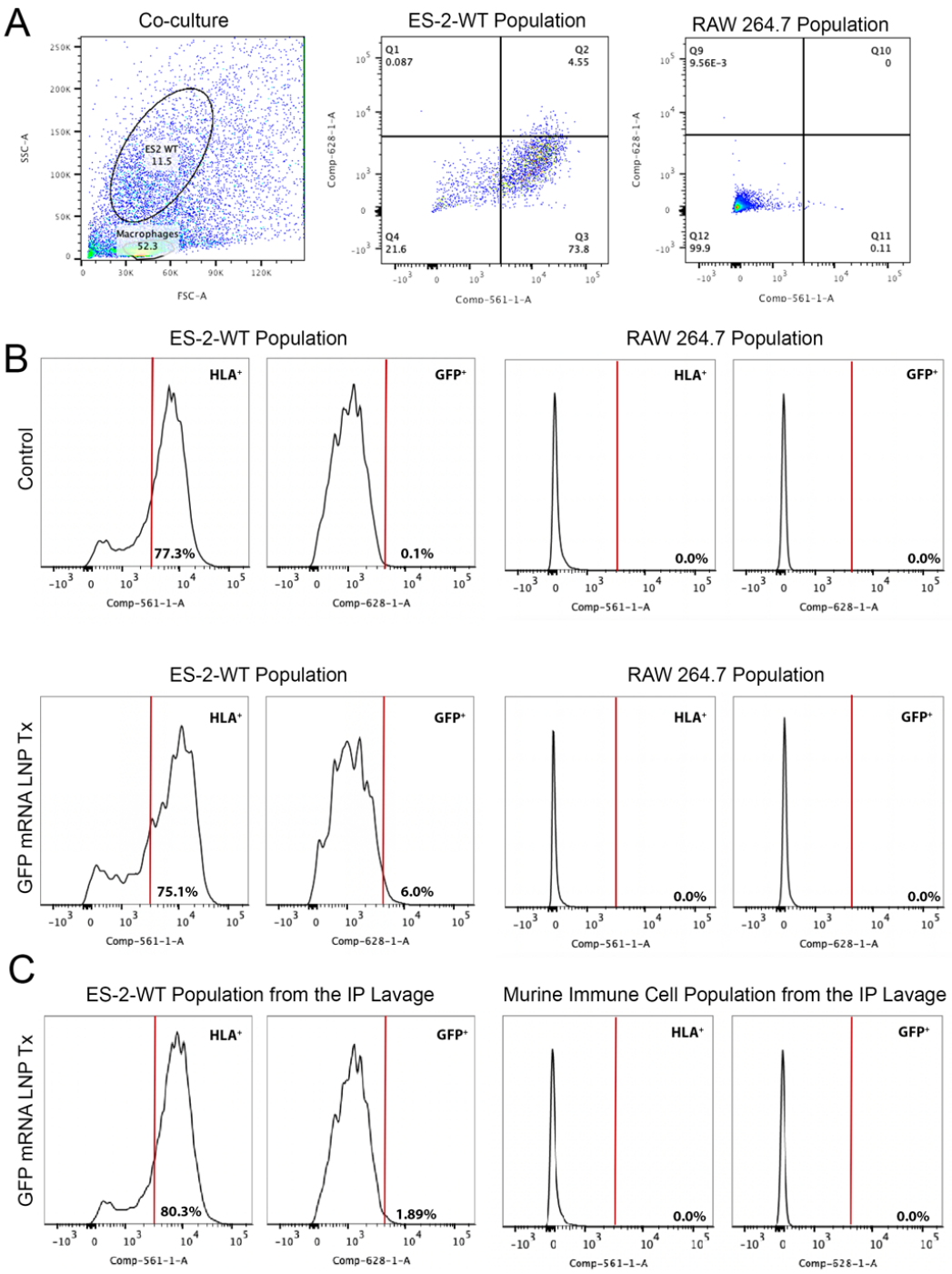

Figure 13: Proportion and cell types internalizing Egfp mRNA LNPs and expressing GFP. (A) Flow cytometry analysis and gating approach in evaluating in vitro and ex vivo samples, Comp–561-1-A–anti-HLA-ABC antibody; Comp-628–1- A–anti-GFP antibody. (B) Analysis of in vitro subculture of ES-2-WT and Raw 264.7 cells (3:1), where controls were treated with PBS and Egfp mRNA LNP Tx samples were treated with Egfp mRNA LNP formulation. (C) ES-2-WT-bearing mice were treated with Egfp mRNA LNPs (2ug mRNA per mouse), control mice were injected with PBS. Collected IP lavage fluid containing mixture of ES-2-WT cells and murine immune cells was subjected to flow cytometry analysis.

Our goal was to achieve transfection of more than just cancer cells within the peritoneal cavity to enable FST expression in the localized tumor microenvironment; we aspired to elevate FST levels in the systemic circulation. Since the *Fst* mRNA used in the experiments translated to the secreted protein isoform (FST-315, see *Fst* mRNA open reading frame sequence, **Table 4**) in comparison to the membrane-tethered isoform, we quantified FST levels in serum samples with FST ELISA. Groups of ES-2-Luc-bearing mice and age-matched sham controls received a single injection of FST_H mRNA LNP, FST_L mRNA LNP*, Egfp* mRNA LNP formulations, or PBS in the negative control group. In sham mice, both *Fst* mRNA formulations exhibited a concentration-dependent increase in serum FST levels (~ 3 and ~1.6-fold increase, **Figure 14 A**). Furthermore, in ES-2-Luc-bearing mice, despite the high basal FST level, FST_H mRNA LNPs increased FST by ~1.6-fold.

Although *in situ* internalization of LNPs by cancer clusters is ideal for autocrine and paracrine inhibition of tumor-derived ActA protein, we expected that the released FST could also affect ActA levels on the systemic level. We aimed to demonstrate the effectiveness of *Fst* mRNA LNP to inhibit ActA by showing the decreasing levels of serum ActA coincident with increased FST LNP uptake. Therefore, we confirmed the synthesis of the fully functional FST protein by evaluating serum ActA levels. FST_H mRNA LNP and FST_L mRNA LNP treatments in sham mice both led to a ~2-fold decrease in serum ActA. In cancer-bearing mice, the decrease was 1.3- and 2-fold for FST_L mRNA LNP and FST_H mRNA LNP treatments, respectively (**Figure 14 B**). The treatment with FST_L mRNA LNP in tumor-bearing mice resulted in a less pronounced reduction in serum ActA levels, indicating that the formulation contained only half the

quantity of *Fst* mRNA loaded into LNPs. Importantly, control (injected with PBS) cancer-bearing mice had a ~4-fold increase in the basal level of ActA compared to sham mice, implying pathological roles of ActA in EOC.

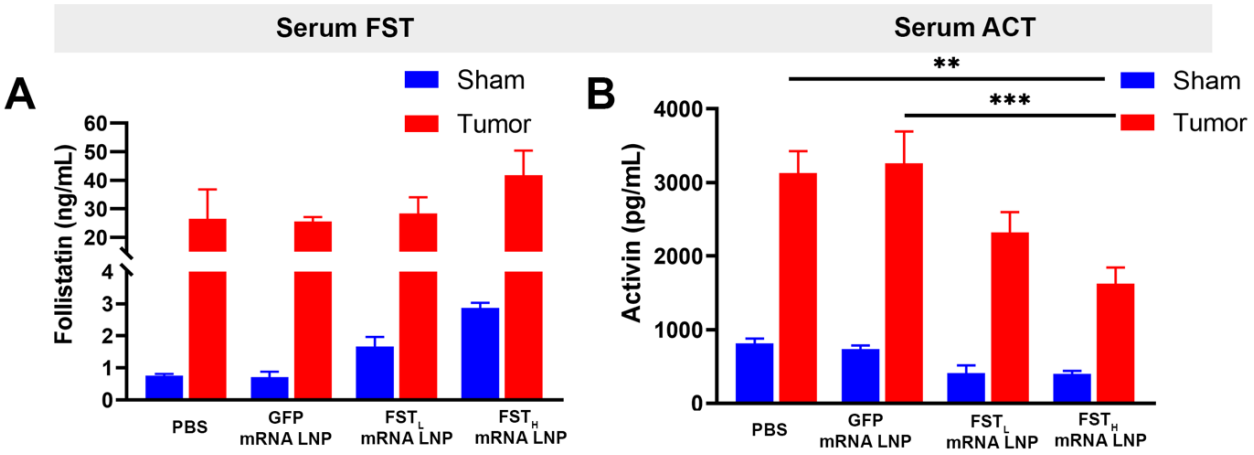

Figure 14. Action of LNP-mediated delivery of *Fst* mRNA leads to a superior therapeutic effect, demonstrated by serum ActA reduction. (A) FST and **(B)** ActA serum protein concentrations expressed as mean ± SEM, *n*=5, ***p*<0.01, ***p<0.001, analyzed by two-way ANOVA followed by Bonferroni's *post hoc* test.

Table 4: mRNA open reading frame sequences utilized in mRNA LNP formulations

Fst mRNA ORF (CleanCap®)

ATGGTCCGCGCGAGGCACCAGCCGGGTGGGCTTTGCCTCCTGCTGCTGCTGCTCTGCCAGTTCATGGAGGA
CCGCAGTGCCCAGGCTGGGAACTGCTGGCTCCGTCAAGCGAAGAACGGCCGCTGCCAGGTCCTGTACAAGA
CCGAACTGAGCAAGGAGGAGTGCTGCAGCACCGGCCGGCTGAGCACCTCGTGGACCGAGGAGGACGTGAA
TGACAACACACTCTTCAAGTGGATGATTTTCAACGGGGGCGCCCCCAACTGCATCCCCTGTAAAGAAACGTGT
GAGAACGTGGACTGTGGACCTGGGAAAAAATGCCGAATGAACAAGAAGAACAAACCCCGCTGCGTCTGCGC
CCCGGATTGTTCCAACATCACCTGGAAGGGTCCAGTCTGCGGGCTGGATGGGAAAACCTACCGCAATGAATG
TGCACTCCTAAAGGCAAGATGTAAAGAGCAGCCAGAACTGGAAGTCCAGTACCAAGGCAGATGTAAAAAGAC
TTGTCGGGATGTTTTCTGTCCAGGCAGCTCCACATGTGTGGTGGACCAGACCAATAATGCCTACTGTGTGACC
TGTAATCGGATTTGCCCAGAGCCTGCTTCCTCTGAGCAATATCTCTGTGGGAATGATGGAGTCACCTACTCCA
GTGCCTGCCACCTGAGAAAGGCTACCTGCCTGCTGGGCAGATCTATTGGATTAGCCTATGAGGGAAAGTGTA
TCAAAGCAAAGTCCTGTGAAGATATCCAGTGCACTGGTGGGAAAAAATGTTTATGGGATTTCAAGGTTGGGAG
AGGCCGGTGTTCCCTCTGTGATGAGCTGTGCCCTGACAGTAAGTCGGATGAGCCTGTCTGTGCCAGTGACAA
TGCCACTTATGCCAGCGAGTGTGCCATGAAGGAAGCTGCCTGCTCCTCAGGTGTGCTACTGGAAGTAAAGCA
CTCCGGATCTTGCAACTCCATTTCGGAAGACACCGAGGAAGAGGAGGAAGATGAAGACCAGGACTACAGCTT
TCCTATATCTTCTATTCTAGAGTGGTAA

fLuc mRNA ORF Sequence (CleanCap® fLuc mRNA, L-7202)

AUGGAGGACGCCAAGAACAUCAAGAAGGGCCCCGCCCCCUUCUACCCCCUGGAGGACGGCACCGCCGGC
GAGCAGCUGCACAAGGCCAUGAAGCGGUACGCCCUGGUGCCCGGCACCAUCGCCUUCACCGACGCCCACA
UCGAGGUGGACAUCACCUACGCCGAGUACUUCGAGAUGAGCGUGCGGCUGGCCGAGGCCAUGAAGCGGU
ACGGCCUGAACACCAACCACCGGAUCGUGGUGUGCAGCGAGAACAGCCUGCAGUUCUUCAUGCCCGUGCU
GGGCGCCCUGUUCAUCGGCGUGGCCGUGGCCCCCGCCAACGACAUCUACAACGAGCGGGAGCUGCUGAA
CAGCAUGGGCAUCAGCCAGCCCACCGUGGUGUUCGUGAGCAAGAAGGGCCUGCAGAAGAUCCUGAACGU
GCAGAAGAAGCUGCCCAUCAUCCAGAAGAUCAUCAUCAUGGACAGCAAGACCGACUACCAGGGCUUCCAG
AGCAUGUACACCUUCGUGACCAGCCACCUGCCCCCCGGCUUCAACGAGUACGACUUCGUGCCCGAGAGCU
UCGACCGGGACAAGACCAUCGCCCUGAUCAUGAACAGCAGCGGCAGCACCGGCCUGCCCAAGGGCGUGG
CCCUGCCCCACCGGACCGCCUGCGUGCGGUUCAGCCACGCCCGGGACCCCAUCUUCGGCAACCAGAUCA
UCCCCGACACCGCCAUCCUGAGCGUGGUGCCCUUCCACCACGGCUUCGGCAUGUUCACCACCCUGGGCU
ACCUGAUCUGCGGCUUCCGGGUGGUGCUGAUGUACCGGUUCGAGGAGGAGCUGUUCCUGCGGAGCCUG
CAGGACUACAAGAUCCAGAGCGCCCUGCUGGUGCCCACCCUGUUCAGCUUCUUCGCCAAGAGCACCCUGA
UCGACAAGUACGACCUGAGCAACCUGCACGAGAUCGCCAGCGGCGGCGCCCCCCUGAGCAAGGAGGUGG
GCGAGGCCGUGGCCAAGCGGUUCCACCUGCCCGGCAUCCGGCAGGGCUACGGCCUGACCGAGACCACCA
GCGCCAUCCUGAUCACCCCCGAGGGCGACGACAAGCCCGGCGCCGUGGGCAAGGUGGUGCCCUUCUUCG
AGGCCAAGGUGGUGGACCUGGACACCGGCAAGACCCUGGGCGUGAACCAGCGGGGCGAGCUGUGCGUGC
GGGGCCCCAUGAUCAUGAGCGGCUACGUGAACAACCCCGAGGCCACCAACGCCCUGAUCGACAAGGACGG
CUGGCUGCACAGCGGCGACAUCGCCUACUGGGACGAGGACGAGCACUUCUUCAUCGUGGACCGGCUGAA
GAGCCUGAUCAAGUACAAGGGCUACCAGGUGGCCCCCGCCGAGCUGGAGAGCAUCCUGCUGCAGCACCC
CAACAUCUUCGACGCCGGCGUGGCCGGCCUGCCCGACGACGACGCCGGCGAGCUGCCCGCCGCCGUGGU
GGUGCUGGAGCACGGCAAGACCAUGACCGAGAAGGAGAUCGUGGACUACGUGGCCAGCCAGGUGACCAC
CGCCAAGAAGCUGCGGGGCGGCGUGGUGUUCGUGGACGAGGUGCCCAAGGGCCUGACCGGCAAGCUGG
ACGCCCGGAAGAUCCGGGAGAUCCUGAUCAAGGCCAAGAAGGGCGGCAAGAUCGCCGUGUGA

Egfp mRNA ORF Sequence (CleanCap® Egfp mRNA, L-7601)

AUGGUGAGCAAGGGCGAGGAGCUGUUCACCGGGGUGGUGCCCAUCCUGGUCGAGCUGGACGGCGACGUA
AACGGCCACAAGUUCAGCGUGUCCGGCGAGGGCGAGGGCGAUGCCACCUACGGCAAGCUGACCCUGAAG
UUCAUCUGCACCACCGGCAAGCUGCCCGUGCCCUGGCCCACCCUCGUGACCACCCUGACCUACGGCGUG
CAGUGCUUCAGCCGCUACCCCGACCACAUGAAGCAGCACGACUUCUUCAAGUCCGCCAUGCCCGAAGGCU
ACGUCCAGGAGCGCACCAUCUUCUUCAAGGACGACGGCAACUACAAGACCCGCGCCGAGGUGAAGUUCGA
GGGCGACACCCUGGUGAACCGCAUCGAGCUGAAGGGCAUCGACUUCAAGGAGGACGGCAACAUCCUGGG
GCACAAGCUGGAGUACAACUACAACAGCCACAACGUCUAUAUCAUGGCCGACAAGCAGAAGAACGGCAUCA
AGGUGAACUUCAAGAUCCGCCACAACAUCGAGGACGGCAGCGUGCAGCUCGCCGACCACUACCAGCAGAA
CACCCCCAUCGGCGACGGCCCCGUGCUGCUGCCCGACAACCACUACCUGAGCACCCAGUCCGCCCUGAGC
AAAGACCCCAACGAGAAGCGCGAUCACAUGGUCCUGCUGGAGUUCGUGACCGCCGCCGGGAUCACUCUCG
GCAUGGACGAGCUGUACAAGUAA

4.4 Chronic regional *Fst* mRNA LNP injections reduce tumor-derived ActA levels

The perturbation of the ActA–FST axis with over-expression of ActA is associated with a number of ovarian disorders, including carcinogenesis. [309] Similarly, previous studies reveal that FST serum levels are elevated in ovarian cancer patients to the extent that FST can be considered a tumor marker for ovarian cancer diagnosis. [310, 311] Even though FST expression correlates with ActA levels, FST does not increase to the same extent as ActA. Indeed, total FST serum levels rise due to pathological increase in ActA but do not exceed the higher end of its normal physiological range in patients. [310, 312] Notably, at least 90% of FST in healthy individuals is ActA-bound and biologically inactive. [313, 314] Given that the maximal suppression of ActA-induced signaling was observed with an FST-to-ActA molar ratio of 4:1 [315], significant overexpression of FST is pivotal in counteracting pathological actions of ActA and its multiple adverse effects in patients with ovarian cancer.

Since the developed therapeutic as an adjuvant treatment for EOC requires multiple injections, we established a chronic daily injection schedule with *Fst* mRNA LNPs (10 µg mRNA equivalent per dose) to study the effect of a long-term FST protein supplementation (**Figure 15 A**). Total *Fst* mRNA levels, including endogenous and exogenous transcripts, in the cancer clusters and various tissues, were quantified using qRT-PCR. We showed that *Fst* mRNA was significantly increased in ES-2-Luc cell clusters and organs of mice treated with seven daily *Fst* mRNA LNP injections (**Figure 15 B-G**).

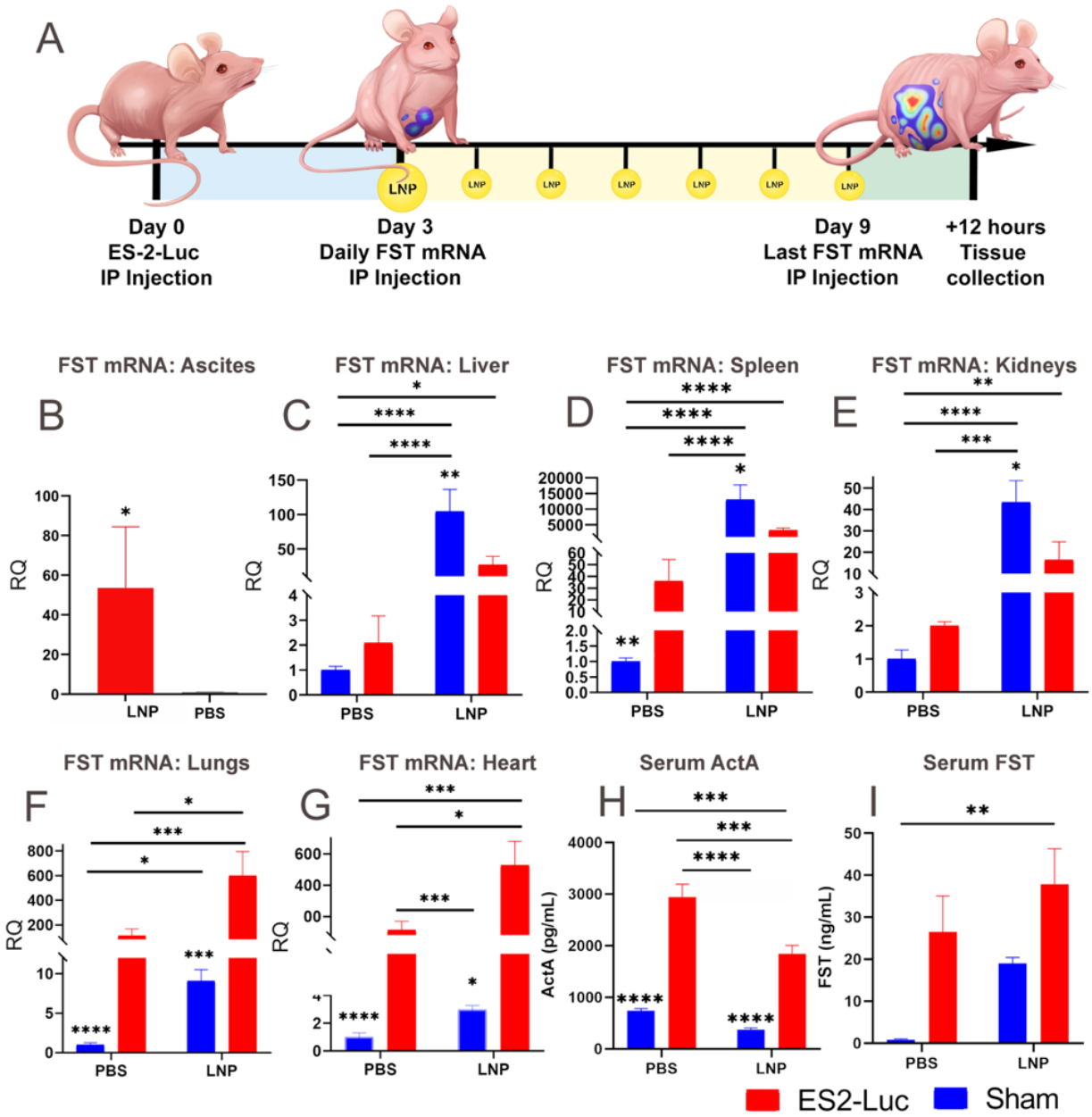

Figure 15. While endogenous upregulation of FST is insufficient to control serum ActA, chronic *Fst* mRNA LNP administration substantially reduces ActA levels. (A) Experimental design demonstrating ES-2-Luc bearing mice receiving seven daily *Fst* mRNA LNP (10 µg mRNA) injections; the sham group is not shown on the graphic for simplicity. qRT-PCR analysis of FST transcript counts in ascites **(B)**, liver **(C)**, spleen **(D)**, kidneys **(E),** lungs **(F),** and heart **(G)**. **(H)** Serum ActA concentration determined by ELISA. **(I)** Serum FST determined by ELISA. For (B-G), results are mean ± SEM, n=10 for treatment groups (LNP) and n=5 for control groups (PBS), *p<0.05, **p<0.01, ***p<0.001, ****p<0.0001. (B) analyzed by t-test; (C-I) analyzed by two-way ANOVA followed by Bonferroni's *post hoc* test.

Similar to a single *Fst* mRNA LNP injection, a daily dosage regimen led to a significant increase of *Fst* mRNA in ES-2-Luc clusters (**Figure 15 B**). It is important to note that serum samples were obtained four hours after LNP injection in the single administration study but twelve hours after the final LNP injection in the chronic administration study. *Fst* mRNA relative quantities in ES-2-Luc clusters after a single and chronic administrations were ~250- and ~50-fold higher than in the control mice, respectively. Notably, we detected a pan-organ upregulation of endogenous *Fst* mRNA and increased serum FST levels in control tumor-bearing mice compared to control sham mice (**Figure 15 C - G**) treated with PBS. Despite this endogenous FST upregulation, *Fst* mRNA LNP treatment resulted in a significant *Fst* mRNA increase in the liver, kidney, and spleen of treated sham animals (100-, 40- and a striking 13,000-fold increase, respectively, **Figure 15 C-E**) compared to control sham mice. Treated ES-2-Luc-bearing mice exhibited a positive trend in Fst mRNA counts in the liver, kidney, and spleen (~25-, ~8-, and ~12-fold increase) in contrast to control cancer-bearing mice. Increase in *Fst* mRNA relative quantities in these organs of cancer-bearing mice was lower than in organs of sham mice, suggesting that ES-2-Luc clusters in the IP cavity are internalizing the majority of *Fst* mRNA LNPs. *Fst* mRNA LNP treatment substantially increased *Fst* mRNA in the lungs and heart of both treated sham and cancer-bearing mice (**Figure 15 F-G**). Treated sham and cancer-bearing mice displayed 8- and 4-fold increase in Fst mRNA in lungs compared to sham and cancer-bearing controls. *Fst* mRNA increase in hearts was 3- fold in both treatment groups compared to the corresponding controls. Interestingly, the lungs and hearts had higher *Fst* mRNA counts in treated cancer-bearing mice than treated sham mice (60 and 300

times higher than in the treated sham mice, respectively), while lower levels are observed in liver, kidney, and spleen. Because the majority of LNPs are internalized by cancer cells, relative quantification of *Fst* mRNA is consequently decreased in the liver, kidneys, and spleen of cancer-bearing animals. The opposite trend is observed in the lungs and heart, where uptake is presumably less affected by the concentration of LNPs in the bloodstream.

Upon observing that the majority of LNPs are targeting cancer clusters, we conducted an evaluation of ActA and FST levels in both serum and ascites. FST bioactivity in cancer-bearing and sham mice was evident from the decrease in serum ActA. ActA serum levels displayed a similar 2-fold decline after a single LNP injection (**Figure 15 H**) in sham and cancer-bearing mice. Importantly, cancer-bearing mice exhibited three-fold levels of ActA in comparison to sham mice. Tumor-bearing mice demonstrated ~10 ng mL^{-1} increase in serum FST after a single or chronic injection (both, ~1.3-fold increase). In sham mice, chronic injections with *Fst* mRNA LNPs increased serum FST levels by ~18 ng mL^{-1} (**Figure 15 I**), compared to a single LNP injection that increased serum FST by only ~2 ng mL^{-1} (**Figure 14 A**), that is 24- and 4-fold increase from baseline, respectively. Smaller increase of FST in tumor-bearing mice in comparison to sham mice was almost certainly due to consumption of FST by pathologically high levels of ActA in serum.

Fst mRNA LNP treatment led to a ~2-fold increase in FST levels in ascites resulting in a ~2-fold decrease in ascitic ActA levels (**Figure 16 A-D**). Importantly, when comparing FST levels in serum and ascites of PBS-treated mice, a 100-fold increase of FST concentration in the ascites compared to FST in serum (25 ng mL^{-1} and 2400 ng

mL^{-1}) strongly suggests both local FST production by cancer cells and demonstrates the applicability of the proposed treatment for efficient protein overexpression without systemic toxicity.

Importantly, the more significant decrease in total ActA (**Figure 16 A**) compared to its normalized levels by total protein in ascites (**Figure 16 B**) may be attributed to variations in the total protein content. When ActA is a predominant species in ascites, a reduction in its absolute levels would result in a noticeable decrease in total ActA and would affect the protein concentration in ascites. Therefore, when normalizing by total protein while taking into account the overall protein concentration, the proportional decrease in normalized ActA may appear less significant. For FST, the total increase after *Fst* mRNA LNP treatment is not significantly evident (**Figure 16 C**), but when normalized by total protein, the increase becomes more pronounced (**Figure 16D**). This phenomenon might be explained by considering the impact of ActA removal from the total protein pool. If ActA is removed from the total protein pool during normalization, it could lead to a decrease in the denominator (total protein), making the increase in normalized FST more apparent. Normalizing by a reduced total protein concentration may amplify the relative increase in FST levels, providing a clearer indication of the treatment's effect on FST expression when ActA is excluded from the normalization process. This adjustment helps highlight changes in FST that might be masked when considering the total protein context that includes ActA.

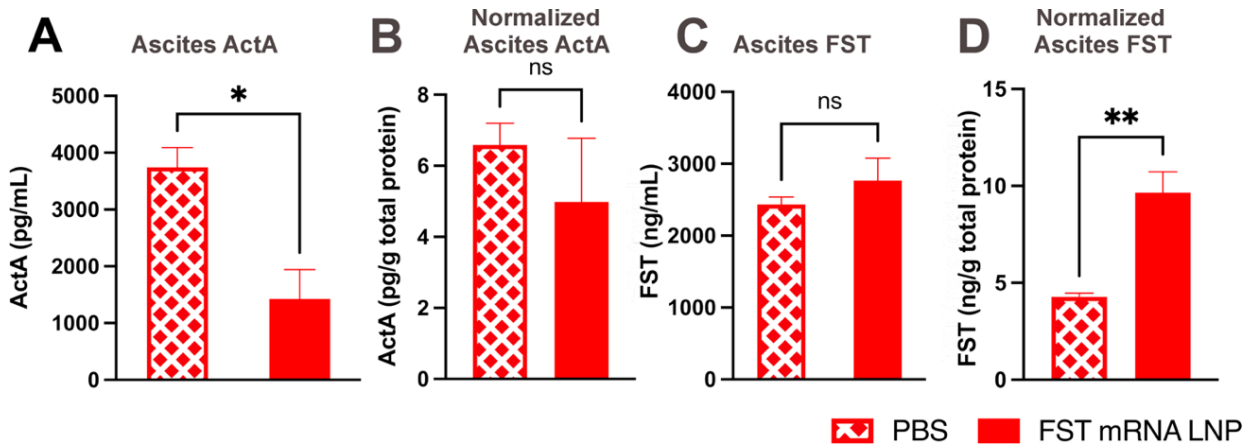

Figure 16. Chronic *Fst* mRNA LNP administration substantially reduces ActA levels in ascites. (A) ActA protein levels in ascites. **(B)** ActA protein levels in ascites normalized by total protein in ascites. **(C)** FST protein levels in ascites. **(D)** FST protein levels in ascites normalized by total protein in ascites. *p<0.05, **p<0.01, ***p<0.001, ****p<0.0001. (J-M) analyzed by t-test.

Moreover, pooled serum samples from control and *Fst* mRNA LNP-treated mice demonstrated negative correlation between levels of FST and ActA (**Figure 17**). This finding aligns with published literature and reinforces the significance of ActA as a marker of EOC aggressiveness and power of FST downregulating ActA levels. Additionally, this data suggests that the FST overexpression including the proposed therapeutic approach can effectively reduce ActA levels in circulation.

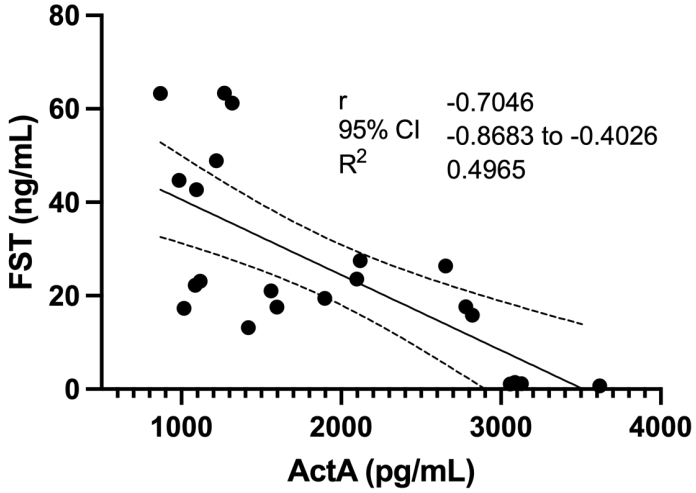

Figure 17: Correlation between FST and ActA concentrations in serum. Data obtained from pooled samples of healthy and ES-2-WT-bearing mice, both treated with PBS and *Fst* mRNA LNP formulation.

Importantly, *Fst* mRNA LNP treatment was able to decrease ascitic concentration of myostatin, another negative muscle regulator from TGF-B family (**Figure 18**). Although the action of FST is multifactorial and involves the inactivation of various factors such as ActA, myostatin, and bone morphogenetic factors, our focus has been on the impact of FST on ActA. This is due to ActA's prominent role in negative muscular control, particularly in humans, as well as ActA's role in increasing the aggressiveness of certain epithelial cancers in terms of proliferation and migration, including EOC.

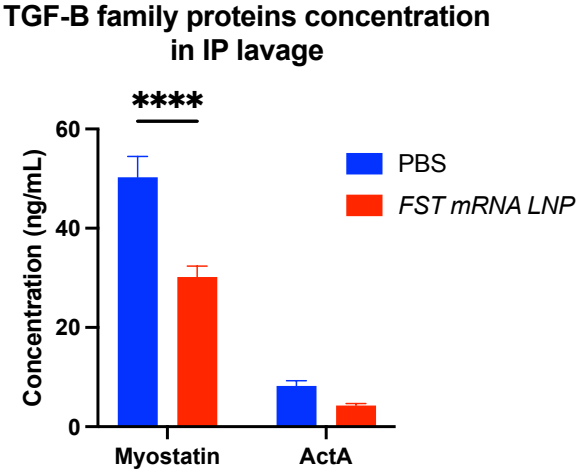

Figure 18: Myostatin and ActA concentration in ES-2-WT malignant ascites. Samples were collected from peritoneal cavity of control and *Fst* mRNA LNP-treated mice. Presented as mean ± SEM, ****p<0.0001, analyzed by two-way ANOVA.

4.5 LNP-guided FST overexpression modulates epithelial and mesenchymal characteristics of malignant ascites

Pathological actions of ActA have both local and systemic implications affecting cancer propagation and associated morbidities. In the context of local effects, we hypothesized that the observed change in the cluster morphology and size was associated with *in situ* reduction of available ActA, leading to a modification in ES-2-Luc cell mobility and its epithelial or mesenchymal phenotype. To evaluate the potential anticancer effect of *Fst* mRNA LNPs, two groups of mice inoculated with ES-2-Luc cells

received seven daily injections with *Fst* mRNA LNPs (treatment group) or PBS (control group). Control mice developed abundant third-spaced fluid infiltrated with diffuse circulating ES-2-Luc cells forming microscopic clusters (**Figure 19 A, B**). Notably, in the treatment group, we observed a minimal formation of malignant ascites (**Figure 19 C**). Volumes of ascites in control mice were ~5-fold higher than in the *Fst* mRNA LNP-treated mice. Instead, ES-2-Luc cells formed self-adhering tumors (aggregates) accumulating in the physiological bottlenecks of IP fluid movement (**Figure 19 A, B**, red arrows). In most cases, the cellular aggregates were found in suprahepatic compartments of the peritoneal cavity. Importantly, the aggregates were nonadherent to the organs or the walls of the peritoneal cavity. Both treatment and control groups had secondary cancer nodules forming on gonadal fat pads (**Figure 19 A, B,** black arrows). We hypothesized that these differences in ES-2-Luc dissemination patterns indicated a treatment-dependent modulation of epithelial-mesenchymal plasticity of ES-2-Luc cells.

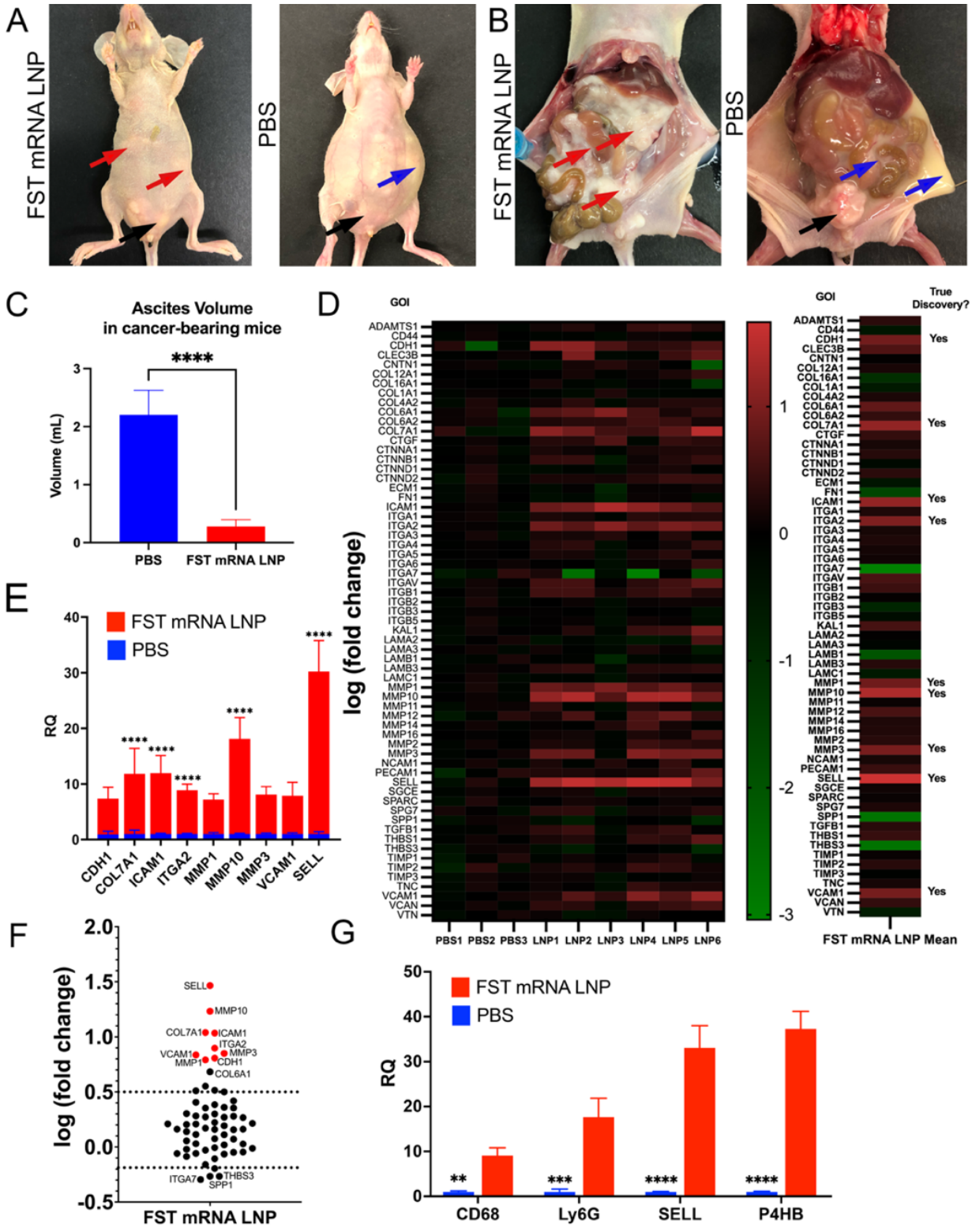

Figure 19. Mice treated with *Fst* mRNA LNPs for 7 days formed ES-2-Luc aggregates in the physiological bottlenecks of IP fluid movement with minimal apparent ascites. (A) and **(B)** representative images of *Fst* mRNA LNP-treated (left) and control (right) mice. In the LNP-treated mouse, red arrows show ES-2-Luc cell

aggregates; no third space/ascitic fluid is present**;** the control (PBS) mice formed third-spaced/ascitic fluid with a suspension of ES-2-Luc clusters (blue arrows). Black arrows in both (**A**) and (**B**) show the formation of secondary nodules on gonadal fat pads. (**C**) Ascites volume in control and LNP-treated mice. **(D)** ECM TaqMan Array heatmap for individual samples (left) and average fold change for ES-2-Luc aggregates (right); analyzed by two-way ANOVA followed by two-stage step-up method of Benjamini, Krieger and Yekutieli with FDR = 0.01. Relative expression of up-regulated genes identified as true discoveries is shown on linear **(E)** and log **(F)** scales. Statistical significance between PBS and LNP groups (**E, F**) was determined by multiple *t-tests* with the Bonferroni-Dunn method, alpha = 0.05; computations assumed the samples from populations with the same scatter. Expressed as mean ± SEM; n=3 for the control group (PBS), n=6 for the treatment group (LNP). **(G)** Relative quantification of fibroblast (*P4HB*), macrophage (*CD68*), neutrophil (*Ly6G*), and immature lymphocyte (*SELL*) markers in control and LNP-treated cancer clusters**;** analyzed by two-way ANOVA followed by Bonferroni's *post hoc* test on raw parametric data (dCt values); expressed as mean ± SEM, n=10 for treatment groups (LNP) and n=5 for control groups (PBS). $p^{*}<0.05$, $p^{**}<0.01$, $p^{***}<0.001$, $p^{****}<0.0001$.

It is well documented that TGF-β family signaling is predominant mechanism in reprogramming gene expression during epithelial-to-mesenchymal transition (EMT). [316] EMT is associated with cancer stemness, its metastatic and invasive potentials, and resistance to treatment. [317] Mesenchymal to epithelial transition (MET), in turn, is observed in the process of colonization and formation of secondary tumors and is associated with the proliferative potential of cancer cells. Indeed, the presence of multiple markers, especially those influenced by ActA, can alter the equilibrium and shift it towards either EMT or MET. For example, ActA-mediated suppression of E-cadherin expression propagates the migration of ovarian cancer cells. [318] To understand if *Fst* mRNA LNP therapy induced epithelial or mesenchymal phenotypic changes in cancer cells, we analyzed the expression of extracellular matrix (ECM) and adhesion molecules in solid aggregates (*Fst* mRNA LNP treatment) and diffuse circulating clusters accumulating in ascitic fluid (PBS, control group). Analyzing the expression of ECM and adhesion proteins is essential to understand how *Fst* mRNA LNP therapy affects the

EMT and MET transition in ES2 cancer clusters. These molecular changes provide valuable insights into how cells move, their invasion capabilities, and potential for metastatic activity. [319, 320] In EMT, cells lose their cell-to-cell connections while acquiring features that enhance interactions with the surrounding matrix. Conversely, in MET, cells regain epithelial characteristics, reestablishing cell-to-cell adhesion. Studying adhesion molecule expression directly assesses these alterations and aids in understanding the migratory and invasive tendencies of cancer cells during both EMT and MET processes modulated by the proposed therapeutic.

In the cancer aggregates formed in *Fst* mRNA LNP-treated mice, we observed upregulation of nine genes involved in both epithelial-mesenchymal (EMT) and mesenchymal-epithelial (MET) transition processes (**Figure 19 D-F**). Compared to cell suspensions from the control mice, the *Fst* mRNA LNP treatment increased *Cdh1* expression (E-cadherin, pro-MET) in ES-2-Luc cell aggregates. We also observed relative upregulation of three matrix metalloproteinases (stromelysins *Mmp3*, *Mmp10,* and collagenase *Mmp1,* pro-EMT), *Col7A1* and *Itga2* (potentially, pro-EMT), as well as *SellL*, *Icam1,* and *Vcam1* genes. FST over-expression leading to inhibition of canonical ActA signaling and related overexpression of E-cadherin most likely changed cluster morphology to large cellular aggregates and decreased cancer cell mobility while imparting ES-2 cells with MET characteristics. Additionally, ES-2-Luc aggregates but not ES-2-Luc suspension from malignant ascites displayed upregulation of neutrophil (*Ly6G*), macrophage (*Cd68*), immature lymphocyte (*Sell*), and fibroblast (*P4BH*) markers (**Figure 19 G**), suggesting cancer clusters undergoing heterogeneous cellular infiltration with innate immune cells.

Also, we observed a positive trend in the expression of cell cycle markers in the ES-2-Luc aggregates formed as a result of *Fst* mRNA LNP treatment that are usually upregulated in actively proliferating cancer cells (*mki67*, *top2A*, *tpx2*; **Figure 20**). Markers of proliferation such as *mki67* (Ki-67), *top2A* (Topoisomerase II alpha), and *tpx2* (Targeting protein for Xenopus kinesin-like protein 2 microtubule nucleation factor) are widely utilized in cancer research and diagnostics due to their ability to reflect various aspects of cell division dynamics. Ki-67 serves as a reliable indicator of actively dividing cells within tumors, allowing for the assessment of tumor aggressiveness and prediction of patient outcomes. [321] Similarly, TOP2A, an enzyme involved in DNA replication and repair, is often overexpressed in rapidly proliferating cells, making it a valuable marker for assessing cell proliferation and predicting response to chemotherapy in cancer patients. [322] On the other hand, TPX2 plays a critical role in spindle assembly during mitosis and is frequently upregulated in cancer cells, contributing to increased tumor aggressiveness and poor prognosis. [323] Together, these markers provide valuable insights into tumor proliferation dynamics, aiding in cancer diagnosis, prognosis, and treatment planning.

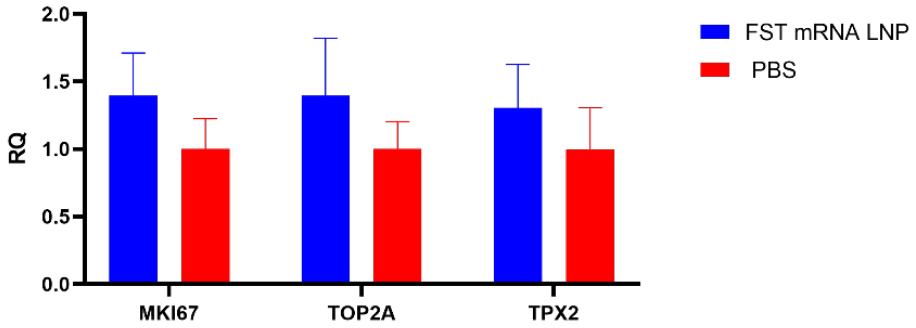

Figure 20. Proliferation markers in ES-2 cell clusters from treatment and control groups. *Fst* mRNA LNP-treated mice had higher expression of *Mki67*, *Top2a* and *Tpx2* in the ES-2-Luc cancer aggregates in comparison to control group treated with PBS.

The cell aggregates treated with *Fst* mRNA LNPs exhibit a positive trend in the expression of *mki67*, *top2A*, and *tpx2*. This pattern is consistent with the observed MET-like changes in the cells, indicating an upregulation of genes associated with active proliferation in cancer cells, even though their migratory activity is comparatively reduced. [324] Other upregulated genes in *Fst* mRNA LNP-treated clusters are recognized as pro-EMT pathway members (**Figure 19 D**). [325-331] Given this differential upregulation of both pro-MET and pro-EMT genes, we hypothesized that FST treatment could trap the cells in the transitional EMT/MET phenotype, where the cells can break the connection between the true epithelial phenotype and cell cycle activation, and become more susceptible to chemotherapy. [332]

4.6 *Fst* mRNA LNP counteracts muscle loss in ES-2-Luc bearing mice exhibiting cancer-associated cachexia

To test whether *Fst* mRNA LNP not only exerts action on ES-2-Luc tumors but also produces bioactive FST protein inhibiting ActA leading to muscle-sparing effects, we assessed terminal gastrocnemius mass, muscle fiber cross-section area, and cachexia-driving gene expression in mice chronically treated with *Fst* mRNA LNPs (**Figure 21 A-E**).

We observed a 37% loss of gastrocnemius muscle mass in control (PBS) cancer-bearing mice. Importantly, our data suggest that *Fst* mRNA LNP treatment reversed bulk muscle loss in tumor-bearing animals to the level of control sham mice (~35% bulk muscle increase) associated with the 2-fold decrease in serum ActA levels. We also observed a 15% increase in muscle mass in sham mice receiving *Fst* mRNA LNP injections (**Figure 21 A**). Muscle fiber cross-section area (CSA) analysis displayed a

40% decrease in CSA in non-treated cancer-bearing mice that supports the 37% bulk muscle loss finding. Interestingly, *Fst* mRNA LNP treatment led to 90% increase in CSA in cancer-bearers, that is ~50% larger CSA than in non-treated sham mice (**Figure 21 B**). Compared to sham mice, gastrocnemius samples from tumor-bearing mice had elevated expression of E3 ubiquitin ligase-related genes *Foxo1* (Foxo1), *Fbxo32* (Atrogin-1/Mafbx), and *Trim63* (Murf1) (**Figure 21 C-E**). The aforementioned genes are known to induce muscle catabolism via the ubiquitin-proteasome axis in cancer-associated cachexia. [333] We observed a decreasing trend in *Foxo1*, *FBXO32*, and *Trim63* expression in the treated cancer-bearing mice relative to control cancer-bearing mice.

Gonadal fat pads from tumor-bearing mice were excluded from the analysis due to infiltration with ES-2-Luc cells. Interestingly, the treated sham mice displayed a significant ~2-fold increase in the adipose tissue mass of gonadal fat pads (**Figure 21 F**). Our results also show a substantial increase in adipocyte uptake of *Fst* mRNA LNPs (relative 3000-fold increase in *Fst* mRNA, **Figure 21 G**). We also observed a modest increase in the expression *of Ucp1*, a marker of white adipose tissue browning, known to be induced by FST signaling leading to a decrease in adiposity (**Figure 21 H**). [334] These highly reproducible results are in dissonance with the FST function to decrease adiposity and thus require thorough investigation to determine if they reflect a true potential to slow fat stores depletion in cachexia.

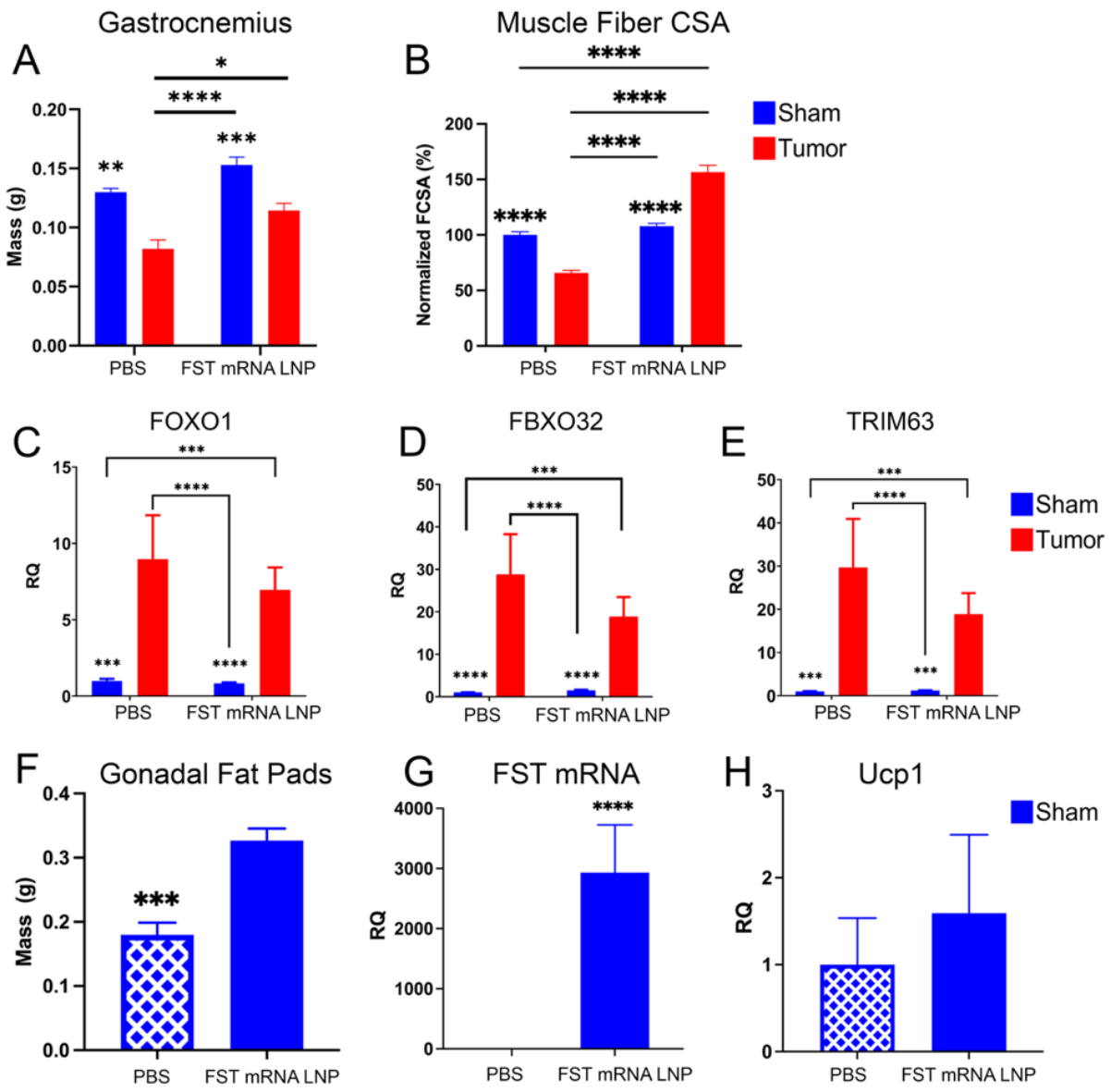

Figure 21. Chronic *Fst* mRNA LNP treatment ameliorates cancer-associated muscle bulk loss and decelerates ubiquitin-proteasome proteolysis program in cancer-bearing mice. **(A)** Gastrocnemius muscles were collected from mice following daily treatment for 7 days with LNPs loaded with 10 µg *Fst* mRNA; data were analyzed by two-way ANOVA followed by Bonferroni's *post hoc* test. **(B)** Muscle fiber cross-section area (FCSA) and **(C-E)** expression of *FOXO1*, *FBXO32,* and *TRIM63* in gastrocnemius. **(F)** Gonadal fat pad mass in control sham and treatment sham groups. **(G)** Relative *Fst* mRNA counts in the gonadal fat pads of control and treatment sham groups. **(H)** *Ucp1* expression in the gonadal fat pads of control and treatment sham groups. **(A-E)** were analyzed by two-way ANOVA followed by Bonferroni's *post hoc* test on raw parametric data (dCt values). All data expressed as mean ± SEM; $p^{*}<0.05$, $p^{**}<0.01$, $p^{***}<0.001$, $p^{****}<0.0001$; n=10 for treatment groups (LNP) and n=5 for control groups (PBS). **(F-H)** analyzed by unpaired *t-test* (n=5) on mass or raw parametric data (dCt values); all data expressed as mean ± SEM; $p^{***}<0.001$, $p^{****}<0.0001$.

4.7 Supplementation of recombinant ActA exacerbates ascites, accelerates cancer progression, and decreases survival, while recombinant FST alleviates these manifestations

Taken together, *Fst* mRNA LNPs decreased the volume of ascites, altered dissemination patterns of ES-2 cells, and provided a muscle-sparing effect in cachectic mice bearing ovarian cancer xenografts. We hypothesized that this was due to a decrease in bioactive ActA signaling. To test this hypothesis, we established three cancer-bearing treatment groups of mice receiving recombinant ActA injections (20 μg per kg of body weight (20 μg kg b.w.$^{-1}$)) or recombinant FST injections (two doses: FST_L, 20 μg kg b.w.$^{-1}$ and FST_H, 100 μg kg b.w.$^{-1}$), as well as a control group receiving PBS (**Figure 22 A**). Daily IP injections of recombinant ActA to ES-2-Luc-bearing mice led to accelerated cancer progression and faster advancement to primary humane endpoint in the comparative survival study (**Figure 22 B, C**). The ActA treatment group developed a more severe disease with excessive ascites and shortened survival.

IP injection of recombinant FST_L led to an insignificant change in serum FST and ActA levels (data not shown), and unaltered disease progression trajectory characterized by the formation of malignant ascites, muscle wasting, and decreased mobility similar to the control group. FST_L and FST_H treatments had a positive impact on survival (**Figure 22 C, D**). An increase of recombinant FST dose to 100 μg kg b.w.$^{-1}$ (FST_H) led to the formation of small ES-2-Luc aggregates in the ascitic fluid and decreased volume of ascites. This group of mice had no signs of lethargy, fatigue, or change in the spinal curvature; euthanasia was performed based on the extent of abdominal distension due to the buildup of ascitic fluid.

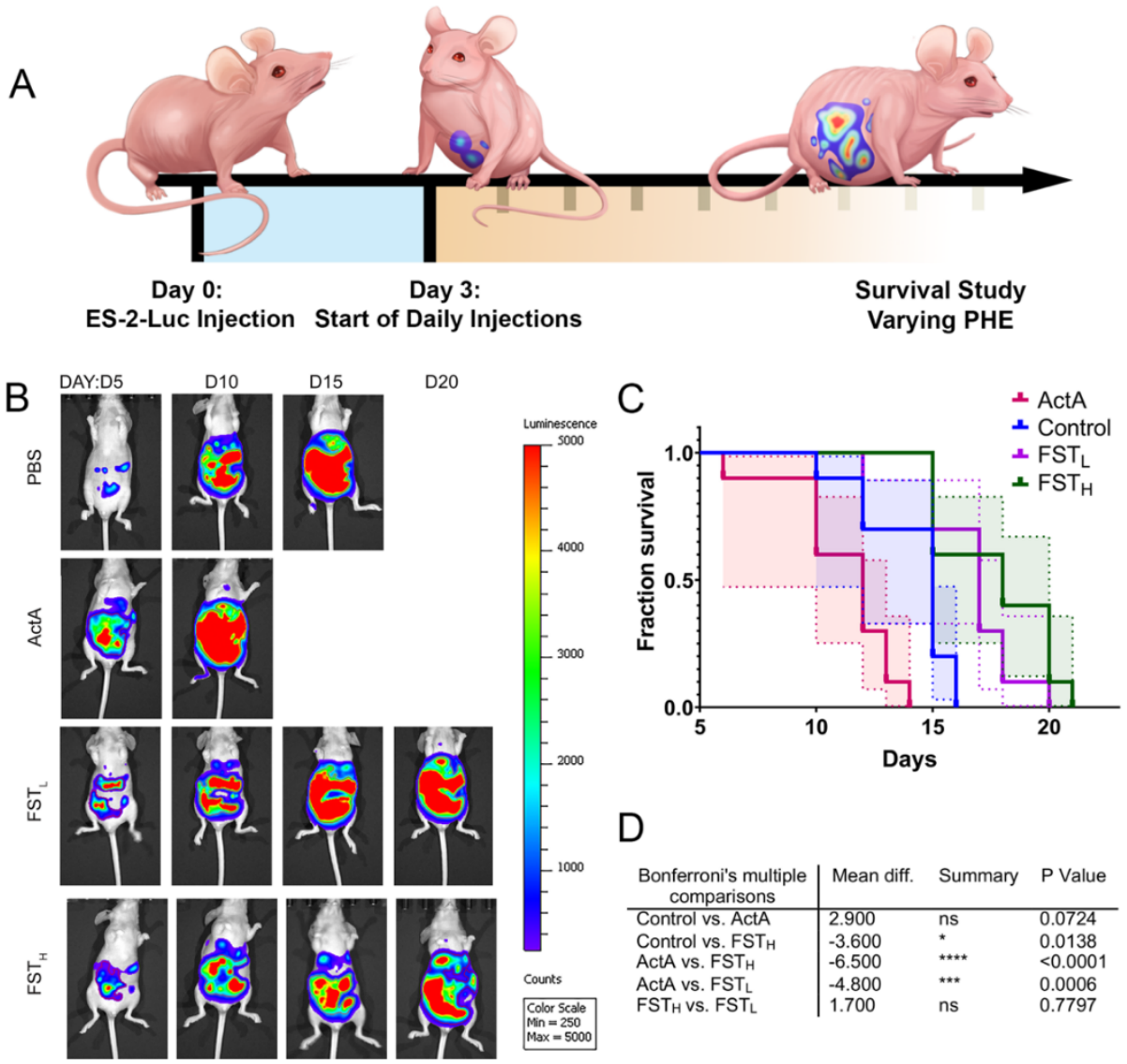

Figure 22. Supplementation with recombinant ActA exacerbates ascites, accelerates cancer progression, and decreases survival, while recombinant FST alleviates these manifestations. (A) Experimental design demonstrating ES-2-Luc bearing mice receiving daily IP recombinant protein injections. **(B)** Representative BLS images of ES-2-Luc mice treated with PBS, recombinant ActA (20 µg kg b.w.$^{-1}$), recombinant FST_L (20 µg kg b.w.$^{-1}$), and FST_H (100 µg kg b.w.$^{-1}$). **(C)** Comparison of survival curves between control, ActA, FST_L, and FST_H recombinant protein treatments. **(D)** Table of significant results of *post hoc* Bonferroni's multiple comparison tests using median survival and standard error (n=5).

Mean survival analyzed in **Figure 22 C, D** was 14.1±0.64, 11.1±0.73, 16±0.92, and 17.7±0.79 days for control, ActA, FST_L, and FST_H groups, respectively (represented as means ± SE). Decrease in mean survival in ActA treatment group was approaching significance (p=0.07, **Figure 22 D**). Mice treated with FST_H displayed a significant increase in mean survival compared to control and ActA treatment groups. **Figure 23** summarizes the apparent volume of malignant ascites in the control mice and mice receiving recombinant ActA, and FST in low and high doses.

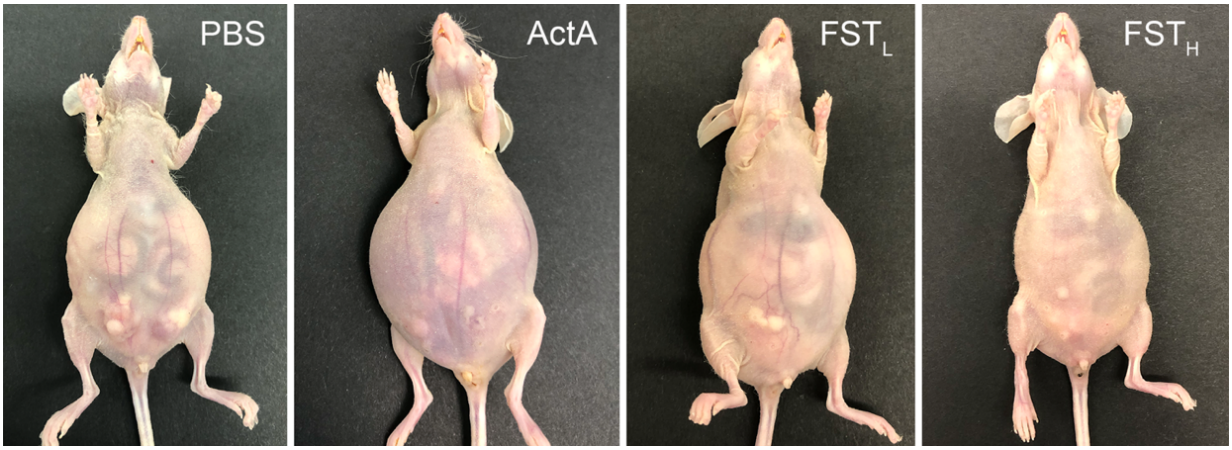

Figure 23. Recombinant ActA increases apparent volume of malignant ascites, while FST decreases it in a concentration-dependent manner: Representative images of mice were taken on day 12 after tumor inoculation for PBS and ActA-treatment groups and day 20 for recombinant FST_L and FST_H treatment groups.

Although all recombinant treatments lead to the formation of ascites nearing the primary humane endpoint, FST_H postponed its formation and led to the development of macroscopic cancer cell aggregates. This promising data encouraged us to compare recombinant and mRNA-based FST supplementation treatments. Sera from the mice treated with recombinant FST_H were analyzed together with sera from mice receiving *Fst* mRNA LNP treatment in the experiment discussed in the next section.

4.8 *Fst* mRNA LNPs in combination with cisplatin prolong survival, decreases tumor burden, and provides muscle sparing effect in ES-2-bearing mice

Cancer-associated inflammation and obstruction of intraperitoneal organs lead to depletion of fat stores, loss of muscle bulk, and compromised nutritional state. [9, 335] These catabolic changes, together with systemic inflammation further propagating the metabolism of fat and muscles, manifest in a complex syndrome of cancer-associated cachexia (CAC). Marked by cancer-associated muscle loss, the declining muscle function in patients deteriorates even further due to the unavoidable iatrogenic burden of chemotherapy. [11] To investigate the potential anti-cachexia effect of our therapy, we next performed a comparative survival study to compare the efficacy of *Fst* mRNA LNPs to recombinant FST in combination with cisplatin chemotherapy (CDDP) (**Figure 24 A**). We established six ES-2-Luc-bearing groups that included mice treated with CDDP (2 mg kg b.w.$^{-1}$, injected every 4 days for 5 weeks), recombinant FST (FST_H, 100 µg kg b.w.$^{-1}$, daily dosage) and *Fst* mRNA LNPs (10 µg mRNA/dose, daily dosage), as well as their combination with CDDP, and a control group receiving PBS injections.

Compared to the control group, mice treated with CDDP displayed decreased volumes of ascites, but still formed dispersed cancer clusters and exhibited wasting similar to controls. Mice treated with recombinant FST_H and *Fst* mRNA LNP had slower cancer progression in comparison to controls and were characterized by strikingly higher mobility and reduced apparent fatigue. Mice receiving CDDP combinations with FST_H or *Fst* mRNA LNPs formed peritoneal aggregates of cancer cells with minimal ascites. **Figure 24 B** shows representative images of mice from each treatment group

and their cancer progression as a function of time to a primary humane endpoint. Combinatorial treatment with CDDP and *Fst* mRNA LNP formulation resulted in the longest survival of mice in comparison to other groups.

Postmortem BLS images of mice treated with CDDP, *Fst* mRNA LNPs, a combination of CDDP and *Fst* mRNA LNPs, or PBS show the extent of cancer progression inside of the peritoneal cavity. Control mice displayed dispersed ES-2-Luc clusters in the ascitic fluid that gave high BLS readings (**Figure 24 C**, white arrow). Although CDDP and FST_H treated mice exhibited slower progression of the disease, lower tumor burden, and formation of small cancer aggregates (**Figure 24 C**, purple arrow), we still observed significant ES-2-Luc cell infiltrates in ascites (**Figure 24 C**, white arrow). *Fst* mRNA LNP-treated mice developed ES-2-Luc aggregates accumulating in the suprahepatic regions and between the folds of the mesentery, small intestines, and other organs (**Figure 24 C**, purple arrow). Minimal volume of ascitic fluid and binding of cells in cancer aggregates allowed us to observe organs on the image (i.e., liver, **Figure 24 C**, yellow arrow) that would not be possible in the case of ES-2-Luc cluster suspension giving an intense and diffuse BLS signal. Combinatorial treatment with CDDP and *Fst* mRNA LNPs led to the formation of small solid tumors nonadherent to organs (**Figure 24 C**, red arrow) and easily removed from the IP cavity (**Figure 24 C**, bottom image).

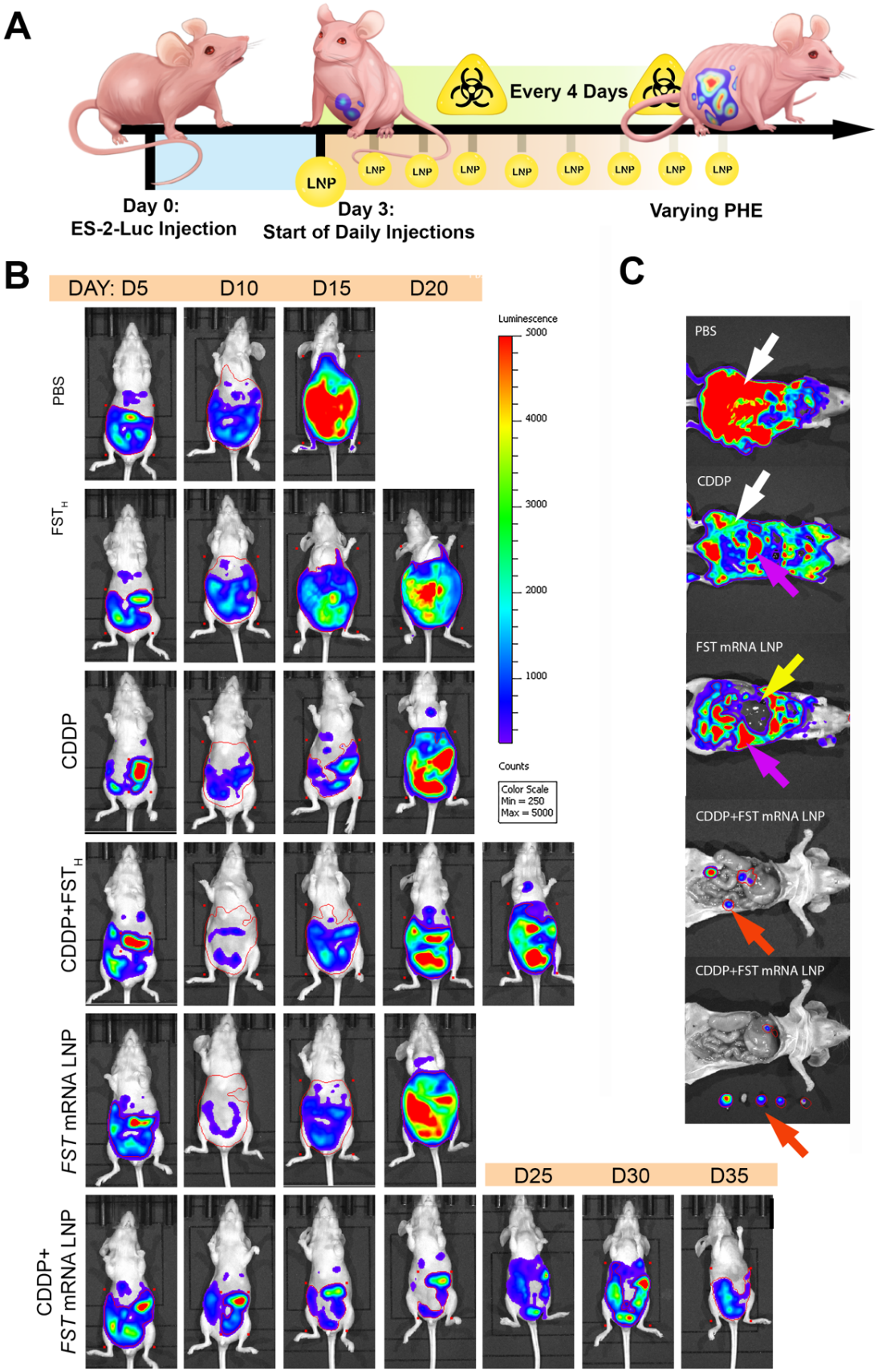
A
Every 4 Days
LNP
Day 0:
ES-2-Luc Injection
Day 3:
Start of Daily Injections
Varying PHE
B
DAY: D5
D10
D15
D20
D25
D30
D35
PBS
FST H
CDDP
CDDP+FST H
FST mRNA LNP
CDDP+
FST mRNA LNP
Luminescence
5000
4000
3000
2000
1000
Counts
Color Scale
Min = 250
Max = 5000
C
PBS
CDDP
FST mRNA LNP
CDDP+FST mRNA LNP
CDDP+FST mRNA LNP

Figure 24. *Fst* mRNA LNP treatment reprograms ES-2-Luc clusters and provides an abscopal effect alleviating cancer-associated cachexia manifestations. (A) Design of survival experiment demonstrating ES-2-Luc-bearing mice receiving the following treatments: PBS (control group, daily), CDDP (every four days, for a maximum of 5 weeks, 2 mg kg b.w.$^{-1}$ dose), recombinant FST (FST_H, 100 μg kg b.w.$^{-1}$ dose, daily) or *Fst* mRNA LNP (10 μg mRNA equivalent dose, daily), or their combination with CDDP. **(B)** Representative whole-body BLS images of mice in each experimental group as a function of time; imaging was performed every 5 days (*n*=5). **(C)** Representative post-mortem BLS images of mice treated with PBS, CDDP, or *Fst* mRNA LNPs, or their combination; white arrows represent ascites, purple arrows – ES-2-Luc cell aggregates, yellow arrow – liver, red arrow –non-adherent solid ES-2-Luc tumors.

Furthermore, **Figure 25 A** depicts ES-2-Luc cell behavior in the peritoneal cavity of the mice at primary humane endpoints showing differential response to treatments with PBS (control), CDDP, *Fst* mRNA LNP, and CDDP+*Fst* mRNA LNP combination. Control mice developed severe ascites with ES-2-Luc cluster suspension (white arrows). Both *Fst* mRNA LNP- and CDDP-treated mice developed minimal ascites (white arrows) and metastatic nodules (purple arrows) forming on organs and mesenteries. However, *Fst* mRNA LNP-treated mice also displayed nonadherent ES-2 aggregates that were easily removed from the abdominal cavity. Combinatorial CDDP+*Fst* mRNA LNP treatment resulted in ES-2-Luc cells aggregating to solid nonadherent tumors (red arrow) with no metastatic nodules forming on organs (also confirmed in **Figure 24 C**).

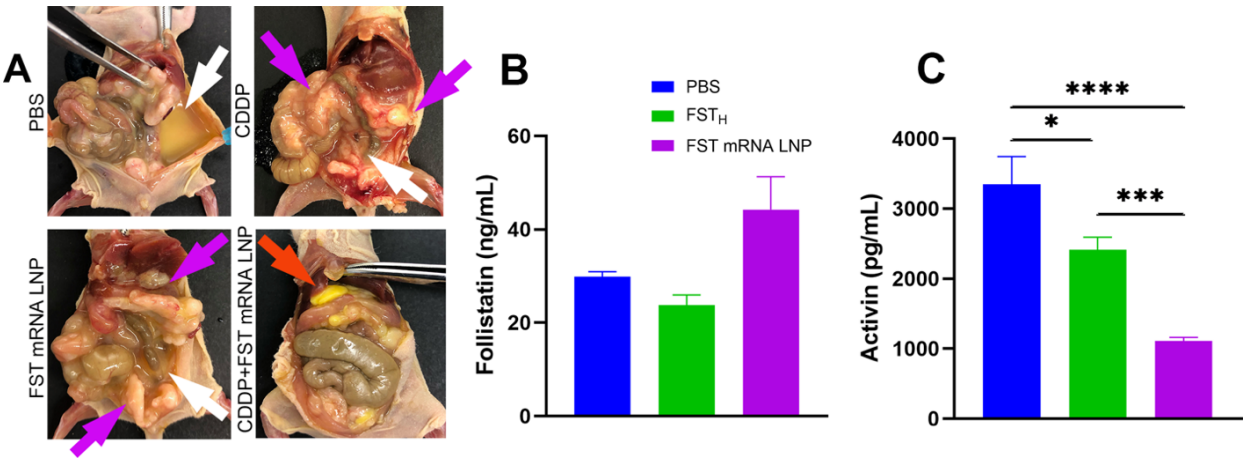

Figure 25. Increased *FST* protein and decreased ActA reshapes ES-2 tumor phenotypes. (A) Representative images of mice from control, CDDP, *Fst* mRNA LNP, and CDDP+*Fst* mRNA LNP groups. Purple arrows show ES-2-Luc cell aggregates, white arrows – ascites, red arrows – non-adherent solid ES-2-Luc tumors. **(B)** Serum FST and **(C)** serum ActA concentrations determined by ELISA; results are mean ± SEM, n=5, **p*<0.05, **p<0.01, ***p<0.001, ****p<0.0001, analyzed by two-way ANOVA followed by Bonferroni's *post hoc* test.

Fst mRNA LNP delivered in daily doses increased serum FST levels and considerably reduced serum ActA (**Figure 25 B, C**). An increasing concentration-dependent effect of FST was reflected by a proportionate decrease of serum ActA in the treatment groups with *Fst* mRNA LNP (10 µg mRNA equivalent per mouse) and recombinant FST_H (100 µg kg b.w.$^{-1}$). Serum ActA levels were decreased by 3- and 1.3-fold in *Fst* mRNA LNP and recombinant FST treatment groups, respectively. Thus, a higher concentration of FST protein transiently expressed from the delivered *Fst* mRNA in the immediate tumor environment not only decreased ActA levels, but also increased systemic serum FST providing therapeutic abscopal effects.

The beneficial therapeutic effect of increased systemic FST was again observed in the context of counteracting cachexia manifestations of progressing cancer and iatrogenic insults of CDDP chemotherapy. Analysis of the cross-sectional area (CSA) of

individual muscle fibers indicated a 25% CSA decrease in muscle fibers of ES-2-Luc-bearing mice receiving CDDP treatments (PBS/PBS vs. PBS/CDDP, **Figure 26**). FST supplementation by FST_H and to the greater extent by *Fst* mRNA LNP treatments attenuated this detrimental effect. FST_H increased CSA by ~1.5-fold in both no chemotherapy (FST_H/PBS) and CDDP-treated (FST_H/CDDP) animals, compared to PBS/PBS and PBS/CDDP groups. *Fst* mRNA LNP treatment led to a ~2-fold increase in CSA of muscle fibers in no chemotherapy (*Fst* mRNA LNP/PBS) and CDDP-treated (*Fst* mRNA LNP/CDDP) animals in comparison to PBS/PBS and PBS/CDDP groups.

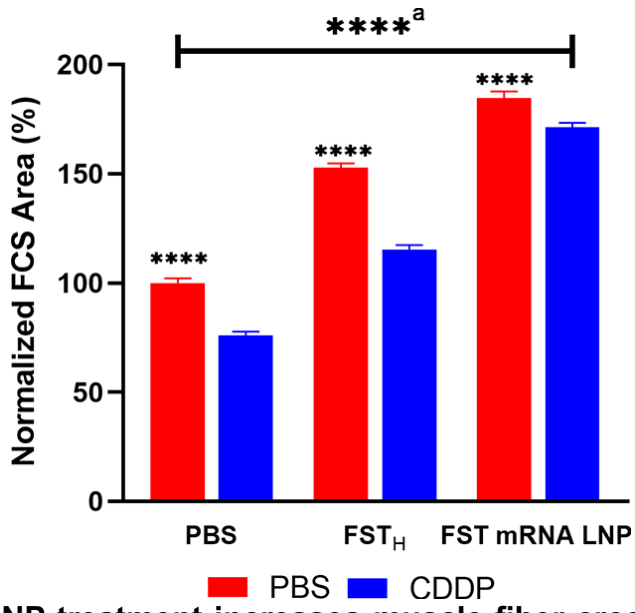

Figure 26. *Fst* mRNA LNP treatment increases muscle fiber cross-sectional area. Muscle fiber cross-section (FCS) area; normalized to double-negative control (PBS/PBS) mice. Results are mean % ± SEM, n=500, analyzed by two-way ANOVA followed by Bonferroni's *post hoc* test. [a]All groups are significant with p****<0.0001, except PBS/CDDP vs. FST_H/CDDP groups (**p<0.01).

We observed muscle fiber atrophy and fibrotic changes in CDDP-treated mice (PBS/CDDP group), as shown on Picrosirius muscle fiber histology with Sirius red stain highlighting regions of increased collagen deposition. Muscle fibers in CDDP-treated mice supplemented with FST protein (both recombinant FST_H and *Fst* mRNA LNP treatments) displayed reduced fibrosis (**Figure 27 A, B**). Although both recombinant

FST_H and *Fst* mRNA LNP treatments prevented muscle fibrosis, *Fst* mRNA LNP treatment exerted a superior muscle-sparing effect compared to recombinant FST_H protein supplementation, as it resulted in a greater CSA in both PBS and CDDP groups (**Figure 26**).

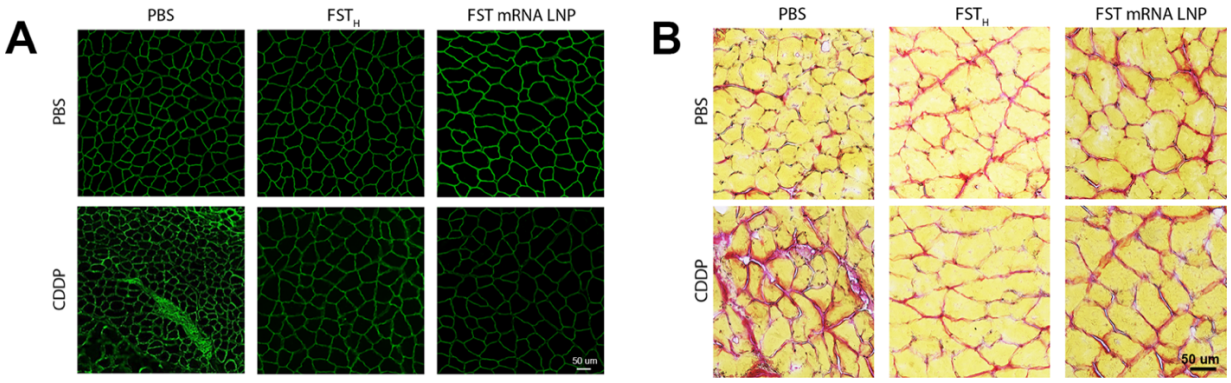

Figure 27. *Fst* mRNA LNP treatment alleviates cancer-associated cachexia by increasing myofiber cross-sectional area and decreasing skeletal muscle fibrosis. (A) Representative anti-laminin immunohistochemistry and (**B**) Picrosirius staining of muscle fibers.

Altogether, cancer-bearing mice treated with *Fst* mRNA LNPs preserved their muscle bulk, as well as displayed a decreased expression of E3 ubiquitin ligase-related genes *FBXO32*, *Trim63*, and *Foxo1*. Thus, the effect of the *Fst* mRNA LNP platform has a potential direct clinical translation for treating muscle catabolic manifestations of CAC and muscle atrophy following chemotherapy. Since antibodies against ActRIIB receptors were shown to ameliorate chemotherapy-dependent cachexia,[336] *Fst* mRNA LNP treatment would be a promising adjuvant approach supplementing chemotherapeutic intervention. Similarly, in our murine model, we observed that the CDDP-treated cancer-bearing mice exhibited signs of iatrogenic muscle atrophy in addition to cancer-dependent skeletal muscle loss. However, the regional combinatorial treatment with CDDP and *Fst* mRNA LNPs exerted an amplified therapeutic effect in terms of more effective eradication of cancer cells in addition to functional and metabolic support of the

organism undergoing chemotherapeutic intervention. It is also important to note that mice treated with *Fst* mRNA LNP/CDDP combination developed small, tightly packed nonadherent tumors easily removed from the IP cavity. This would likely be of great benefit clinically, as it would facilitate surgical resection of most ovarian tumor tissues and prevent malignant intestinal obstructions.

4.9 Synergistic effect of *Fst* mRNA LNP treatment with CDDP chemotherapy prolongs survival of mice with ovarian cancer characterized by peritoneal metastases

The mean survival of mice treated with *Fst* mRNA LNPs (25.8±2.8 days, mean ± SE**, Table 5**), but not FST_H therapy (17.0±1.3 days), differed significantly from the negative control group (12.2±1.15 days) treated with PBS (**Figure 28 A-D**). The combination of *Fst* mRNA LNP with CDDP significantly increased the mean survival (33.8±2.4 days) in comparison to CDDP treatment alone (21.2±1.66 days). However, there was no statistically significant difference in mean survival between negative control and CDDP groups, as well as between *Fst* mRNA LNP alone and CDDP+*Fst* mRNA LNP treatment groups. Importantly, the combination of CDDP with *Fst* mRNA LNPs substantially increased the mean survival of cancer-bearing mice (33.8±2.4 days) compared to CDDP+FST_H (23.8±2.0 days) treatment (**Figure 28 B**). These findings suggest an essential role of *Fst* mRNA LNP treatment in increasing mean survival of cancer-bearing mice when compared to recombinant FST and further support the importance of local and systemic mRNA-mediated FST increase in addition to CDDP therapy.

Table 5: Survival analysis for evaluation of combinatorial treatment efficacy

Treatment Group	Mean Survival	Std. Error	95% LCL	95% UCL
PBS	12.2	1.16	9.93	14.47
CDDP	21.2	1.66	17.96	24.44
FST_H	17.0	1.34	14.37	19.63
CDDP+FST_H	23.8	1.96	19.96	27.64
Fst mRNA LNP	25.8	2.80	20.31	31.29
CDDP+ *Fst* mRNA LNP	33.8	2.35	29.19	38.41

Bliss modeling of therapeutic independence demonstrated a synergistic effect of CDDP+*Fst* mRNA LNP, but not CDDP+FST_H treatments (**Figure 28 E, F**). Therefore, synergistic CDDP+*Fst* mRNA LNP treatment led to a superior ~2-fold increase in mean survival compared to negative control and ~1.3-fold increase compared to single treatments used in this experiment. These findings summarize the importance of adjuvant *Fst* mRNA LNP therapy in combination with regional administration of CDDP chemotherapy.

The synergistic effect of CDDP and ActA inhibition in the treatment of EOC may derive from three mechanisms. First, ActA inhibition may reduce the activity of the non-canonical ActA pathway, thereby decreasing activation of ERK1/2 and p38 MAPKs through type 1 ActA receptor. This would be particularly beneficial for the treatment of chemotherapy-induced cachexia associated with ERK1/2 and p38 activation. [316, 317] Second, downregulation of the canonical ActA pathway could reduce the activation of the proteolytic program in muscle by inhibiting the SMAD 2/3 signaling that mediates the expression of Atrogin-1 and Murf-1. [280] Third, guiding ES-2-Luc cells towards a MET state, characterized by increased proliferation, could enhance the susceptibility of cells to chemotherapy. Simultaneously, this transition may result in the aggregation of cancer

cells into compact clusters, potentially confining them and influencing their response to chemotherapy.

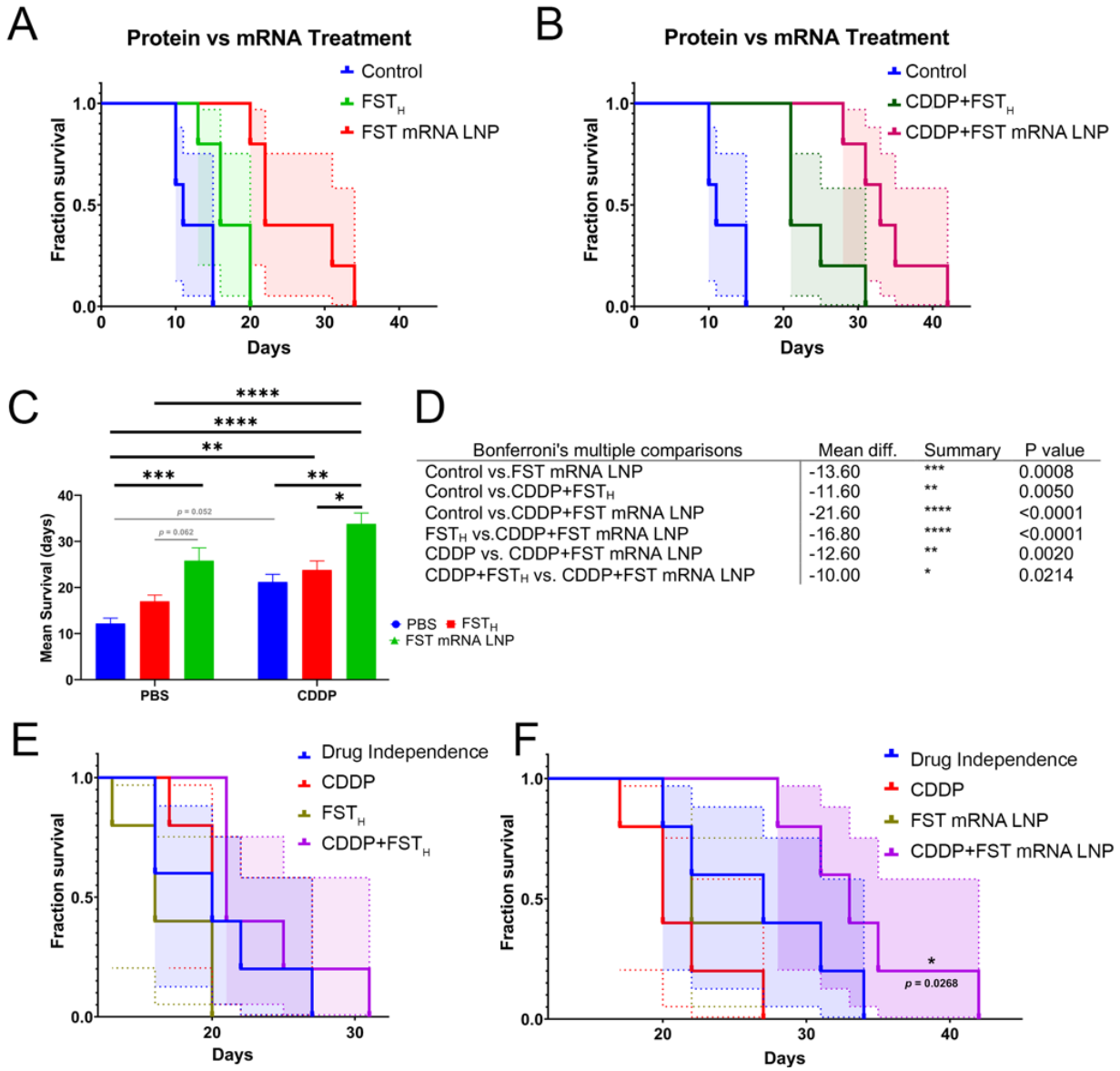

Figure 28. *Fst* mRNA LNP therapy has a potential synergistic effect with CDDP chemotherapy. (A) Comparison of survival curves between control, FST_H, and *Fst* mRNA LNP treatments. **(B)** Comparison of survival curves between control, CDDP+FST_H, and CDDP+*Fst* mRNA LNP treatments. **(C)** Results of *post hoc* Bonferroni's multiple comparisons using median survival **(D)** Table of significant results of *post hoc* Bonferroni's multiple comparisons using median survival **(E)** Bliss modeling of treatment independence for therapeutic synergy analysis between FST_H and its combination with CDDP **(F)** Bliss modeling of treatment independence for therapeutic synergy analysis between *Fst* mRNA LNP and its combination with CDDP.

4.10 Methods

Fst, *Egfp*, and *Luc* mRNA, including fluorophore-labeled mRNA, were purchased from TriLink Biotechnologies Inc. (TriLink Biotechnologies Inc San Diego, CA, USA). DLin-MC3-DMA, cholesterol, DSPC, DMG-PEG2k were obtained from BioFine International (BioFine International, Vancouver, BC, Canada) or Avanti Polar Lipids (Avanti Polar Lipids, Alabaster, AL, USA. Cell culture reagents, including RPMI media, FBS, PBS, and penicillin and streptomycin were purchased from Gibco (Gibco BRL, Gaithersburg, MD, USA), nuclease-free water from Cytiva (Cytiva, Hyclone Laboratories, South Logan, UT, USA). D-luciferin reagent, Halt Protease Inhibitor Cocktail, Prolong Gold anti-fade mountant, Pierce BCA protein assay, Quant-iT RiboGreen RNA kit and ribosomal RNA standards were obtained from Thermo Fisher Scientific (Thermo Fisher Scientific, Waltham, MA, USA). DNA-free Kit and TRIzol reagent were obtained from Ambion (Ambion Co., Carlsbad, CA, USA). Proteinase K reagent and Qiagen RNeasy Mini kit were purchased from Qiagen (Qiagen Corporation, Hilden, Germany). TaqMan Reverse Transcription Reagents Kit, TaqMan Gene Expression Master Mix, Power SYBR Green Master Mix, and other TaqMan assay reagents were purchased from Applied Biosystems (Applied Biosystems, Foster City, CA, USA). Human follistatin and activin A ELISA kits were purchased from Ray Biotech (Ray Biotech, Peachtree Corners, GA, USA). All antibodies were obtained from Invitrogen (Invitrogen, Thermo Fisher Scientific, Waltham, MA, USA). PicroSirius Red Stain Kit was purchased from Abcam (Abcam, Cambridge, UK). Human recombinant follistatin protein, mouse recombinant activin A, and human recombinant activin A were

purchased from Enzo Life Sciences (Enzo Life Sciences, Farmingdale, NY, USA). Cisplatin reagent was obtained from Tocris Bioscience (Tocris Bioscience, Bristol, UK).

LNP preparation and characterization: The LNPs containing different mRNA transcripts (CleanCap *Fst*, *Egfp*, and *Luc* mRNA) were prepared by the previously reported microfluidic procedure. [301] Briefly, LNPs were synthesized in the ratios 50:38.5:10:1.5 of the ionizable lipid DLin-MC3-DMA, cholesterol, DSPC, and DMG-PEG-2k using NanoAssemblr Spark or Benchtop (Precision Nanosystems Inc., Vancouver, Canada). Between ionizable lipids and nucleic acids, an N:P ratio of 5.67 was maintained to produce the nanoparticles that were further concentrated using Amicon Ultra centrifugal filters (Millipore, Bedford, MA, USA) after being buffer exchanged with phosphate-buffered saline (PBS; pH 7.4). Hydrodynamic size, PDI and ζ potential of the developed LNPs were evaluated by Zetasizer Nano ZS (Malvern Panalytical, Malvern, UK) according to the previously reported procedure. [337] All LNPs used in the study exhibited >90% mRNA encapsulation efficiency characterized by a modified Quant-iT RiboGreen assay as previously described. [301] Cryo-TEM micrographs were prepared by depositing 2-3 µL of LNP suspension onto a lacey carbon grid (Electron Microscopy Sciences, Cu 300 mesh), blotting for 1s using Vitrobot (FEI), and rapidly plunging the grid into liquid ethane to produce vitrified ice. The grids were then clipped and imaged on Glacios Cryo-TEM (Thermo Fisher Scientific, Cleveland, OH, USA) equipped with Gatan K3 camera (Gatan, Pleasanton, CA, USA).

In vivo studies: All animal studies were approved by the Institutional Animal Care and Use Committees at Oregon Health and Science University and Oregon State University (approval number: IP00000690).

Animal Model: We utilized a previously reported murine model of ovarian cancer with extensive invasive and metastatic properties. [338, 339] Our experiments were performed in female nude mice (Nu/Nu, Charles River Laboratories, Wilmington, MA, USA) bearing ES-2 intraperitoneal (IP) xenograft. ES-2 human ovarian clear cell carcinoma cell line was purchased from ATCC (Manassas, VA, USA). ES-2-Luc cells were a kind gift from Glen S. Kwon from the School of Pharmacy at the University of Wisconsin–Madison. Cells were grown in RPMI (Gibco BRL, Gaithersburg, MD, USA) growth media supplemented with 10% fetal bovine serum (Gibco BRL, Gaithersburg, MD, USA) and 5% Penicillin/Streptomycin (Gibco BRL, Gaithersburg, MD, USA). All cultures were grown at 37°C with 5% CO_2.

The ES-2 cell line is a human ovarian cancer that expresses an intermediate phenotype between high-grade serous cell carcinoma (HGSCC) and clear cell carcinoma (CCC), the two most aggressive types of ovarian cancer in humans. [340-342] Mixed surface epithelial carcinomas display CCC- and HGSCC-derived characteristics, including resistance to platinum-based chemotherapy, tumors with high mitotic rates, and increased mutational burden. [343, 344] Compared to other mixed CCC/HGSCC cell lines, the ES-2 line is characterized by both malignant ascites and a formation of solid tumors. [345] Taken together, the rationale behind choosing the ES-2 line for this model was based on its characteristics of a short doubling time (t=19 h), invasiveness, and high metastatic potential with tropism for metastasis to organs and fat pads in the peritoneal cavity. [341, 346, 347] Accordingly, after IP injection of ES-2-WT or ES-2-Luc cells (3×10^6 cell per 100 µL in PBS), we observed the growth of malignant ascites with multi-cellular clusters in a third-spaced fluid. PBS was used for sham

injection in control groups. The mice developed multiple cancer clusters, ultimately colonizing secondary sites, and forming metastatic nodules in the omentum, ovaries, and gonadal fat pads. Cancer-bearing mice also displayed a profound cachexic phenotype that was previously described in the literature. [339]

Biodistribution of Luc mRNA *LNPs in sham and ES-2-WT cancer-bearing mice:* The ES-2-WT bearing mice (n=3, day ten after ES-2-WT cells injection) and the sham mice (n=3) were injected with a single *Luc* mRNA LNP dose (10 μg mRNA per dose). Mice injected with ES-2-Luc cells served as positive controls. ES-2-WT-bearing mice and sham mice injected with PBS served as negative controls. The positive and negative control groups (both, n=3). Four hours after injections, mice were injected with D-luciferin (150 mg kg b.w.$^{-1}$ in 100 μL PBS). After fifteen minutes, BLS was captured with IVIS Lumina XRMS imaging system (Perkin Elmer, Hopkinton, MA, USA). BLS data were analyzed using Living Image software (Perkin Elmer, Hopkinton, MA, USA). Organs and ascitic fluid were collected and assessed for BLS distribution.

Biodistribution of mRNA *LNPs in ES-2-Luc cancer-bearing mice:* Five groups of ES-2-Luc bearing mice (n=5, day ten after ES-2-WT cells inoculation) were injected with single doses of Cy5-*Egfp*, *Egfp*, equimolar *Egfp/Sft*, *Fst* mRNA LNPs (10 μg total mRNA per dose) or PBS. Four hours after injection, mice were euthanized, organs and ascitic fluid was collected for further analysis. Fluorescence images of ascites were visualized using Cy5 and GFP filters on the Keyence BZ-X700 microscope (Keyence Corp., Osaka, Japan). Absolute quantification of *Egfp* mRNA by qRT-PCR on cells from the ascitic fluid was performed as described in the *Quantitative RT-PCR* section.

Quantitative RT-PCR: Cells from ascites were centrifuged, ascitic fluid removed. Total RNA was extracted with TRIzol (Ambion Co., Carlsbad, USA) and Chloroform (Sigma-Aldrich, Merck KGaA, Darmstadt, Germany). RNA was precipitated with 200 proof ethanol (Decon Labs, Inc.; King of Prussia, PA, USA). Qiagen RNeasy Mini kit (Qiagen Corporation, Hilden, Germany) was used for further extraction following the modified manufacturer's instructions. DNA-free Kit (Ambion, Catalog #1906, Invitrogen, Carlsbad, CA, USA) was used to remove genomic DNA contaminants. Total RNA was eluted with nuclease-free water (Cytiva, Hyclone Laboratories, South Logan, UT, USA). Total RNA from liver, spleen, lungs, and gonadal fat pads was extracted using the method above. Total RNA from fibrous tissues (muscle, kidneys) was extracted using Qiagen RNeasy Mini kit (Qiagen Corporation, Hilden, Germany) following the manufacturer's protocol. Proteinase K (Qiagen Corporation, Hilden, Germany) was employed after the tissue homogenization step. DNA-free Kit was used to remove genomic DNA contaminants.

cDNA was synthesized with TaqMan Reverse Transcription Reagents Kit (Applied Biosystems, Foster City, CA, USA). Relative quantification with qRT-PCR was performed by using TaqMan Gene Expression Master Mix (Applied Biosystems, Foster City, CA, USA) and TaqMan assay reagents (**Table 6**, TaqMan assay reagents) on the 7300 PCR system (Applied Biosystems). Gene expression was normalized to 18S expression.

Table 6: TaqMan assay reagents and corresponding TaqMan assay identifiers.

Gene of interest	*TaqMan assay*
FST	Hs01086902_m1
CD68	Mm03047343_m1
Ly6G	Mm04934123_m1
SELL	Mm00441291_m1
P4HB	Mm01243188_m1
FOXO1	Mm00490671_m1
FBXO32	Mm00499523_m1
TRIM63	Mm01185221_m1
Ucp1	Mm01244861_m1
MKI67	Hs01032443_m1
TOP2A	Hs03063307_m1
TPX2	Hs00201616_m1
18S	CN: 4333760F

Absolute quantification with qRT-PCR was performed using Power SYBR Green Master Mix (Applied Biosystems, Foster City, CA, USA). *Egfp* primer sequences were: forward -CACATGAAGCAGCACGACTT, reverse – GGTCTTGTAGTTGCCGTCGT; efficiency – 108%, dissociation T=82.5 ^{0}C, single peak. Levels of detection (LoD) and level of quantification (LoQ) were calculated as previously described. [348]

For the ECM gene expression experiment, total RNA from ascitic fluid containing dispersed ES-2-Luc cells and solid ES-2-Luc aggregates was analyzed with TaqMan Array Human Extracellular Matrix & Adhesion Molecules. A 1.5-fold change threshold was used to identify over- and under-expressed genes, and a 0.01 false discovery rate was used to validate a finding of differentially expressed genes.

Evaluation of serum FST and ActA levels after single Fst mRNA *LNP injection:* FST_L mRNA LNP and FST_H mRNA LNP formulations were prepared by encapsulating equimolar *Egfp/Fst* mRNAs and *Fst* mRNAs, respectively. The mice were injected on the 10th day after ES-2-WT cells inoculation. Serum and ascites were collected for

analysis. FST and ActA serum concentrations were quantified using ELISA as described below in the *Enzyme-linked immunosorbent assays* section. Relative quantification of *Fst* mRNA by qRT-PCR on cells from the ascitic fluid was performed as described above in the *Quantitative RT-PCR* section.

Enzyme-linked immunosorbent assays: For ELISA analysis, blood was collected by cardiac puncture in 2 mL tubes with the addition of EDTA and protease inhibitor (Halt Protease Inhibitor Cocktail; Thermo Scientific, Waltham, MA, USA) and was let to sit at room temperature for a minimum of 30 minutes. Blood samples were centrifuged for 15 minutes at 3000 g within one hour of collection (Eppendorf, 5430R, Hamburg, Germany). Serum was then transferred to clean tubes for storage or immediate analysis. Ascitic fluid was centrifuged to separate from the cellular pallet. Total protein in the ascitic supernatant was quantified with the Pierce BCA protein assay (Thermo Scientific, Waltham, MA, USA). Colorimetric quantification was performed on BioTek Synergy 2 microplate reader (BioTek, Winooski, USA) and analyzed on BioTek Gen5 Data Analysis Software. Serum and ascitic fluids were analyzed for FST or ActA concentrations using human follistatin and activin A ELISA kits according to the manufacturer's protocol (Ray Biotech, Norcross, USA). Samples were diluted 1:2 and 1:10 for FST and ActA quantification, respectively. Results were read using BioTek Synergy 2 microplate reader and analyzed on BioTek Gen5 Data Analysis Software. Ascitic fluid results were normalized to total protein.

Chronic Fst mRNA *LNP injections:* Two control groups, ES-2-Luc-bearing and sham mice (both, n=5) and two treatment groups, ES-2-Luc-bearing and sham mice (both, n=10), received PBS or *Fst* mRNA LNP injections (10 μg mRNA per dose),

respectively. Treatment was initiated on day three after ES-2-Luc cell inoculation in cancer-bearing mice and sham PBS injection in age-matched sham mice and continued for seven days. Mice were euthanized twelve hours after the final LNP injection; serum, ascitic fluid, and organs were collected for further analysis. Relative quantification of *Fst* mRNA in organs and ascites, and *CD68, Ly6G, Sell, P4Hb, Mki67, Top2A and Tpx2* mRNA transcripts in ascites was performed by qRT-PCR. Extracellular matrix and adhesion molecules assay were analyzed as described in the *Quantitative RT-PCR* section. FST and ActA quantification in the ascites and serum samples was performed as described above in the *Enzyme-linked immunosorbent assays* section. Gastrocnemius muscles and gonadal fat pads were analyzed by qRT-PCR for quantification of *Foxo1*, *Fbxo32*, *Trim63* and *Ucp1* mRNA transcripts as described in the *Quantitative RT-PCR* section. Gastrocnemius muscles were flash frozen and sectioned (10 μm) on Leica CM1850 UV (Leica Biosystems Nussloch, GmbH, Germany) at -18 ^{0}C. IHC and Picrosirius staining was perfumed as described below in the *Histology and immunohistochemistry* section.

Flow cytometry studies: ES-2-WT cells were co-cultured with RAW 264.7 murine macrophages in RPMI medium with 10% fetal bovine serum and 5% Penicillin/Streptomycin, and initial proportion of 3:1 of ES-2-WT cells and RAW 264.7, respectively. Nude mice were injected with ES2-WT cells (3×10^6 cells per 100 μL in PBS). After 10 days, the control group received PBS injection (100 uL), and the treatment group received injections with Egfp mRNA LNP formulation (2 ug mRNA/mouse in 100 uL PBS). Ascitic fluid was collected by IP lavage. Both in vitro and in vivo samples were fixed with 1:1 acetone/methanol solution pre-cooled to -20 °C and

blocked with 1:1 mixture of TruStain FcX Fc receptor blocking solutions (human and murine, Biolegend, San Diego, CA, USA) for 30 minutes at room temperature, followed by conjugated antibodies staining for HLA-ABC (HLA-ABC Monoclonal Antibody (W6/32), PE eBioscience, Thermofisher Scientific, Waltham, MA, USA) and GFP (APC Anti-GFP antibody, Abcam, Cambridge, UK). Flow cytometry was performed on BD FACSymphony S6 cell sorter (BD, Franklin lakes, NJ, USA) using laser excitation wavelength of 561 nm and 628 nm for HLA-ABC and GFP detection, respectively. Data was analyzed using FlowJo (FlowJo LLC, Ashland, OR, USA).

Histology and immunohistochemistry: Muscle samples were flash frozen followed by 10-μm cryosectioning. For IHC studies, the slides were incubated in blocking buffer for 1 hour at room temperature, followed by primary antibody (mouse laminin, Invitrogen, rabbit, 1:200) incubation overnight at 4 °C. Secondary antibody utilized in the experiment was goat anti-rabbit AF488 (Invitrogen, 1:1000). Sections received three PBS washes between each step. Slides were mounted using Prolong Gold anti-fade media (Thermo Scientific, Waltham, MA, USA). PicroSirius staining was performed according to the manufacturer's protocol (PicroSirius Red Stain Kit, Abcam, Cambridge, UK). Histopathological examinations of liver slices from the mice treated with three daily injections of *Luc* mRNA LNP were performed to evaluate safety and tolerability of the platform. Livers were collected into 4% PFA, stored for 24 hours before a transfer to 70% ethanol for further paraffin embedding and sectioning. Liver sections from control (PBS) and treatment (*Luc* mRNA LNP, 10 ug/mRNA/mouse) were then stained with hematoxylin and eosin (H&E) and evaluated for pathologically observable changes in morphology, infiltration with immune cells, fibrotic or inflammatory changes.

FST and ActA recombinant protein injections in survival experiment: Human recombinant follistatin protein (Enzo Life Sciences, Farmingdale, NY, USA) or mouse recombinant activin A (Enzo Life Sciences, Farmingdale, NY, USA) were reconstituted according to the manufacturer's recommendations and further diluted in PBS as needed on the injection days. ActA was injected in doses of 20 µg kg b.w.$^{-1}$, FST was injected in doses of 20 µg kg^{-1} or 100 µg kg b.w.$^{-1}$ according to the experimental procedure. BLS was read as described above.

Fst mRNA *LNP and CDDP combinatorial treatment in survival experiment:* In the experiments requiring cisplatin (CDDP, >98% purity, Tocris Bioscience, Bristol, UK) injections, the CDDP working solution was prepared in sterile PBS. CDDP was injected in a dose of 2 mg kg b.w.$^{-1}$, delivered every four days for a maximum of five weeks.

Statistical Analysis: All experiments were performed with $n = 5$ unless specified otherwise. Significance was determined using paired t-tests, multiple comparison *t*-tests, two-way ANOVA using GraphPad Prism software. *$p \leq 0.05$, **$p \leq 0.01$, ***$p \leq 0.001$, ****$p \leq 0.0001$.

4.11 Chapter summary

Chapter 4 outlines the development of an mRNA LNP therapeutic aimed at addressing metastatic EOC and cancer-associated muscle wasting, within the context of a syndrome known as CAC. [349] The conceptual advance of this work was centered around *in situ* mRNA-guided reprogramming of cancer cells from mesenchymal to epithelial phenotypes, leading to increased chemotherapy sensitivity with the abscopal effect ameliorating the iatrogenic burden of chemotherapy and simultaneously treating CAC manifestations. **Figure 29** provides graphical summary of the proposed therapeutic.

[349] In fulfillment of **Objectives 1.3** and **1.4**, Chapter 4 provides a comprehensive review of the formulation and characterization of a lipid nanoparticle-based delivery system for follistatin mRNA. Furthermore, it evaluates the formulation's effectiveness in treating EOC and managing CAC within a preclinical nude mouse model, marking the culmination of **Aim 1** in my dissertation.

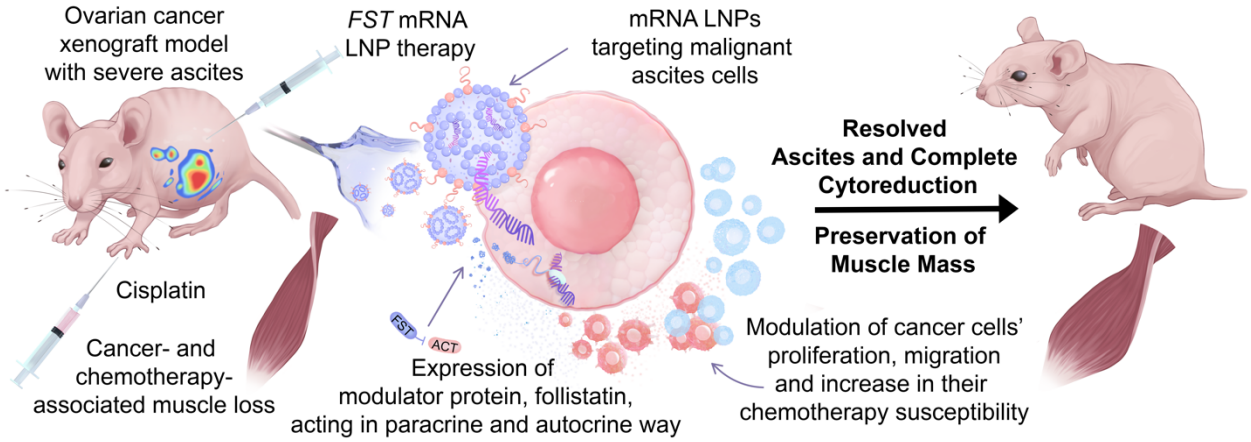

Figure 29. ***Fst* mRNA LNP therapy in combination with cisplatin chemotherapy reprograms metastatic ovarian cancer and reduces CAC manifestations.** LNPs deliver mRNA encoding the therapeutic protein follistatin primarily to cancer cells, locally reducing metastatic potential of peritoneal malignant ascites and, on the systemic level, exerting inhibitory effects on negative muscle regulator activin A leading to preservation of muscle mass. The phenotypic reprogramming of cancer cells results in an increased sensitivity to chemotherapy leading to complete cytoreduction and enhanced resilience during aggressive chemotherapy in a murine model of advanced ovarian cancer.

The main findings of the Chapter include the following:

1) We developed an LNP-based therapy that, following intraperitoneal administration, delivered mRNA encoding the therapeutic protein follistatin primarily to cancer cells.
2) The developed *follistatin* mRNA therapy prevented malignant ascites, delayed cancer progression, consolidated solid tumors, and reversed muscle loss in cancer-bearing mice.

3) Combined with cisplatin, *follistatin* mRNA therapy increased mouse survival while counteracting chemotherapy-induced muscle atrophy and cancer-associated cachexia.
4) The mice receiving combinatorial chemotherapy and *follistatin* mRNA LNP therapy developed a few nonadherent solid tumors that were surgically removed from the peritoneum.

In conclusion, *Fst* mRNA LNP therapy led to durable responses providing synergistic effects in combination with cisplatin chemotherapy in a murine model of disseminated ovarian carcinoma and CAC. This study established a promising translatable therapeutic option for treatment of unresectable EOC with distant metastases that limits cancer progression while enhancing resilience during an aggressive chemotherapeutic intervention. Clinically, the proposed combinatorial treatment could improve overall survival in advanced ovarian cancer patients by facilitating complete cytoreduction and increasing resilience during aggressive chemotherapy.

Chapter 5: Improving LNP platforms for mRNA-based protein replacement therapies

Preamble

In the following two chapters of my dissertation, I focus on the reactions caused by LNP formulations when chronically injected into wild-type mice. The main hypothesis I am investigating is whether the LNPs themselves might cause reactogenic manifestations and, therefore, should be formally evaluated to enhance their safety profiles. This idea emerged when I transitioned my experimental model from using nude athymic mice to more biologically relevant wild-type C57BL/6 mice. This transition aligns with the overarching objective of translating a developed *Fst* mRNA LNP formulation to humans, necessitating assessment within the context of a wild-type immune system. During these studies, I observed that the mice became unwell even with the empty LNP formulation, showing signs of reduced movement, lower food intake, and weight loss. These reactions were not only associated with the chronic injection schedule needed for the therapeutic approach of mRNA-based protein supplementation but were also observed after a single injection of LNPs. The significance of these findings extends

beyond the studies of sickness behavior in experimental models and contributes to the larger goal of improving mRNA LNP formulations, especially when considering their use in mRNA LNP therapies for protein supplementation or replacement in human patients requiring chronic injections. Therefore, it is crucial to address the observed effects on the mice, emphasizing the need to fully understand how LNPs may cause these reactogenic manifestations. This focus on understanding the reactions is a key element in the ongoing effort to develop mRNA therapies that are not only effective but also safe, laying the groundwork for potential use in clinical applications.

5.1 Optimizing LNPs: Balancing efficacy and safety

Nanomaterial-based delivery vehicles are often praised for their ability to encapsulate both hydrophobic and hydrophilic payloads, including small molecule drugs, imaging agents, and nucleic acids, resulting in enhanced solubility, extended circulation time, and their delayed degradation in the systemic circulation. [160] These properties make nanomedicines an attractive alternative to traditional therapeutic and diagnostic modalities, and they are now commonly used clinically and pre-clinically in various biomedical applications. [350] Extensive research has been conducted on the efficacy of LNPs for the delivery of mRNA as a vaccination tool for the prevention of SARS-CoV-2 during the recent pandemic. [351-355] The potential applications of mRNA LNPs for non-infectious diseases, including those necessitating protein supplementation or replacement therapies, were significantly enhanced by the progress made in the field. [356] These therapeutic interventions are applicable to a range of disorders, encompassing those linked to chronic inflammation, such as cancer, autoimmune diseases, cardiovascular disorders, diabetes, and other conditions. However, caution

must be exercised when considering already reactogenic xenobiotic substances in the presence of pre-existing inflammation. Such a combination is likely to aggravate the underlying inflammation, hamper therapeutic mRNA translation, and interfere with the repeated administration of mRNA therapeutics.

The studies of the reactogenicity of mRNA LNP formulations were conducted by leveraging the abundance of data derived from clinical trials of SARS-CoV-2 vaccines. Systemic and local reactogenic symptoms are known to occur after administration of SARS-CoV-2 mRNA vaccines, including formulations developed by Pfizer-BioNTech and Moderna. [352, 357] The observed side effects include fever, muscle aches, headaches, fatigue, chills, and pain at the injection site. [351, 354, 355] These symptoms are usually mild to moderate in severity and are more common after the second dose of the vaccine. [358] Individuals with underlying chronic inflammation may be at an increased risk of experiencing severe side effects from mRNA LNP-based therapies and may also have a reduced response to the treatment itself. [359] Furthermore, as shown by SARS-CoV-2 vaccines reactogenicity studies, overactivation of immune responses triggered by mRNA LNP formulations could lead to new-onset autoimmune disorders, such as autoimmune liver diseases, Guillain-Barré syndrome, immune thrombotic thrombocytopenia, IgA nephropathy, rheumatoid arthritis, systemic lupus erythematosus, and others. [359-361] Despite the reported unfavorable outcomes, research demonstrates that the manifestation of vaccination side effects is linked to a more robust immune reaction and enhanced protection against SARS-CoV-2. [362, 363] However, the development and optimization of LNP carrier species for therapeutic use beyond vaccines and infectious disease prevention, which do not

require immune activation, require a thorough investigation of their toxicity and reactogenicity to guarantee their safety and effectiveness in clinical applications.

The influence of multiple pro-reactogenic elements of mRNA LNP formulations, such as ionizable lipids, polyethylene glycol (PEG) coating, and mRNA cargo, should be studied with great caution. Extensive investigation concerning mRNA's reactogenicity, stability, and translatability, creates a favorable environment for the current applications of modified mRNA in various therapeutic settings. [364-366] For LNP reactogenicity research, the current focus is now centered on investigating the reactogenic adjuvanticity of LNP formulations to enhance the immunogenicity of mRNA LNP vaccine formulations. [16] Although a thorough investigation of the LNP carrier's reactogenicity is yet to be accomplished, the current data raises important questions revolving around LNP-associated side effects. For instance, the use of a greater mRNA LNP dose in the mRNA-1273 vaccine and different ionizable lipids used in the formulation are potential explanations for the increased reactogenicity of mRNA-1273 compared to BNT162b formulations in Modena and Pfizer-BioNTech SARS-CoV-2 vaccines, respectively. [367, 368] Therefore, further research and standardization in the area of reactogenic manifestations and their association with the LNP formulations are necessary to develop effective and safe LNP carrier formulations. By addressing the issue of reactogenicity, mRNA LNP therapies hold promise for treating a wide range of non-infectious diseases, including those associated with chronic inflammation.

Therefore, this chapter summarizes the current understanding of the reactogenicity of LNP carriers, including their potential to exacerbate underlying inflammation, impede the delivered mRNA translation, and potentially interfere with the

repeated administration of mRNA therapeutics. Addressing a significant gap in the current literature regarding the reactogenicity of empty LNPs, I seek to bridge this critical void by providing a thorough and comprehensive analysis of the reactogenic manifestations associated with LNP carriers.

5.2 Exploring LNPs as xenobiotics in reactogenic responses

Reactogenicity is a recognized phenomenon that manifests in individuals, who are administered xenobiotics, which are defined as any foreign substances introduced into the body. This phenomenon encompasses a range of unfavorable events that may arise due to the immune system's response to these substances, such as mRNA LNP formulations, which are presently employed in SARS-CoV-2 vaccines. These reactogenic outcomes in the form of adverse reactions stem from the immune system's response to the LNPs themselves, rather than the intended antigen of the vaccine. Although immunogenicity is an anticipated feature of LNP-based vaccines, the reactogenicity of mRNA LNP leads to undesirable therapeutic outcomes and unfavorable effects such as pain, fever, chills, and fatigue. [352, 357, 369-371]

Studies are underway to evaluate the reactogenicity of LNPs and their structural components (**Table 7**) independent of the intended cargo. The typical composition of LNP carriers consists of ionizable lipids, helper lipids, such as distearoylphosphatidylcholine (DSPC), as well as cholesterol and PEG-lipids (**Figure 30**). [17]

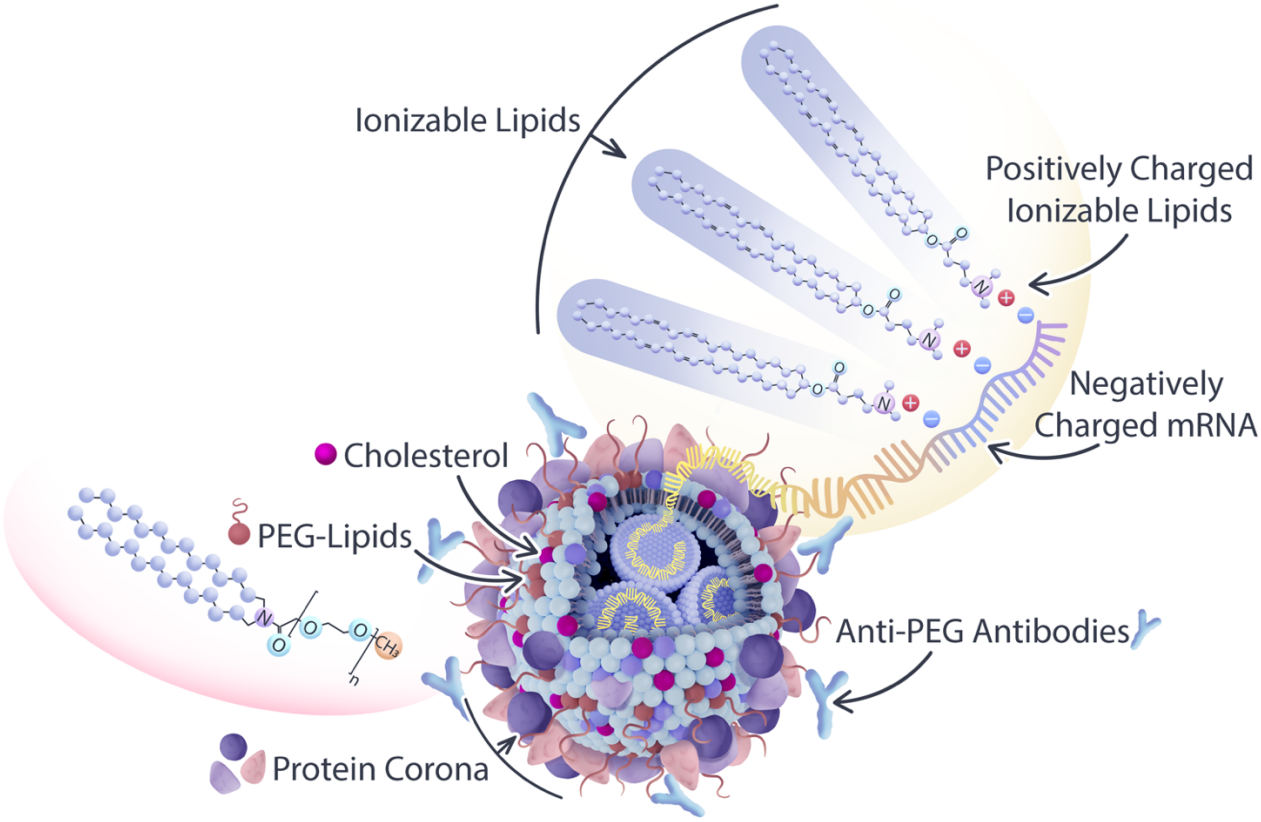

Figure 30. Composition of LNP carriers used in drug delivery: LNPs are composed of ionizable lipids, helper lipids such as distearoyl-phosphatidylcholine (DSPC), cholesterol, and polyethylene glycol (PEG)-conjugated lipids. PEG-lipids assume a significant role in LNP self-assembly, creating a hydrophilic steric barrier with protruding PEG chains surrounding the particle, while ionizable lipids bind to the nucleic acid payload through electrostatic interactions. Among these components, ionizable lipids and PEG-lipids are considered to be the most reactogenic, posing potential risks for unfavorable immune stimulation and adverse effects.

Table 7. Key building blocks of FDA-approved mRNA LNP formulations

Category	Common Name	IUPAC Name	Chemical Structure
Ionizable Lipid	Dlin-MC3-DMA[a]	(6Z,9Z,28Z,31Z)-6,9,28,31-Heptatriacontatetraen-19-yl 4-(dimethylamino)butanoate	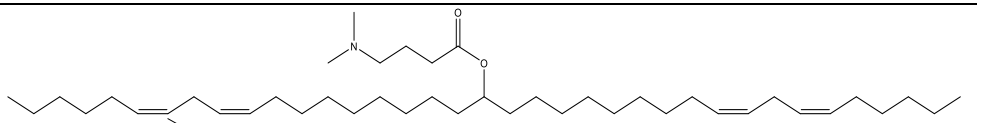
Ionizable Lipid	SM-102[b]	9-Heptadecanyl 8-{(2-hydroxyethyl)[6-oxo-6-(undecyloxy)hexyl]amino}octanoate	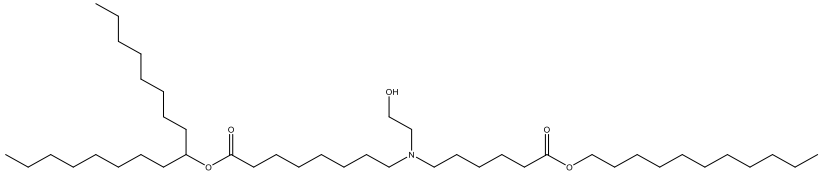
Ionizable Lipid	ALC-0315[c]	[(4-Hydroxybutyl)imino]di-6,1-hexanediyl bis(2-hexyldecanoate)	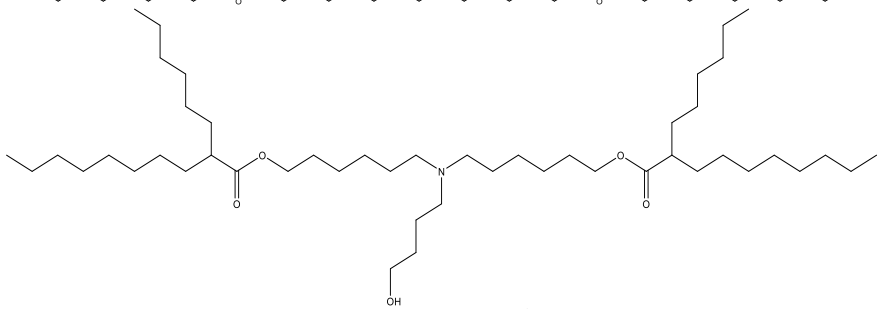
Helper Lipid	DSPC	(2R)-2,3-Bis(stearoyloxy)propyl 2-(trimethylammonio)ethyl phosphate	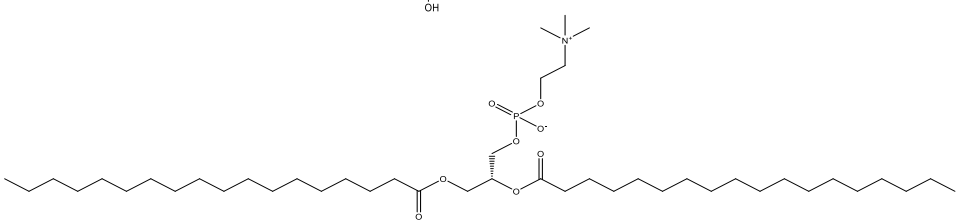
Stabilizing component	Cholesterol	(3β)-Cholest-5-en-3-ol	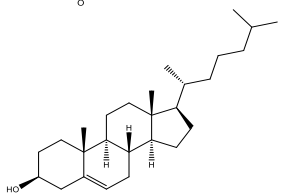
Shielding component	PEG	poly(oxyethylene)	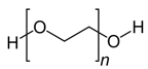

Ionizable lipids used in [a]Onpattro therapy, [b] Moderna, and [c] Pfizer-BioNTech SARS-CoV-2 vaccines.

Ionizable lipids are a key component of LNPs, as they provide the positive charge that facilitates the encapsulation of negatively charged nucleic acids. [372] Helper lipids, such as DSPC, are often used to optimize the biophysical properties of LNPs. Helper lipids can enhance the stability of the LNP formulation and promote cellular uptake and endosomal escape. [373] Cholesterol is another essential component of LNPs, as it also can influence the biophysical properties of the LNP formulation. The presence of cholesterol within the LNP membrane can enhance its fluidity, thereby promoting the efficient release of nucleic acids from the LNP and facilitating their uptake by cells via enhanced fusogenicity. [374] Lastly, the incorporation of PEG-lipids into LNP formulations serves to augment their stability, decrease the activation of phagocytic immune cells, and enhance their pharmacokinetic properties. [372] In the process of LNP self-assembly, PEG-lipids assume a crucial role by creating a hydrophilic steric barrier through the formation of PEG chains on the LNP surface. [375] Van der Waals forces between hydrocarbon chains of DSPE, PEG-lipids and cholesterol molecules are essential for holding the LNP together and maintaining its structural integrity. [376] The collective result is the formation of a PEG layer around the intact LNP, with the PEG chains protruding from the particle's surface. This arrangement enhances the stability and integrity of the LNP structure, contributing to its overall functionality and effectiveness as a delivery vehicle. PEG-lipids form a protective layer around the LNP, which can minimize recognition by the immune system and improve circulation time *in vivo*, but can also increase the immunogenicity of the formulation. [377]

Among the components of LNP platforms, ionizable lipids and PEG-lipids are recognized as the most reactogenic elements. [378] Ionizable lipids such as Dlin-MC3-

DMA (hereafter referred to as MC3), initially introduced in the therapeutic Onpattro (patirisan), SM-102 employed in the Moderna SARS-CoV-2 vaccine, and ALC-0315 utilized in the Pfizer-BioNTech SARS-CoV-2 vaccine, are frequently evaluated, and contrasted based on their reactogenicity and immunogenicity profiles, especially in the context of their implementation in vaccines (**Table 7**). [379-381] Ionizable lipids are cationic in low pH and play a crucial role in encapsulating nucleic acids and promoting endosomal escape with the efficient release of cargo into the cytosol. [380] However, their positive charge can also interact with negatively charged endosomal membranes or proteins, resulting in cellular damage and undesired immune activation. Additionally, incorporating PEG-lipids into LNPs to enhance their stability, evade immune cell recognition, and impede opsonization by complement effector molecules, can potentially lead to undesirable consequences. These may include the production of anti-PEG antibodies or the accumulation of PEG in various organs and tissues. [377] Importantly, the molecular weight of PEG was shown to play a crucial role in both the production of anti-PEG antibodies and their binding to the PEG moieties. A reduction in anti-PEG IgM formation was observed in mice when treated with LNPs conjugated to a fast-shedding PEG-lipid with short acyl chains and hence lower molecular weight in comparison to LNPs conjugated to a slow-shedding PEG-lipid with long acyl chains. [382] Moreover, the pretreatment of mice with slow-shedding PEG-containing LNPs resulted in suboptimal performance (i.e., loss of RNA interference) of LNP formulations containing nucleic acids. [382] Interestingly, the administration of high molecular weight PEG as a pre-treatment in mice, before introducing PEGylated liposomal formulation, effectively sequestered the existing pool of anti-PEG antibodies. [383] The decrease in available

anti-PEG antibodies enabled prolonged circulation of PEGylated liposomes, avoiding the induction of accelerated clearance and preserving their efficacy. Additionally, PEG with a molecular weight of 2000 Da and larger exhibited the highest affinity for binding anti-PEG antibodies. [384]

Therefore, it can be inferred that LNPs themselves, independent of their cargo, possess structural components capable of inducing reactogenic and immunogenic responses. Evaluating the reactogenicity of individual components of LNP carriers (hereafter referred to as empty LNPs, eLNPs) in isolation is often challenging due to the integral role played by the assembled eLNPs in delivering nucleic acids. As such, the comprehensive assessment of the safety and efficacy of the assembled product usually involves the evaluation of the reactogenicity of the complete eLNP platform.

When conducting studies that include reactogenic profiling of mRNA LNP formulations, researchers use multiple controls beyond the eLNP carriers. These include phosphate-buffered saline, placebo mRNA LNPs incorporating luciferase or *Egfp* mRNA, diluents, or naked nucleic acids. [385-390] Although LNPs are frequently employed as carriers for mRNA, utilizing eLNPs as a control for comparing their reactogenic effects to mRNA-loaded LNPs and attempting to separate the reactogenic profiles of mRNA cargo and eLNP may not yield optimal results. This is due to the possibility that eLNPs differ from mRNA-loaded LNPs in their size, composition, surface interactions, and fusibility potential. The molar ratio of PEG-lipids, the lipid-to-mRNA mass ratio, and the N/P ratio (representing positively charged nitrogen of ionizable lipids and negatively charged phosphates of nucleic acids) are critical factors that influence the ultimate composition of LNPs containing ionizable lipids for mRNA complexation.

[391] eLNPs with a lower concentration of helper lipids and interference from ionizable lipids on the surface, often display variations in physicochemical and biological properties compared to mRNA-loaded LNPs, including a positive surface charge, increased splitting dynamics, and an altered protein corona composition. [391] Consequently, there is a possibility that eLNPs display different organ tropism, as a result of their differential interaction with homing proteins such as ApoE in comparison to mRNA-loaded LNPS. [391] This, in turn, may augment the local and systemic eLNP reactogenicity.

Considering the major concerns surrounding the reactogenicity of eLNPs and their components, various efforts are underway to develop alternative lipid formulations that can minimize their adverse effects, while still maintaining the desirable properties of LNP platforms. The process of constructing LNP formulations involves adhering to similar protocols and ratios of structural components, with the primary variance arising from the application of different ionizable lipids (**Table 7**) but following similar LNP composition ratios (**Table 8**). For instance, the currently approved mRNA LNP vaccines demonstrate a similarity in their structural compositions (**Table 7**). These compositions encompass a diverse range of ionizable lipids, each unique to the specific vaccine formulation, alongside the inclusion of diverse PEGylated lipids. Although the ionizable lipids utilized in each vaccine formulation differ, they all share certain structural features. These structural similarities, such as the amino-alcohol head group and branched hydrocarbon lipid tails characterized by ester linkages contribute to the stability, mRNA encapsulation efficiency, and facilitation of cellular uptake of mRNA LNP vaccines.

Table 8. Empty LNP composition and doses utilized in reactogenicity studies.

Reference	eLNP composition (molar ratios)	Ionizable Lipid	eLNP dose
[392]	IL: DSPC: cholesterol: PEG-lipid 50:10:38.5:1	MC3 and YK009	Not provided; mRNA LNP dose was equivalent to 10 µg mRNA administered via the IM, SQ, or ID routes
[370]	IL: phosphatidylcholine: cholesterol: PEG-lipid 50:10:38.5:1.5 [393]	IL under US10221127B2 patent (Acuitas Therapeutics)	10 µg administered in 4 spots, 2.5 µg/spot, ID, and IV; 10 µg administered IN
[394]	IL: DSPC: cholesterol: PEG-lipid: GLA at a molar ratio of 50:9.83:38.5:1.5:0.17*	Not discussed	50 µg administered per site, injected ID
[395]	IL: DSPC: cholesterol: PEG-lipid at a molar ratio of 50:10:38.5:1.5	MC3 ionizable lipid	Equivalent to 0.3 mg/kg mRNA LNP dose, injected IV
[396]	IL: DSPC: cholesterol: PEG-lipid at a molar ratio of 55:10:32.5:2.5 as described in [397]	IL under US10221127B2 patent (Acuitas Therapeutics)	5 µg/mL (total lipids, or~7.5 µg/mL ionizable lipid) empty LNP in vitro study
[398]	The LNP formulation used in this study is proprietary to Acuitas Therapeutics	IL under US10221127 patent (Acuitas Therapeutics)	Total lipid content: 900 µg; equivalent to the lipid content of 30 µg mRNA-LNP ID and IV
[399]	IL: DSPC: cholesterol: PEG-lipid at a molar ratio of 50:20:28:2 for the MC3 or 50:10:38.5:1.5 for the SM-102 formulations	MC3 and SM-102	eLNP doses are not provided, eLNP injected IV
[400]	IL: phosphatidylcholine: cholesterol: PEG-lipid at a molar ratio of 50:10:38.5:1.5 mol/mol) as described in [393, 401]	IL under US10221127 patent (Acuitas Therapeutics)	Equivalent to the lipid content of 2.5 µg mRNA-LNP injected ID
[402]	IL: DSPC: cholesterol: PEG-lipid at a molar ratio of 50:10:38.5:1.5	MC3 and C12-200	2 mg/kg lipids or dose equivalent to 0.32 mg-mRNA/kg, injected IV

IL = ionizable lipid; Distearoylphosphatidylcholine = DSPC. ID = intradermally, IV = intravenously, IM = intramuscularly, SQ = subcutaneously, IN = intranasally. * Valera LLC, a Moderna Therapeutics Venture, supplied all vaccines.

Despite the development of new formulations, the current Food and Drug Administration (FDA)-approved LNP platforms and their modified versions, which employ similar structural components, continue to serve as the established standard for delivering nucleic acids. Consequently, a comprehensive evaluation of their reactogenicity is imperative to expand the scope of their clinical applications. In light of this, it is essential to note that there are different types of reactogenicity assessments that can be used to evaluate the safety and efficacy of LNP-based therapies.

5.3 Assessment of reactogenic manifestations following LNP administration

Evaluation of reactogenicity is a crucial component of preclinical safety studies for LNP formulations. Assessing reactogenicity can be done in several ways, depending on the formulation being administered and the specific adverse events being monitored. While the assessment of reactogenicity in human subjects mainly involves evaluating the frequency and severity of local and systemic reactions, as well as monitoring for severe adverse events such as anaphylaxis, preclinical studies involving animal models, including murine models, typically employ a range of approaches. The employed methodologies in animal models encompass behavioral observations, hematological, immunological and biochemical analyses, histopathological examinations, and measurements of specific pro-inflammatory markers through immunohistochemistry and gene expression assays (**Figure 31**). The comprehensive application of these methods facilitates a more thorough understanding of the reactogenic manifestations associated with administered formulations.

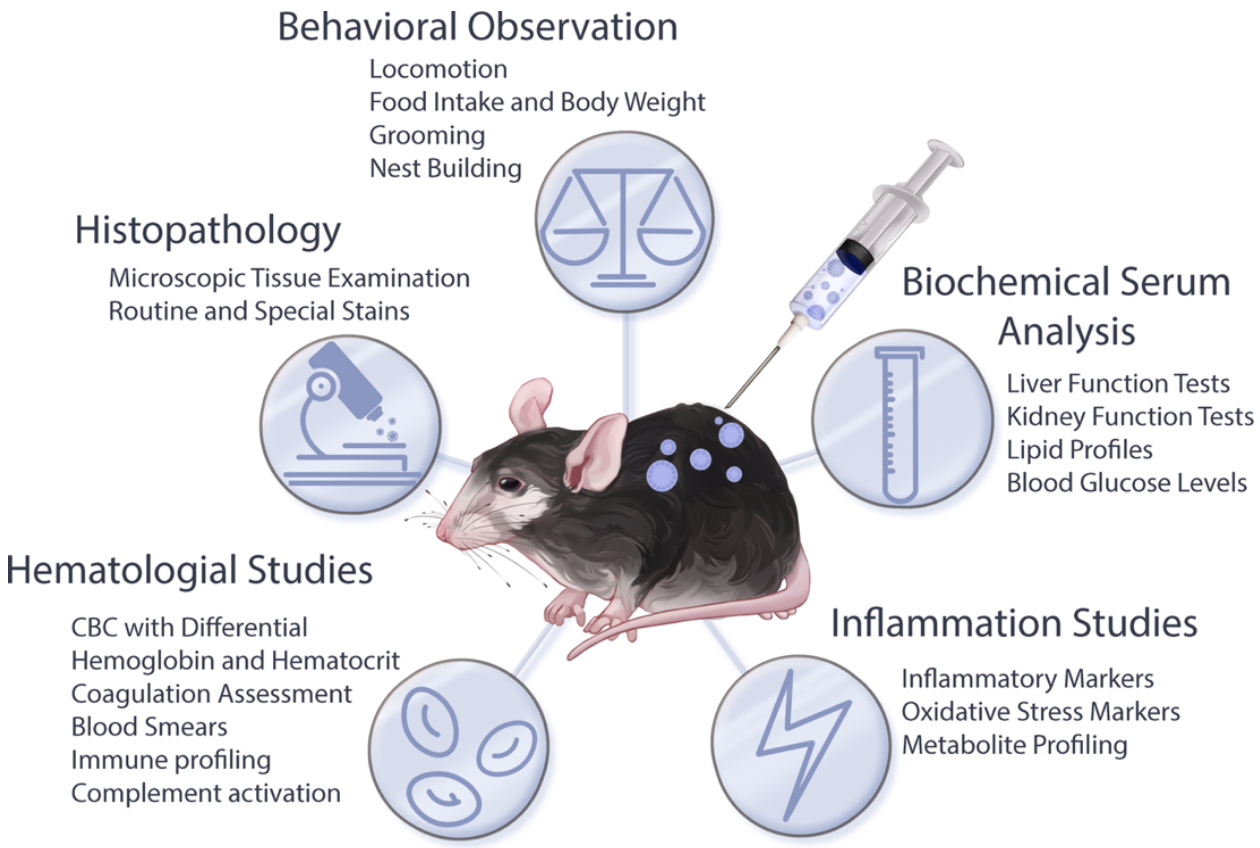

Figure 31. Methodological approaches for investigating reactogenic manifestations in animal models: By integrating different methodologies, such as behavioral observations, histopathological studies, and hematological, biochemical and inflammation analyses, a more comprehensive understanding of the cause-and-effect relationship between treatments and reactogenic manifestations can be achieved, aiding in the development of improved LNP platforms.

Behavioral observation involves monitoring mice for signs of reactogenicity or toxicity, such as changes in behavior, activity level, grooming, and respiratory distress. Food intake and body weight are essential parameters often closely examined in preclinical studies. Changes in food intake and body weight provide valuable insights into the overall health of the animals and serve as early indicators of potential reactogenicity to xenobiotics. Therefore, in this Chapter, food intake and body weight will be discussed further as important indicators of reactogenicity in mice.

The *hematological analyses* focuses on assessing blood samples for parameters such as platelet, white blood cell (WBC), and red blood cell (RBC) counts (i.e., complete

blood count with differential), hemoglobin concentration, and RBC characteristics. For instance, in rats and monkeys treated with MC3 eLNPs, no change was observed in RBC counts, hemoglobin, hematocrit, and RBC distribution width compared to PBS administration. [395] However, an increase in all these parameters was observed in response to mRNA-loaded LNPs. Additionally, rats exhibited a systemic increase in total WBC count resulting from mRNA-LNP treatment, but not from MC3 eLNPs. [395] The systemic increase in WBCs found in this study mirrored the increasing mRNA concentration per administered dose. Interestingly, despite greater WBC counts in the mRNA-LNP treatment group, neutrophils and monocytes were increased in both mRNA LNP and MC3 eLNP treatment groups. [395] Transient increase in monocytes and neutrophils in the MC3 eLNP treatment group was observed for a shorter period (specifically, day 9 post-administration), in comparison to mRNA LNP treatment groups where this increase was sustained (up to day 16 post-administration). [395] In addition to complete blood cell count with differential, immunological investigations, including immune profiling and complement activation studies, play a crucial role in identifying specific components or characteristics of eLNPs that contribute to their reactogenic properties. Despite the absence of specific studies examining the activation of complement by eLNPs, ample evidence exists regarding complement activation through classical, mannose-binding lectin, and properdin-mediated pathways involving liposomes. [403-407] The activation of the complement cascade can occur through the recognition of structural components of liposomes or antibodies that target these components on the liposomal surface, including cholesterol, PEG, or structural lipids.

[408-410] Additionally, the complement cascade can be initiated by the interaction of specific proteins that form the protein corona surrounding the nanoparticles. [407, 411]

In addition to hematological and immunological assessment, blood samples for reactogenic studies can be evaluated for *biochemical parameters*, including liver enzymes, kidney function, and electrolyte balance. The most common biochemical approach utilized to assess systemic reactogenicity in animal models involves the evaluation of hepatic and renal function, as these organs are integral to the metabolism and elimination of foreign substances, including nanoparticles. [412] Exposure to reactogenic substances can result in liver or kidney damage, which is generally reflected by changes in liver enzyme levels such as alanine and aspartate aminotransferases (AST, ALT), or markers of renal function such as increased blood urea nitrogen (BUN) or plasma creatinine levels. [413, 414] For instance, in mice, AST (but not ALT or alkaline phosphatase) was the only parameter significantly elevated compared with placebo treatment after MC3 eLNPs administration. [392] In rats, the same type of eLNPs containing MC3 ionizable lipids increased AST and ALT levels. Moreover, these parameters were increased to the same extent in the rats treated with the highest dose of mRNA LNP under investigation. [395]

In response to LNP administration, rodents typically manifest edema, redness, and infiltration of innate immune cells at the injection site as well as in organs penetrated by LNP-based formulations, such as lungs in the studies with intranasal drug administration, mirroring similar responses observed in humans. [370, 395] To evaluate the impact of xenobiotics on affected tissues, reactogenicity studies employ *histopathological examination* involving collection and microscopic analysis of tissue

samples from various organs for signs of tissue damage, inflammation, or immune cell infiltration. For instance, histopathological assessment of liver samples showed that MC3 eLNPs induced individual cell necrosis in the livers of rats. [395] Similarly, histopathological approaches are employed to assess the infiltration of immune cells into organs and tissues. In mice, injection site immune cell infiltrates consist of neutrophils, macrophages and dendritic cells, and demonstrate the localized release of chemokines in response to eLNPs. [370] The intranasal delivery of labeled LNPs resulted in leukocytic infiltration of lung tissues, with a predominant presence of neutrophils and eosinophils. [370] Additionally, in rhesus macaques, injections with eLNPs and, to a greater extent, mRNA-loaded LNPs lead to CD45-positive cell infiltration that denotes non-specific infiltration with hematopoietic cells. [394] Liang *et al.* also reported that neutrophil and monocyte infiltration in rhesus macaques was similar for mRNA-loaded LNP and eLNP treatments, regardless of administration route where intramuscular and intradermal routes of injection were compared from immunogenic and reactogenic perspectives. [394]

Finally, the assessment of pro-inflammatory effector molecules released in response to eLNP administration encompasses a range of *studies targeting inflammation*, that include a wide array of methodologies, including ELISA, flow cytometry, cytokine profiling, quantitative PCR, and microarray analysis. Specifically, chemokine and cytokine expression studies can provide valuable insights into the reactogenicity pathways of eLNPs as a drug delivery system. For instance, the expression of chemokines at the injection site is known to facilitate trafficking and recruitment of more circulating innate immune cells to the site of active inflammation.

[415] Accordingly, eLNPs induce the local release of multiple chemokines, including CCL2, CCL3, CCL4, CCL7, CCL12, CXCL1, and CXCL2, that further attract macrophages and monocytes. [370] The potent chemokine CCL2 was also overexpressed by monocytes in response to Acuitas eLNP administration to human peripheral blood mononuclear cells (PBMCs) *ex vivo.* [396] Collectively, eLNP carriers devoid of payload elicit the recruitment of monocytes and neutrophils, which subsequently amplify this cascade through the local expression of chemokines. However, eLNP administration elicits a response of shorter duration when contrasted with mRNA-loaded LNP treatments. Our observation suggests that this disparity may stem from the unique molecular-level responses to mRNA payloads and eLNP carriers, which can be recognized as danger- (DAMPs) or pathogen-associated molecular patterns (PAMPs).

5.4 Cellular and molecular responses to LNP carriers

Within the intricate landscape of molecular interactions involving LNPs, innate immune cells emerge as the primary first responders to these therapeutics. Among these cellular "arenas," macrophages and neutrophils take center stage as pivotal participants in the dynamic interplay with LNP formulations. Employing complex molecular processes, innate immune cells orchestrate a series of reactions that significantly impact the efficacy and safety of LNP-based therapeutics. Neutrophils play a critical role in the initiation of acute inflammation and are among the earliest immune cells to be recruited into tissues during such inflammatory processes. [416] Functioning as polymorphonuclear cells, they demonstrate remarkable versatility and contribute significantly to the innate immune response against invading pathogens and tissue

damage. [417] Their rapid mobilization to inflamed sites is regulated by a diverse array of signaling molecules, including chemokines and cytokines, which guide their directed migration from the bloodstream to the sites of tissue inflammation. [418-420] Neutrophils interact with different nanoparticles, including LNPs and cationic liposomes. [421-424] Studies reveal that the surface characteristics of lipid-containing nanoparticles, such as PEG density and surface charge, play a pivotal role in modulating the neutrophils' capacity to internalize LNPs. [422, 424] Monocytes, the second most abundant cell type responding to LNPs, assume a pivotal role in the context of tissue inflammation. This significance is attributed to their selective recruitment and guided migration into inflamed tissues, regulated by an array of inflammatory mediators, encompassing cytokines, chemokines, and complement effector molecules. [415] Their extravasation mechanism enables monocytes to actively participate in immune surveillance and host defense, as they engage with inflamed tissues to facilitate pathogen clearance, tissue repair, and the maintenance of tissue homeostasis. [425, 426] Monocytes demonstrate proficient phagocytic capabilities and are equipped with pattern recognition receptors (PRRs), enabling monocytes and macrophages to actively interact with microbial pathogens, cellular debris, and diverse xenobiotics [427], including LNPs. Macrophages are also widely recognized to be one of the initial and principal cell types responsible for nanoparticle processing. [428] As nanoparticles enter the bloodstream, they become coated with opsonins, such as antibodies to PEG or complement effector molecules, which mark them for recognition by the mononuclear phagocytic system. [428] The mononuclear phagocytic system, including monocytes and macrophages, identifies opsonized nanoparticles, facilitating

their efficient uptake and clearance from circulation. [429-431] This finely tuned process is essential for the immune surveillance and removal of foreign particles, contributing significantly to the body's defense against potential threats posed by xenobiotics in the bloodstream.

While hematologic studies indicate a systemic increase in WBCs in the bloodstream following the administration of LNP formulations, a more thorough understanding of the biological responses to these formulations can be gained by examining the reactions of innate immune cells at the immediate site of administration. For instance, regardless of the administration mode, whether it is intravenous (IV), intramuscular (IM), intradermal (ID), or intranasal (IN), the formulation administration sites undergo infiltration by diverse innate immune cells. Among these cellular constituents, neutrophils, monocytes, macrophages, and to a lesser extent eosinophils and dendritic cells, were predominant species. [370, 394, 396] This infiltration pattern highlights the robust and multifaceted response of the innate immune system to the presence of administered xenobiotics. Furthermore, this localized approach that defines innate immune cell populations offers a comprehensive view of the early molecular events and interactions that shape the subsequent immune responses.

The broad and diverse molecular pathways that underlie eLNP-related reactogenic manifestations as part of DAMP- and PAMP-mediated signaling involve the activation of toll-like receptors (TLRs), including TLR4 and TLR2. [396, 432] The interactions between eLNPs and TLRs are studied using downstream effectors and adaptor proteins that facilitate further signal transduction. Signal transduction from TLR4 and TLR2 necessitates the presence of the myeloid differentiation primary response 88

(MyD88) adaptor protein, which is essential for downstream signaling. [433] Additionally, some TLRs, such as TLR4, are known to modify their homophilic interactions with adjacent adaptor proteins based on the acidity of the local environment. [433, 434] When TLR4 is internalized along with the forming endosome, the decrease in endosomal pH influences the exchange of the MyD88 adaptor protein for the TIR-domain-containing adaptor-inducing interferon-β (TRIF) adaptor protein. [435] It remains unclear which component of the LNP construct or its protein corona is responsible for TLR ligation, and it is also unknown whether the ligation occurs on the plasma membrane, where TLR4 associates with MyD88, or in the endosome, where TLR4 associates with TRIF for further signal transduction. Furthermore, TLR ligation can be facilitated in the endosome by both LNP surface structures or released LNP components (**Figure 32**). The acidification of the endosomal environment as endosomes undergo maturation induces the degradation of LNPs, releasing ionizable lipids from the LNP core. [436, 437] In the case of LNP-mediated cargo delivery, this conversion occurs during the LNP processing within the endosomal compartment, followed by their escape from the endosomes to facilitate the release of their cargo into the cytosol. It is facilitated by the interactions between the surface of LNPs and the negatively charged membrane of the endosomes, in addition to the decrease in ambient pH or the action of helper lipids, cholesterol or its derivatives. [438, 439] Apart from the destabilization of the endosomal membrane caused by LNPs, additional factors, such as the elevation of osmotic pressure or the swelling of particles within the endosome can contribute to the facilitation of LNP disintegration and subsequent escape from the

endosomes. [437] This process allows for the liberation of LNP contents into the cytosol, inevitably compromising the integrity of the intact particles.

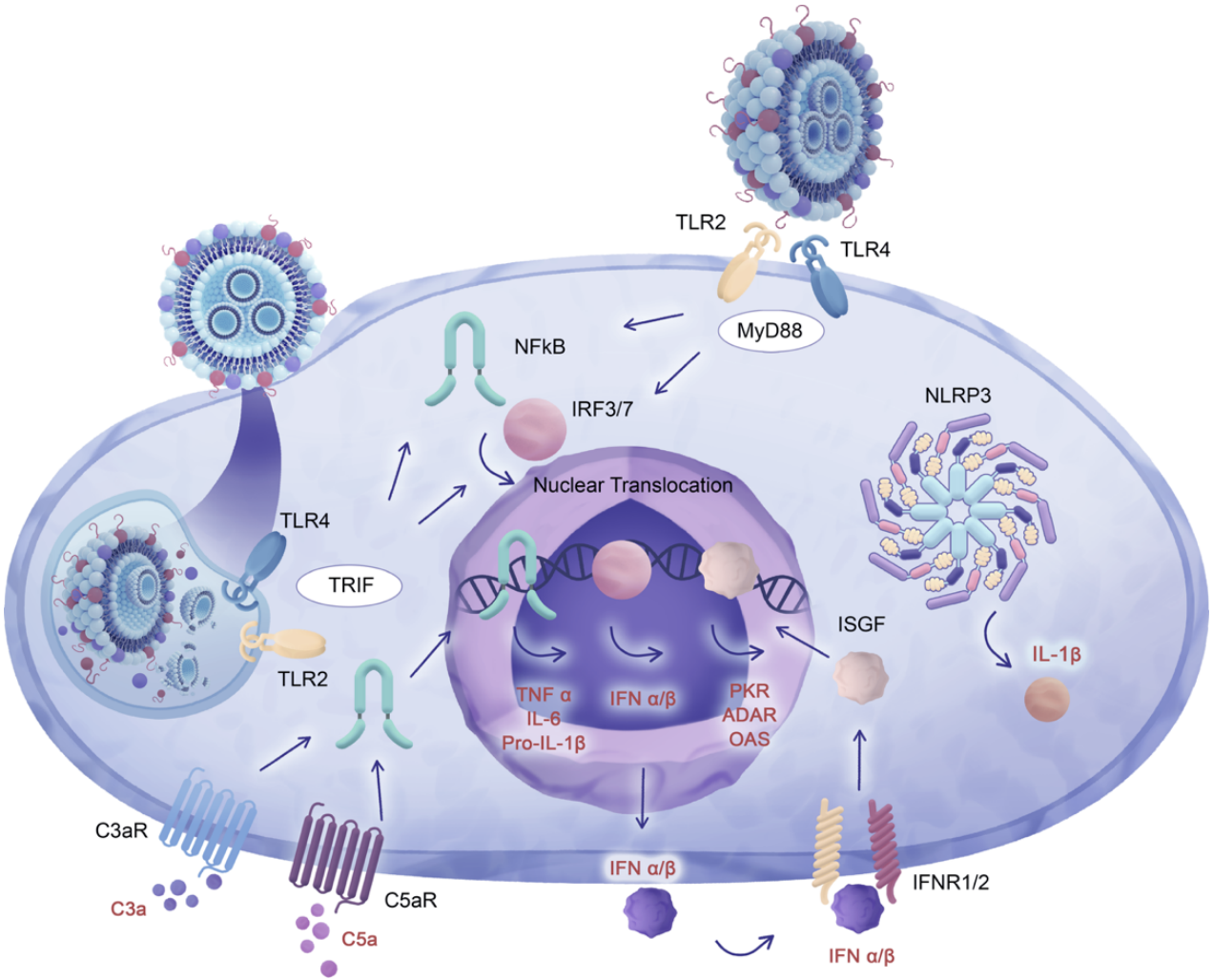

Figure 32. TLR4 signal propagation mediated by MyD88 and TRIF adaptor proteins: Converging pathways involving MyD88 and TRIF adaptors activate cytokines TNF-α, IL-6, and IL-1β through nuclear translocation of NF-κB, IRF3, and IRF7 transcription factors. Positive feedback loops and type I interferons enhance cytokine expression, activating additional pro-inflammatory effectors and inducing cessation of mRNA expression. Complement cascade activation exacerbates cytokine-dependent reactogenicity, with C5a and C3a promoting inflammation via their receptors. TLR4 and C3aR/C5aR activation converge on MAPKs, increasing cytokine production by APCs.

While considering reactogenic signal propagation via two main pathways, namely MyD88-dependent and TRIF-dependent pathways (refer to **Figure 32**), it is crucial to employ both adaptor proteins in reactogenicity studies and investigate their involvement in eLNP-mediated induction of reactogenic manifestations. Therefore, studying the involvement of these proteins in propagating pro-inflammatory signals, researchers utilized genetic ablation approaches such as MyD88 and TRIF knock-out (KO) mouse models to investigate the impact of eLNPs on TLR receptors. For instance, MyD88 KO mice showed no response to empty LNPs in terms of follicular T helper and germinal center B cell upregulation, indicating that adjuvant properties and possibly reactogenicity of eLNPs rely on signal transduction via MyD88 adaptors. [398] Moreover, the convergence of signaling pathways dependent on MyD88 and TRIF adaptors results in the activation of a common set of cytokines, namely tumor necrosis factor-alpha (TNF-α), interleukin 6 (IL-6) and interleukin 1 β (IL-1β). This activation occurs through the induction of nuclear translocation of transcription factors such as nuclear factor-kappa B (NF-κB) and interferon regulatory factors 3 (IRF3) and 7 (IRF7). The expression of these cytokines is further enhanced by positive feedback loops involving type I interferons and interferon-stimulated gene factors (ISGFs) (**Figure 32**). Consequently, this amplification of cytokine expression leads to the activation of additional effectors, ultimately resulting in the cessation of mRNA translation and the maturation of cytokines (i.e., IL-1β) associated with physiological reactogenic responses such as fever and painful sensations. Importantly, within the context of investigations concerning MyD88 and TRIF adaptors in LNP reactogenicity studies, mice with a dual knockout of MyD88 and TRIF exhibited reduced expression of downstream effectors,

specifically TNF-α and IL-6, in comparison to wild-type (WT) mice when exposed to mRNA-loaded LNPs. [440] The study has a limitation in that it did not distinguish between the effects of mRNA-loaded LNPs and empty LNPs on the Myd88/Trif dual KO model. This is further complicated by the fact that both TRIF and MyD88 proteins also function as adaptors to TLRs that detect nucleic acids, such as TLR3, which recognizes double-stranded RNA (dsRNA). [441] Moreover, the MyD88 adaptor is involved in signal transduction from TLR7 that is activated by single-stranded RNA. [435] As such, it is unclear whether the observed response is due to the nucleic acid payload, the LNP carrier or both. A further puzzle that arises in the decoding of reactogenicity of mRNA-loaded LNPs and eLNPs is that both the induction of TLRs by nucleic acids and eLNPs results in the expression of a similar subset of cytokines and chemokines involved in reactogenic symptoms.

Cytokine-dependent reactogenic manifestation can be exacerbated following complement cascade activation, where pro-inflammatory effects of complement effector molecules acting on their respective receptors result in upregulation of IL-6, TNF-α, and IL-1β expression (**Figure 32**). The anaphylatoxins, C5a and C3a, are produced through proteolytic processes during the complement cascade activation, which involves the previously mentioned liposome-dependent activation of the classical, mannose-binding lectin, and properdin-mediated complement pathways. [403-407, 442] The administration of LNPs possibly causes similar activation patterns, resulting in the generation of C3a and C5a effectors through the action of proteolytic convertases. [443, 444] While functioning as anaphylatoxins, attracting innate and adaptive immune cells and promoting the maturation of adaptive immune cells, they also interact with the C3a

receptor (C3aR) and the C5a receptor (C5aR), thus propagating and amplifying the TLR-dependent inflammatory cascade. [445-451] For instance, the activation of TLR4 and C3aR/C5aR converges on the activation of mitogen-activated protein kinases (MAPKs), leading to the nuclear translocation of NF-κB, resulting in a significant upregulation of IL-6, TNF-α, and IL-1β by antigen-presenting cells (APCs). [452, 453]

5.5 Enhanced cytokine gene expression in response to eLNP administration

Reactogenic symptoms such as fever, chills, and localized inflammation at the injection site of the LNP-based vaccines are known to be driven by cytokine expression by the resident and migratory immune cells attracted to the injection site. [454] Recent research shed light on the mechanisms underlying reactogenic manifestations revealing that they are driven by certain cytokines, including IL-6, IL-1β, and TNF-α. [455] These cytokines are part of the body's innate immune response and are responsible for inducing inflammation and fever, which help to mobilize the immune system to fight off the perceived target pathogen. The regulation of pro-inflammatory cytokines is tightly controlled by previously introduced transcription factors NF-κB, IRF3, and IRF7, which play crucial roles in the molecular mechanism of acute and chronic inflammation. [456, 457]

The TRIF-dependent signaling via TLR4 following ligation by eLNPs, and TLR3 by dsRNA as part of secondary mRNA structures both govern the activation of transcription factors IRF3/7. [396, 458, 459] The activation through phosphorylation and following nuclear translocation of IRF3/7 results in the expression of interferon β (IFN-β) and other interferon-stimulated genes factors (ISGFs). Moreover, TLRs stimulation with the subsequent MyD88-dependent signal transduction results in the expression and

phosphorylation of another transcription factor, NF-κB, indicating the initiation of the "early" NF-κB pathway. [460] The phosphorylated NF-κB protein translocates to the nucleus, where it acts as a transcription factor, regulating the expression of pro-inflammatory effector molecules, including TNF-α, IL-1β, and IL-6. [456] Together with IRF activation, the TRIF-dependent signaling pathway also guides the "late" activation of NF-κB, further emphasizing the convergence of TRIF- and MyD88-dependent pathways. [460] The converging nature of these pathways is elucidated in **Figure 33**.

Overall, the pathway involving TLR activation leading to NF-κB nuclear translocation, regardless of whether it is MyD88- or TRIF-dependent, leads to the expression of cytokines such as TNF-α, IL-6, interleukin 8 (IL-8), IL-1β, and others, but differ in the timing of expression. In this context, the mechanism of transcriptional activation of IL1β is somewhat complicated, because the interleukin-1 receptor (IL-1R) requires MyD88 as an adaptor molecule to transmit signals following IL-1R ligation by IL-1β (**Figure 33**). [461] Therefore, the expression of *IL1β* in cells and tissues that encounter eLNPs presents a challenge in distinguishing the initial TLR-dependent expression of *IL1β* from its subsequent expression self-potentiated by IL-1β binding to IL-1R. Furthermore, at the protein level, post-translational modifications are necessary to activate the inactive form of IL-1β (pro-IL-1β) and release the mature, biologically active form of IL-1β. Proteolytic activation of IL-1β is induced by the enzyme caspase-1 that is activated by the multi-protein complex inflammasome NLRP3, which is assembled in response to TLR activation (**Figure 33**). [462] Once activated, caspase-1 cleaves pro-IL-1β into its mature, active form IL-1β, which can then be secreted by the cell and can exert its pro-inflammatory effects. In summary, the ligation of TLRs with

subsequent activation of different signaling pathways leads to the expression and post-translational activation of cytokines, including IFN-β, IL-6, TNF-α, and IL-1β, which are commonly used as outcome measures to study eLNP-induced reactogenicity.

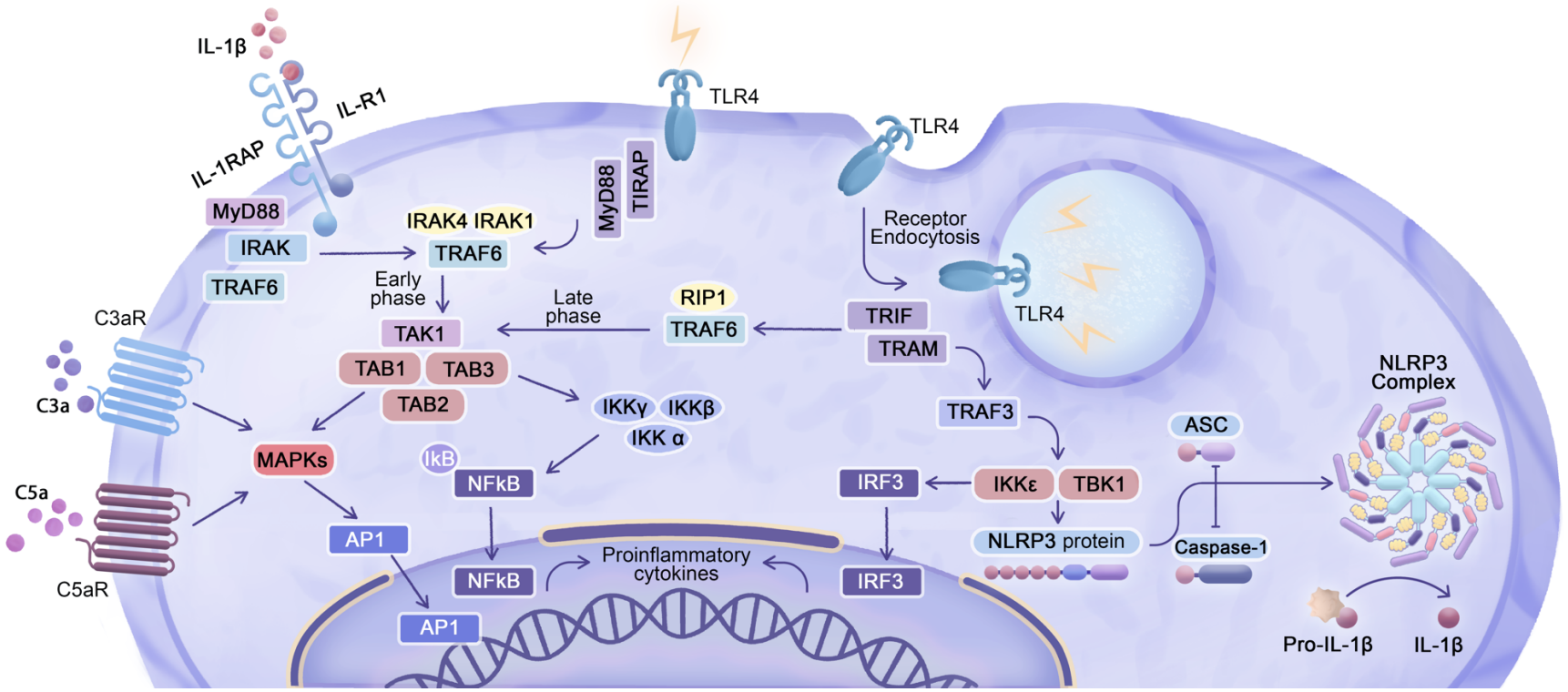

Figure 33. Integration of TLR4 signaling, inflammasome activation, and complement anaphylatoxin receptors in cytokine regulation: Upon TLR4 stimulation on the plasma membrane, a MyD88-dependent pathway is initiated, leading to the phosphorylation of interleukin-1 receptor-associated kinases (IRAKs), particularly IRAK1 and IRAK4. The recruited TNF Receptor Associated Factor 6 (TRAF6) undergoes ubiquitination, facilitating the formation of polyubiquitin chains that recruit transforming growth factor-β-activated kinase 1 (TAK1), TGF-beta activated kinase 1 (MAP3K7) binding protein 1/2/3 (TAB 1/2/3), and inhibitor of nuclear factor-κB kinases (IKKs). These molecules are crucial for activating NF-κB and mitogen-activated protein kinases (MAPKs) signaling. NF-κB translocates to the nucleus, acting as a transcription factor for pro-inflammatory cytokines such as TNF-α, IL-1β, and IL-6. Activation of TLR4 in the endosome triggers a TRIF-dependent pathway, where translocating chain-associating membrane protein (TRAM) serves as an adaptor molecule connecting TLR4 and TRIF. TRAF6, recruited via TRIF, undergoes ubiquitination and interacts with receptor-interacting serine/threonine-protein kinase 1 (RIP1), facilitating the recruitment and activation of IKK for "late" NF-κB activation. Regardless of MyD88 or TRIF dependence, TLR activation induces NF-κB nuclear translocation, resulting in the expression of cytokines such as TNF-α, IL-6, IL-1β, and others, with temporal variations. Additionally, TNF Receptor Associated Factor 3 (TRAF3) interacts

with TRIF and recruits TANK-binding kinase 1 protein (TBK1) and IκB kinase epsilon (IKKε) kinase, which phosphorylate and activate IRF3/7. IRF3/7 translocates to the nucleus, promoting the expression of type I interferons. Post-translational modifications are necessary to activate pro-IL-1β, with caspase-1 and apoptosis-associated speck-like protein containing CARD (ASC) adaptor activation by the NOD-, LRR- and pyrin domain-containing protein 3 (NLRP3) inflammasome complex playing a key role. TRAF3, through IKKε and TBK1, can interact with NLRP3 inflammasome components in certain cellular contexts. Activated IL-1β via interaction with IL-1R can upregulate NF-κB nuclear translocation via a MyD88-dependent mechanism. Furthermore, C3aR and C5aR receptors ligated by C3a and C5a complement anaphylatoxins, lead to activation of AP-1 and NF-κB transcription factors, either by interacting with MAPKs or IKKs, further propagating pro-inflammatory cytokine expression.

The upregulation of pro-inflammatory cytokines in response to eLNP treatment has been studied in both *ex vivo* experiments and *in vivo* murine studies, with results showing increased expression over time and across different proprietary lipid formulations. eLNPs containing Acuitas proprietary lipids were assessed in experiments with *ex vivo* human PBMCs and *in vivo* murine studies. [396, 398] Expression of IL-1β and IL-6 was upregulated in monocytes and increased in a time-dependent manner after treatment with eLNPs. [396] Furthermore, Tahtinen and Alameh showed that eLNP containing SM-102 utilized in the Moderna SARS-CoV-2 vaccine and eLNPs containing Alnylam ionizable lipid led to an increase in IL-1β levels in purified monocytes and draining lymph node lysate, respectively. [398, 399] IL-1β and IL-6 were also increased in the sera of mice treated with eLNPs containing MC3 and YK009 ionizable lipids compared to a control group treated with phosphate-buffered saline (PBS). [392] Furthermore, serum TNF-α in this study was higher in MC3 eLNPs than in mRNA MC3 LNPs in the first 6 hours post-treatment, although no information was provided about dosing considerations of eLNPs in comparison to mRNA LNPs. [392] Interestingly, in contrast to TNF-α, both IL-1β and IL-6 were increased in the eLNP treatment group, similarly to the mRNA-loaded LNP treatment group. [392] Parhiz *et al.* also found that MC3 eLNPs upregulated serum IL-6 expression in mice but were less reactogenic in terms of IL-6 levels compared to C12-200 ionizable lipid-containing eLNPs. [402] In contrast, Tahtinen *et al.* reported that MC3 eLNPs did not change IL-1β levels; however, doses of eLNPs administered to mice were not reported in the study, [399] Sedic *et al.* found no change in IL-6 and TNF-α expression in rats subjected to MC3 eLNPs in comparison to the control group. [395] As highlighted in **Table 8** (Section 5.2), a

selection of representative studies illustrates the range of eLNP doses ranging from 2.5 µg to 50 µg per administration in mice. Therefore, the introduction of standardization in the doses and dosage regimens of eLNPs is crucial for facilitating a comparative evaluation of eLNP reactogenicity. Furthermore, standardization is particularly important for evaluating the safety profile of eLNPs to identify potential adverse reactions and to determine the optimal dose range for clinical use. Since pre-existing inflammation can increase the risk of adverse reactions to eLNPs, utilizing standardized dosing in research settings could help to identify the optimal dose range for minimizing this risk of exacerbating inflammation or inducing further damage to cells and tissues.

Despite the limited availability of data concerning eLNP reactogenicity in inflamed tissues, there is evidence indicating that pre-treatment with lipopolysaccharide (LPS), which is known to induce a TLR4-dependent innate immune response and acute inflammation, exacerbates existing inflammation following subsequent eLNP administration. [402] The exacerbation of inflammation induced by LPS may arise from various factors, such as heightened eLNP internalization or the self-potentiation of chemokine and cytokine expression via parallel or converging reactogenic pathways induced by LPS and eLNP. Furthermore, LPS induces not only peripheral inflammation but also hypothalamic inflammation, thereby introducing a brain axis that leads to the induction of sickness behavior components, such as fatigue, fever, weight loss, decreased food intake and anhedonia. [463-465] These findings emphasize the need to mitigate the reactogenic effects of LNPs to ensure their safe and effective application.

5.6 LNP-inducible expression of cytokines modulating sickness behavior

The physiologic responses to eLNPs include a typical sickness response, consisting of attenuation of food intake and loss of body weight (**Figure 34**). This is driven, at least partially, by the action of pro-inflammatory cytokines on hypothalamic centers regulating appetite and metabolism. Cytokines such as IL-6, IL-1β and TNF-α play a role in the negative regulation of body weight in rodents as part of sickness behavior in response to inflammatory conditions. [466-471] IL-6 is mainly expressed by innate immune cells, such as monocytes, but is also produced by skeletal muscle and adipose tissues and has both pro- and anti-inflammatory effects. [306, 472-474] In terms of body weight regulation, IL-6 exhibits a biphasic effect, where acute increases in IL-6 levels decrease food intake and increase energy expenditure, while chronic increases in IL-6 levels are associated with increased body weight and insulin resistance. [469, 475] IL-1β is produced by a variety of cells, including innate immune cells such as macrophages, monocytes and dendritic cells, and is known to be a potent pro-inflammatory cytokine. [476, 477] Both IL-6 and IL-1β act on the hypothalamus, a key regulatory center in the brain that controls feeding behavior and energy expenditure. [478] IL-6 acts on the hypothalamus to increase the expression of anorexigenic (appetite-reducing) neuropeptides. [479, 480] Although IL-1β increases the expression of orexigenic (appetite-stimulating) neuropeptides, such as neuropeptide Y (NPY) and agouti-related protein (AgRP), its potent induction of hypothalamic inflammation leads to a reduction in food intake and consequent decrease of body weight. [481, 482]

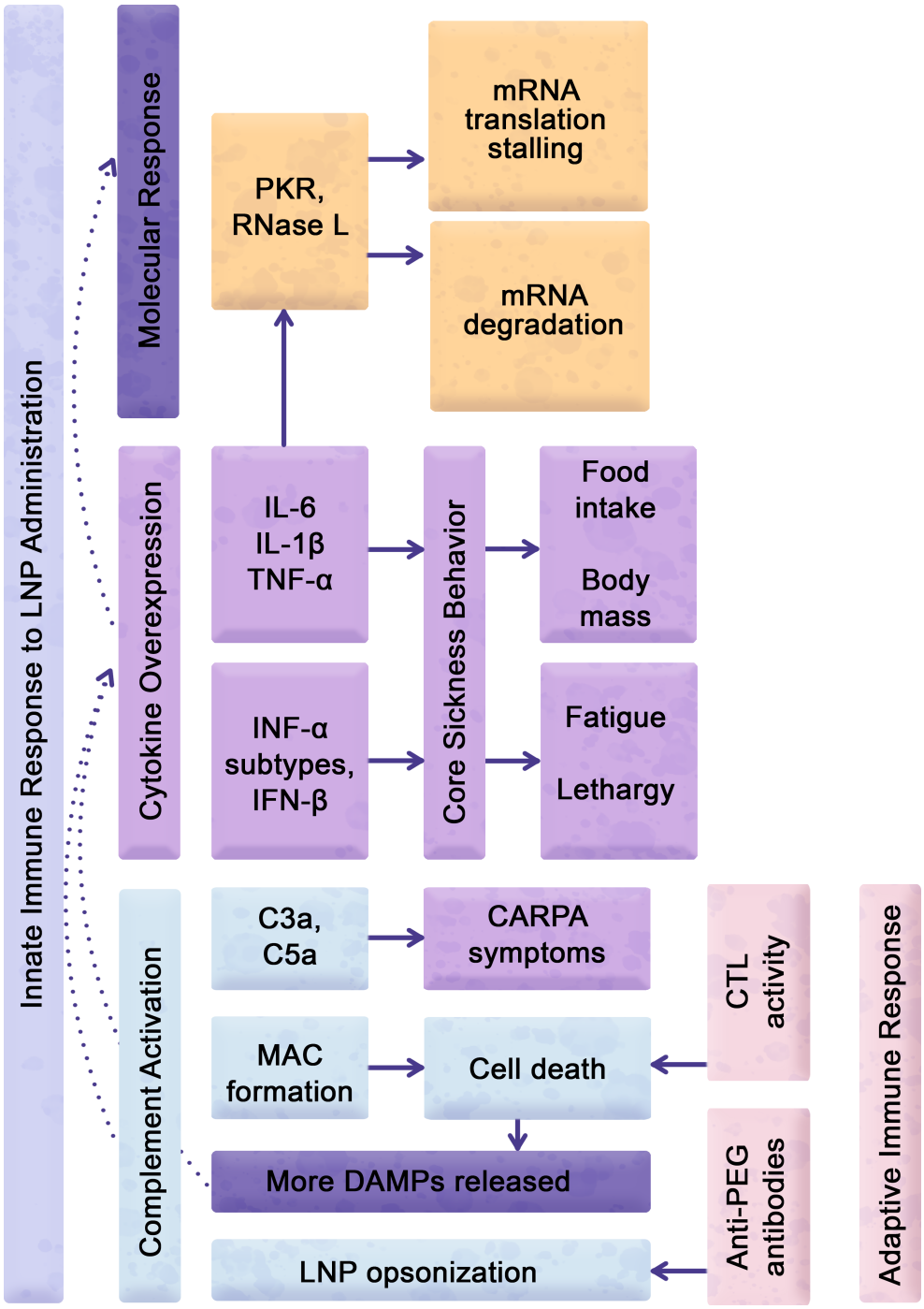

Figure 34. Mechanistic insights into reactogenic manifestations and therapeutic challenges in LNP administration: Complex mechanisms underlie reactogenic manifestations of LNP administration. Cytokine expression, including IL-6, IL-1B, TNF-a, and interferons, initiate core sickness behaviors such as decreased food-motivated behaviors, fatigue, and lethargy. Concurrent LNP-dependent complement activation can result in CARPA symptoms, including anaphylaxis, chills, headache, and cardiopulmonary distress. Moreover, complement activation-dependent MAC formation potentially eliminates cells actively internalizing LNPs, leading to the release of DAMPs signals and further cytokine expression. CTLs also contribute to removing cells presenting LNP-

related antigens from the treated cell pool. Complement opsonization of LNPs, along with anti-PEG antibodies, may further increase systemic and local reactogenicity by sequestering particles and reduce their therapeutic efficacy. Additionally, activated PKR and RNase L enzymes can hinder mRNA translation or degrade the mRNA therapeutic payload, further decreasing therapeutic efficacy.

The findings suggest that the increased levels of IL-6 and IL-1β induced by eLNPs lead to decreased body weight through the modulation of hypothalamic function. IL-6 and IL-1β were shown to be increased on both mRNA and protein levels in mice treated with eLNPs containing non-disclosed proprietary ionizable lipids. [370] Importantly, IL-6 and IL-1β overexpression were also associated with a decrease in murine body weight. [370] Of note, the authors also observed high mortality at the 10 μg eLNP dose delivered intranasally in this study, with just 20% survival on day 1 post-treatment. [370] Therefore, the observed weight reduction could be due to TLR-dependent septic shock involving cytokine storm with possible overexpression of IL-6, IL-1β, and TNF-α, as discussed in. [483] Importantly, the results of studies utilizing MyD88/Trif KO mice administered mRNA LNP injections suggest that MyD88/Trif dual KO mice did not exhibit weight loss. [440] These findings suggest that effector molecules produced due to the LNP activation of Trif- or MyD88-dependent reactogenic pathways play a pivotal role in inducing sickness behavior. Therefore, incorporating food intake and body weight as key indicators of systemic reactogenicity in the routine evaluation of eLNP is crucial, as they not only form an integral part of sickness behavior, but are also paramount in assessing the efficacy and safety of LNP therapies for conditions that afflict patients' frailty, such as cancer and other chronic diseases.

Together with a decrease in food-motivated behavior, fatigue is an important indicator of the severity of the reactogenic insult (**Figure 34**). Type I and II interferons play a critical role in developing disease-associated and iatrogenic fatigue syndromes.

[484-489] Hence, the assessment of interferons expression holds significant importance due to their role in causing symptomatic reactogenic manifestations, including fatigue, in response to mRNA LNP formulations. This is particularly relevant in the context of SARS-CoV-2 vaccine administration, where fatigue is a frequent side effect. [490, 491] The role of interferons, along with other pro-inflammatory cytokines, is considered significant in both localized and systemic inflammation and the development of fever. [492] Type I interferons, including IFN-α subtypes and IFN-β, are expressed as part of the pro-inflammatory cascade induced by unmodified mRNA acting on TLR 3, 7, 9 and eLNPs acting on TLR2 or TLR4. [396, 493, 494] Interferon-gamma (IFN-γ) or type II interferon has lower pro-inflammatory potency and is important for the induction of adaptive immunity against intracellular pathogens. [495] Liang *et al.* reported that, in comparison to mRNA-loaded LNPs, eLNPs do not increase Type I IFN-inducible myxovirus resistance gene A (MxA) expression that is used as a marker for the induction of endogenous type I interferons. [394] However, protein levels of IFNα and IFNγ were significantly increased after 24 h of Acuitas eLNP stimulation. [396] Connors also reports that eLNPs induced increased levels of phosphorylated IRF7, leading to the expression of ISGs. [396] Although there is a slight increase in IRF7 activation when TLR4 is ligated, significant activation only occurs when TLR7 or TLR9 are engaged, such as in the case of an LNP-encapsulated payload of nucleic acids acting on these receptors. [494]

5.7 Reactogenicity interference with translation of mRNA delivered by LNP carriers

The immune response triggered by the injection of mRNA LNP formulations can result in the downregulation of protein translation from the delivered mRNA, which limits the efficacy of mRNA-based therapies (**Figure 34, Section 5.6**). [496, 497] The production of pro-inflammatory effector molecules downregulates expression of the delivered mRNA through various mechanisms, including the inhibition of translation initiation and the degradation of mRNA. [19, 498] The immune system may recognize the eLNP carriers or eLNP structural components as a threat and mount an immune response, even in the absence of an mRNA payload. Significantly, compelling evidence suggests that mRNA LNP formulations exhibit a substantial abundance of eLNPs that lack the incorporation of any therapeutic payload. [391] Hence, it is imperative to explore the reactogenic effects of eLNP, which may trigger immune responses and ultimately diminish mRNA expression, in order to ensure optimal protein expression.

The delivery of mRNA using LNPs was observed to result in reduced mRNA translation when mice were simultaneously exposed to mild doses of LPS. [497] This finding holds significance as LPS are capable of binding to TLR4 and eLNPs are speculated to have the same tropism to this receptor. Lokugamage *et al.* further showed that administering a TLR4 inhibitor increased mRNA translation; however, it did not fully restore it to the levels observed in the absence of LPS treatment. [497] Importantly, the reduction in mRNA expression was not attributed to a decline in the particle endocytosis or endosomal escape of LNPs, but rather to the action of RNA-dependent protein kinase R (PKR) subsequent to TLR4 ligation. PKR, which reduces mRNA translation in

the cell, is an intermediary component downstream of TLR signaling that, upon its activation, phosphorylates eukaryotic initiation factor 2 (eIF2). [364, 499, 500] This phosphorylation event prevents the recruitment of the initiator transfer RNA (tRNA) to the ribosome and activation of eIF2 by binding to guanosine triphosphate (GTP), thereby inhibiting the initiation of translation. [500-503] Furthermore, one of the innate immune mechanisms by which effector molecules such as TNF-α, IL-1 family cytokines, type I IFNs, and other pro-inflammatory cytokines can inhibit translation initiation is by controlling phosphorylation of the alpha subunit of eIF2, eIF2α. [503, 504] Consequently, the initial event of TLR4 ligation, along with the subsequent expression of downstream molecules such as TNF-α, members of the IL-1 family, and type I interferons, contributes to the decreased expression of both therapeutic mRNA and the entire pool of mRNA within the cell, as part of a reactogenic outcome.

In addition to inhibiting translation initiation, cytokines can also induce the degradation of mRNA molecules (**Figure 34**). One mechanism by which this occurs is through the activation of ribonuclease L (RNase L), an enzyme that degrades mRNA in response to exogenous nucleic acid insults such as those arising from viral infection. [505] The activation of RNase L by pro-inflammatory cytokines can lead to both viral and host mRNA degradation, thereby reducing the overall level of mRNA available for translation. [506, 507] Moreover, pro-inflammatory cytokines can activate signaling pathways that lead to the induction of cell death, which also contributes to the downregulation of mRNA expression by the cells actively internalizing mRNA LNP formulations. [508] Despite the low-reactogenicity modified mRNA formulations used in clinical practice, [365, 366] the use of LNP carriers may still cause reactogenic

manifestations and subsequently lead to cytokine-dependent downregulation of mRNA expression.

The reduction in exogenous mRNA expression can be further modulated by activating complement and adaptive immunity by removing the cells internalizing mRNA LNPs. Activation of the complement pathway by LNPs can initiate the formation of membrane attack complexes (MACs), which often inflict cellular damage. The formation of MACs as a result of activation through classical, mannose-binding lectin, and properdin-mediated complement pathways [509] not only poses a direct threat to the targeted cells but can also impact the uptake and internalization of LNP formulations, leading to a decrease in their therapeutic effectiveness.

Furthermore, PEG incorporated into the LNP coating induces anaphylactoid, complement activation-related pseudoallergy (CARPA) rection. [510, 511] CARPA is a harmful immune reaction triggered by the activation of the complement system, leading to adverse symptoms and potentially life-threatening complications in response to certain medications or therapeutic agents. [512] In their study, Ndeupen *et al.* put forth the hypothesis that PEGylated lipids present in LNPs may elicit CARPA in individuals who possess preexisting PEG-specific antibodies. These antibodies could arise from the previous administration of mRNA LNP formulations, including SARS-CoV-2 vaccines. [370] Of significant importance, extensive evidence exists regarding the activation of the adaptive immune system by LNP delivery, resulting in the generation of antibodies against immunogenic LNP components, including the formation of anti-PEG antibodies. [513, 514]

Furthermore, the activation of cytotoxic T lymphocytes (CTLs) cells and their accumulation in draining lymph nodes adjacent to the xenobiotic injection site can lead to the destruction of the cells, such as APCs that have taken up the LNPs containing immunogenic components (**Figure 34**). Consequently, CTLs can facilitate an increase in the clearance of PEGylated LNPs, thereby causing a further decrease in the expression of the delivered mRNA. The actions of CTLs are indeed advantageous in therapeutic approaches that utilize mRNA LNPs as cancer vaccines. The delivery of therapeutic mRNA LNPs can lead to the expression of novel antigens in cancer cells, potentiated by a triggered immune response. [515] However, this approach may be counterproductive in mRNA therapeutics aimed at applications beyond the elimination of diseased cells. These immune responses highlight the immunogenic potential of LNPs bridging to reactogenic manifestations and emphasize the need for careful evaluation and monitoring of immune reactions in LNP-based therapeutic applications.

5.8. Reactogenicity interference with multiple injections of LNP formulations

Similar to the immune system's ability to interfere with mRNA translation after a single injection, there is growing apprehension regarding the possibility of decreased mRNA expression in response to repeated administrations or after prior exposure to mRNA LNP formulations. This phenomenon can be attributed to the recognition of the LNP delivery system as a foreign entity by the adaptive immune system, leading to an immediate immune response that may result in mRNA degradation prior to its translation into proteins. As the utilization of mRNA vaccines and therapeutics continues to expand, it is imperative to gain a comprehensive understanding of the potential long-term ramifications that may arise from repeated administrations. If repeated injections or

pre-exposure to LNPs leads to a decrease in mRNA expression, it could impact the efficacy of these treatments and may require changes to dosing, dosage or delivery methods. Therefore, understanding the potential risks associated with repeated administration of mRNA LNPs is important to improve the safety and efficacy of mRNA-based therapies.

Despite the limited amount of research on the pre-exposure to mRNA LNP formulations decreasing mRNA expression, the available evidence suggests that there are significant implications and thus a need to understand its impact. In a study aiming to express an mRNA-encoded antigen, Qin *et al.* reported that pre-exposure to eLNPs or mRNA-loaded LNPs decreased the response in terms of both antibody production and germinal center B cell expansion. [400] Further, upon administering mRNA LNPs repeatedly, there was an observed transition in LNP distribution from the liver to the spleen after the third successive injection. [516] This observation was attributed to increased internalization of LNPs by splenic APCs, possibly recognizing the protein corona surrounding LNPs. Additionally, exposure of LNPs to plasma from LNP-immunized mice revealed the enhancement of immunoglobulins attached to the protein corona encircling the LNPs. [516] In line with prior research, the opsonizing immunoglobulins detected in this study included antibodies against PEG. [516] These findings again suggest that the LNP carriers themselves, and not the mRNA payload, play a crucial role in the immune elimination of mRNA LNP formulations. Of note, the physical characteristics of LNPs and their interactions with serum proteins can be altered by employing diverse ionizable lipid components, leading to variations in LNP accumulation across different tissues, such as liver, spleen, and lung. [517] Hence, the

redistribution of LNPs following multiple injections may depend on the composition of the LNPs themselves.

In addition to stimulating adaptive immunity, pre-exposure to LNP formulation can also alter the innate immune response that could aggravate mRNA elimination, decreasing its expression. For instance, the use of BNT162b2 mRNA LNP formulation as a vaccine resulted in the upregulation of pro-inflammatory and IFN-stimulated genes such as chemokine CXCL10 and cytokine IL6 in monocytes. [518] These effects were more pronounced after the booster vaccination with BNT162b2 than after the initial vaccination. [518] Despite these findings, mRNA LNP-based vaccines continue to play a crucial role in the ongoing battle against the SARS-CoV-2 pandemic, and their success provides a foundation for developing novel and innovative mRNA LNP formulations for the treatment of various other diseases.

5.9 Chapter summary

In **Chapter 5** of my dissertation, I investigate reactogenicity induced by mRNA LNP formulations, focusing on the impact of eLNPs. The in-depth literature review in this chapter highlights how reactogenic outcomes stem from the LNPs themselves and not necessarily the payload, such as mRNA cargo, and delves into the components within eLNPs that induce reactogenic and immunogenic responses.

The main theses of the chapter are outlined below:

1) The reactogenicity, a result of the immune system's response to the structural components of LNPs, notably ionizable lipids and PEG-lipids, introduces various unfavorable effects, including headaches, fevers, fatigue, and inflammation at the injection site.

2) Innate immune cells, particularly macrophages and neutrophils, are central to the complex molecular interactions, orchestrating critical reactions that influence the therapeutic efficacy and safety of LNP-based therapeutics.
3) On the molecular level, TLR signaling pathways and complement cascade activation play essential roles in modulating reactogenic manifestations in response to LNPs. They can converge, leading to overexpression of key pro-inflammatory chemokines and cytokines.
4) Reactogenic symptoms triggered by LNP formulations are driven by the expression of pro-inflammatory cytokines, including IL-6, IL-1β, and TNF-α, which are tightly regulated by NF-κB, IRF3, and IRF7 transcription factors.
5) Administration of eLNPs leads to increased production of pro-inflammatory cytokines, particularly IL-6 and IL-1β, which are associated with reduced body weight due to their influence on hypothalamic function and can result in symptoms of sickness, including decreased food intake, locomotor activity, and reduced grooming behavior in mice.
6) mRNA LNP formulations can trigger an immune response that not only suppresses protein translation from the delivered mRNA but also initiates complement activation, elicits adaptive immune reactions against LNPs, including anti-PEG antibody formation, and promotes cytotoxic T lymphocyte (CTL)-mediated LNP clearance, raising potential implications for therapeutic applications.
7) There is growing concern about the potential for reduced mRNA expression following repeated administrations of mRNA LNP formulations or prior exposure

to these formulations, which could be attributed to the adaptive immune system's recognition of LNPs as foreign entities, leading to an immediate immune response.

In conclusion, in **Chapter 5** of my dissertation, I underscored the significance of assessing reactogenicity in eLNP formulations and their components, emphasizing the need for comprehensive preclinical safety studies. I explored the pivotal roles played by innate immune cells, the complement cascade, and TLR signaling pathways in modulating reactogenic manifestations, ultimately contributing to a deeper understanding of the safety of LNP-based drug delivery systems. In pursuit of **Objective 2.1**, I conducted a comprehensive review of the existing literature to explore the role of TLRs and their associated adaptor proteins in recognizing LNPs, laying the foundation for my subsequent investigation into the role of TLR4 and TRIF/MyD88 adaptors in the initiation and amplification of reactogenic responses. Importantly, I identified that the involvement of TLR4 in eLNP-dependent reactogenicity, although suspected, was never formally studied. Recognizing this gap, I investigated this aspect in **Chapter 6** of my dissertation.

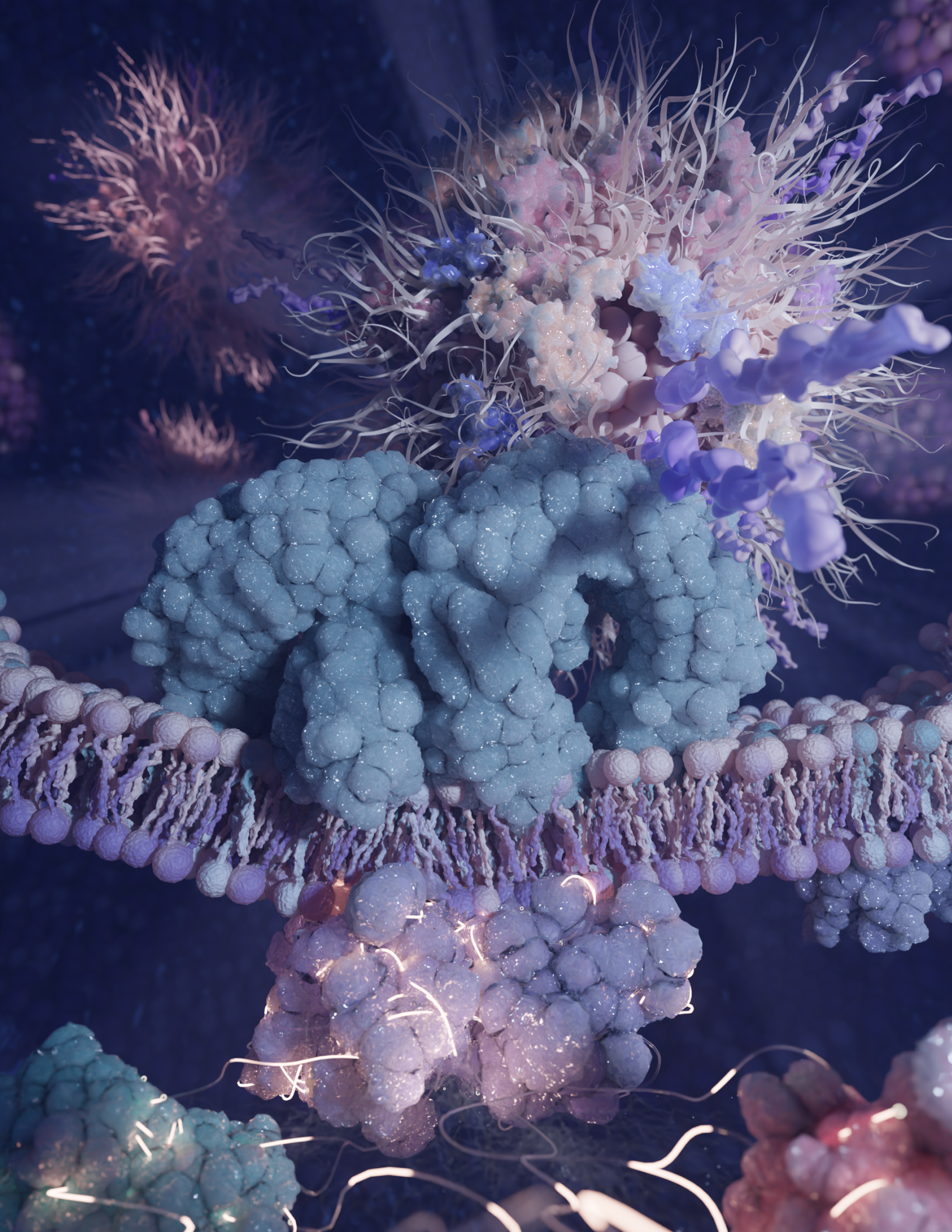

Chapter 6. Ionizable lipids modulate lipid nanoparticle biodistribution and reactogenic profile

6.1 Probing reactogenicity mechanisms for safer mRNA LNP formulations

The development of messenger RNA (mRNA) vaccines demonstrates the power of mRNA therapeutics in preventing infectious diseases. [519, 520] The therapeutic action of mRNA is accomplished through lipid nanoparticle (LNP)-mediated transport of messenger RNA molecules that are translated into proteins inside cells. [521] mRNA LNP vaccines promote immunity via the immunogenic properties of antigen proteins synthesized from exogenous mRNA. While immunogenicity is an expected characteristic of some mRNA LNP formulations, such as mRNA vaccines, their reactogenicity results in suboptimal therapeutic outcomes and adverse effects, including pain, fever, chills, and fatigue. [352, 369, 370, 522, 523] The adverse effects of mRNA LNP vaccine formulations as part of their reactogenicity profile are known to affect patients' decisions about vaccination and adherence to immunization schedules. [524] Vaccine hesitance and partial immunization were linked to SARS-CoV-2 vaccine side

effects and response severity after the initial dose. [525] While some suggest that reactogenicity, when not affecting mRNA expression, could enhance the adaptive immune response in mRNA vaccines intended for infectious disease control and vaccinology, it is generally considered undesirable for mRNA LNP formulations designed for purposes beyond infections, such as those for protein replacement and supplementation.

Co-administration of cyclooxygenase (COX) inhibitors or dexamethasone can alleviate certain reactogenicity-related symptoms following mRNA LNP administration. However, this transient immunosuppression does not address the concerns related to decreased vaccine potency caused by mRNA degradation or reduced mRNA translation due to translational stalling, which are also consequences of the reactogenicity of the administered formulations. [526] Even in the context of a single mRNA vaccine administration, where an adaptive immune response is a foremost goal, innate immune responses initiate mRNA degradation and diminish mRNA translation to immunizing protein. [527, 528] Notably, these manifestations are not dependent on mRNA as a sole reactogenic species.

Reactogenic and immunologic responses to LNP components, including polyethylene glycol (PEG) and ionizable lipids, are observed to reduce the expression of therapeutic mRNA. [529, 530] Moreover, the LNP vehicle's adjuvanticity and pro-inflammatory characteristics are hypothesized as probable causes of SARS-CoV-2 mRNA vaccines' side effects, as opposed to the immunological responses induced by the translated immunogen. [370] Importantly, ionizable lipids cause inflammation characterized by the expression of signature pro-inflammatory cytokines, including

interleukin 1B and 6 (IL-1B, IL-6), and chemokines, such as chemokines CC motif ligand 2 and 4 (CCL2, CCL4), and chemokines (C-X-C motif) ligand 2 and 10 (CXCL2, CXCL10). [370] Although the precise mechanism by which LNPs initiate the chemokine-cytokine cascade has yet to be determined, ionizable lipids as part of LNPs activate the immune system via binding to toll-like receptors (TLR). [527, 531, 532] Activation of toll-like receptor 4 (TLR4) is implicated in the production of cytokines associated with the inflammation-driven adverse effects of LNP formulations but also in diminishing mRNA expression delivered by LNP carriers. [529] While it is established that concurrent TLR4 activation decreases mRNA LNP efficacy by reducing mRNA expression, it remains unknown whether LNPs themselves activate TLR4 signaling.

Since TLR4 adaptor proteins are gatekeepers to the expression of multiple cytokines, including IL-1B, IL-6, tumor necrosis factor-alpha (TNF-α), and lipocalin-2 (LCN2), as well as secretion of type I interferons, deconvolution of the complex pathways downstream of TLR4 is important for improving mRNA LNP reactogenicity profiles. It is well established that distinct adaptors promote TLR4 dimerization in different cell compartments. The adaptor protein myeloid differentiation primary response 88 (MyD88) is required for TLR4 dimerization on the plasma membrane, whereas the adaptor protein TIR-domain-containing adapter-inducing interferon-β (TRIF) dimerizes TLR4 in the endosomal compartment, as reviewed in [533, 534]. Differential TLR4 dimerization and association with distinct adaptor proteins could provide insights into whether LNPs activate TLR4 on the plasma membrane or inside the endosome, revealing the preferred pathway of reactogenic signal propagation.

In addition to investigating the role of TLR4 and its adaptors in LNP-induced reactogenicity, a gap exists in understanding the physiologically relevant innate immune responses triggered by empty LNP (eLNP) vehicles activating TLR4. Therefore, our work described in this chapter focuses on animal sickness behavior as a measurable physiological response to acute or chronic inflammation, elucidating TLR4 downstream signaling leading to sickness outcomes induced by LNP administration. We establish that the activation of TLR4 by an eLNP formulation induces distinct physiological responses in mice. Moreover, our findings highlight the indispensable role of the MyD88 adaptor protein in the development of sickness behavior triggered by LNP administration in mice.

6.2 Dosing strategies for induction of murine sickness behavior

To enhance LNP formulation safety, we aimed to distinguish immune responses triggered by eLNPs from those induced by mRNA cargo. Although therapeutic considerations often treat mRNA cargo and LNP vehicles as a combined entity, it is essential to recognize the unique contribution of eLNPs in initiating and amplifying reactogenic manifestations. [526] This understanding is crucial to supplement existing safety measures applied for mRNA, such as the incorporation of pseudouridine substitutions, currently employed in mRNA vaccines. [364]

For the purpose of investigating eLNP reactogenicity, we carefully selected the eLNP formulation, administration route (intraperitoneal (IP) injection over intravenous (IV) or subcutaneous (SQ)), dose, and dosage regimens to systematically investigate eLNP-dependent reactogenicity in mice. For candidate LNP formulation synthesis, we maintained a composition ratio of 50:38.5:10:1.5 for key LNP components, including the

ionizable lipid, cholesterol, DSPC, and DMG-PEG-2k. In our examination of ionizable lipids, we investigated DLin-MC3-DMA (MC3), ALC-0315, and SM-102, all integral to FDA-approved LNP formulations. [164, 351, 379] Ensuring purity, subsequent dialysis effectively eliminated small contaminants, yielding eLNP batches with sizes between 58nm and 84nm and a polydispersity index (PDI) ranging from 0.064 to 0.098. To validate our administration approach, we used *luciferase* (*Luc*) mRNA LNPs to monitor the biodistribution of each formulation, distinguished by the ionizable lipid they incorporated. We used the same composition ratio of 50:38.5:10:1.5 for the *Luc* mRNA LNP preparation described above, in addition to the nitrogen to phosphate (N:P) ratio of 5.67 between ionizable lipids and nucleic acid.

While the intravenous (IV) administration route provided the most signal in the liver (**Figure 35 A**) from ALC-0315-containing LNPs, the IP administration route demonstrated superior liver distribution for MC3 and SM-102-containing LNPs (**Figure 35 B**). Conversely, the subcutaneous (SQ) administration route (**Figure 35 C**) resulted in minimal liver localization of LNPs, with most of the signal originating from draining lymph nodes (data not shown). Peritoneal lavage samples after IP administration exhibited bioluminescence due to innate cell infiltration to the peritoneum (**Figure 35 D**).

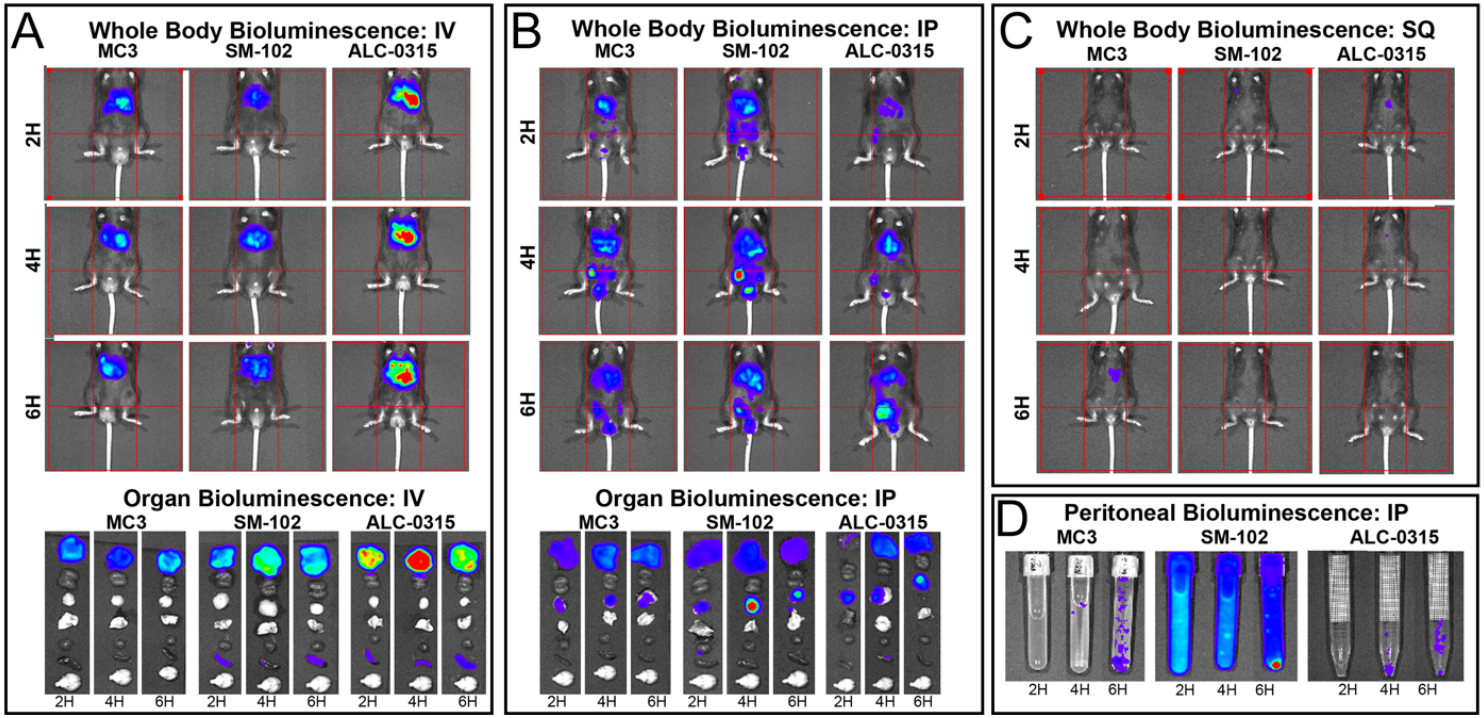

Figure 35. Biodistribution study using *Luc* mRNA LNP formulations for optimizing administration strategies to study reactogenic manifestations in LNP formulations. Representative bioluminescence images of WT mice injected with Luc mRNA LNP formulation at 2, 4, 6 hours following IV **(A)**, IP **(B)**, SQ **(C)** administration routes for three LNP formulations, containing MC3, SM-102, ALC-0315 ionizable lipids. **(D)** Bioluminescence signal from peritoneal lavage samples following administration of MC3-, SM-102, and ALC-0315-containing Luc mRNA LNPs at 2, 4, 6 hours post-injection.

The quantitative summary of bioluminescence signals from the whole body and livers is presented in **Figure 36 E** for IV and IP administrations.

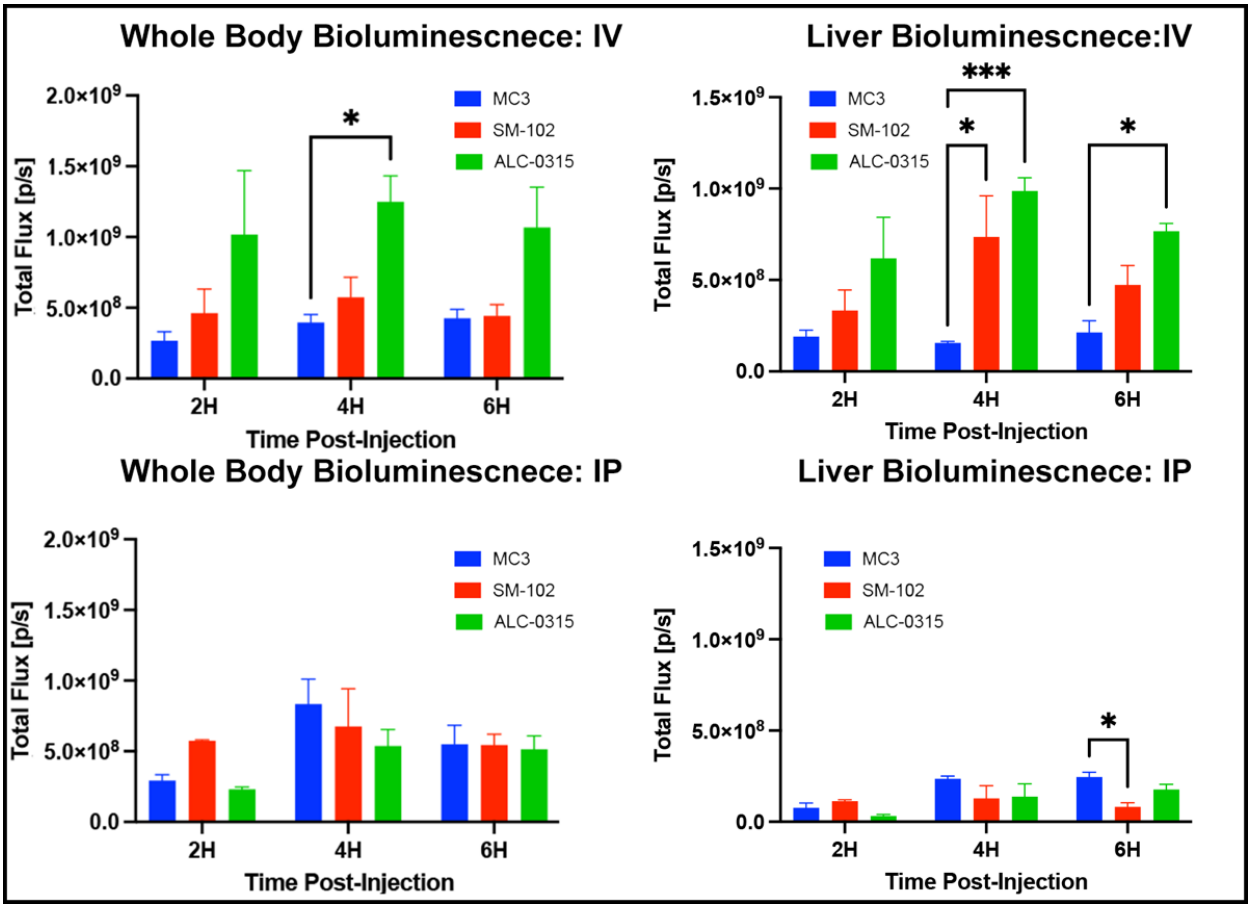

Figure 36. Quantitative assessment of bioluminescence from the expressed luciferase protein. Quantitative assessment of whole-body and liver bioluminescence following IV and IP administrations of Luc mRNA LNP formulations. Expressed as mean ± SEM, n=5, *p<0.05, **p<0.01, ***p<0.001 analyzed by two-way ANOVA followed by Bonferroni's *post hoc* test.

Notably, SQ administration appeared to be the most reactogenic route of Luc mRNA LNP administration. Although SQ administration appeared to induce increased reactogenicity in the liver for some, but not all, reactogenicity markers after a single eLNP administration, this effect is likely attributed to the delayed onset of reactogenic manifestations (**Figure 37A**). This delay is a result, at least in part, of the additional time

required for *Luc* mRNA LNPs to reach the liver when administered SQ. This is particularly evident in the expression levels of cytokines that are promptly downregulated after immune induction, such as *Il1B* and *Il6* for IV and IP administrations (**Figure 37 A**). Therefore, their apparent expression is lower in IV and IP administration routes, compared to SQ. Furthermore, we normalized hepatic reactogenic markers in the mice receiving IV formulations to the relative counts of *Luc* mRNA in liver samples (**Figure 37 B**) to satisfy the assumption of comparable liver targeting efficiency among all three tested nanoparticles delivered via IV administration. Interestingly, *Luc* mRNA LNPs containing MC3 demonstrated the most pronounced hepatic reactogenic outcome as evidenced by elevated levels of *Il1b*, *Tnf*, *Il6*, *Orm1*, and *Cxcl10* (**Figure 37 C**).

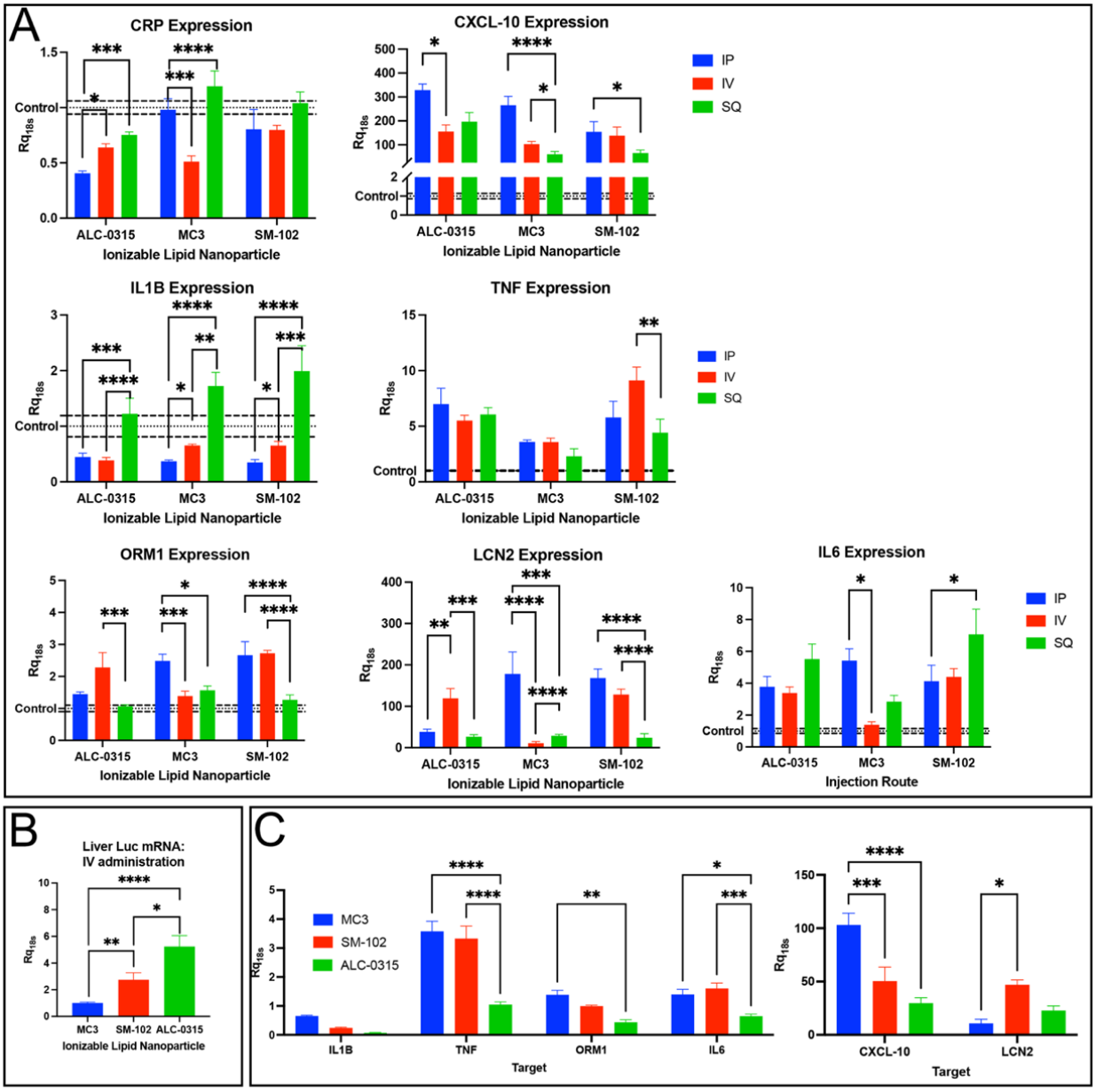

Figure 37. Expression of innate immunomodulatory components following single Luc mRNA LNP administration in WT mice: (A) Hepatic pro-inflammatory gene expression following administration (IP, IV, SQ) of ALC-0315, MC3 and SM-102 containing Luc mRNA LNPs, assessed 6 hours post-injection. Expressed as mean ± SEM, n=5, **p*<0.05, ***p*<0.01, ****p*<0.001, *****p*<0.0001; analyzed by two-way ANOVA followed by Bonferroni's *post hoc* test. (B) Relative quantification of Luc mRNA delivered to mice via IV administration of three Luc mRNA LNP formulations. Expressed as mean ± SEM, n=5, **p*<0.05, ***p*<0.01, *****p*<0.0001 analyzed by one-way ANOVA followed by Bonferroni's *post hoc* test. (C) Innate effector protein expression in liver samples from the mice subjected to IV *Luc* mRNA LNP administration normalized to *Luc* mRNA as a measure of transfection efficiency.

We observed that Luc mRNA LNPs with SM-102 ionizable lipid efficiently recruited various innate immune cells to the peritoneal cavity, leading to luciferase expression upon transfection, and those with ALC-0315 exhibited minimal innate cell recruitment to the peritoneal compartment (**Figure 35 D and Figure 38**). Therefore, we chose MC3 LNPs for formulating eLNPs for subsequent studies. This decision was driven by a balanced distribution of luciferase signal following Luc mRNA LNPs administration containing MC3 ionizable lipid, recruiting cells to the peritoneum while effectively directing the formulation to the liver after IP injection.

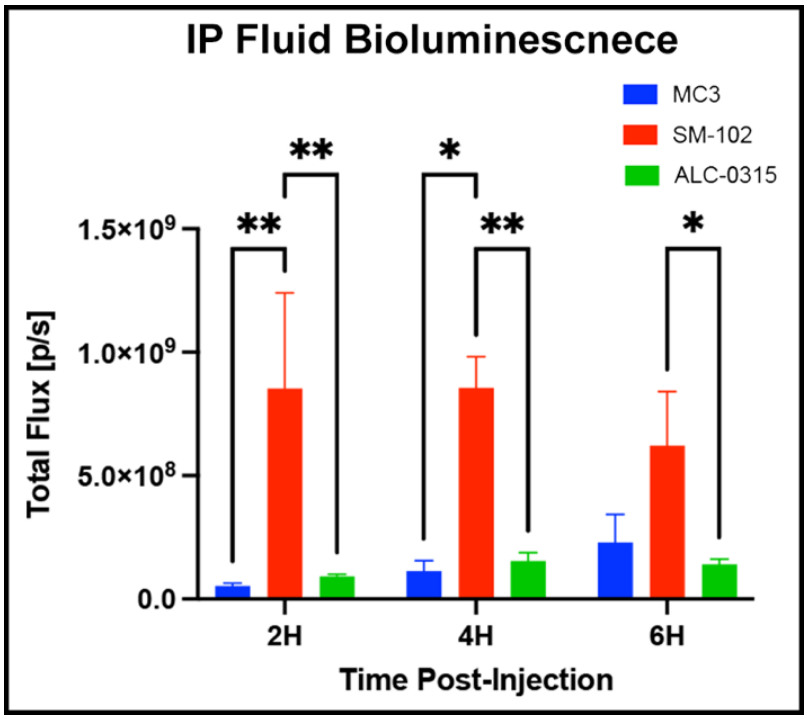

Figure 38. Quantification of peritoneal lavage bioluminescence following IP Luc mRNA LNP administration using three Luc mRNA LNP formulations. Quantitative assessment of peritoneal lavage samples following IP administrations of Luc mRNA LNP formulation. Expressed as mean ± SEM, n=5, *p<0.05, **p<0.01, analyzed by two-way ANOVA followed by Bonferroni's *post hoc* test. Statistically significant difference is displayed only for intra group analysis for each of three described time points (2, 4 and 6 hours).

We then employed fluorescence-assisted cell sorting (FACS) to study subpopulations of innate immune cells driven to the peritoneum following Luc mRNA LNP administration via IP injection. ALC-0315 did not induce significant cell infiltration to the peritoneum, resembling the cell proportions observed after PBS injection (**Figure 39 A**). On the other hand, SM-102 LNPs recruited considerably higher numbers of macrophages and neutrophils, while MC3 LNPs predominantly recruited lymphocytes. Furthermore, MC3 LNPs resulted in a moderate increase in chemokine expression and exhibited comparable expression levels of cytokines and chemokines relative to ALC-0315 LNPs (**Figure 39 B**).

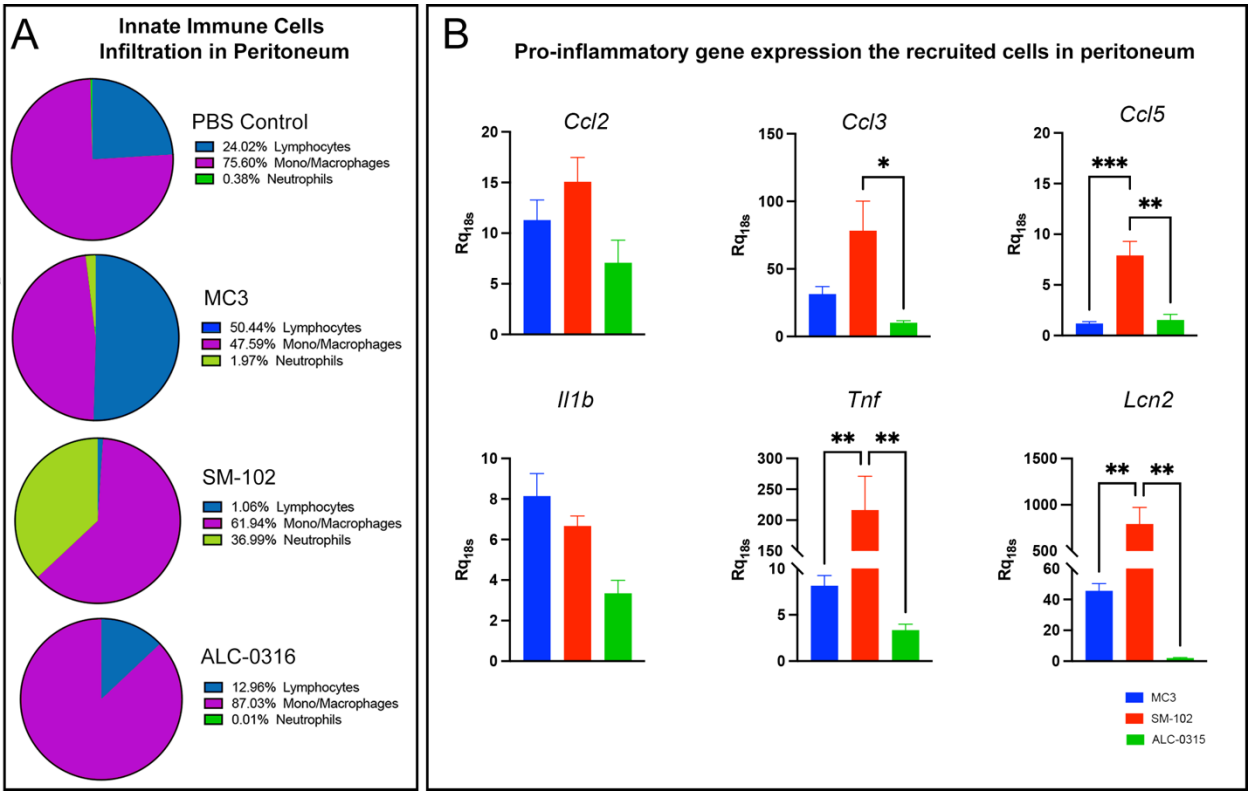

Figure 39. Optimizing administration strategies to study reactogenic manifestations in LNP formulations. (A) Innate immune cell populations in peritoneal lavage samples following IP administrations of Luc mRNA LNP formulations. Expressed as a proportion of total cells. (B) Relative gene expression in peritoneal lavage samples following IP administrations of Luc mRNA LNP formulations, normalized to PBS-treated mice whose expression is equal to one. Expressed as mean ± SEM, n=5, *p<0.05, **p<0.01, ***p<0.001 analyzed by one-way ANOVA followed by Bonferroni's *post hoc* test.

Furthermore, we explored various eLNP doses and dosing regimens with the aim of finding a delicate balance between sufficiently stimulating the immune system and avoiding a fulminant immune response. Our objective was to induce reactogenicity for both quantitative and qualitative assessment while mitigating the risk of severe immune responses, such as the overexpression of immune effector molecules that could set off a positive feedback loop and potentially lead to sepsis in mice. Three eLNP formulations were assembled simultaneously with at least one batch of LNPs containing Luc mRNA in order to compare and scale LNP constituents' concentrations (**Figure 39**). eLNP and mRNA-containing LNPs were then assessed using nanoparticle tracking analysis (NTA) to ensure equivalent concentration of particles in the carrier solution (PBS).

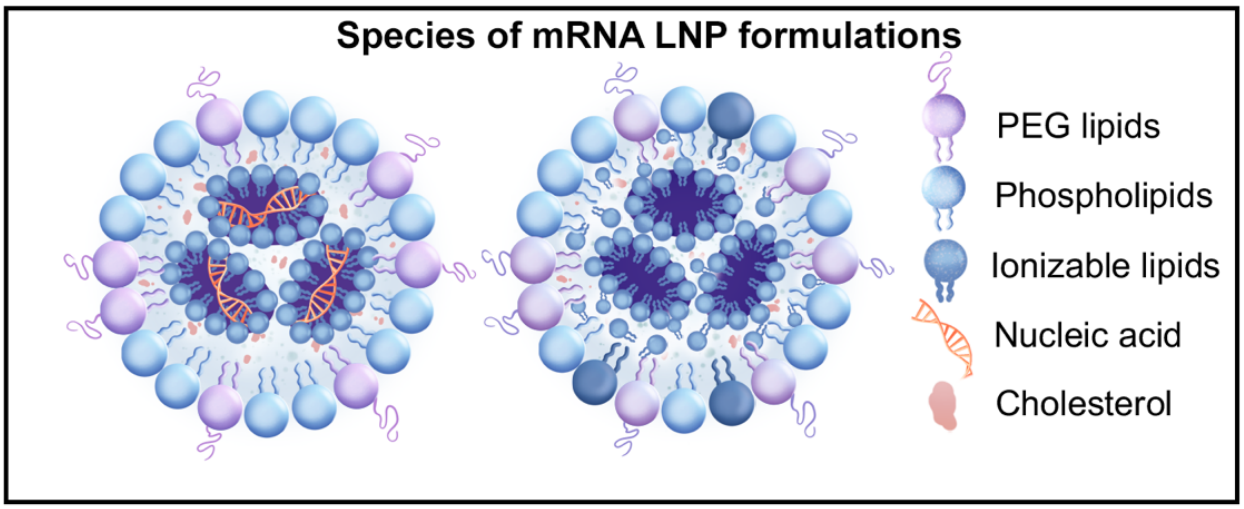

Figure 39. Schematic representation of mRNA LNPs and eLNPs. Illustration of eLNP and mRNA-loaded LNP structure, emphasizing the arrangement and components. It is important to note that certain ionizable lipids in eLNP may exhibit a less organized configuration due to the absence of electrostatic interactions with mRNA molecules.

After thorough investigations, we chose to administer eLNP doses equivalent to 5 μg of *Luc* mRNA LNPs per mouse, delivering the eLNPs in phosphate-buffered saline (PBS). Moreover, we implemented two distinct dosage regimens to assess both acute and chronic reactogenic outcomes of eLNP administration. After the initial induction of the immune response, there is a well-established pattern of downregulating pro-inflammatory genes. [535, 536] This process is crucial to acknowledge, as a failure to assess local immune response induction at the correct time could erroneously imply the absence of an immune response. Notably, in the case of chronic administration, involving three daily IP injections, the downregulation of pro-inflammatory markers induced by MC3 eLNPs was not as profound as observed with SM-102 and ALC-0315 eLNPs (**Figure 40**). Furthermore, the localized initiation of an immune response, notably in the liver due to the pronounced hepatic tropism of LNPs, requires thorough evaluation. Typically, inflammation spreads systemically even after subsiding locally. Consequently, a prompt response occurs in the central nervous system (CNS), including the hypothalamus, triggering behavioral responses in animal models. [537] This includes sickness behavior induction in mice, involving decreased food intake, locomotion, and grooming behaviors. [538] Therefore, by utilizing both single and three consecutive daily injections, we aimed to evaluate reactogenic responses to eLNPs after acute and chronic stimulation.

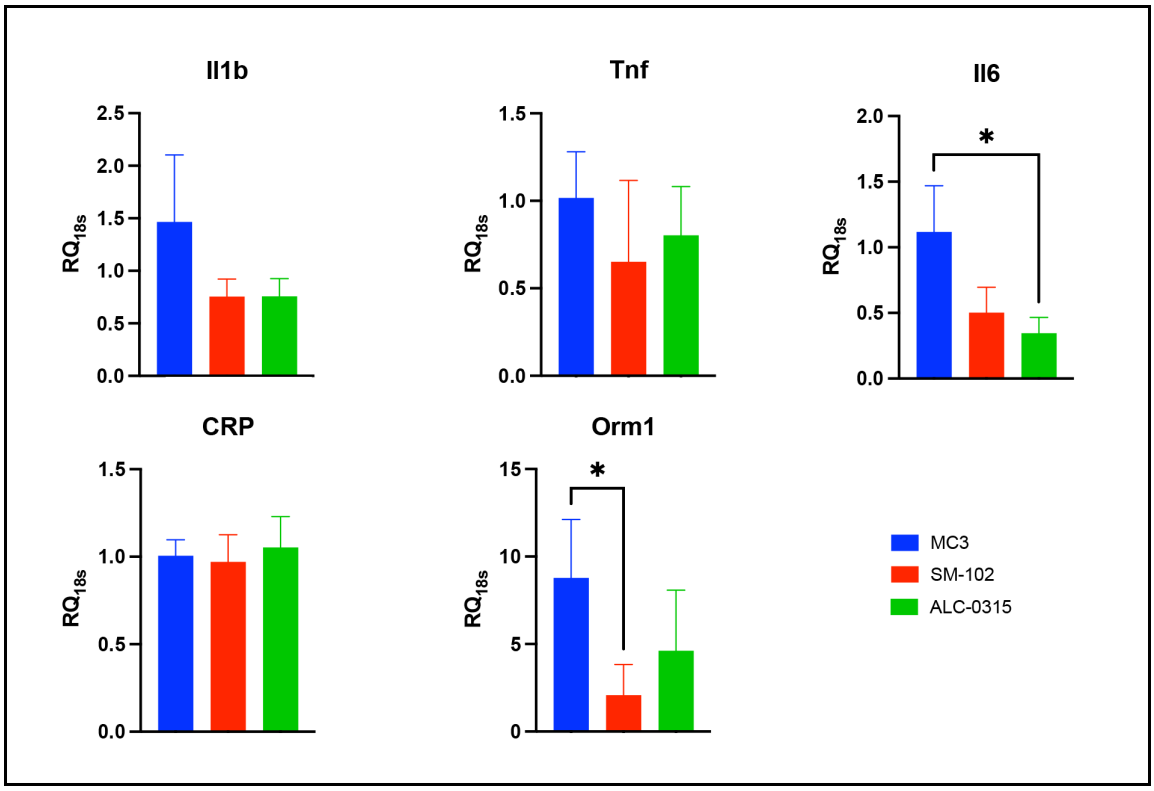

Figure 40. Expression of cytokine and acute-phase proteins in response to chronic administration of eLNPs containing three ionizable lipids. Hepatic relative gene expression following chronic IP administration of Luc mRNA LNP formulations, normalized to the expression in PBS-treated mice, whose expression is equal to one. Expressed as mean ± SEM, n=5, *p<0.05, **p<0.01, ***p<0.001 analyzed by one-way ANOVA followed by Bonferroni's *post hoc* test.

Ultimately, three chronic administrations of the eLNP formulations enabled the evaluation of physiological responses, particularly sickness-induced anorexia resulting in reduced body weight (**Figure 41**). Our findings revealed that eLNPs containing MC3 induced the most significant decrease in body weight compared to those containing ALC-0315 and SM-102. This observation aligns with the sustained upregulation of pro-inflammatory genes in the liver observed with MC3 eLNPs (refer to **Figure 40**).

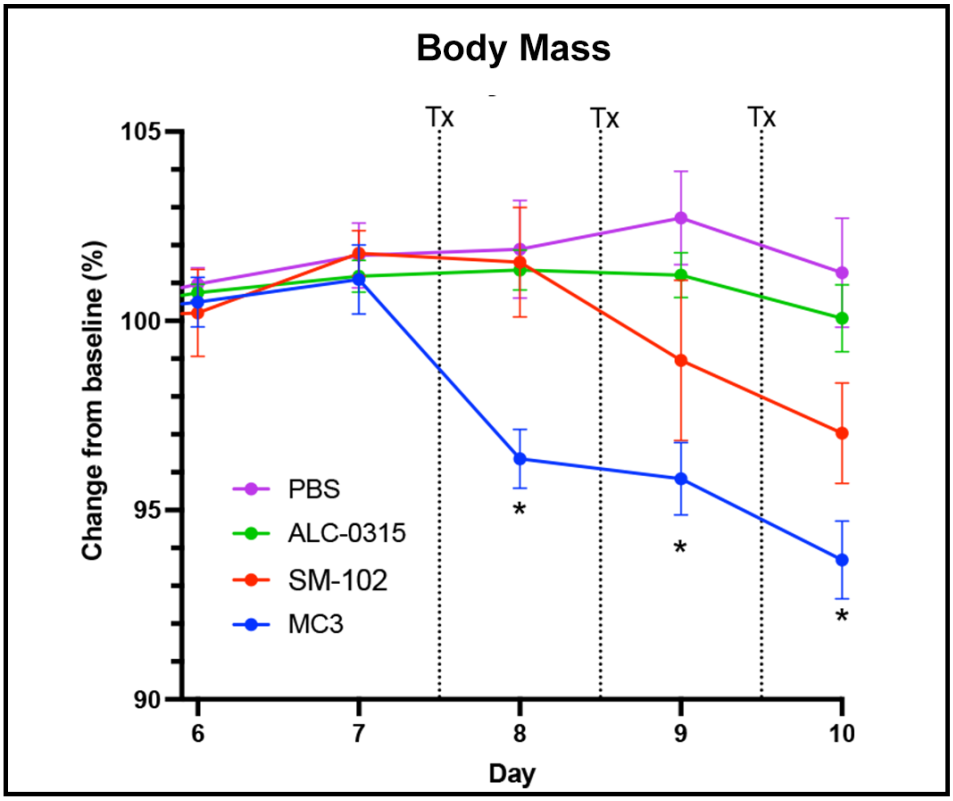

Figure 41. MC3-containing eLNP formulation led to the most profound body weight loss following three chronic injections. Body weight assessment following eLNP formulations chronic administration. Expressed as mean ± SEM normalized to baseline, n=5, *p<0.05 analyzed by two-way repeated measures ANOVA.

For further investigation of eLNP-induced reactogenicity mechanism, we selected IP injection over IV or SQ routes to streamline our experimental approach. This decision aligns with our strategy to compartmentalize LNPs within the peritoneal cavity while directing them to the liver. Our IP administration approach not only ensured controlled responses and localized hepatic inflammation but also facilitated experiments by allowing easy separation of extravasating cells through simple peritoneal lavage for subsequent analysis, including FACS. Moreover, in an effort to achieve a balance between effectively stimulating the immune system for physiological changes (especially in light of the minimal physiological changes with the ALC-0315 eLNP formulation) and preventing an overly intense localized molecular response (as

observed with the SM-102 eLNP formulation), we chose to administer doses of MC3-containing eLNPs equivalent to 5 μg of Luc mRNA LNPs per mouse via intraperitoneal (IP) injection. While acknowledging the potential limitations of generalizing findings from a single eLNP formulation to the overall reactogenicity of LNP formulations, we emphasize the structural similarities among ionizable lipids and other LNP components, as well as the consistency in the methods employed for LNP preparation described in previous chapters. These similarities suggest the potential relevance of our observations to a broader spectrum of LNP formulations.

6.3 Involvement of toll-like receptor adaptors in eLNP-induced reactogenicity

In our investigation of TLR4 involvement in eLNP-induced reactogenicity (**Figure 42 A**), we initiated the investigation with MyD88 and TRIF, toll-like receptor adaptors essential for downstream signal propagation. Utilizing genetic ablation studies targeting MyD88 and TRIF, allowed us to address fundamental questions regarding their roles in reactogenic propagation following toll-like receptors activation. Additionally, these studies provided a platform for further inquiries, such as whether LNPs interact with TLR4 on the plasma membrane or within endosomes. This distinction is significant because MyD88 serves as an adaptor protein for TLR4 when it is located on the plasma membrane. However, when TLR4 undergoes changes in dimerization due to pH changes in the maturing endosome, MyD88 is replaced by TRIF. Regardless of the location of the adaptor association, the absence of MyD88 or TRIF prevents the propagation of signals downstream of TLR4 in the membrane or in the endosome, respectively. Therefore, our approach with genetic ablation studies helps elucidate the

specific involvement of these adaptors and sheds light on the dynamics of TLR4 interaction with eLNPs in different cellular compartments.

In our experimental setup, we included MyD88 knock-out (MyD88 KO), TRIF knock-out (TRIF KO), and wild-type (WT) mice, all of which shared a C57Bl/6 background (**Figure 42 B**). We subjected each genotype group to either a single injection or three consecutive daily injections, allowing us to assess both acute and chronic reactogenic manifestations to eLNPs. Tissues were harvested 6 hours after the last injection for all groups.

Given that food intake and body weight are robust indicators of an animal's sickness response, we utilized these metrics to observe how mice responded to the three consecutive daily injections of eLNPs (**Figure 42 C**). Notably, deletion of MyD88 completely normalized food intake and body weight to the pre-injection baseline. However, both WT mice and TRIF KO mice exhibited a decrease in both parameters. Using food intake reduction as a sensitive method to detect ongoing sickness in mice, we observed no significant difference between WT and TRIF KO mice. However, there was a statistically significant difference between these two groups and MyD88 KO mice. These findings underscore the specific influence of MyD88, but not TRIF, on the sickness response in mice following eLNP injections.

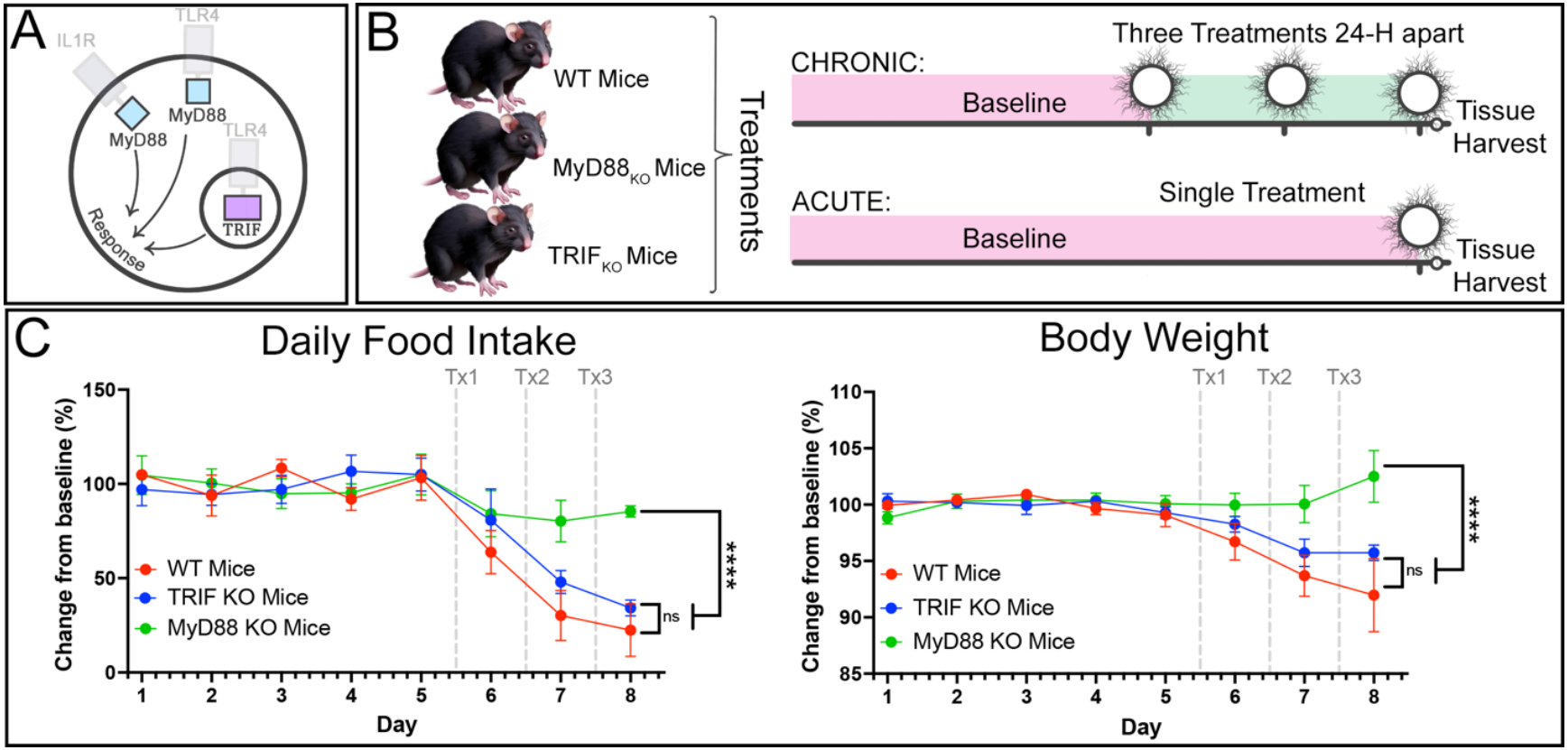

Figure 42. Physiological response to eLNP administration shows the adaptor protein MyD88 to be necessary for reactogenic signal transduction following eLNP administration. (A) Schematic representation of TLR4 interactions with MyD88 and TRIF adaptors, emphasizing proteins of interest for the current section. **(B)** Methodologic approach using genetic ablation to study acute and chronic reactogenic manifestations in WT, MyD88 KO and TRIF KO mice. Percent change in **(C)** Food intake and body weight following MC3 eLNP chronic administration in WT, MyD88 KO and TRIF KO mice. Expressed as mean ± SEM normalized to baseline, n=5, ****p<0.0001 analyzed by two-way repeated measures ANOVA

Given the pronounced tropism of LNPs for the liver, we next focused on assessing the expression of hepatic inflammatory genes to investigate the primary site of immune response induction (**Figure 43**). Notably, *Il1B* and *Tnf* exhibited a more significant upregulation in WT and TRIF KO mice in comparison to MyD88 KO mice, particularly under acute administration conditions. *Il6* showed a slight upregulation in WT and TRIF KO mice, but no apparent increase was observed in MyD88 KO mice (data not shown). Lipocalin 2 (*Lcn2*), a marker of propagating inflammation expressed by neutrophils and endothelial cells, demonstrated robust and sustained upregulation in WT and TRIF KO mice. *Lcn2* levels were also elevated during chronic administration compared to the acute phase in these groups. Conversely, in MyD88 KO mice, *Lcn2* expression remained at the similar levels as control MyD88 KO mice treated with PBS after single injection (5-fold increase). A non-significant increase (74-fold increase, p=0.3102, **Table 9**) was observed only after chronic injections, yet it remained approximately seven times lower compared to WT and TRIF KO animals.

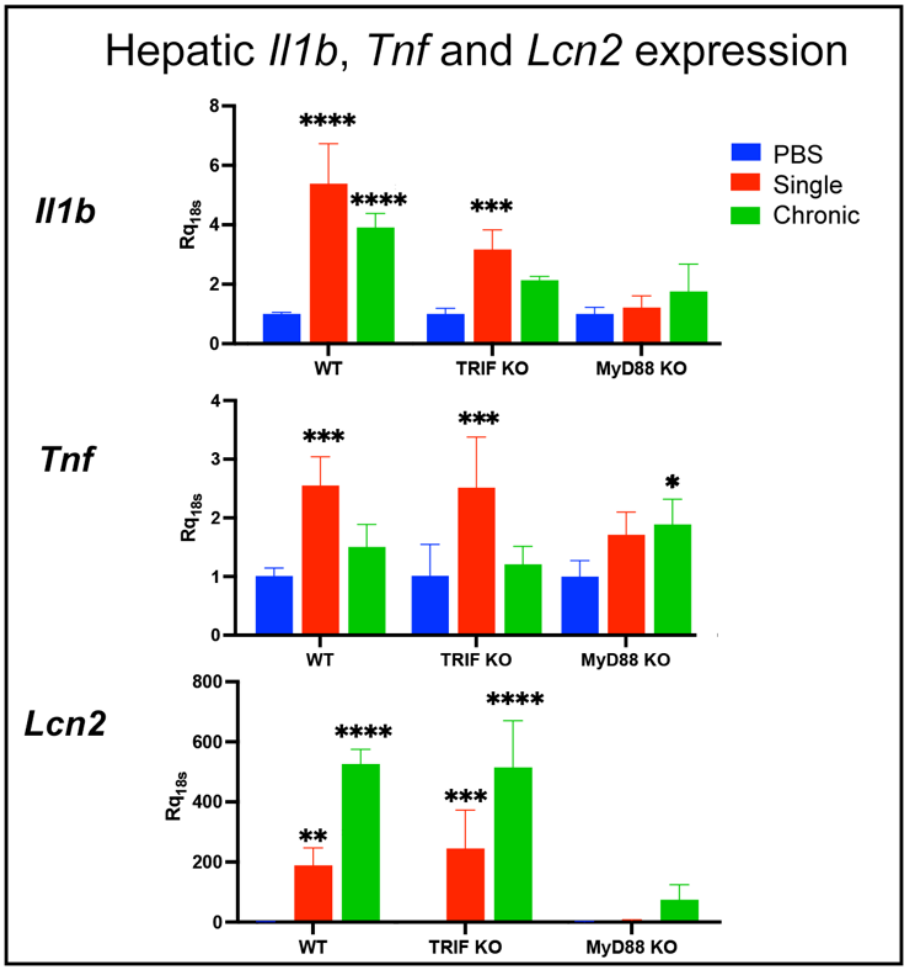

Figure 43. Hepatic pro-inflammatory gene expression in MyD88 KO, TRIF KO and WT mice following eLNP administrations. Relative gene expression in MyD88 KO, TRIF KO, WT murine livers at the baseline (PBS, and after single and chronic MC3 eLNP injections. Expressed as mean ± SEM, n=5, **p*<0.05, ***p*<0.01, ****p*<0.001, *****p*<0.001 analyzed by two-way ANOVA followed by Bonferroni's *post hoc* test. Statistical significance is exclusively illustrated within each genotype group relative to the PBS treatment with additional information provided in **Table 9**.

Table 9. Statistical significance in multiple comparisons following gene expression analysis using two-way ANOVA.

Two-way ANOVA for *Il1b* expression

Bonferroni's multiple comparisons test	Predicted (LS) mean diff.	95.00% CI of diff.	Below threshold?	Summary	Adjusted P Value
MyD88 KO					
Acute vs. Chronic	-0.5420	-1.640 to 0.5562	No	ns	0.6576
Acute vs. PBS	0.2150	-0.9262 to 1.356	No	ns	>0.9999
Chronic vs. PBS	0.7570	-0.2732 to 1.787	No	ns	0.2154
TRIF KO					
Acute vs. Chronic	1.038	-0.1652 to 2.241	No	ns	0.1095
Acute vs. PBS	2.171	0.8716 to 3.470	Yes	***	0.0006
Chronic vs. PBS	1.133	-0.1661 to 2.433	No	ns	0.1039
WT					
Acute vs. Chronic	1.473	0.2697 to 2.676	Yes	*	0.0126
Acute vs. PBS	4.381	3.082 to 5.680	Yes	****	<0.0001
Chronic vs. PBS	2.908	1.609 to 4.208	Yes	****	<0.0001
Acute					
MyD88 KO vs. TRIF KO	-1.956	-3.159 to -0.7533	Yes	***	0.0009
MyD88 KO vs. WT	-4.167	-5.370 to -2.964	Yes	****	<0.0001
TRIF KO vs. WT	-2.210	-3.413 to -1.007	Yes	***	0.0002
Chronic					
MyD88 KO vs. TRIF KO	-0.3766	-1.475 to 0.7216	No	ns	>0.9999
MyD88 KO vs. WT	-2.152	-3.250 to -1.054	Yes	****	<0.0001
TRIF KO vs. WT	-1.775	-2.978 to -0.5725	Yes	**	0.0024
PBS					
MyD88 KO vs. TRIF KO	-0.0003141	-1.243 to 1.242	No	ns	>0.9999
MyD88 KO vs. WT	-0.0007808	-1.243 to 1.242	No	ns	>0.9999
TRIF KO vs. WT	-0.0004667	-1.390 to 1.389	No	ns	>0.9999

Two-way ANOVA for *Tnf* expression

Bonferroni's multiple comparisons test	Predicted (LS) mean diff.	95.00% CI of diff.	Below threshold?	Summary	Adjusted P Value
MyD88 KO					
Acute vs. Chronic	-0.1790	-0.8846 to 0.5265	No	ns	>0.9999
Acute vs. PBS	0.7108	-0.02616 to 1.448	No	ns	0.0616
Chronic vs. PBS	0.8898	0.1842 to 1.595	Yes	**	0.0098
TRIF KO					
Acute vs. Chronic	1.308	0.4842 to 2.132	Yes	**	0.0011
Acute vs. PBS	1.505	0.6149 to 2.395	Yes	***	0.0005
Chronic vs. PBS	0.1967	-0.6932 to 1.087	No	ns	>0.9999
WT					
Acute vs. Chronic	1.044	0.2196 to 1.868	Yes	**	0.0095
Acute vs. PBS	1.540	0.6504 to 2.430	Yes	***	0.0004
Chronic vs. PBS	0.4968	-0.3932 to 1.387	No	ns	0.5003
Acute					
MyD88 KO vs. TRIF KO	-0.8055	-1.587 to -0.02381	Yes	*	0.0417
MyD88 KO vs. WT	-0.8393	-1.621 to -0.05769	Yes	*	0.0321
TRIF KO vs. WT	-0.03388	-0.8578 to 0.7901	No	ns	>0.9999
Chronic					
MyD88 KO vs. TRIF KO	0.6817	-0.07044 to 1.434	No	ns	0.0859
MyD88 KO vs. WT	0.3833	-0.3689 to 1.135	No	ns	0.6169
TRIF KO vs. WT	-0.2984	-1.122 to 0.5255	No	ns	>0.9999
PBS					
MyD88 KO vs. TRIF KO	-0.01141	-0.8624 to 0.8395	No	ns	>0.9999
MyD88 KO vs. WT	-0.009808	-0.8608 to 0.8412	No	ns	>0.9999
TRIF KO vs. WT	0.001605	-0.9498 to 0.9530	No	ns	>0.9999

Two-way ANOVA for *Lcn2* expression

Bonferroni's multiple comparisons test	Predicted (LS) mean diff.	95.00% CI of diff.	Below threshold?	Summary	Adjusted P Value
MyD88 KO					
Acute vs. Chronic	-69.07	-180.2 to 42.10	No	ns	0.3758
Acute vs. PBS	4.498	-111.6 to 120.6	No	ns	>0.9999
Chronic vs. PBS	73.56	-37.60 to 184.7	No	ns	0.3102
TRIF KO					
Acute vs. Chronic	-270.4	-400.2 to -140.5	Yes	****	<0.0001
Acute vs. PBS	243.9	103.7 to 384.1	Yes	***	0.0004
Chronic vs. PBS	514.2	374.0 to 654.5	Yes	****	<0.0001
WT					
Acute vs. Chronic	-337.6	-467.4 to -207.8	Yes	****	<0.0001
Acute vs. PBS	187.9	47.71 to 328.1	Yes	**	0.0059
Chronic vs. PBS	525.5	385.3 to 665.7	Yes	****	<0.0001
Acute					
MyD88 KO vs. TRIF KO	-239.4	-362.6 to -116.3	Yes	****	<0.0001
MyD88 KO vs. WT	-183.4	-306.6 to -60.28	Yes	**	0.0021
TRIF KO vs. WT	55.98	-73.84 to 185.8	No	ns	0.8467
Chronic					
MyD88 KO vs. TRIF KO	-440.7	-559.2 to -322.2	Yes	****	<0.0001
MyD88 KO vs. WT	-452.0	-570.5 to -333.5	Yes	****	<0.0001
TRIF KO vs. WT	-11.28	-141.1 to 118.5	No	ns	>0.9999
PBS					
MyD88 KO vs. TRIF KO	-0.01447	-134.1 to 134.1	No	ns	>0.9999
MyD88 KO vs. WT	-0.003078	-134.1 to 134.1	No	ns	>0.9999
TRIF KO vs. WT	0.01140	-149.9 to 149.9	No	ns	>0.9999

When administering LNP formulation, including mRNA cargo, we noted an increase in *Il1b*, *Tnf*, *Il6*, and *Lcn2* levels in MyD88 KO mice after a single administration of *Luc* mRNA LNPs (**Figure 44**). In contrast, WT mice demonstrated relatively lower levels of these markers, likely due to either a prior significant overexpression followed by signal dampening or a potential compensatory mechanism in MyD88 KO and TRIF KO mice, leading to substantial overexpression of these cytokines. Additionally, our observation underscores the importance of alternative innate defense mechanisms triggered by mRNA cargo, activating a distinct subset of innate immunity receptors beyond those requiring MyD88 and TRIF adaptors, such as RIG (Retinoic Acid-Inducible Gene) and MDA5 (Melanoma Differentiation-Associated protein 5). [539]

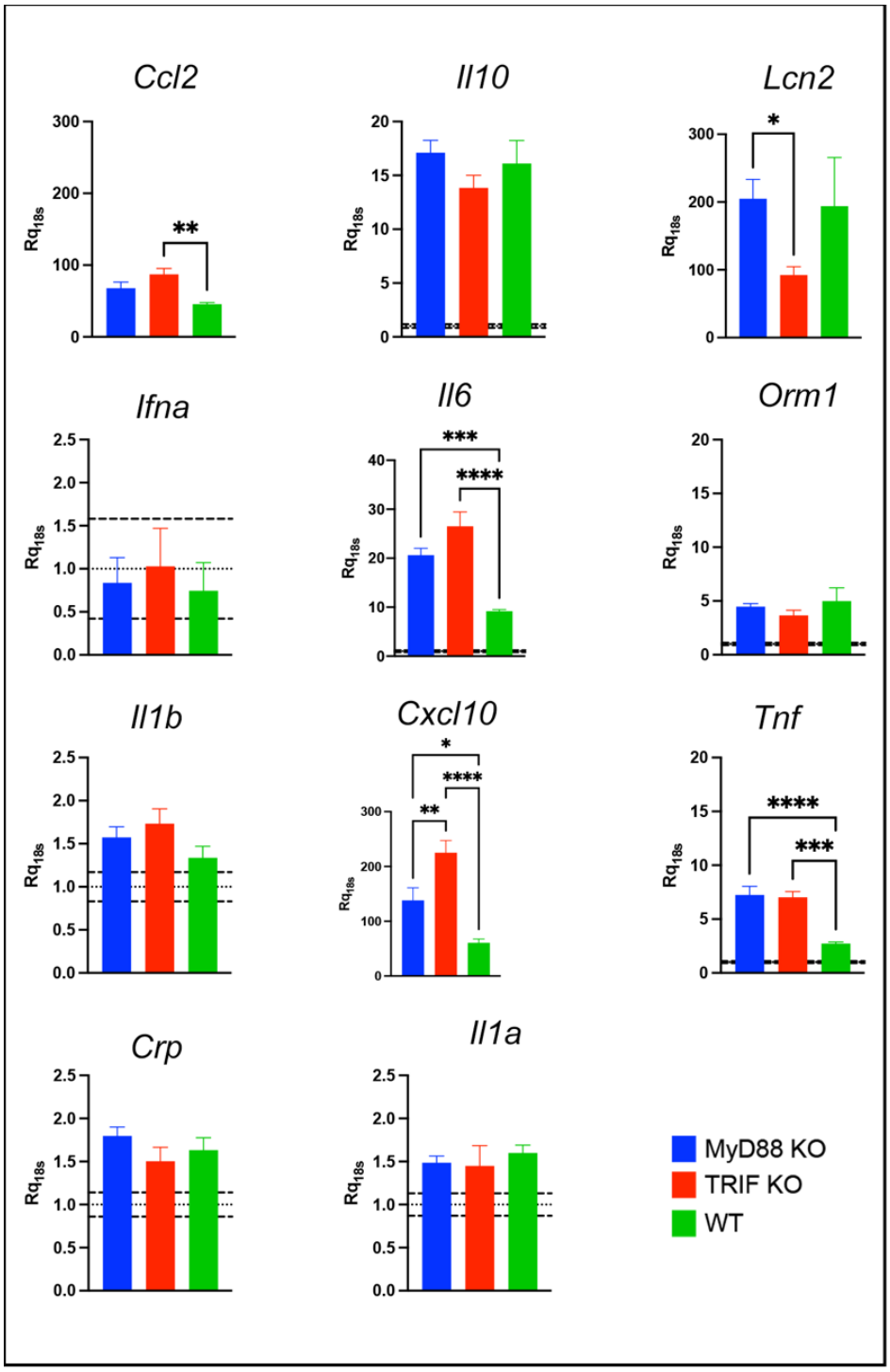

Figure 44. MyD88 is dispensable in propagating reactogenicity associated with intact mRNA LNP formulation, as evident by increased pro-inflammatory gene expression in MyD88 KO mice. Relative gene expression in MyD88 KO, TRIF KO, WT murine livers following Luc mRNA LNP administration. Expressed as mean ± SEM, n=5, **p*<0.05, ***p*<0.01, ****p*<0.001, *****p*<0.001 analyzed by one-way ANOVA followed by Bonferroni's *post hoc* test. Intragroup significance compared to PBS, normalized to a relative expression equals to 1 ± SEM within each genotype.

Despite increased levels of pro-inflammatory cytokines in MyD88 and TRIF KO mice, these animals exhibited increased quantities of *Luc* mRNA delivered by LNPs relative to WT control mice, which implies that the activation of MyD88- and TRIF-dependent reactogenic pathways by both mRNA cargo and LNP vehicles may diminish the efficacy of mRNA LNP therapeutics (**Figure 45**). The observed increase in *Luc* mRNA levels in MyD88 KO mice may be attributed to the influence of eLNP-induced reactogenicity via MyD88-dependent pathways. This underscores the essential task of disentangling reactogenic responses induced by eLNPs from mRNA-dependent manifestations, particularly those induced by activation of TLR3, TLR7 in mice and TLR8 in humans that require MyD88 and TRIF adaptors. [540]

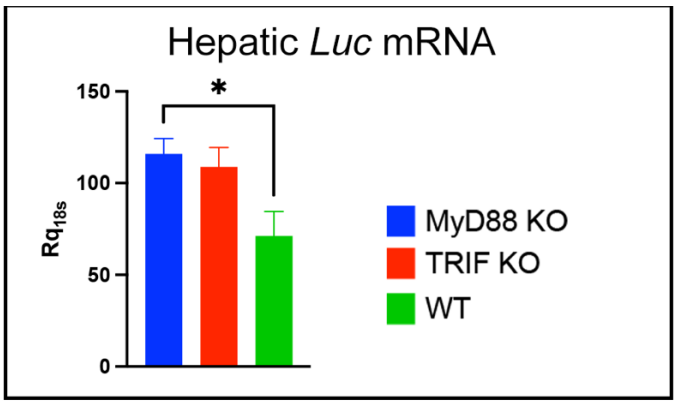

Figure 45. MyD88 KO mice exhibit increased levels of hepatic Luc mRNA. Relative abundance of Luc mRNA in MyD88 KO, TRIF KO, WT murine livers. Expressed as mean ± SEM, n=5, *p<0.05, analyzed by one-way ANOVA followed by Bonferroni's *post hoc* test.

Next, we assessed serum levels of pro-inflammatory cytokines. Following a single eLNP injection, serum IL-1B levels were undetectable; however, they increased in WT and TRIF KO mice after three chronic injections. Serum IL-1B was elevated in WT mice and increased to an even greater extent in TRIF KO mice (**Figure 46 A**). IL-1B was undetectable after single and chronic injections in MyD88 KO mice. Interestingly, IL-1B levels were higher in TRIF KO mice compared to WT mice. TNF-alpha levels were

below the limit of quantification in the serum of all three groups for both administration approaches (data not shown). Serum LCN2 levels in WT animals increased from 100 to almost 1000 ng/mL after a single injection (**Figure 46 B**). Following chronic injection, LCN2 levels continued to rise in WT mice, reaching up to 2500 ng/mL, and increased to 1500 ng/mL in TRIF KO mice. It's noteworthy that we observed a positive trend in serum LCN2 increase in MyD88 KO mice, but the difference was not statistically significant. While IL-6 increased in MyD88 KO mice, the elevation was notably lower compared to the other groups (**Figure 46 C**). These findings shed light on the differential responses of inflammatory markers in serum after eLNP injections, with notable distinctions among MyD88 KO in comparison to TRIF KO and WT mice. They underscore the pivotal role of the MyD88 adaptor in propagating reactogenic signals, as evidenced by the observed differences between MyD88 KO mice and TRIF KO and WT mice

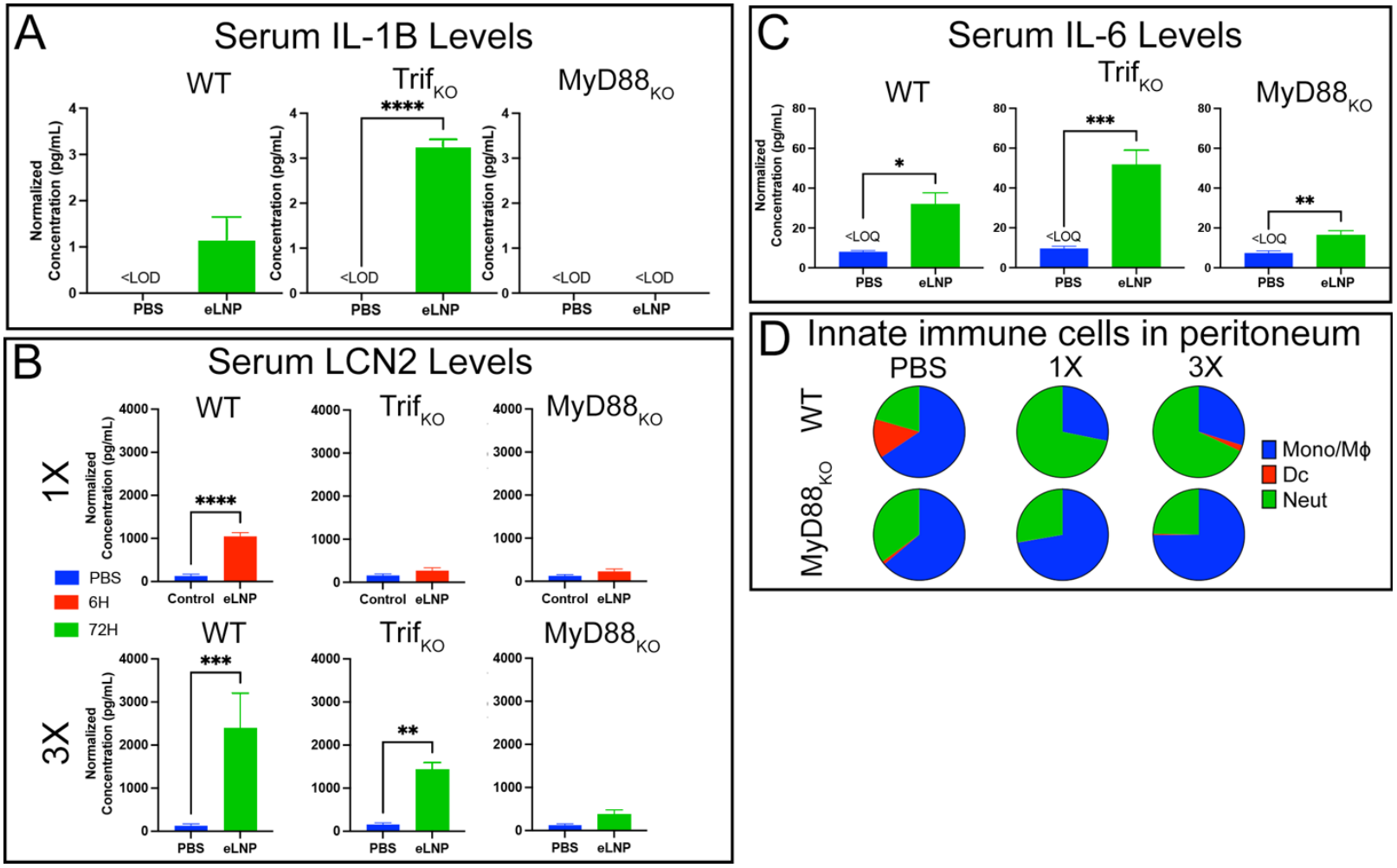

Figure 46. MyD88 KO prevents increase in serum pro-inflammatory cytokines and prevents innate cell infiltration to the peritoneum after eLNP administration. (A) Serum IL-1B levels in WT, TRIF KO, and MyD88 KO mice at the baseline (PBS) and after chronic MC3 eLNP administration (eLNP). **(B)** Serum LCN2 levels in WT, TRIF KO, and MyD88 KO mice at the baseline (PBS) and following single (1X) MC3 eLNP administration and after chronic (3X) MC3 eLNP administration. **(C)** Serum IL-6 levels in WT, TRIF KO, and MyD88 KO mice at the baseline and after chronic MC3 eLNP administration. **(D)** Innate immune cells in peritoneal lavage samples at baseline and following IP administrations of eLNP formulations (1X and 3X) for WT and MyD88 KO mice. (A-C) Expressed as mean ± SEM, n=5, *p<0.05, **p<0.01, ***p<0.001, ****p<0.0001 analyzed by one-way ANOVA followed by Bonferroni's *post hoc* test. (D) Expressed as a proportion of total cells.

We next examined the dynamics of innate cell recruitment between WT and MyD88 KO mice using FACS on peritoneal lavage samples following eLNP administration. In WT mice, a single injection resulted in a predominant increase in neutrophils, whereas in MyD88 KO mice, the primary cell type was macrophages/monocytes (**Figure 46 D**). Considering that neutrophils are the primary responders to xenobiotic administration and ongoing inflammation, we evaluated LCN2 levels in peritoneal lavage after single and chronic eLNP injections in both WT and MyD88 KO mice (**Figure 47**). Despite the well-known rapid degranulation of neutrophils upon physical perturbation, we observed higher LCN2 levels in peritoneal lavage samples from WT animals. This intriguing finding suggests potential differences in the dynamics or magnitude of the response between the two groups, which also aligns with LCN2 levels in serum. Notably, levels of LCN2 after a single eLNP injection were lower in MyD88 KO mice compared to WT and TRIF KO levels. After chronic administration, quantifying LCN2 was challenging due to technical difficulties involving neutrophil netosis.

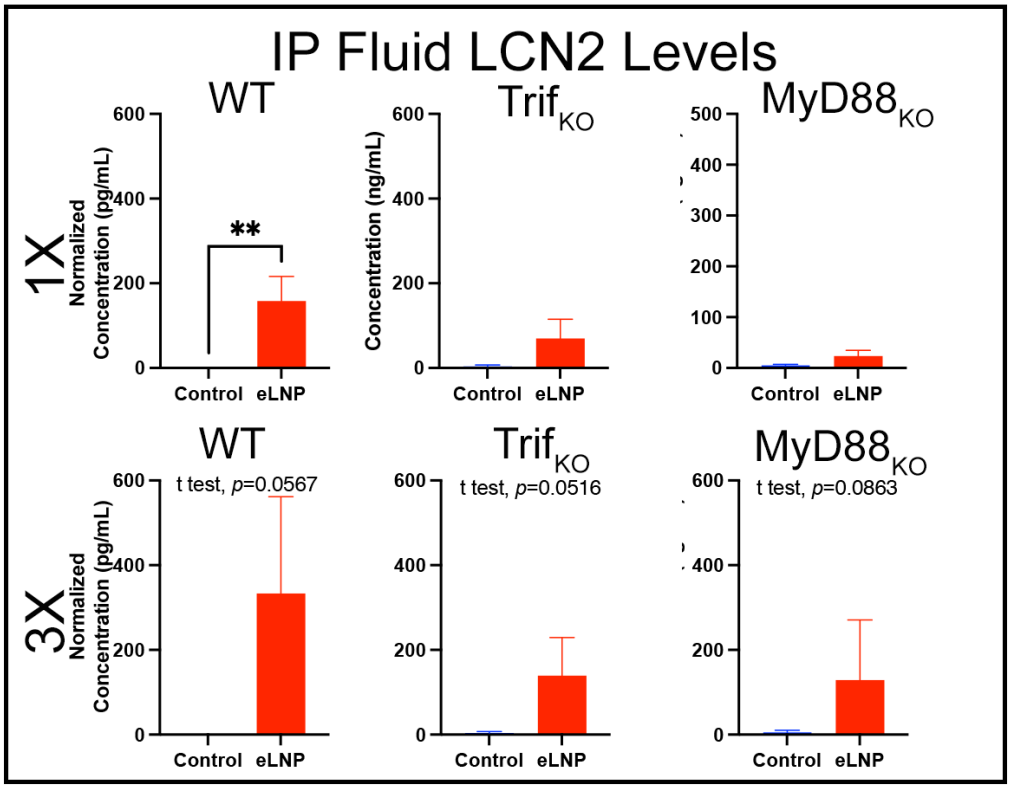

Figure 47. LCN2 levels in peritoneum are reduced after a single IP eLNP administration in MyD88 KO mice. LCN2 levels in peritoneal fluid of WT, TRIF KO, and MyD88 KO mice at the baseline (PBS-treated) and following single (1X) and chronic (3X) MC3 eLNP administration (eLNP). Expressed as mean ± SEM, n=5, $^{**}p<0.01$, analyzed by one-way ANOVA followed by Bonferroni's *post hoc* test.

Furthermore, in wild-type (WT) mice, there was an increased rate of extravasation of innate immune cells, as evidenced by a decrease in leukocytes in the blood after a single eLNP injection, in comparison to the rapid increase in blood leukocyte cellularity (i.e., number per blood sample determined by Hemavet) following three consecutive eLNP administrations (**Figure 48**). This observation suggests that WT mice exhibit a faster and more pronounced response of innate immune cells upon repeated exposure to eLNPs, indicating a heightened reactivity and adaptability of the immune system to the formulation with successive administrations. Specifically, we observed an increase in neutrophils and lymphocytes in WT blood samples. Notably, lymphocytes in MyD88

KO mice remained at the same level after chronic treatment compared to acute treatment with a slight increase in neutrophils, highlighting the impact of MyD88 adaptor protein involvement in the dynamic response of specific immune cell populations (**Figure 48**).

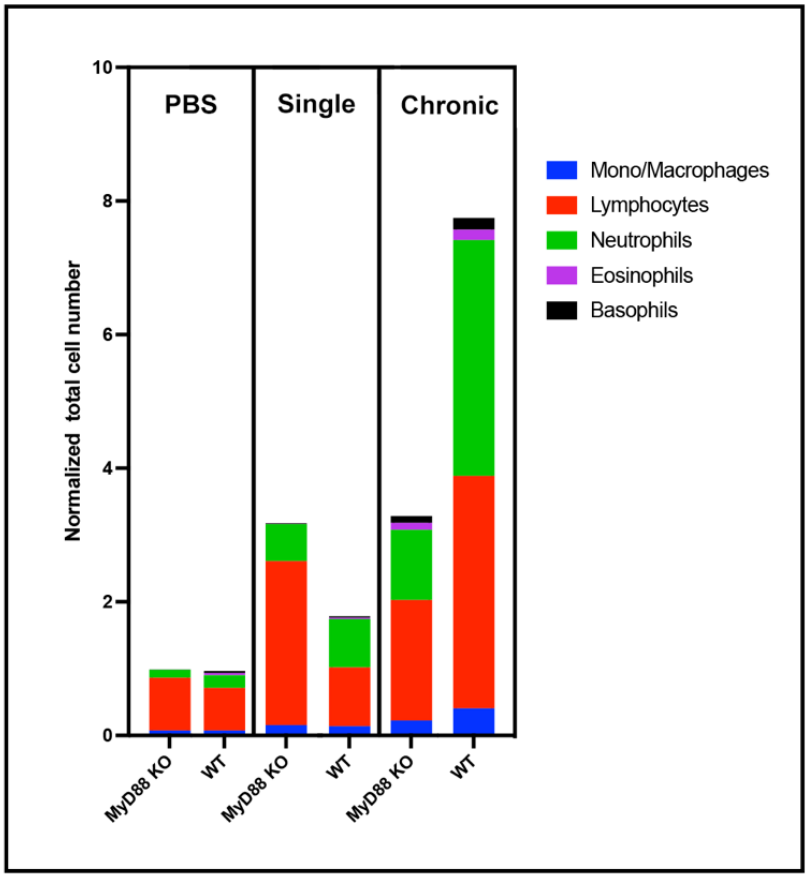

Figure 48. Blood count with differential reveals a likely slower extravasation of innate cells from the bloodstream after acute reactogenicity induction and a gradual increase in innate cell numbers in the state of chronic inflammation in MyD88 KO mice following eLNP administration in comparison to WT animals. LCN2 levels in peritoneal fluid of WT and MyD88 KO mice at the baseline (PBS-treated) and following single (1X) and chronic (3X) MC3 eLNP administration (eLNP). Expressed as mean ± SEM, n=5, $^{**}p<0.01$, analyzed by one-way ANOVA followed by Bonferroni's *post hoc* test.

6.4 TLR4 KO partially rescues food intake and body weight and decreases upregulation of pro-inflammatory effector molecules in response to eLNP administration

After establishing the crucial role of MyD88 in propagating reactogenic signals, we turned our attention to the TLR4 receptor itself (**Figure 49 A**). We started with genetic ablation studies, using TLR4 knock-out (TLR4 KO) mice. Employing a similar dosage approach, both TLR4 KO and WT mice received either single or chronic injection regimens (**Figure 49 B**). As expected, food intake exhibited a marked decrease in WT mice following chronic eLNP administration. This was attenuated, but not completely reversed in TLR4 KO mice (**Figure 49 C**). Similarly, there was some recovery in food intake observed in TLR4 KO mice compared to their WT counterparts. Furthermore, TLR4 KO mice displayed reduced sensitivity to eLNP induced changes in body weight, with no statistically significant difference observed after the third injection when compared to WT mice subjected to PBS injections (**Figure 49 C)**.

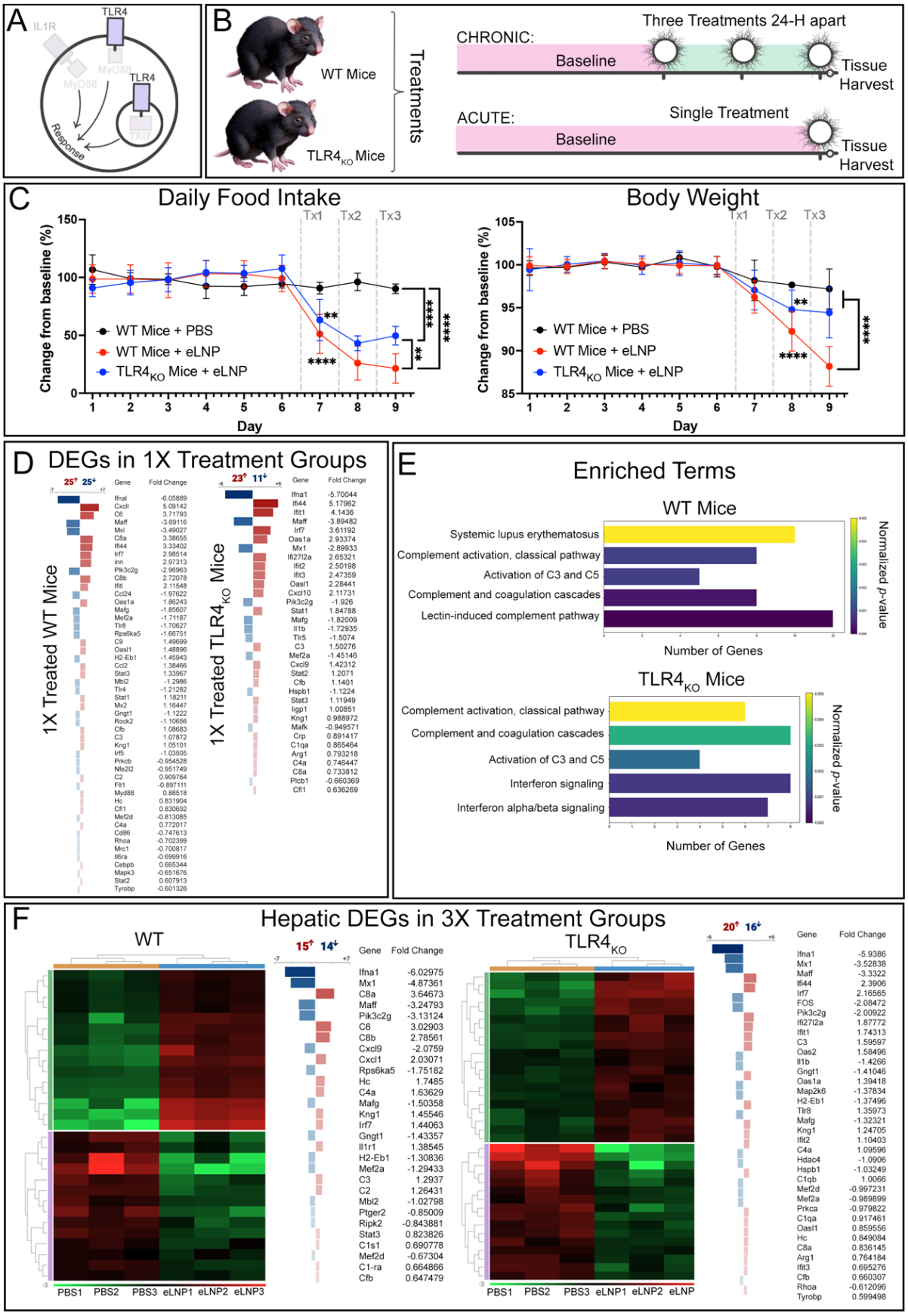
A
IL1R
TLR4
MyD88
MyD88
TLR4
Response
TRIF
B
WT Mice
TLR4KO Mice
Treatments
CHRONIC:
Three Treatments 24-H apart
Baseline
Tissue Harvest
ACUTE:
Single Treatment
Baseline
Tissue Harvest
C
Daily Food Intake
Tx1
Tx2
Tx3
Change from baseline (%)
WT Mice + PBS
WT Mice + eLNP
TLR4KO Mice + eLNP
Day
Body Weight
Tx1
Tx2
Tx3
Change from baseline (%)
WT Mice + PBS
WT Mice + eLNP
TLR4KO Mice + eLNP
Day
D
DEGs in 1X Treatment Groups
25↑ 25↓
1X Treated WT Mice
Gene
Fold Change
Ifnal -6.05889
Cxcll 5.09142
C6 3.71793
Maff -3.69116
Mxl -3.49027
C8a 3.38655
Ifi44 3.33402
Irf7 2.98514
inn 2.97313
Pik3c2g -2.96963
C8b 2.72078
Ifitl 2.11548
Ccl24 -1.97622
Oas1a 1.86243
Mafg -1.85607
Mef2a -1.71187
Tlr8 -1.70627
Rps6ka5 -1.66751
C9 1.49699
Oasl1 1.48896
H2-Eb1 -1.45943
Ccl2 1.38466
Stat3 1.33967
Mbl2 -1.2986
Tlr4 -1.21282
Stat1 1.18211
Mx2 1.16447
Gngt1 -1.1222
Rock2 -1.10656
Cfb 1.08683
C3 1.07872
Kng1 1.05101
Irf5 -1.03505
Prkcb -0.954528
Nfe2l2 -0.951749
C2 0.909764
Flt1 -0.897111
Myd88 0.88518
Hc 0.831904
Cfi1 0.830692
Mef2d -0.813085
C4a 0.772017
Cd86 -0.747613
Rhoa -0.702399
Mrc1 -0.700817
Il6ra -0.699916
Cebpb 0.665344
Mapk3 -0.651676
Stat2 0.607913
Tyrobp -0.601326
23↑ 11↓
1X Treated TLR4KO Mice
Gene
Fold Change
Ifna1 -5.70044
Ifi44 5.17962
Ifit1 4.1436
Maff -3.89482
Irf7 3.61192
Oas1a 2.93374
Mx1 -2.89933
Ifi27l2a 2.65321
Ifit2 2.50198
Ifit3 2.47359
Oasl1 2.28441
Cxcl10 2.11731
Pik3c2g -1.926
Stat1 1.84788
Mafg -1.82009
Il1b -1.72935
Tlr5 -1.5074
C3 1.50276
Mef2a -1.45146
Cxcl9 1.42312
Stat2 1.2071
Cfb 1.1401
Hspb1 -1.1224
Stat3 1.11949
Igp1 1.00851
Kng1 0.988972
Mafk -0.949571
Crp 0.891417
C1qa 0.865464
Arg1 0.793218
C4a 0.746447
C8a 0.733812
Plcb1 -0.660369
Cfi1 0.636269
E
Enriched Terms
WT Mice
Systemic lupus erythematosus
Complement activation, classical pathway
Activation of C3 and C5
Complement and coagulation cascades
Lectin-induced complement pathway
Number of Genes
Normalized p-value
TLR4KO Mice
Complement activation, classical pathway
Complement and coagulation cascades
Activation of C3 and C5
Interferon signaling
Interferon alpha/beta signaling
Number of Genes
Normalized p-value
F
Hepatic DEGs in 3X Treatment Groups
WT
PBS1 PBS2 PBS3 eLNP1 eLNP2 eLNP3
15↑ 14↓
Gene
Fold Change
Ifna1 -6.02975
Mx1 -4.87361
C8a 3.64673
Maff -3.24793
Pik3c2g -3.13124
C6 3.02903
C8b 2.78561
Cxcl9 -2.0759
Cxcl1 2.03071
Rps6ka5 -1.75182
Hc 1.7485
C4a 1.63629
Mafg -1.50358
Kng1 1.45546
Irf7 1.44063
Gngt1 -1.43357
Il1r1 1.38545
H2-Eb1 -1.30836
Mef2a -1.29433
C3 1.2937
C2 1.26431
Mbl2 -1.02798
Ptger2 -0.85009
Ripk2 -0.843881
Stat3 0.823826
C1s1 0.690778
Mef2d -0.67304
C1-ra 0.664866
Cfb 0.647479
TLR4KO
PBS1 PBS2 PBS3 eLNP1 eLNP2 eLNP
20↑ 16↓
Gene
Fold Change
Ifna1 -5.9386
Mx1 -3.52838
Maff -3.3322
Ifi44 2.3906
Irf7 2.16565
FOS -2.08472
Pik3c2g -2.00922
Ifi27l2a 1.87772
Ifit1 1.74313
C3 1.59597
Oas2 1.58496
Il1b -1.4266
Gngt1 -1.41046
Oas1a 1.39418
Map2k6 -1.37834
H2-Eb1 -1.37496
Tlr8 1.35973
Mafg -1.32321
Kng1 1.24705
Ifit2 1.10403
C4a 1.09596
Hdac4 -1.0906
Hspb1 -1.03249
C1qb 1.0066
Mef2d -0.997231
Mef2a -0.989899
Prkca -0.979822
C1qa 0.917461
Oasl1 0.859556
Hc 0.849084
C8a 0.836145
Arg1 0.764184
Ifit3 0.695276
Cfb 0.660307
Rhoa -0.612096
Tyrobp 0.599498

Figure 49. Genetic ablation studies with TLR4 KO mice shed light on TLR4 involvement in eLNP-induced reactogenicity in mice. (**A)** Schematic representation of the TLR4 receptor's role in reactogenic signal transduction as a central focus for the current section. **(B)** Methodologic approach using genetic ablation to study acute and chronic reactogenic manifestations in WT and TLR4KO mice. **(C)** Food intake and body weight following MC3 eLNP chronic administration in WT and TLR4 KO mice. WT mice subjected to PBS act as a negative control, TLR4KO mice receiving PBS omitted from the graph for simplicity as they follow the same trans as WT-PBS group. **(D)** Differentially expressed genes (DEGs) in WT and TLR4 KO murine livers normalized to their corresponding genetic control groups following single MC3 eLNP injection. **(E)** Enriched terms based on DEGs for WT and TLR4 KO mice receiving single MC3 eLNP injection. **(F)** Differentially expressed genes (DEGs) in WT and TLR4 KO murine livers normalized to their corresponding genetic control groups following chronic MC3 eLNP injection. (C) Expressed as mean ± SEM normalized to baseline, n=5, ****p<0.0001 analyzed by two-way repeated measures ANOVA. (D) and (F) Fold change is an average for n=3.

We next investigated liver Differentially Expressed Genes (DEGs) using a curated gene list associated with inflammation in mice (Inflammation V2 panel, Nanostring). A comparison was made between the hepatic gene expression profiles of eLNP-treated mice and PBS-treated controls with the same genotypes. Our initial focus was on the hepatic DEGs under conditions of acute inflammation following a single eLNP injection assessed 6 hours post-administration (**Figure 49 D**). Notably, *Ifna1*, *Maff*, and *Mx1* displayed consistent downregulation in both WT and TLR4 KO mice after a single injection, with similar magnitudes of downregulation persisting through chronic injections. These genes are associated with the antiviral response, and their downregulation could suggest a suppression of antiviral defenses, possibly influenced by the fact that LNPs mimic the milieu of viruses. Additionally, both WT and TLR4 KO mice exhibited upregulation in *Ifl44* and *Irf7* in the acute inflammation setting. In WT mice, there was a pronounced upregulation of complement cascade molecules (*C6, C8a, C8b*, and *C9*) alongside a substantial increase in *Cxcl1* after single injection. In contrast, TLR4 KO mice did not show this upregulation in *Cxcl1* and did not upregulate complement effector molecules after single injection, with the exception of C3. In

contrast, TLR4 KO mice exhibited an upregulation in *Cxcl10*, a chemokine, after a single injection, which subsequently returned to normal levels after chronic injections. Furthermore, TLR4 KO mice uniquely upregulated *Ifit1*, *Ifit2*, *Ifit3*, *Oasl1*, and *Oas1a*, responses not observed in WT mice. The Bioplanet analysis of enriched terms [541] revealed that both WT and TLR4 KO mice exhibited DEGs linked to the activation of *C3* and *C5* complement effector molecules, as well as the complement and coagulation cascades (**Figure 49 E**). Notably, in WT mice, the majority of DEGs were associated with the lectin-induced complement pathway, while TLR4 KO mice displayed genes linked to interferon signaling and interferon alpha/beta signaling.

Following three eLNP injections, the persistent sickness behavior in mice prompted us to study hepatic DEGs after chronic eLNP injections (**Figure 49 F**). Notably, chronic eLNP injections induced a more pronounced upregulation of complement pathway molecules in WT mice, specifically *C8a, C6, C8b,* and *C4a*. These specific genes were absent in the battery of upregulated DEGs in TLR4 KO mice, with only *C3* showing a 1.6-fold upregulation. Furthermore, WT mice exhibited a threefold upregulation of *Cxcl1*, also known as keratinocyte-derived chemokine, which plays a crucial role in inflammation and immune response, often recruiting neutrophils to sites of injury or infection. Furthermore, in both WT and TLR4 KO mice, we observed a consistent downregulation in *Ifna1, Mx1*, and *Maff*. Additionally, the upregulation of *Irf7* in TLR4 KO mice may indicate a compensatory mechanism in response to the absence of TLR4 signaling.

The comparison between WT and TLR4 KO responses reveals distinct patterns in gene expression. The mentioned genes belong to various functional categories,

including interferon-stimulated genes (ISGs: *Ifna1, Mx1, Ifl44, Irf7, Ifit44, Ifit1, Ifit2, Ifit3, Oasl1, Oas1a*), complement cascade molecules (*C6, C8a, C8b, C9, C3*), and chemokines (*Cxcl1 and Cxcl10*). While both groups exhibit sustained downregulation of *Ifna1, Maff*, and *Mx1*, TLR4 KO mice show a unique upregulation in *Cxcl10, Ifit1, Ifit2, Ifit3, Oasl1*, and *Oas1a*, suggesting a specific response in the absence of TLR4 signaling. Upregulation of *Irf7* and ISGs in TLR4 KO mice prompted us to use a different strategy of pharmacological receptor manipulation due to possible compensatory mechanisms often found with germline receptor deletion.

6.5 Pharmacological receptor manipulation selectively inhibiting TLR4 completely eliminates reactogenicity of eLNPs

To validate TLR4's role in eLNP reactogenicity and account for potential compensatory mechanisms in TLR4-deficient mice (**Figure 50 A**), we employed the TLR4 inhibitor TAK-242 for focused pharmacological receptor manipulation. TAK-242 is a small molecule that acts as a potent inhibitor of TLR4 signaling. This compound is designed to selectively inhibit TLR4 activation, and act as an uncompetitive antagonist. TAK-242 exerts its inhibitory effects by disrupting the interaction between TLR4 and its adaptor proteins, thereby suppressing downstream signaling cascades. The level of specificity inherent in TAK-242 ensures a targeted impact on TLR4, distinguishing it from other receptors and signaling pathways.

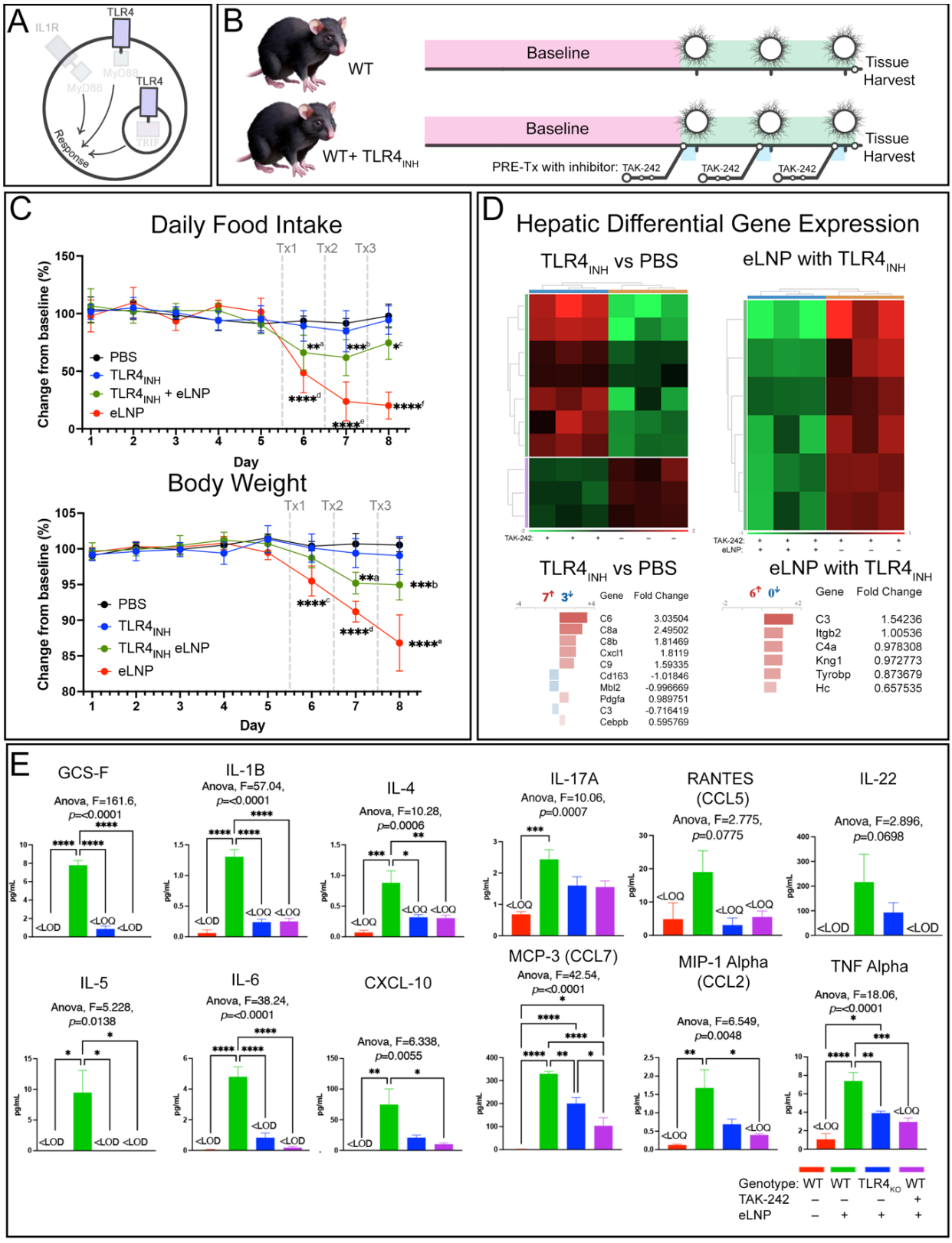
A
IL1R
TLR4
MyD88
MyD88
TLR4
TRIF
Response
B
WT
WT+ TLR4INH
Baseline
Tissue Harvest
Baseline
Tissue Harvest
PRE-Tx with inhibitor: TAK-242 TAK-242 TAK-242
C
Daily Food Intake
Tx1 Tx2 Tx3
Change from baseline (%)
PBS
TLR4INH
TLR4INH + eLNP
eLNP
Day
Body Weight
Tx1 Tx2 Tx3
Change from baseline (%)
PBS
TLR4INH
TLR4INH eLNP
eLNP
Day
D
Hepatic Differential Gene Expression
TLR4INH vs PBS
eLNP with TLR4INH
TLR4INH vs PBS
Gene Fold Change
C6 3.03504
C8a 2.49502
C8b 1.81469
Cxcl1 1.8119
C9 1.59335
Cd163 -1.01846
Mbl2 -0.996669
Pdgfa 0.989751
C3 -0.716419
Cebpb 0.595769
eLNP with TLR4INH
Gene Fold Change
C3 1.54236
Itgb2 1.00536
C4a 0.978308
Kng1 0.972773
Tyrobp 0.873679
Hc 0.657535
E
GCS-F
Anova, F=161.6, p=<0.0001
IL-1B
Anova, F=57.04, p=<0.0001
IL-4
Anova, F=10.28, p=0.0006
IL-17A
Anova, F=10.06, p=0.0007
RANTES (CCL5)
Anova, F=2.775, p=0.0775
IL-22
Anova, F=2.896, p=0.0698
IL-5
Anova, F=5.228, p=0.0138
IL-6
Anova, F=38.24, p=<0.0001
CXCL-10
Anova, F=6.338, p=0.0055
MCP-3 (CCL7)
Anova, F=42.54, p=<0.0001
MIP-1 Alpha (CCL2)
Anova, F=6.549, p=0.0048
TNF Alpha
Anova, F=18.06, p=<0.0001
pg/mL
<LOD
<LOQ
Genotype: WT WT TLR4KO WT
TAK-242 – – – +
eLNP – + + +

Figure 50. TLR4 antagonist rescues food intake and body weight of eLNP-treated mice. (**A)** Schematic representation of the TLR4 receptor's role in reactogenic signal transduction as a central focus for the current section. **(B)** Methodologic approach using pharmacologic receptor manipulation to study acute and chronic reactogenic manifestations in WT and WT mice subjected to TLR4 inhibitor, TAK-242. **(C)** Food intake and body weight following MC3 eLNP chronic administration in WT mice pre-treated with TAK-242 inhibitor. WT mice subjected to PBS with and without TAK-242 pre-treatment act as negative controls, WT mice receiving MC3 eLNP act as a positive control. **(D)** Hepatic DEGs in WT mice receiving TAK-242 pre-treatment (left) and DEGs in WT mice receiving TAK-242 pre-treatment and MC3 eLNP treatment (right) all normalized to WT mice receiving PBS. **(E)** Serum immune markers following chronic eLNP injection to WT, TLR4 KO and TLR4 antagonized mice. (C) Expressed as mean ± SEM normalized to baseline, n=5, ****p<0.0001 analyzed by two-way repeated measures ANOVA. (D) Fold change is an average for n=3. (E) Expressed as mean ± SEM, n=5, *p<0.05, **p<0.01, ***p<0.001, ****p<0.0001 analyzed by one-way ANOVA followed by Bonferroni's *post hoc* test.

In the experimental setup (**Figure 50 B**), WT mice were either pre-treated with TAK-242 two hours before each eLNP injection or received eLNP injections without pre-treatment. We only tested chronic responses in the setting of three daily eLNP injections. The comparison group did not undergo pre-treatment and received three eLNP injections, while a negative control group received PBS. Additionally, we assessed whether TAK-242 itself influenced murine sickness behavior. Notably, there was no significant change in food intake and body weight in the PBS and TAK-242 injected mice (**Figure 50 C**). In contrast, eLNP-treated animals experienced a substantial decrease in food intake by almost 75% and a close to 15% drop in body weight. Remarkably, mice pre-treated with TAK-242 exhibited a statistically significant decrease in food intake (-23%) and body weight (-7%) compared to the negative control; however, these reductions were considerably less severe than those observed in the eLNP-treated group. This indicates that specific TLR4 inhibition in WT mice rescues these crucial physiological parameters, underscoring the pivotal role of the TLR4 receptor in inducing reactogenic responses to eLNPs.

Pre-treatment with TAK-242 somewhat perturbed the equilibrium of complement effector molecules, evident in the upregulation of *C6, C8a, C8, C9*, and *Cxcl1* cytokine genes following TAK-242 administration (**Figure 50 D**). Strikingly, the analysis revealed only six DEGs in TAK-242-pretreated mice after eLNP administration compared to the mice receiving PBS. These genes included *C3*, *C4a*, and *Hc*, which encodes complement factor *C5*, all associated with the activation of the complement system. Additionally, *Itgb2, Kng1*, and *Tyrobp* showed upregulation that did not achieve statistical significance. The limited number and magnitude of DEGs, especially the singular upregulation of *C3* with a fold change higher than 1.5, stand in stark contrast to the diverse and pronounced gene expression changes observed in WT mice receiving eLNPs without pre-treatment, as depicted in **Figure 49**.

We conducted a comprehensive analysis of sixty-four immune markers in murine serum (**Figure 50 E**). Notably, the most consistently altered markers were pro-inflammatory cytokines (IL-1B, TNF-alpha, IL-6, IL-17A), anti-inflammatory cytokines (IL-4, IL-5, IL-22), chemokines (CXCL-10, CCL5, CCL7, CCL2), and the hematopoietic growth factor GCS-F, following chronic eLNP injections. In WT mice, we observed a consistent upregulation of these markers, indicating an intensified immune response. However, TLR4 KO and TLR4-inhibited mice did not exhibit significant changes in these markers, except for an increase in IL-22, CCL7, and TNF-alpha in TLR4 KO mice. This again suggests potential compensatory mechanisms triggered by knock-out of *TLR4*.

6.6 Extending considerations from reactogenicity to mRNA degradation in mRNA LNP-based therapies

Our work reveals that mice exhibit signs of sickness following the administration of eLNPs and mechanistically proves that sickness behavior is induced by the reactogenicity facilitated through the TLR4 and MyD88 receptor-adaptor tandem. This finding serves as a link to understanding possible adverse reactions in humans following mRNA LNP administration, similar to what has been observed with mRNA vaccines.

An additional side of reactogenic manifestations explored in existing literature delves into mRNA cargo degradation associated with TLR4 activation. As highlighted by Lokugamage et al., administering a TLR4 agonist, such as lipopolysaccharide (LPS) from gram-negative bacteria, inhibited mRNA translation. [497] TLR4 inhibition simultaneously administered with LPS attenuated but did not fully restore mRNA expression to levels observed without LPS treatment. [497] Importantly, the reduction in mRNA expression was attributed not to a decline in particle endocytosis or endosomal escape of LNPs, but rather to the action of RNA-dependent protein kinase R (PKR) subsequent to TLR4 activation. RNA typically present during viral infections, serves as a key component of the host's defense against viral invasion. Upon activation, PKR phosphorylates the eukaryotic initiation factor 2 alpha (eIF2α), hindering the initiation of translation, a critical step in protein synthesis. [364, 499, 500] This phosphorylation event prevents the formation of the pre-initiation complex, impeding the binding of initiator tRNA to the small ribosomal subunit and resulting in a global reduction in protein synthesis. Additionally, PKR activation may contribute to mRNA degradation by

phosphorylating other proteins involved in mRNA stability, accelerating the decay of specific mRNA molecules. [364, 499, 500] To corroborate these findings, we demonstrate that hepatic bioluminescence decreases with consecutive daily administrations of Luc mRNA LNPs (**Figure 51**, WT mice 4x vs 1x Luc mRNA LNP administration), indicating a potential reduction in the delivered Luc mRNA translation. Additionally, the decrease in bioluminescence signal is not rescued by knocking down MyD88 adaptor (**Figure 51**, MyD88 KO mice, 4x vs 1x Luc mRNA administration).

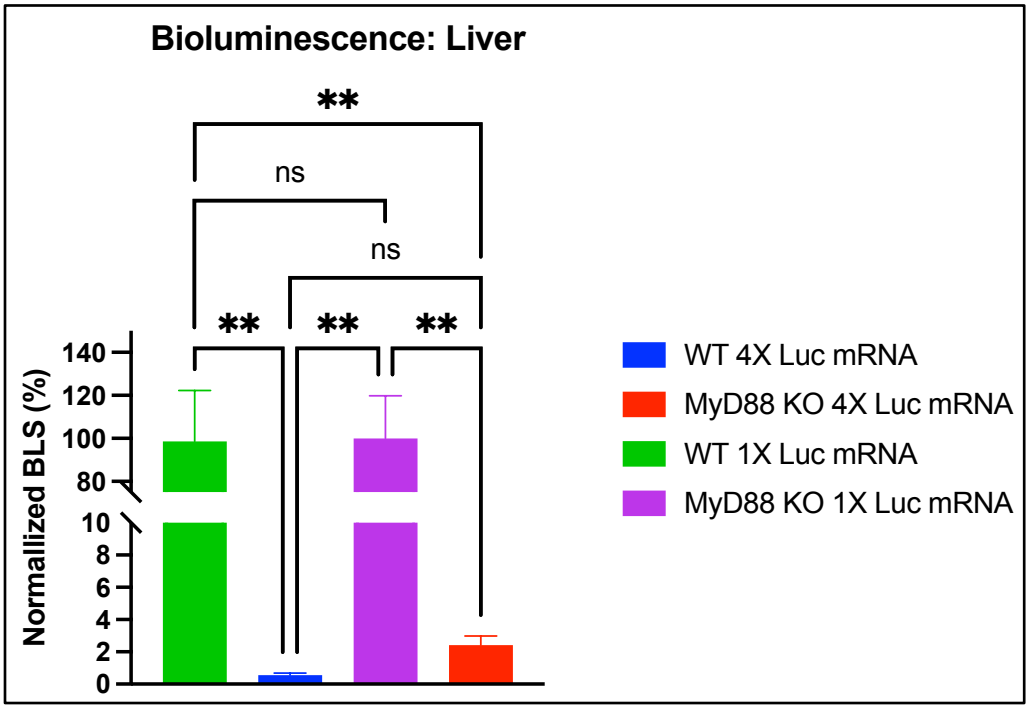

Figure 51. A comparative analysis of liver bioluminescence in mice, subjected to either chronic or a single administration of Luc mRNA LNPs, indicates a significant decrease in bioluminescence following chronic administration. Both WT and MyD88 KO mice had a profound decrease in bioluminescence signal following chronic Luc mRNA LNP administration. Expressed as mean ± SEM, n=5, $^{**}p<0.01$, analyzed by one-way ANOVA followed by Bonferroni's *post hoc* test.

In another experiment, we demonstrate that both WT and MyD88 KO mice exhibit an approximately 90% reduction in Luc mRNA levels after the first administration of three consecutive Luc mRNA LNP doses (**Figure 52**). In this experimental setup, mice

in each group (1x, 2x, 3x) received injections of Luc mRNA lipid nanoparticles (LNPs) once, twice, or thrice, and they were euthanized 6 hours after the last injection.

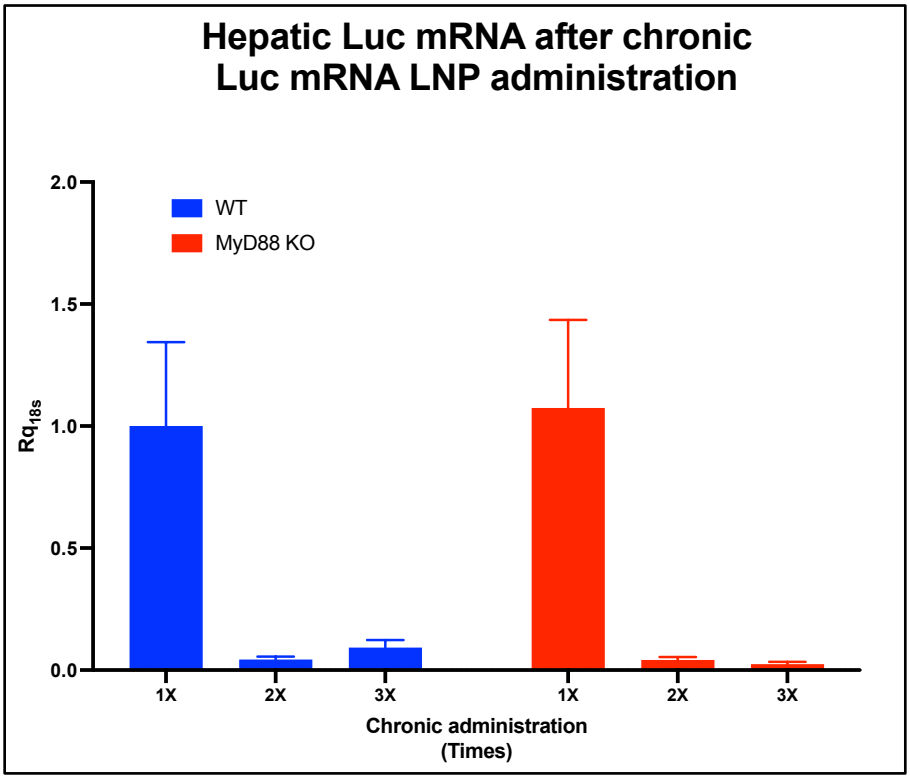

Figure 52. Quantification of hepatic Luc mRNA after chronic Luc mRNA LNP administration suggests potential heightened mRNA degradation in both WT and MyD88KO murine genotypes. MyD88 KO genotype does not prevent mRNA degradation in mice receiving chronic Luc mRNA LNP doses. Expressed as mean ± SEM, n=5, analyzed by two-way ANOVA followed by Bonferroni's *post hoc* test.

The observed drastic reduction in mRNA levels after the second administration, assessed 6 hours following the second injection, may be attributed to either mRNA degradation or decreased internalization of *Luc* mRNA LNPs. The potential decrease in internalization with subsequent administrations could suggest a significant influence of LNPs as a vector on the experimental outcomes. Therefore, to understand this phenomenon further, we pre-treated mice with three consecutive daily injections of MC3 eLNPs before the final *Luc* mRNA LNP injection, comparing it to PBS pre-treated mice receiving a single *Luc* mRNA LNP. We observed only a minor decrease in whole-body,

splenic, and hepatic bioluminescence (**Figure 53**), with no change in *Luc* mRNA counts (data not shown).

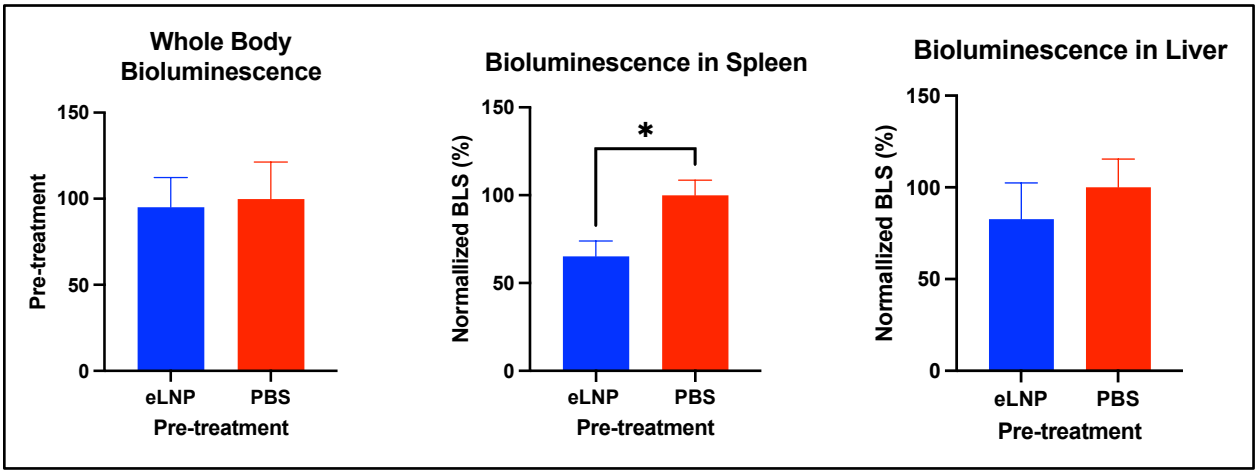

Figure 53. Whole body and organ-specific bioluminescence in WT mice pre-treated with eLNPs reveals minor involvement of LNP vectors in inducing mRNA degradation. Parallel bioluminescence patterns in whole-body and liver bioluminescence indicate a slight reduction in Luc expression in mice subjected to three daily eLNP pre-treatments before Luc mRNA administration. However, the observed significant decrease in spleen bioluminescence is more likely attributed to shifts in the innate immune cell population, which takes up Luc mRNA LNPs following priming with eLNPs, rather than being directly linked to increased mRNA degradation. Expressed as mean ± SEM, n=5, **p*<0.05, analyzed by unpaired t-test.

Consequently, our conclusion is that the mRNA cargo alone prompts reactogenic mechanisms, setting off nucleic acid degradation pathways, aligning with findings from Lokugamage et al. [497] Moreover, this process may be intensified by background inflammation, as illustrated by the introduction of LPS. [497] Therefore, administering mRNA LNP-based therapies to individuals with pre-existing chronic inflammation requires caution. This precaution stems from the potential of mRNA LNP reactogenicity to exacerbate underlying inflammatory conditions, coupled with its observed low efficacy in the presence of ongoing inflammation. Additionally, even in healthy individuals, reactogenicity could pose a risk to the effectiveness of mRNA translation and may hinder the repeated administration of mRNA therapeutics. The current understanding of

the effects of LNP composition, associated temporal kinetics, chronic dosage, and dosing on their ability to evoke reactogenic manifestations is still evolving, and further investigations are needed to develop safe and effective LNP carrier formulations.

Future research should prioritize understanding the mechanisms behind LNP-induced inflammation and finding strategies to mitigate their reactogenicity. Our data underscores the importance of considering temporal kinetics in the study of eLNP reactogenicity, as prolonged presence of LNP carriers may induce propagation of immune responses and compromise therapeutic efficacy. Consequently, an in-depth evaluation of the optimal timing and frequency of LNP-based therapy administration is essential to minimize the risk of adverse reactions. Optimization of LNP carrier dosage and mRNA payload distribution per particle is equally crucial for achieving the desired therapeutic outcome, especially in cases of chronic administration. Additionally, it is vital to acknowledge that variations in ionizable lipids, mRNA cargo, and PEG coating can significantly impact LNP carrier reactogenicity. Therefore, standardizing and optimizing LNP carrier formulations in reactogenicity studies should be prioritized for enhancing both safety and effectiveness, providing a solid foundation for the development of these innovative treatments.

6.7 Methods

6.6.1 Materials

Lipid Nanoparticle Components for eLNP and mRNA LNP synthesis, including ALC-0315, SM-102, DLin-MC3-DMA, cholesterol, DSPC, and DMG-PEG2k, were sourced from BioFine International (BioFine International, Vancouver, BC, Canada) or Avanti Polar Lipids (Avanti Polar Lipids, Alabaster, AL, USA). For mRNA LNP synthesis,

Luc mRNA was obtained from TriLink Biotechnologies Inc. (TriLink Biotechnologies Inc., San Diego, CA, USA). For LNPs concentration, Amicon ultra centrifugal filters were obtained from MilliporeSigma (MilliporeSigma, Burlington, MA, USA). For cell culture consumables, Gibco (Gibco, Gaithersburg, MD, USA) supplied RPMI, DMEM media, FBS, PBS, and penicillin-streptomycin. Nuclease-free water was obtained from Cytiva (Hyclone Laboratories, South Logan, UT, USA). For chemical reagents, Thermo Fisher Scientific (Thermo Fisher Scientific, Waltham, MA, USA) provided a d-luciferin reagent, Halt Protease Inhibitor Cocktail, Pierce BCA protein assay, Quant-iT RiboGreen RNA kit, and RNA standards. Ambion (Ambion, Carlsbad, CA, USA) supplied a DNA-free Kit and TRIzol reagent. Proteinase K reagent and Qiagen RNeasy Mini kit were purchased from Qiagen Corporation (Qiagen, Hilden, Germany). Applied Biosystems (Applied Biosystems, Foster City, CA, USA) supplied molecular biology reagents, including TaqMan Reverse Transcription Reagents Kit, TaqMan Gene Expression Master Mix, Power SYBR Green Master Mix, and other TaqMan and SYBR assay reagents. Nanostring nCounter Mouse Inflammation Assay and consumables were obtained from NanoString Technologies (NanoString Technologies, Seattle, WA, USA). Primers for Luc mRNA detection were ordered from Integrated DNA Technologies (IDT, Coralville, IA, USA). R&D Systems (R&D Systems, Minneapolis, MN, USA) provided IL-6, IL-1B, TNF, and LCN2 ELISA kits. Assay for polyplex cytokine and chemokine assessment in mouse sera, ProcartaPlex™ Mouse Cytokine & Chemokine Panel 1A, was obtained from Thermo Fisher Scientific (Thermo Fisher Scientific, Waltham, MA, USA). TAK-242 inhibitor was obtained from MilliporeSigma (MilliporeSigma, Burlington, MA, USA).

6.6.2 LNP preparation

The eLNP and Luc mRNA LNP formulations were created using a microfluidic method previously established in the literature. [374] The synthesis involved combining ionizable lipids, cholesterol, DSPC, and DMG-PEG-2k in proportions of 50:38.5:10:1.5, utilizing NanoAssemblr Spark or Benchtop (Precision Nanosystems Inc., Vancouver, Canada). For Luc mRNA LNPs we maintained an N:P ratio of 5.67 between ionizable lipids and nucleic acids. LNPs were subsequently concentrated through following buffer exchange with PBS (pH 7.4). LNP characterization, including hydrodynamic size, PDI, and ζ potential, was evaluated using Zetasizer Nano ZS (Malvern Analytical, Malvern, UK) and nanoparticle-tracking analysis using NanoSight LM-20 (Malvern Instruments, Worcestershire, UK). All LNPs employed in the study exhibited mRNA encapsulation efficiency exceeding 90%, as determined by a modified Quant-iT RiboGreen assay.

6.6.3 Animal Studies

All mouse studies were conducted in accordance with the National Institutes of Health Guide for the Care and Use of Laboratory animals. The Institutional Animal Care approved all animal experiments at Oregon Health and Science University and Oregon State University (Approval Number: IP00000690).

6.6.3.1 Animal model

The animal studies were performed using wild-type mice (C57BL/6J, IMSR_JAX:000664), MyD88 KO mice (B6.129P2(SJL)-Myd88tm1.1Defr/J, IMSR_JAX:009088), TRIF KO mice (C57BL/6J-Ticam1Lps2/J, IMSR_JAX:005037), and TLR4 KO mice (B6(Cg)-Tlr4tm1.2Karp/J, IMSR_JAX:029015), all on a C57BL/6 background, obtained from The Jackson Laboratory. The experiments included both male and female mice aged between 8 to 10 weeks. All mice were housed in a

dedicated mouse room with a euthermic environment set to murine body temperature (26°C) to avoid any cold-related stress potentially interfering with the behavioral studies**.** The room was set to a 12-hour light/dark cycle. Animals had *ad libitum* access to water and standard food, Purina rodent diet 5001 (Purina Mills, St. Louis, MO, USA).

6.6.3.2 Administration routes, doses and dosages

Luc mRNA LNPs were administered at doses of 5 µg per mouse, while eLNPs were administered in volumetric equivalents to 5 µg of mRNA LNPs after confirming comparable particle concentration through nanoparticle tracking analysis (NTA). LNPs were delivered in PBS. Negative control groups administered with PBS were injected with equivalent volumes to the treatment groups. Biodistribution studies involved administration through intravenous (IV), subcutaneous (SQ), and intraperitoneal (IP) routes.

For reactogenicity studies, a single IP injection was administered for the single dosage group, with mice euthanized 6 hours post-injection. In the chronic dosage group, mice received three IP injections 24 hours apart, with euthanasia performed 6 hours following the last injection.

The TAK-242 inhibitor (3 mg/kg) was administered two hours before eLNP treatment, with both injections given IP three times, 24 hours apart. Mice were euthanized 6 hours post-last injection. TAK-242 was initially dissolved in DMSO, followed by dilution in PBS, and subjected to 1 hour of sonication. A 1% DMSO solution in PBS was administered to mice as a negative pre-treatment control.

6.6.3.4 Biodistribution analysis

For biodistribution studies, we administered 5 µg doses of Luc mRNA LNPs to mice through intraperitoneal (IP), intravenous (IV), and subcutaneous (SQ) routes, each in 100 µL PBS volumes. At 2-, 4-, and 6-hours post-injection, mice were injected with d-luciferin (150 mg/kg in 100 µL PBS). Following a 15-minute interval, whole-body bioluminescent signal (BLS) was captured using the IVIS Lumina XRMS imaging system (Perkin Elmer, Hopkinton, MA, USA). Organs and ascitic fluid were promptly collected and again imaged for BLS distribution. Analysis of BLS data was performed with Living Image software (Perkin Elmer, Hopkinton, MA, USA).

6.6.3.5 Behavioral studies

In preparation for behavioral studies, animals underwent a 7-day acclimation period, during which they were individually housed. Baseline measurements for food intake and body weight were then established following this acclimation period. Murine weight and food consumption were assessed each day at a consistent time to ensure accuracy and reliability. Additionally, food was pre-dried to ensure consistency in measurements. The baseline data was recorded before the administration of eLNP formulations and then was continued throughout the duration of LNP administration. Food intake and body weight data following treatment administration were normalized to mean baseline measurements to represent percent (%) change from a baseline.

6.6.4 Fluorescence-assisted cell sorting (FACS)

Six hours post last Luc mRNA LNP or eLNP injections in the chronically injected mice, the mice were euthanized, and the peritoneal cavity was washed to collect immune cells that were then centrifuged (200 g, 2 minutes) and resuspended in the

equal volumes of PBS for initial counting. For FACS, pooled samples (n=5) were prepared to investigate the composition of immune cell populations. The cell preparation involved washing to achieve a single-cell suspension, adjusting the cell number to a concentration of 10X10^6 cells/ml in ice-cold FACS buffer (PBS, 1% FBS). Staining with ice-cold reagents and conducting the procedure at 4°C prevented modulation and internalization of surface antigens. Staining was conducted in polystyrene round-bottom 12 x 75 mm BD Falcon tubes. Cell viability was confirmed to be 90-95%. Each tube received 100 µl of cell suspension. A blocking antibody step using Fc block (TruStain FcX, Clone 93, Cat#101320) for 30 minutes was included to mitigate non-specific binding. After washing with ice-cold FACS buffer (2X2mL) and resuspending in 100 µl FACS buffer, primary labeled antibodies (1 µg per test) were added and incubated for 30 minutes at room temperature. Subsequently, after ice-cold FACS buffer (3X2mL) washes, cells were resuspended in 100 µl FACS buffer with addition of DNAse (50 µg/mL), and analyzed on FACSymphony™ S6 Cell Sorter (BD Bioscience, Franklin Lakes, NJ, USA).

The gaiting included a live/dead discrimination step, utilizing an Aqua dye to distinguish viable and non-viable cells. Subsequently, the CD45 marker was used to encompass all CD45-positive cells, providing a broad group of various immune cell types. Myeloid cell identification was achieved through the use of CD11B staining. Further classification of myeloid cells involved specific markers, including Ly6G for the segregation of neutrophils. Monocytes, macrophages, and dendritic cells within the myeloid population were identified using F4/80. Additionally, the characterization of monocytes and macrophages was accomplished by staining for Ly6C marker. The

staining of CD11C allowed for the identification of dendritic cells within the myeloid subset.

FACS reagents				
Antigen	**Clone**	**Fluorophore**	**Company**	**Cat #**
CD45	30-F11	PerCP-Cy5.5	BioLegend	103132
CD11b	M1/70	FITC	BioLegend	101206
Ly-6G	1A8	BV421	BioLegend	127628
F4/80	BM8	APC	BioLegend	123116
Ly-6C	HK1.4	PE Cy7	BioLegend	128018
CD11C	N418	APC-Cy7	BioLegend	117324
Live/Dead Aqua		BV510	ThermoFisher	L34966

6.6.5 Quantitative rtPCR

For total RNA extraction we employed the TRIzol (Ambion Co., Carlsbad, USA) and Chloroform (Sigma-Aldrich, Merck KGaA, Darmstadt, Germany) method [542], followed by Qiagen RNeasy Mini kit (Qiagen Corporation, Hilden, Germany) extraction using modified manufacturer's protocol. The removal of genomic DNA was accomplished using the DNA-free Kit (Ambion, Invitrogen, Carlsbad, CA, USA). For cDNA synthesis, the TaqMan Reverse Transcription Reagents Kit (Applied Biosystems, Foster City, CA, USA) was employed. Relative quantification for all targets, excluding Luc mRNA, utilized the TaqMan Gene Expression Master Mix (Applied Biosystems, Foster City, CA, USA) and TaqMan assay reagents. The rtPCR on Luc mRNA was conducted with SYBR Green PCR Master Mix. Absolute quantification of Luc mRNA levels and expression levels of TaqMan targets were normalized to 18S. The primer sequences for Luc mRNA were as follows:

forward: ACTTCGAGATGAGCGTTCGG,

reverse: CCAACACGGGCATGAAGAAC.

Data acquisition was performed using a QuantStudio 3 real-time PCR system (Applied Biosystems, Foster City, California). Data were analyzed using the QuantStudio Analysis Suite Cloud Software (Thermo Fisher Scientific, Waltham, MA, USA).

TaqMan Reagents	
Ccl2	Mm00441242_m1
Ccl3	Mm00441258_m1
Ccl5	Mm01302427_m1
Il1b	Mm00434228_m1
Tnf	Mm00443258_m1
Lcn2	Mm01324470_m1
Il6	Mm00446190_m1
Crp	Mm00455996_m1
Cxcl10	Mm00445235_m1
Orm1	Mm00435456_g1
Il10	Mm01288386_m1
Ifna	Mm03030145_gH
Il1A	Mm00439620_m1

6.6.7 Nanostring experiments

Liver samples were homogenized in Trizol Reagent (Ambion Co., Carlsbad, USA), and mRNA extraction was carried out following the previously outlined procedure. Subsequently, 100 ng of RNA per sample was used for hybridization, following the

Nanostring protocol. The analysis was conducted using the XT_PGX_MmV2_Inflammation_CSO panel on nCounter Pro analysis system (NanoString, Seattle, WA, USA), enabling the assessment of multiple hepatic RNA markers associated with murine inflammation. Rosalind software (Rosalind, San Diego, CA, USA) was employed to generate heatmaps from calculated z-scores and conduct enrichment analysis.

6.6.8 Protein quantification in serum

Blood was collected by cardiac puncture in BD Microtainer serum separator tubes (BD Biosciences, Franklin Lakes, NJ) and was let to sit at room temperature for a minimum of 30 min. Blood samples were centrifuged for 15 min at 1000g in refrigerated centrifuge within 1 h of collection. Following serum separation, protease inhibitor (Halt Protease Inhibitor Cocktail; Thermo Scientific, Waltham, MA, USA) was added to serum samples. Mouse IL-6, IL-1B, LCN2 and TNF-Alpha ELISAs were performed according to the manufacturer's protocols (R&D Systems, Minneapolis, MN, USA). To evaluate LCN2 levels in peritoneal lavage, mice were euthanized, and their peritoneal cavities were washed with 2 mL of PBS. Samples were then centrifuged for 15 min at 1000g in refrigerated centrifuge. The collected supernatant fluid was then utilized in ELISA analyses according to the manufacturer's protocol (R&D Systems, Minneapolis, MN, USA).

Mouse inflammatory factors in serum were quantified using the ProcartaPlex assay and measured with a Luminex 200 Instrument System (MAGPIX; Thermo Fisher Scientific, Waltham, MA, USA). To investigate the mouse reactogenic response, a ProcartaPlex Mouse Cytokine and Chemokine Panel 1A 36-plex (Thermo Fisher

Scientific, Waltham, MA, USA) was employed. The ProcartaPlex assay was carried out following the manufacturer's instructions to ensure consistency and accuracy in the measurements.

6.6.9 Data analysis

All experimental protocols employed a sample size (n) of 5, unless otherwise specified. The determination of statistical significance utilized various analyses, including one-way ANOVA, two-way ANOVA, and repeated-measures one-way ANOVA, followed by Bonferroni's *post hoc* test, conducted with GraphPad Prism software. Significance levels were indicated as follows: *$p \leq 0.05$, **$p \leq 0.01$, ***$p \leq 0.001$, ****$p \leq 0.0001$.

6.8 Chapter summary

In **Chapter 6** of my dissertation, I investigated the reactogenicity induced by LNP formulations, with a specific focus on the impact of empty lipid nanoparticles (eLNPs). Building upon the foundational literature review presented in **Chapter 5**, I aimed to identify the distinct mechanisms by which eLNPs induce and propagate reactogenic manifestation on both behavioral and molecular levels. The key theses of this chapter are summarized as follows:

1) Careful selection of eLNP formulation, administration route, dose, and dosage regimens was crucial for achieving controlled responses and localized hepatic inflammation.
2) A composition ratio of 50:38.5:10:1.5 for the ionizable lipids, cholesterol, DSPC, and DMG-PEG-2k was maintained, and ionizable lipids (MC3, ALC-0315, SM-102) were investigated for biodistribution using *luciferase* (*Luc*) mRNA LNPs.

3) MC3 LNPs were chosen based on balanced cell recruitment and efficient liver targeting after intraperitoneal (IP) injection.
4) Various eLNP doses equivalent to 5 µg of Luc mRNA LNPs per mouse, along with acute and chronic dosing regimens, were explored to find a balance between immune stimulation and avoiding severe responses.
5) Investigation of toll-like receptor adaptors (MyD88 and TRIF) revealed MyD88's crucial role in eLNP-induced reactogenicity, particularly in the sickness response.
6) TLR4 KO mice displayed reduced sensitivity to eLNP-induced behavioral changes, highlighting TLR4's involvement in reactogenic responses.
7) Pharmacological receptor manipulation using the TLR4 inhibitor TAK-242 validated TLR4's role in eLNP reactogenicity, rescuing physiological parameters and limiting gene expression changes.

In conclusion, **Chapter 6** provides insights into dosing strategies, eLNP formulations, and administration routes, along with specific roles of receptors in inducing murine sickness behavior following eLNP administration. This chapter addresses **Objectives 2.2** and **2.3**, filling a critical gap by formally investigating the role of TLR4 and its adaptor proteins MyD88 and TRIF in eLNP-dependent reactogenicity. **Chapters 5** and **6** collectively contribute to accomplishing **Specific Aim 2** of my dissertation. The synthesis of these chapters establishes a solid foundation for advancing our knowledge of the safety and efficacy of lipid nanoparticle-based drug delivery systems.

Chapter 7: Adapting improved follistatin mRNA LNP therapy: A proof of concept in metastatic epithelial carcinoma, paving the way for ovarian cancer application

Preamble

In Chapter 7 of my dissertation, the focus shifts toward refining *Fst* mRNA LNP therapy, specifically addressing observed reactogenic manifestations linked to LNPs (Chapter 6). The motivation for this exploration stems from recognizing adverse effects in wild-type C57BL/6 mice subjected to chronic LNP injections, prompting a re-evaluation of the therapeutic efficacy undermined by observed reactogenicity. Prioritizing safety in mRNA therapies, I identified the least reactogenic LNP formulation. The integration of the ALC-0315 ionizable lipid became a foundational element, guiding safety improvements. In addition to optimizing LNP components, an adjustment was introduced to the *Fst* mRNA cargo itself – the incorporation of pseudouridine

substitution. This choice, influenced by the Nobel Prize-winning concept [364], aimed to enhance mRNA stability and alleviate cargo immune recognition, bolstering the overall safety and efficacy of the therapeutic approach.

Choosing the formulation with the most favorable safety profile wasn't the sole challenge; selecting an appropriate syngeneic model also presented difficulties. My goal was to replicate metastatic and cachexia phenotypes observed in the ES2 model within wild-type C57BL/6 mice. Initial attempts with the syngeneic ID8 ovarian cancer model [543] proved inadequate, as the model was not producing metastases with sub-bursal ovarian inoculation and had low levels of activin A (ActA). As a proof-of-concept, I subsequently shifted to the B16 syngeneic melanoma model, known for its high metastatic potential. [544] However, it lacked the required elevated ActA levels. Therefore, I turned my attention to an MLM3 head and neck cancer model, distinct from ovarian cancer but exhibiting promising traits. This model showcased both metastatic features and a severe cachexia phenotype, coupled with increasing ActA levels corresponding to increasing tumor burden.

7.1 Metastases, cachexia, and elevated activin A background in head and neck squamous cell carcinoma

Activin A (ActA), a member of the transforming growth factor-beta superfamily, has been increasingly recognized for its pivotal role in the pathogenesis of various cancers. This multifunctional cytokine regulates key processes in cellular growth, differentiation, and repair, extending its influence beyond reproductive and embryonic development. [296, 545] The overexpression of ActA has been implicated in the progression of various tumors, including melanoma, epithelial ovarian (EOC), head and

neck, prostate, pancreatic, colorectal, lung, and liver cancers. [299, 546-552] The upregulated ActA signaling was also involved in cancer-associated cachexia, a debilitating syndrome characterized by severe muscle wasting, weight loss, and systemic inflammation, further contributing to the morbidity and mortality of cancer patients. [288, 553] Therefore, ActA was considered as a potent therapeutic target. The mechanisms underlying ActA, functioning as a significant negative regulator of muscle mass, play a pivotal role in inducing muscle wasting and upregulating the expression. [554, 555] This action significantly amplifies the severity of cachexia, a condition prevalent among cancer patients, highlighting ActA's pivotal role in the detrimental progression of this syndrome.

Given these multifaceted roles, inhibiting ActA signaling presents a promising therapeutic strategy. Follistatin (FST), a well-known antagonist of activin A, emerges as a potential therapeutic agent by neutralizing activin A's activity, offering hope for a novel approach to cancer treatment. [556] In our pursuit of improved therapies for ActA-overexpressing tumors and Act-A-driven cancer-associated cachexia, we propose a novel approach that leverages the potent inhibitory properties of FST, an endogenous antagonist of ActA. By overexpressing FST in the tumor microenvironment and systemically, we aim to disrupt the paracrine action of ActA that drives disease progression while simultaneously alleviating cancer cachexia by inhibiting ActA's endocrine function in the systemic circulation.

For a proof-of-concept, we utilize murine head and neck squamous cell carcinoma (HNSCC) model characterized by both heightened systemic ActA levels derived from tumors and severe phenotype of cancer-associated cachexia. ActA has

emerged as a key player in the pathogenesis of not only EOC, as discussed in Chapters 2 and 4, but also of HNSCC. Given the lack of syngeneic models that overexpress ActA for EOC, we instead selected a murine HNSCC model for our investigations. Our murine HNSCC model accurately mirrors the full spectrum of characteristics observed in human HNSCC, effectively encompassing its complexity and heterogeneity.

In humans, HNSCC is a devastating malignancy characterized by its aggressive nature and late-stage diagnosis, recapitulating observed outcomes in epithelial EOC patients. [557] HNSCC represents heterogeneous cancers that share a common histological origin in the squamous epithelial cells lining the upper aerodigestive tract, including the oral cavity, pharynx, and larynx. [558] Similarly, EOC encompasses a spectrum of diverse malignancies, united by a shared histological origin in the epithelial cells lining the ovaries and adjacent structures within the pelvic region (refer to Chapter 2). Despite the advancements in early diagnosis and treatment, both EOC and HNSCC remain a considerable burden on public health owing to their aggressiveness and tendency for metastasis, accounting for a significant proportion of cancer-related morbidity and mortality worldwide. [25, 559, 560] Similarly to EOC, the burden of HNSCC is further exacerbated by the emergence of debilitating cancer-associated cachexia syndrome. [561-563] This syndrome not only contributes to the decrease in patients' quality of life but also hinders their ability to tolerate and respond to cancer therapies. [555, 561, 564] Addressing cachexia in HNSCC patients is crucial not only for their overall well-being but also for improving treatment outcomes. [562, 565]

Elevated levels of ActA have been observed in both the tumor microenvironment and the systemic circulation of HNSCC patients. [566, 567] ActA is known to promote

tumor growth, migration, angiogenesis, and immune evasion, contributing to the aggressive behavior of HNSCC. [566, 568-570] In EOC, overexpressed ActA stimulates proliferation, migration, and invasion of ovarian cancer cells contributing to ovarian tumor metastasis and aggressiveness in later stages. [283, 284]

Therefore, in our pursuit for enhanced therapies targeting EOC, we redirected our focus to a broad category of epithelial cancers characterized by elevated ActA expression and concurrent cachexia, encompassing HNSCC. [556] Our approach to achieving a therapeutic effect through FST overexpression, which inhibits ActA, incorporates an improved formulation of *Fst* mRNA lipid nanoparticles (LNPs). This strategy leverages an LNP delivery system that has demonstrated significant efficacy, particularly in the development of SARS-CoV-2 vaccines. [571] In addition, we utilize pseudouridine-substituted *Fst* mRNA to enable multiple injections, fostering both constituent and transient overexpression of FST without eliciting an overactivation of innate immune mechanisms that could degrade the delivered mRNA molecules. Therefore, as a proof-of-concept approach, the use of LNPs allows for targeted and controlled delivery of *Fst* mRNA into HNSCC tumors and livers, providing a specific localized and systemic therapeutic effect.

7.2 *Fst* mRNA LNP formulation and in vitro assessment

The LNPs were synthesized with specific ratios of constituent lipids: 50% ionizable lipid ALC-0315, 38.5% cholesterol, 10% DSPC, and 1.5% DMG-PEG-2k. We maintained an N:P ratio of 5.67 to ensure optimal ionizable lipid-nucleic acid complexation (**Figure 54 A**). LNPs were spherical in shape with the average size of 78.56 nm, 0.074 polydispersity index, and encapsulation efficiency of 90% (**Figure 54**

B, C). CryoEM images of prepared formulation revealed that the LNPs had distinctive blebs, thought to enhance in vivo transfection. [572] Pseudouridine substitution (N1-methyl-Ψ), a chemical modification employed to mitigate the immune response and augment mRNA translation, [364] was integrated into the *Fst* mRNA sequence to decrease its reactogenicity. To explore the impact of pseudouridine substitution, known for inducing +1 ribosomal frameshifts at ribosomal slippery sequences, [573] we conducted a thorough *in vitro* investigation focused on mRNA expression to bioactive FST protein (**Figure 54 D-H**).

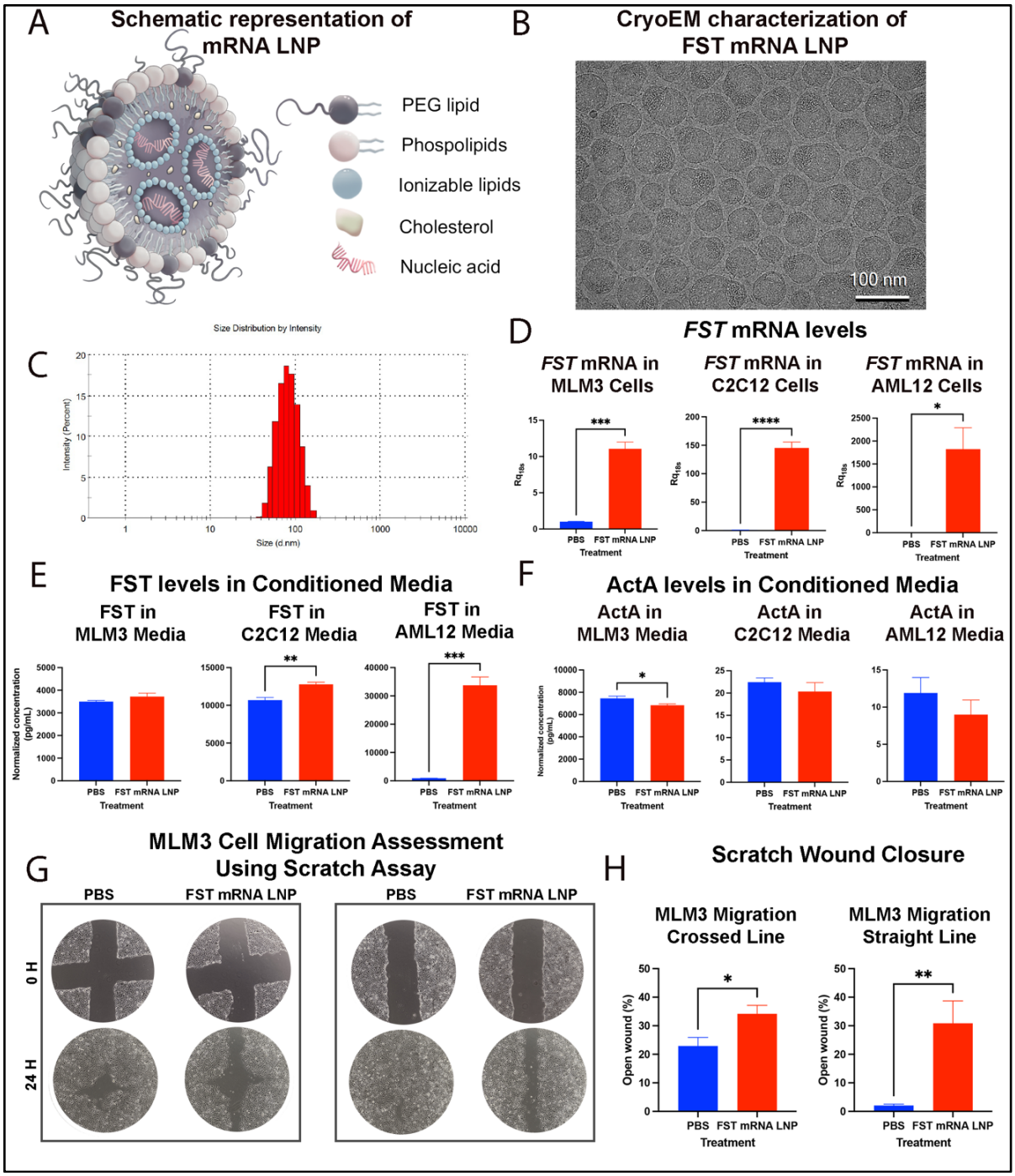

Figure 54. Incorporation of N1-methyl-Ψ to *Fst* mRNA sequence encapsulated in ALC-0315 LNP had high performance in expressing bioactive FST for ActA downregulation. **(A)** Schematic representation of *Fst* mRNA LNPs. **(B)** Representative CryoEM image of *Fst* mRNA LNPs showcasing LNP's spherical structure and formation of characteristic blebs. **(C)** Histogram for Fst mRNA LNP size distribution characterized by dynamic light scattering (DLS). **(D)** Quantitative rt-PCR results for *Fst* mRNA levels in MLM3, C2C12 and AML12 cell lines normalized to 18S levels 8 hours after transfection with *Fst* mRNA LNPs. FST **(E)** and ActA **(F)** levels normalized to total protein in conditioned media of MLM3, C2C12 and AML12 cells 8

hours after transfection with *Fst* mRNA LNPs **(G)** Representative images of scratch assay incorporating both cross and straight-line scratches for comprehensive assessment of MLM3 cell migration and **(H)** its quantitative assessment. (D-F) and (H) expressed as mean ± SEM, n=5, *p<0.05, **p<0.01, ***p<0.001 analyzed by t-test (*n*=3).

To evaluate the efficacy of our formulation, we performed a series of *in vitro* experiments employing three distinct murine cell lines: MLM3 head and neck carcinoma, C2C12 skeletal muscle cells, and AML12 normal hepatocytes. MLM3 cells served as our syngeneic murine HNSCC model, and the inclusion of C2C12 cells was relevant to addressing cancer cachexia and muscle fiber catabolism. The choice of AML12 hepatocytes was based on the propensity of LNPs to migrate and accumulate in the liver. Our investigations revealed a successful upregulation of *Fst* mRNA expression in all three cell lines following nanoparticle-mediated delivery (**Figure 54 D**).

FST protein levels were profoundly increased in the conditioned media of AML12 hepatocytes mirroring dramatic increase in *Fst* mRNA in AML12 cells after transfection (**Figure 54 E**). The MLM3 and C2C12 cell lines demonstrated higher levels of FST upregulation in the conditioned media. Concurrently, there was a decrease in ActA levels observed in C2C12 and AML12 media (**Figure 54 F**). Particularly noteworthy is the reduction in ActA levels in MLM3, which had baseline levels approximately 550 times higher than in C2C12 and AML12 media.

Furthermore, we evaluated the influence of FST overexpression on MLM3 cells migration using a scratch assay, that revealed a notable decrease in wound closure, indicative of reduced cellular mobility (**Figure 54 G, H**). This observation has significant implications for controlling invasive and metastatic characteristics of MLM3 cells. Moreover, it highlights broader ramifications for therapeutics targeting HNSCC,

especially given the well-documented influence of ActA in promoting these aggressive cell behaviors. [574, 575]

7.3 Experimental model selection and *Fst* mRNA LNP safety evaluation

The *Inhba* gene, responsible for encoding ActA, is significantly overexpressed in HNSCC patients, as revealed by The Cancer Genome Atlas (TCGA) data analysis. The upregulation of *Inhba*, measured in transcripts per million (TPM), is particularly pronounced in HNSCC cases, compared to other cancers showing statistically significant upregulation of *Inhba* compared to TCGA normal and Genotype-Tissue Expression (GTEx) data (**Figure 55 A**). [576] Additionally, an analysis using GEPIA [576] for HNSCC patients' survival demonstrates a correlation between higher *Inhba* gene expression and a lower survival rate especially in the first 50 months (**Figure 55 B**). The observed correlation between increased gene expression and reduced survival implies an association between ActA overexpression and an unfavorable prognosis in HNSCC patients, which also corroborated with the published evidence. [577, 578]

In our studies, we utilized the MLM3 syngeneic model to replicate HNSCC in mice, concentrating on its key features of HPV-positive nature [558, 579], presence of cancer-associated co-morbidities such as cachexia [561-563], as well as its primary site of distal metastasis in the lungs. [580] This model is especially relevant as it mimics HPV-positive HNSCC by overexpressing E6/E7 HPV proteins, making it a representative system for the majority of HNSCC cases. [581] Furthermore, implantation of MLM3 cells subcutaneously (SubQ) leads to a robust cachexia phenotype in mice, marked by reduced food intake (**Figure 55 C**) and substantial weight loss (**Figure 55 D**), including depletion of muscle and fat stores. MLM3 model was extensively validated in our

laboratory with respect to its cancer cachexia phenotype. [582] Importantly, as MLM3 tumors progress, there is a noticeable rise in ActA levels associated with increasing tumor burden (**Figure 55 E**). Moreover, allowing the MLM3 model to advance beyond 28 days post-implantation consistently leads to the observation of distal metastases in the lungs with 100% penetrance (**Figure 55 F**).

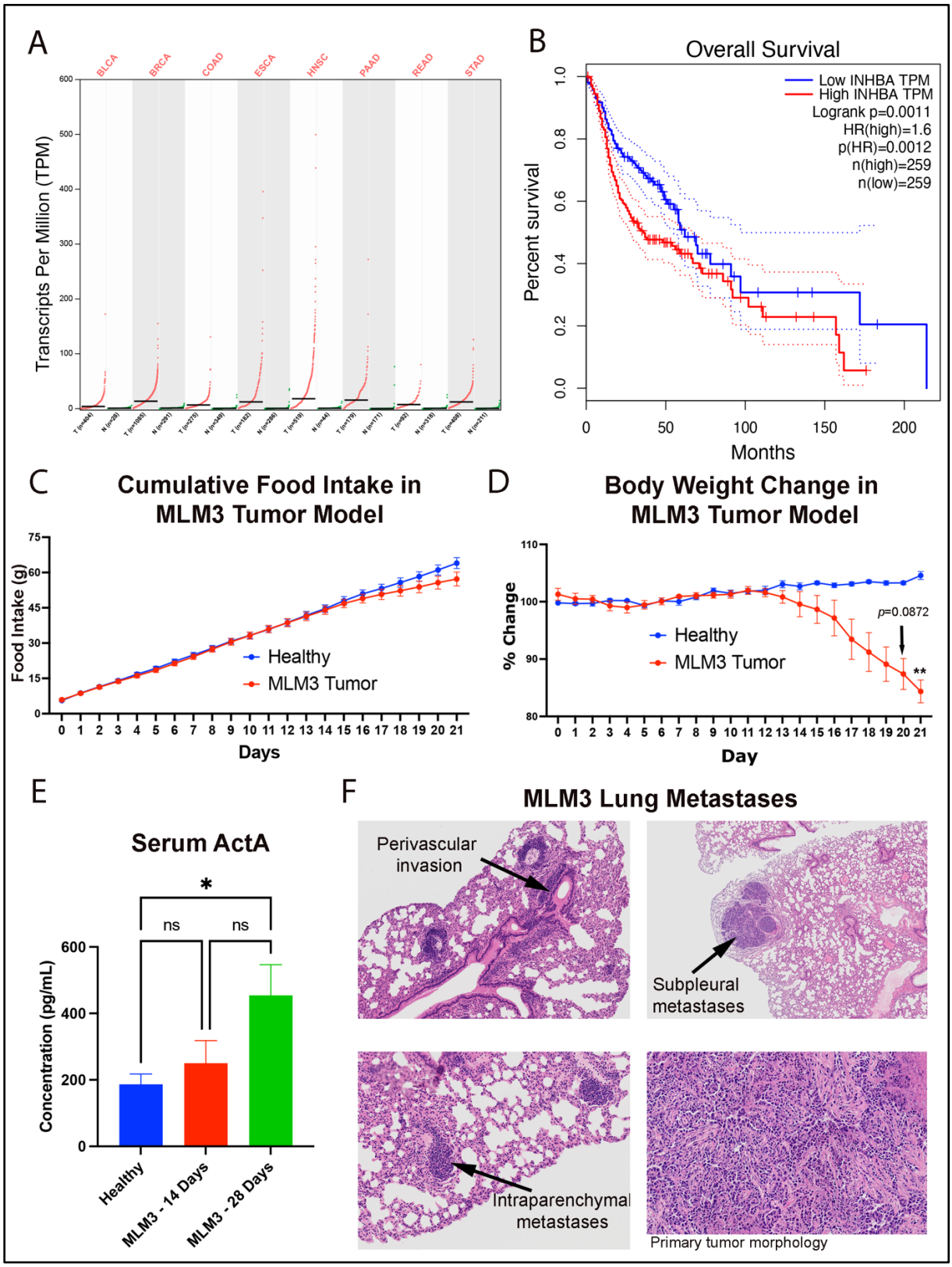

Figure 55. Syngeneic MLM3 model is characterized by high ActA, cancer-associated cachexia and distant lung metastases that is similar to human HNSCC manifestations. (A) *Inhba* upregulation in cancers, including HNSCC in comparison to

TCGA normal and GTEx data expressed in transcripts per million (TPM). **(B)** Overall survival in HNSCC patients with high and low *Inhba* expression. Cumulative food intake **(C)** and body weight change **(D)** in MLM3 model are indicative of cancer-associated cachexia. **(E)** Serum ActA in healthy C57Bl6 and MLM3-bearing mice 14- and 28-days following cancer cells implantation. **(F)** MLM3 lung metastases from primary SubQ tumors following 28 days post-implantation. (C-D) expressed as mean ± SEM, n=10, analyzed by repeated measures one-way ANOVA, followed by Bonferroni's *post hoc* test. (E) expressed as mean ± SEM, n=5 *p<0.05, **p<0.01, ***p<0.001 analyzed by one-way ANOVA (*n*=5).

The syngenetic MLM3 model on the background of C57Bl/6 mice establishes a robust foundation for exploring therapeutic strategies in HNSCC. This method allows for a thorough examination of potential immune responses to the developed *Fst* mRNA LNP therapeutic, enhancing its applicability to human patients. The use of wild-type C57Bl/6 mice enabled the identification of an LNP formulation with a favorable reactogenic profile, particularly with the ALC-0315 ionizable lipids showing the least reactogenic manifestations. Hence, we observed only a slight reduction in food intake following three consecutive intraperitoneal (IP) daily injections, which remained within an acceptable physiological range. This reduction was comparable to the administration of empty LNPs (eLNP) (**Figure 56 A**). In contrast, LNPs containing the MC3 ionizable lipids, similar to Onpattro therapy [379], induced a substantial and prolonged reduction in food intake, exceeding 50%, characteristic for reactogenic anorexia [583] (also, refer to **Figure 41** in Chapter 6). Additionally, our *Fst* mRNA LNP formulation led to a negligible decline in body weight, confirming their tolerability *in vivo* (**Figure 56 B**). The analysis of liver samples following a single IP administration of *Fst* mRNA LNPs revealed an increase in pro-inflammatory cytokines, including *Cxcl1, Cxcl2, Il1b, Il6*, and *Tnf* (**Figure 56 C**). Noteworthy is that these elevated cytokines returned to baseline with successive administrations, mirroring levels observed in mice eLNPs or PBS. This distinctive cytokine profile sheds light on the response to the LNP formulation and

emphasizes the transient and self-limiting nature of the immune reactions triggered by ALC-0315-containing LNPs.

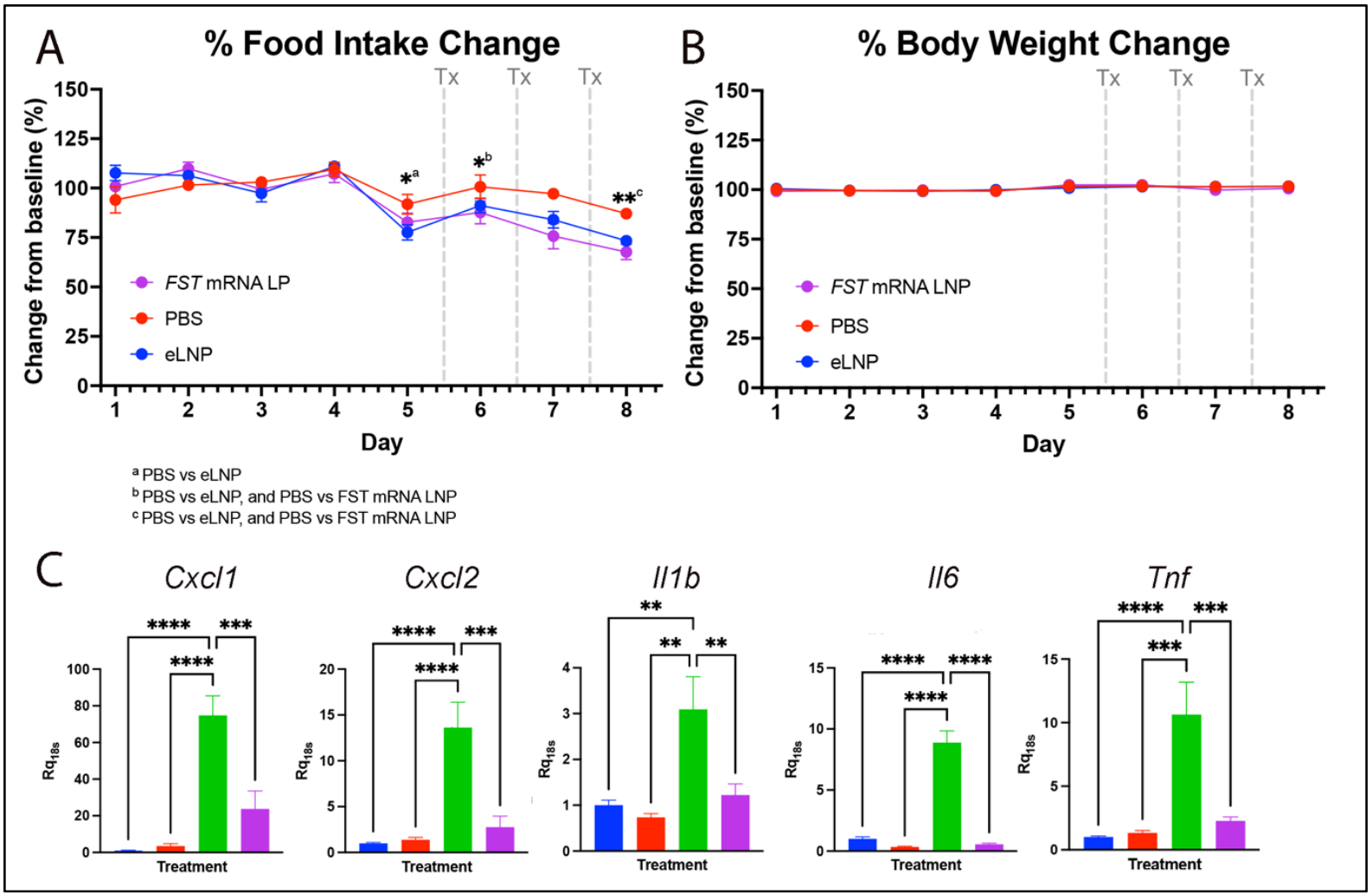

Figure 56: Characterization of *Fst* mRNA LNP safety profile. Food intake **(A)** and body weight **(B)** assessment in wild-type C57Bl/6 mice subjected to three consecutive daily administrations of *Fst* mRNA LNPs, containing ALC-0315 ionizable lipids. **(C)** Expression of *Cxcl1*, *Cxcl2*, *Il1b*, *Il6*, *Tnf* following single IP administrations of *Fst* mRNA LNP formulation in comparison to PBS, empty LNP (eLNP) and three chronic *Fst* mRNA LNP administrations. (A) and (B) expressed as mean ± SEM, *n*=5, analyzed by repeated measures one-way ANOVA, *p<0.05, **p<0.01. (C) expressed as mean ± SEM, n=5 *p<0.05, **p<0.01, ***p<0.001 analyzed by one-way ANOVA (n=5).

Furthermore, as measured by the complete blood count with differential and complete metabolic assessments after three chronic injections, the *Fst* mRNA LNP formulation had minimal impact on red blood cell characteristics (**Figure 57**).

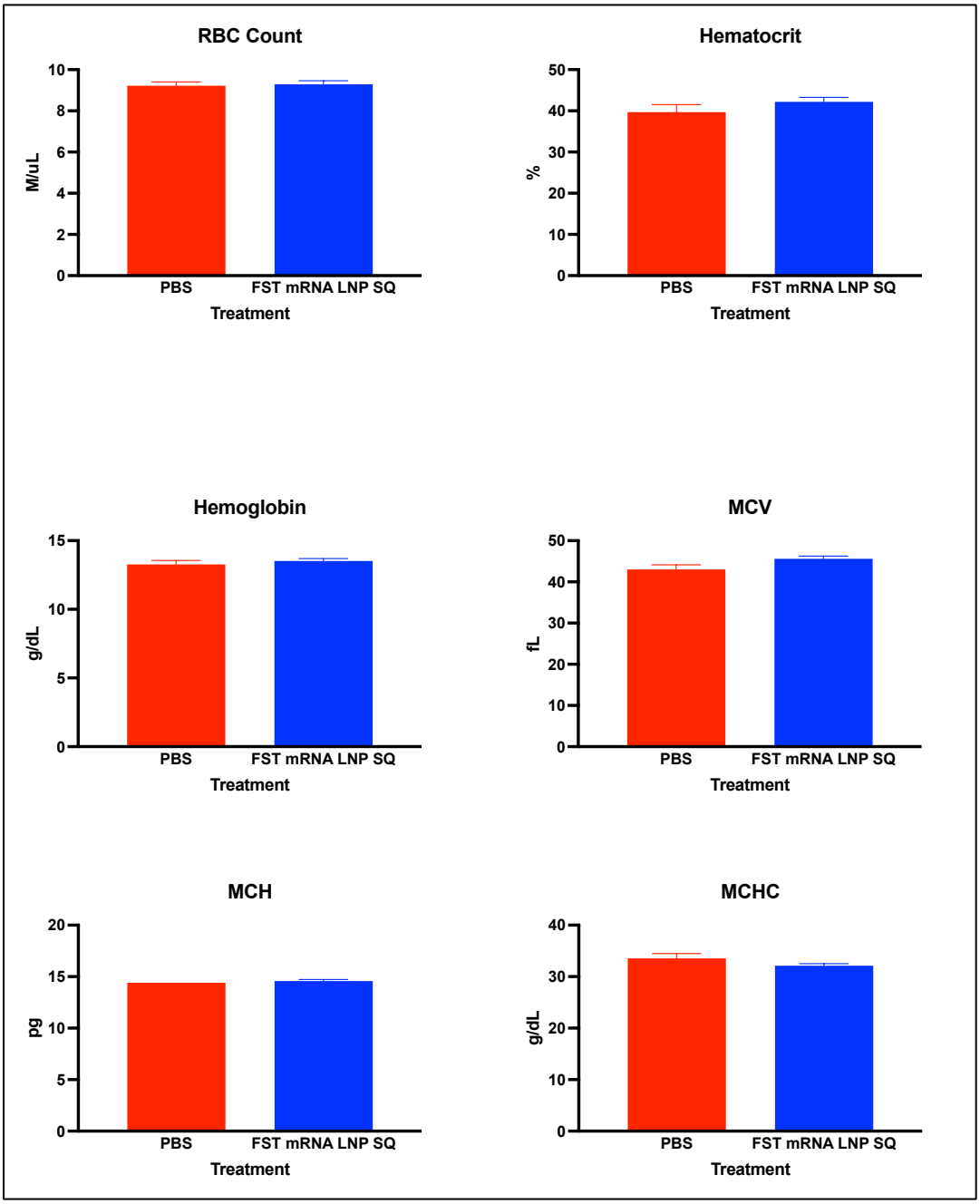

Figure 57. Examining the impact of *Fst* mRNA LNP administration on red blood cell characteristics reveals no observable effects. Red blood cell (RBC) count, hematocrit, hemoglobin levels, mean corpuscular volume (MCV) of RBCs, mean corpuscular hemoglobin (MCH) and its concentration (MCHC) are unaffected by *Fst* mRNA LNP administration. Data expressed as mean ± SEM, *n*=5, analyzed by t-test.

We observed a decrease in white blood cell (WBC) count, indicating potential WBC migration to the peritoneum (**Figure 58**). Furthermore, absolute counts of neutrophils, lymphocytes and monocytes were all decreased in blood.

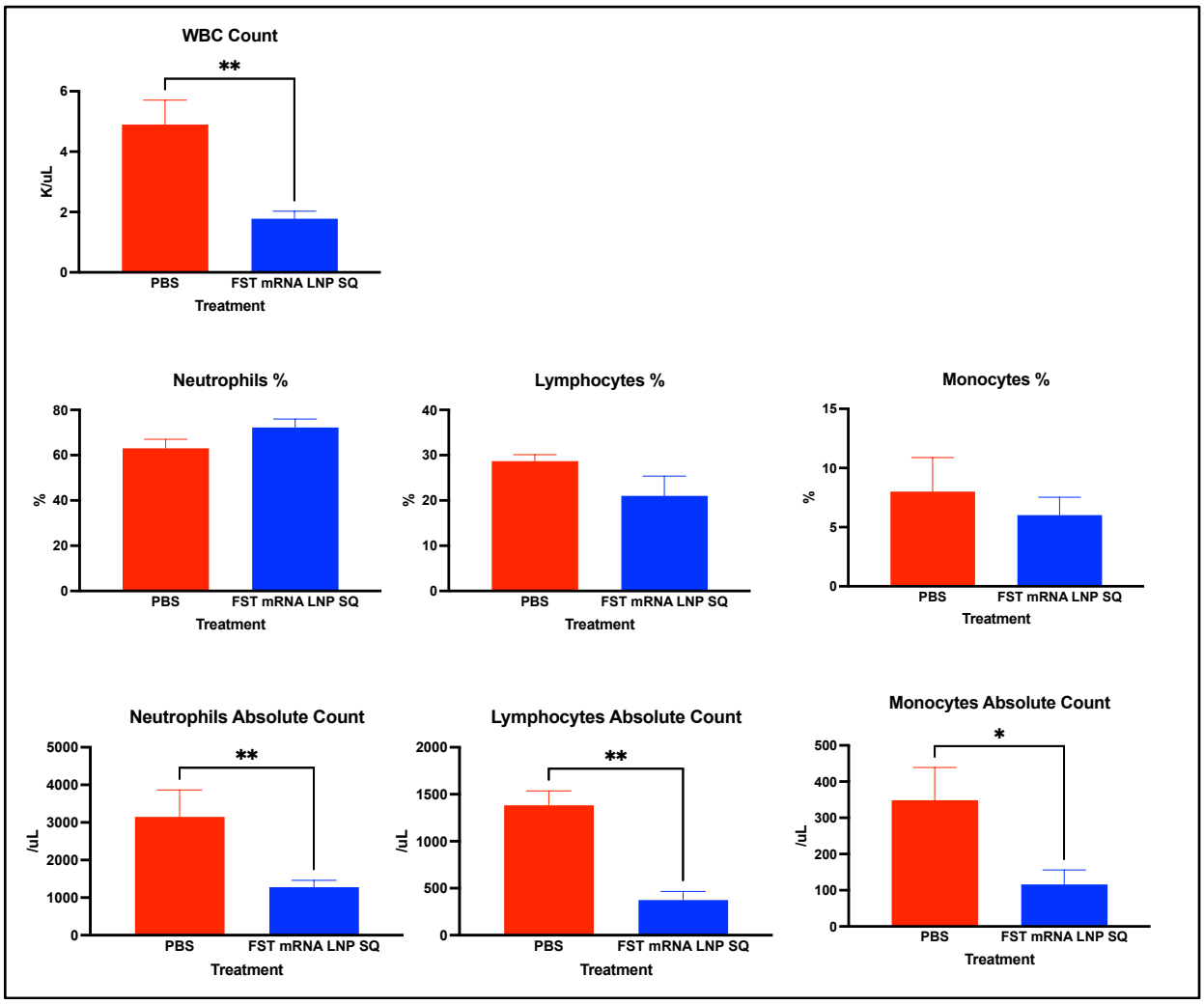

Figure 58. Intraperitoneal administration of *Fst* mRNA LNP formulation leads to decrease of leukocytes in blood. White blood cell (WBC) count, as well as neutrophil, lymphocytes, and monocytes percent and absolute counts were assessed as part of complete blood count analysis with differential. Data expressed as mean ± SEM, *n*=5, analyzed by t test, **p*<0.05, ***p*<0.01.

No significant changes were identified in blood chemistry parameters (**Figure 59**), except for a marginal decrease in total protein levels and reduced albumin levels (**Figure 60**). Similar decreases in total protein and albumin were observed following IP administration of MC3-containing LNP formulation in nude mice (refer to Chapter 4).

This observation may be attributed to the formation of a protein corona around LNPs, which absorbs albumin and leads to a decrease in total protein, as albumin is the most prevalent protein in the blood serum.

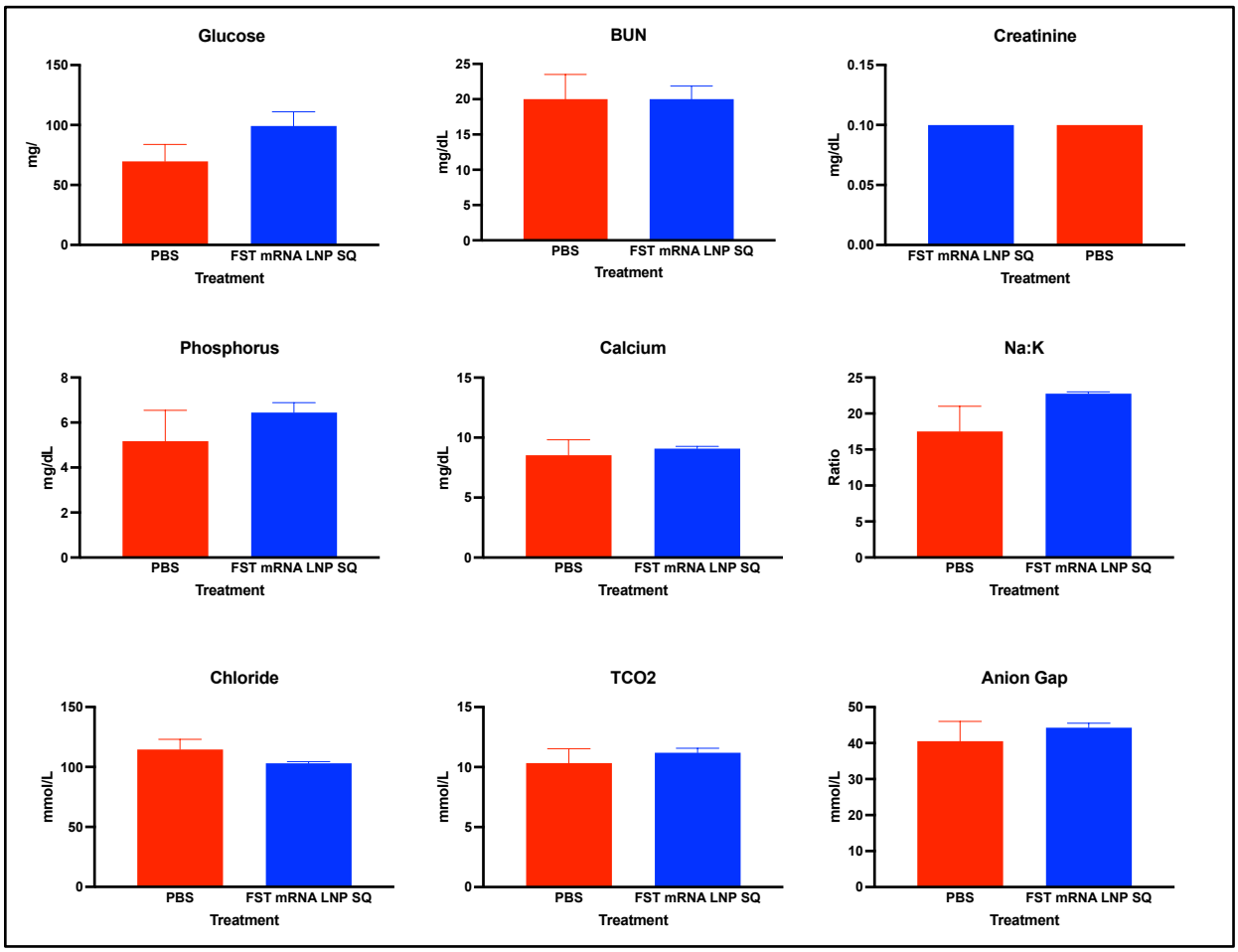

Figure 59. Intraperitoneal injection of *Fst* mRNA LNP formulation does not perturb blood chemistry. Glucose, blood urea nitrogen (BUN), creatinine, phosphorus, calcium, ratio of sodium to potassium, chloride, as well as blood bicarbonate levels and anion gap were assessed as part of blood chemistry analysis. Data expressed as mean ± SEM, *n*=5, analyzed by t-test.

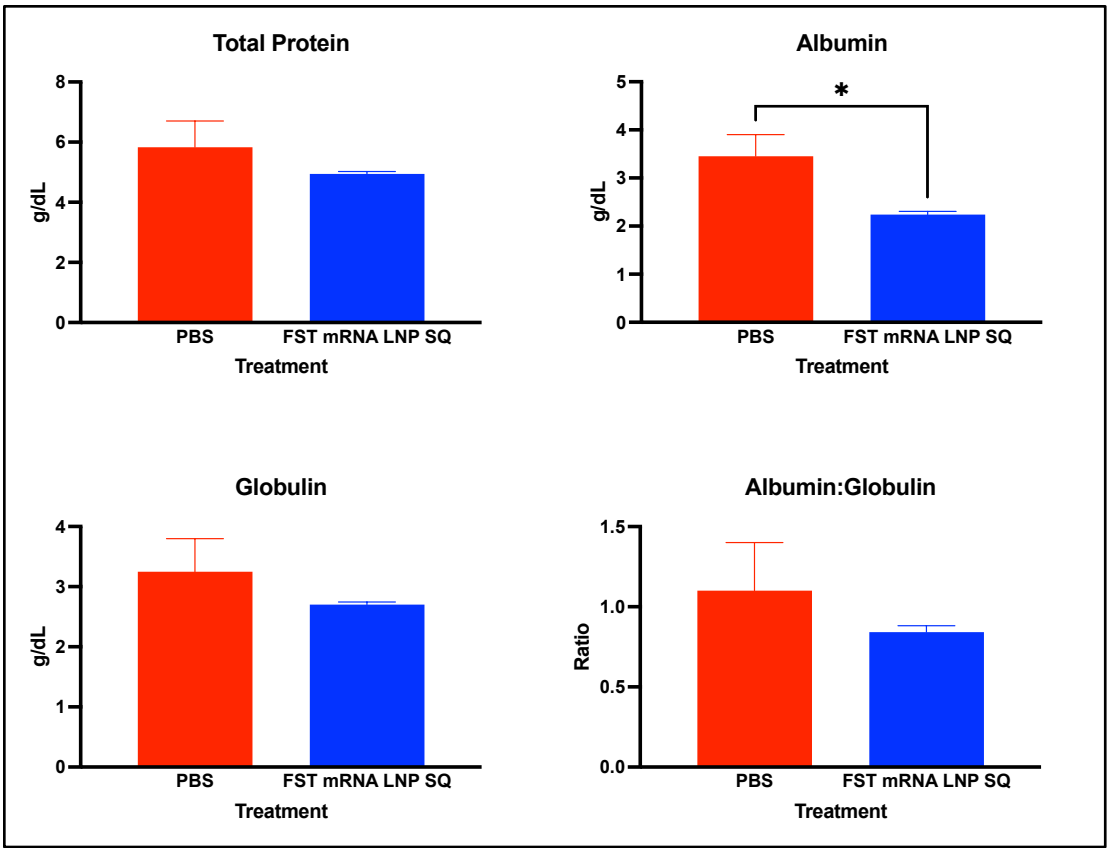

Figure 60. Intraperitoneal injection of *Fst* mRNA LNP formulation decreases serum albumin and as a result influences total protein concentration. Total protein, albumin, globulin and ratio of albumin to globulin were studied as part of blood chemistry analysis. Data expressed as mean ± SEM, *n*=5, analyzed by t test, *p<0.05.

Additionally, intraperitoneal injection of the *Fst* mRNA LNP formulation induced decreases in blood levels of alanine transaminase (ALT) and aspartate transaminase (AST), while alkaline phosphatase (ALP) was non-significantly increased (**Figure 61**). Importantly, amylase, lipase, and creatine kinase levels remained consistent with the control group. Cholesterol levels in treated mice were notably lower compared to their PBS control groups. In summary, our comprehensive assessment of the *Fst* mRNA LNP formulation indicates a favorable safety profile with minor molecular reactions, primarily cytokine responses. Importantly, these immune reactions do not manifest as reactogenicity on a behavioral level, as observed in food intake and body weight studies (**Figure 56**).

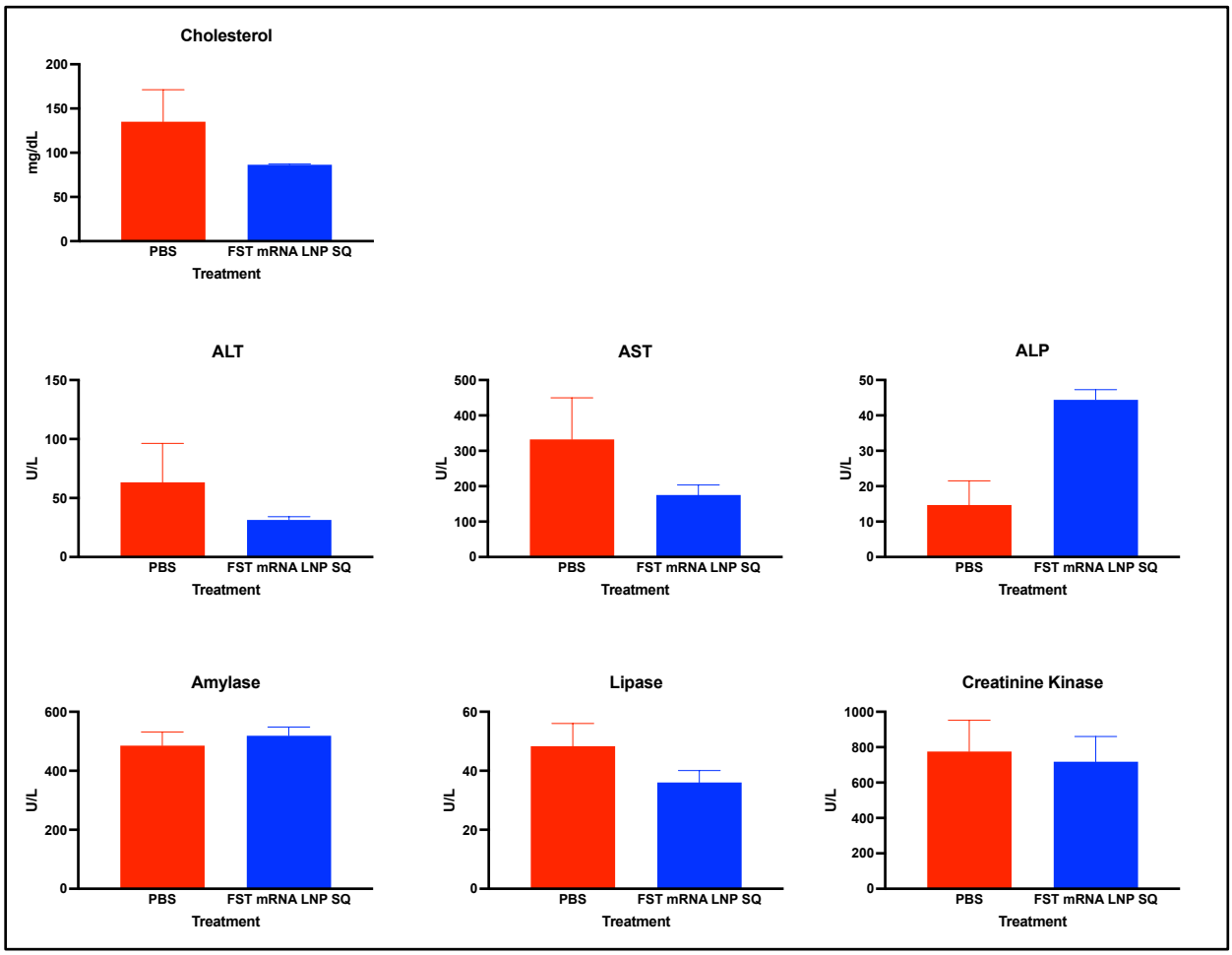

Figure 61. The intraperitoneal injection of the *Fst* mRNA LNP formulation does not disrupt the enzymes commonly used to evaluate hepatic inflammation. Cholesterol, ALT, AST, ALP, amylase, lipase, and creatinine kinase were included in the blood chemistry analysis. The safety assessment of the Fst mRNA LNP formulation via intraperitoneal injection reveals no disturbances in ALT and AST, commonly used indicators of hepatic inflammation, as well as in ALP, amylase, and lipase, extending the analysis beyond hepatic parameters. Data expressed as mean ± SEM, *n*=5, analyzed by t-test.

After confirming the favorable safety profile, we demonstrated a significant upregulation of *Fst* mRNA in both the liver and spleen, indicating successful delivery of therapeutic mRNA in these critical organs, especially following chronic injections known to induce mRNA degradation in wild-type mice (**Figure 62 A**). Importantly, the systemic levels of FST protein in the serum exhibited a robust and sustained increase, reaffirming the effectiveness of our LNP-mediated mRNA delivery system for multiple injections.

Most significantly, our therapeutic intervention demonstrated a pronounced impact on the levels of ActA in the serum (**Figure 62 B**). This finding implies that our LNP-based therapy effectively facilitated the ongoing overexpression of bioactive FST protein in wild-type mice from *Fst* mRNA with pseudouridine (N1-methyl-Ψ) substitution. This success, encompassing increased *Fst* mRNA levels, elevated systemic FST levels, and reduced ActA levels in wild-type mice, underscores the potential of our approach to mitigate key pathophysiological mechanisms driven by ActA. The effectiveness of the proposed therapeutic indicates a promising intervention for HNSCC specifically and, by extension, for epithelial cancers overexpressing ActA, including EOC.

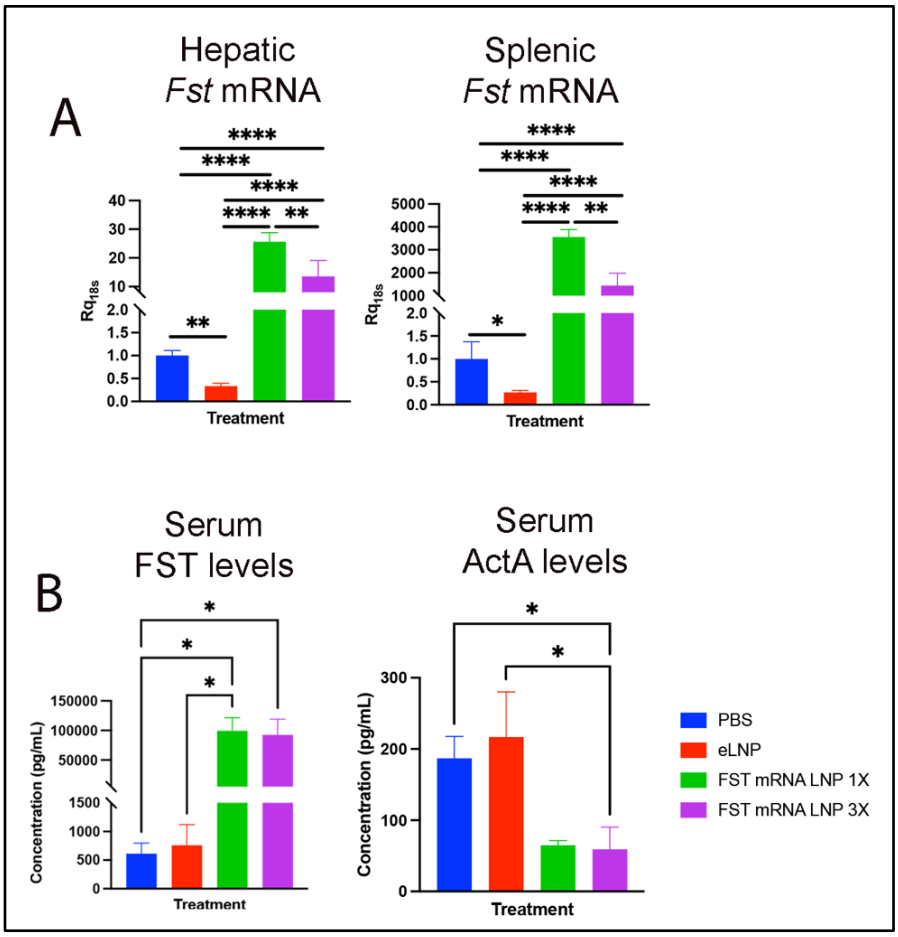

Figure 62: Characterization of *Fst* mRNA LNP safety profile. **(A)** Relative quantification of *Fst* mRNA in livers following single and chronic *Fst* mRNA LNP injections **(B)** FST and ActA level in serum of mice subjected to single and chronic *Fst* mRNA LNP injections. (A) and (B) expressed as mean ± SEM, *n*=5, analyzed by repeated measures one-way ANOVA, *p<0.05, **p<0.01. (C-E) expressed as mean ± SEM, n=5 *p<0.05, **p<0.01, ***p<0.001 analyzed by one-way ANOVA (*n*=5).

7.4 Therapeutic assessment and experimental approaches of *Fst* mRNA LNPs in MLM3 tumor model

In our initial evaluation of the efficacy of *Fst* mRNA LNPs on decreasing growth of MLM3 tumors *in vivo*, we administered the formulation via IP injection to evaluate abscopal effect of ActA downregulation systemically (**Figure 63 A**). The mice were initially subcutaneously injected with MLM3 cells, resulting in spherical subcutaneous tumors in the lower dorsal regions of C57BL/6 mice. After seven days, upon confirming the presence of spherical tumors, mice received daily IP injections of *Fst* mRNA LNP at doses equivalent to 5 ug mRNA for the subsequent seven days of the study. *Fst* mRNA LNP therapy led to a significant reduction in tumor mass, suggesting the impact of systemic FST upregulation (**Figure 63 B and C**). The effect of the *Fst* mRNA LNP formulation was compared to a negative control (PBS), eLNPs, and a non-specific mRNA LNP formulation (erythropoietin (*Epo*) mRNA LNPs).

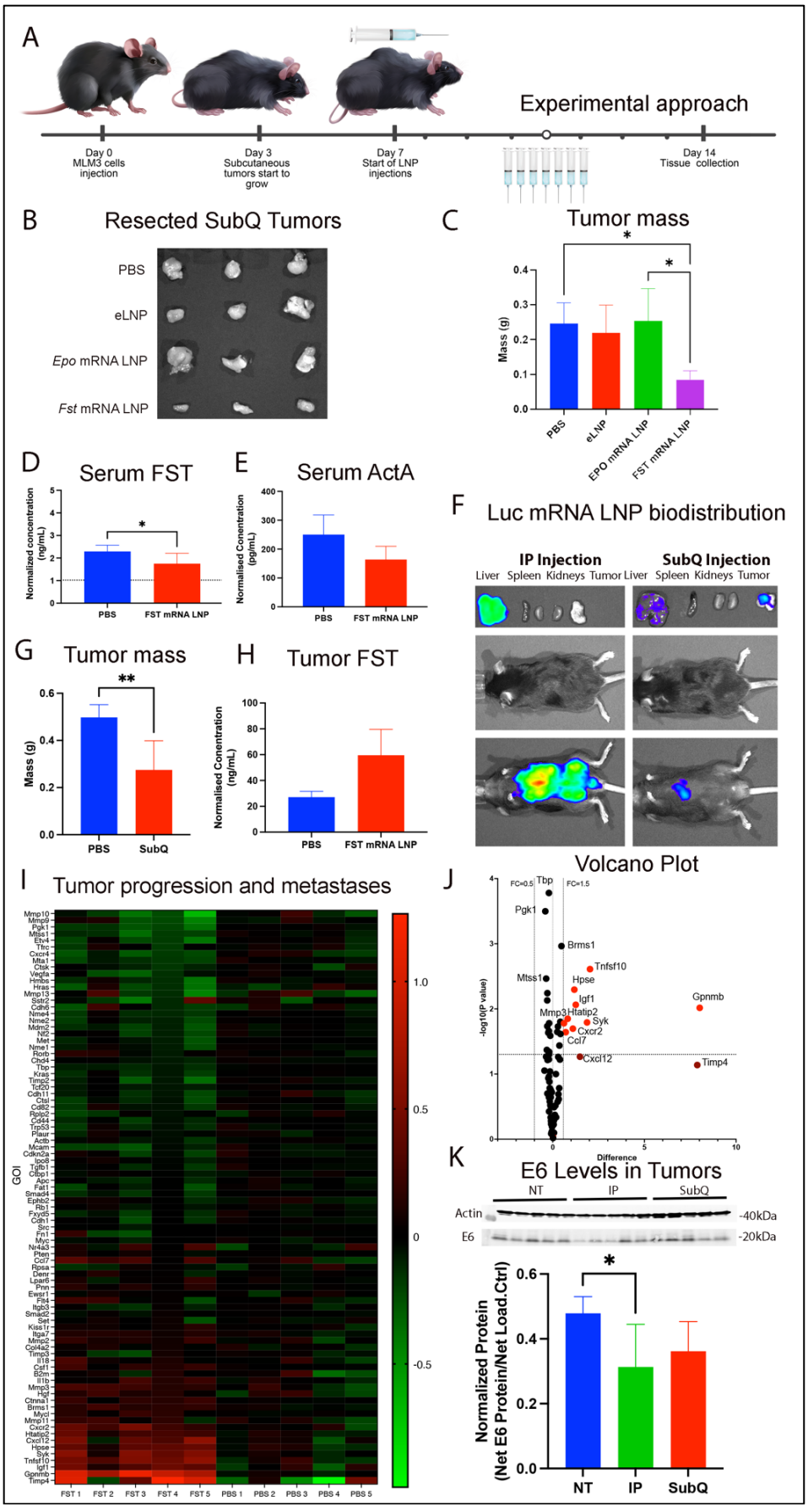
A
Experimental approach
Day 0
MLM3 cells
injection
Day 3
Subcutaneous
tumors start to
grow
Day 7
Start of LNP
injections
Day 14
Tissue collection
B
Resected SubQ Tumors
PBS
eLNP
Epo mRNA LNP
Fst mRNA LNP
C
Tumor mass
Mass (g)
PBS
eLNP
EPO mRNA LNP
FST mRNA LNP
D
Serum FST
Normalized concentration (ng/mL)
PBS
FST mRNA LNP
E
Serum ActA
Normalised Conentration (pg/mL)
PBS
FST mRNA LNP
F
Luc mRNA LNP biodistribution
IP Injection
SubQ Injection
Liver Spleen Kidneys Tumor Liver Spleen Kidneys Tumor
G
Tumor mass
Mass (g)
PBS
SubQ
H
Tumor FST
Normalised Conentration (ng/mL)
PBS
FST mRNA LNP
I
Tumor progression and metastases
GOI
FST 1 FST 2 FST 3 FST 4 FST 5 PBS 1 PBS 2 PBS 3 PBS 4 PBS 5
J
Volcano Plot
FC=0.5
FC=1.5
-log10(P value)
Difference
Tbp
Pgk1
Brms1
Tnfsf10
Mtss1
Hpse
Igf1
Gpnmb
Mmp3
Htatip2
Syk
Cxcr2
Ccl7
Cxcl12
Timp4
K
E6 Levels in Tumors
NT
IP
SubQ
Actin
E6
-40kDa
-20kDa
Normalized Protein
(Net E6 Protein/Net Load.Ctrl)
NT
IP
SubQ

Figure 63. The impact of *Fst* mRNA LNPs on MLM3 tumor progression reveals promising therapeutic potential in reducing tumor growth. (A) Experimental Design: MLM3 SubQ inoculation and 7-day tumor growth period, were followed by daily *Fst* mRNA administration for 7 days**. (B)** Representative images of resected SubQ tumors, following PBS, empty LNP (eLNP), *Epo* mRNA LNP and *Fst* mRNA LNP formulations administration for 7 days. **(C)** Massed of the resected tumors. Serum levels of FST **(D)** and ActA **(E)**. **(F)** Biodistribution of Luc mRNA LNPs administered via IP and SubQ ipsilateral. **(G)** Tumor mass following SubQ *Fst* mRNA LNP administration of 7 days. **(H)** FST levels from the tumor tissue. **(I)** TaqMan gene array assessment of genes associated with tumor progression in SubQ-injected MLM3 tumors, and metastases and the corresponding volcano plot **(J)**. **(K)** E6 levels in MLM3 tumors following IP and SubQ ipsilateral *Fst* mRNA LNP administration. (B-C) expressed as mean ± SEM, *n*=3 for all but *Fst* mRNA LNP group, where *n*=5, analyzed by one-way ANOVA, *p<0.05. (D-H) expressed as mean ± SEM, *n*=5 *p<0.05, analyzed by unpaired t-test. (I) expressed as fold change and -log10(p value), *n*=5, analyzed by multiple t-tests. (K) expressed as mean ± SEM, *n*=5, analyzed by one-way ANOVA, * p<0.05.

Surprisingly, serum FST levels were observed to decrease in mice treated with *Fst* mRNA LNP (**Figure 63 D**). This observation is likely linked to the therapy-induced reduction in ActA levels (**Figure 63 E**), resulting in a simultaneous downregulation of endogenous FST by the body. The underlying reason for this finding lies in the delivered *Fst* mRNA, designed to express an excess of FST protein in the serum, leading to a decrease in ActA-dependent tumor growth. Consequently, the decreased tumor burden triggers a reduction in serum ActA. In a self-regulating manner, FST-ActA equilibrium decreases FST systemic concentration while still maintaining levels higher than those in healthy age-matched controls, as indicated by the dotted line (**Figure 63 D**).

To improve translatability to human applications, we investigated the SubQ injection route, aligning with common clinical injection practices. We initially investigated whether SubQ injection, positioned ipsilateral to the growing tumor but not intratumoral, would enable transfection in both tumors and the liver. This was aimed at facilitating FST expression locally in tumors and systemically by utilizing the liver as a factory for FST upregulation. Upon single injection of Luc mRNA LNPs, we observed a

bioluminescence signal in both the livers and tumors, while IP injection resulted in bioluminescence originating solely from the livers (**Figure 63 E**). Therefore, we proceeded with SubQ administration of *Fst* mRNA formulation to assess its therapeutic efficacy.

Employing a comparable experimental setup (**Figure 63 A**) but utilizing a SubQ injection regimen, our investigation demonstrated noticeable changes in tumor morphology within the initial seven days of administration. Tumors in the treatment group exhibited a noticeable softening (as measured by palpitation), suggesting a potential therapeutic impact on the tumor microenvironment. We observed a noteworthy reduction in tumor size (**Figure 63 G**), accompanied by an increase in tumor FST concentration (**Figure 63 H**). The tumors again exhibited increased softness and mobility, as assessed by enhanced palpability and displacement beneath the skin, in comparison to the PBS-injected group. Consistent findings across multiple experimental replicates confirm the effectiveness of *Fst* mRNA LNPs in reducing the growth of MLM3 tumors.

In our further analysis of the MLM3 tumors subjected to SubQ *Fst* mRNA LNP administration we used TaqMan gene array to explore modulation of metastases and proliferation in MLM3 tumors. We identified the upregulation of nine genes (*Mmp3*, *Tnfsf10*, *Hpse*, *Syk*, *Igf1*, *Cxcr2*, *Ccl7*, *Htatip2*, *Gpnmb*) and two genes that were highly upregulated but had marginal -log10(p value) significance (*Cxcl12* and *Timp4*) (**Figure 63 I, J,** and **Table 10**). The genes *Ccl7*, *Igf1*, *Tnfsf10*, and *Gpnmb*, identified in the top enrichment results using Bioplanet, had the highest association with the TGF-beta regulation of the extracellular matrix pathway. This finding is particularly relevant since

ActA, a key component of the TGF-beta superfamily, is crucial in this context. The inhibition of ActA through FST becomes especially important, highlighting the potential significance of these identified genes in the intricate regulatory network of the extracellular matrix (ECM). Targeting the regulation of the ECM is crucial for impeding tumor invasion, metastasis, and angiogenesis, as the ECM plays a central role in providing structural support and influencing cell signaling. [584]

HPV E6 and E7 proteins are known to fuel tumorigenesis in HNSCC, making their suppression a significant therapeutic target. [585] As an indicator of a slower-progressing tumor burden, we assessed the expression of HPV E6 protein within the tumors after seven days of both IP and SubQ administrations of the *Fst* mRNA LNP formulation (**Figure 63 K**). The observed reduction in HPV E6 expression in MLM3 tumors from mice receiving the *Fst* mRNA LNPs indicates an inhibitory impact of the developed therapy on key pathways associated with tumor progression.

Table 10. Statistical analysis summary of differentially expressed genes in tumor proliferation and migration assay

GENE	*P* value	Treatment Group Mean	Difference	SE of difference	t ratio	df	-log10 (P value)
Pgk1	0.000317	0.5959	-0.4041	0.06489	6.228	7.56	3.498
Mtss1	0.00343	0.643	-0.357	0.08638	4.133	7.842	2.465
Etv4	0.042673	0.6777	-0.3223	0.1272	2.533	6.303	1.37
Mta1	0.007394	0.6982	-0.3018	0.07969	3.787	6.707	2.131
Mcam	0.01841	0.703	-0.297	0.1003	2.962	7.875	1.735
Mdm2	0.005733	0.709	-0.291	0.07788	3.737	7.999	2.242
Ctsl	0.023218	0.7554	-0.2446	0.08737	2.799	8	1.634
Nme2	0.049335	0.7832	-0.2168	0.08385	2.586	4.971	1.307
Smad4	0.021811	0.789	-0.211	0.06002	3.515	4.3	1.661
Tbp	0.000166	0.7917	-0.2083	0.03139	6.636	7.97	3.78
Kras	0.047524	0.7973	-0.2027	0.07786	2.603	5.058	1.323
Cd44	0.016593	0.802	-0.198	0.05587	3.543	4.985	1.78
Fxyd5	0.045533	0.8039	-0.1961	0.08288	2.366	7.997	1.342
Tcf20	0.02582	0.8674	-0.1326	0.04851	2.733	7.963	1.588
Pnn	0.022526	1.248	0.2478	0.07785	3.182	5.306	1.647
Itga7	0.018659	1.283	0.2831	0.08488	3.335	5.348	1.729
Mmp2	0.036526	1.364	0.3644	0.1432	2.545	7.44	1.437
Ctnna1	0.015758	1.414	0.4137	0.1117	3.705	4.668	1.802
Csf1	0.024243	1.42	0.4204	0.1261	3.334	4.503	1.615
Brms1	0.001085	1.477	0.4772	0.09583	4.98	7.987	2.965
Mmp3	0.016604	1.612	0.612	0.1934	3.164	6.757	1.78
Ccl7[a]	0.022779	1.711	0.7111	0.2505	2.839	7.683	1.642
Htatip2	0.014178	1.817	0.8168	0.233	3.506	5.619	1.848
Cxcr2	0.020131	2.099	1.099	0.3318	3.311	5.178	1.696
Hpse	0.005063	2.177	1.177	0.2787	4.223	6.248	2.296
Igf1[a]	0.008643	2.255	1.255	0.3429	3.659	6.738	2.063
Syk	0.016119	2.871	1.871	0.4807	3.891	4.198	1.793
Tnfsf10[a]	0.002453	3.033	2.033	0.3942	5.159	5.693	2.61
Gpnmb[a]	0.009625	9.016	8.016	1.726	4.644	4.014	2.017

[a] Genes identified in the top enrichment results indicate a significant association with the TGF-beta regulation of the extracellular matrix pathway.

7.5 *Fst* mRNA LNP therapy prevents formation and growth of distant MLM3 metastases in the lung

We next evaluated the therapeutic potential of *Fst* mRNA LNP therapy in a longitudinal study with MLM3 cancer-bearing mice, demonstrating remarkable efficacy in impeding tumor progression and reducing the incidence of metastasis. In this study, MLM3 mice were administered with SubQ *Fst* mRNA LNPs starting day 7 following MLM3 cells inoculation (**Figure 64 A**). The therapeutic intervention led to a spectrum of notable outcomes, underscoring the efficacy of our formulation.

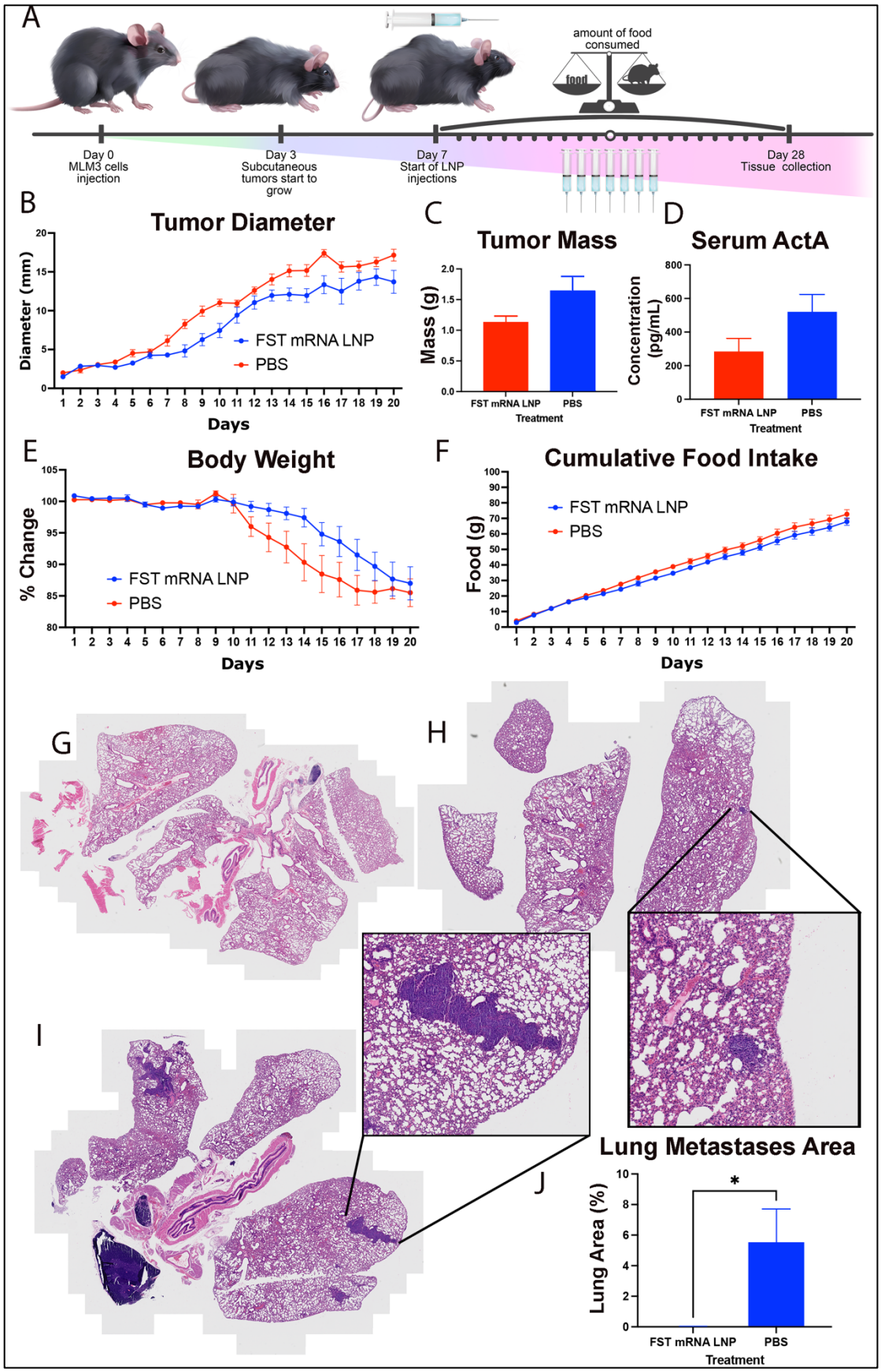
A
amount of food consumed
food
Day 0
MLM3 cells injection
Day 3
Subcutaneous tumors start to grow
Day 7
Start of LNP injections
Day 28
Tissue collection
B
Tumor Diameter
Diameter (mm)
Days
FST mRNA LNP
PBS
C
Tumor Mass
Mass (g)
FST mRNA LNP
PBS
Treatment
D
Serum ActA
Concentration (pg/mL)
FST mRNA LNP
PBS
Treatment
E
Body Weight
% Change
FST mRNA LNP
PBS
Days
F
Cumulative Food Intake
Food (g)
FST mRNA LNP
PBS
Days
G
H
I
J
Lung Metastases Area
Lung Area (%)
*
FST mRNA LNP
PBS
Treatment

Figure 64. A longitudinal assessment of *Fst* mRNA LNPs reveals a decrease in the formation of lung metastases in the treatment group, highlighting the potential efficacy of the developed therapy in inhibiting metastatic spread. (A) Experimental Design: MLM3 cells were subcutaneously inoculated, allowing for 7 days of tumor growth, followed by daily administration of *Fst* mRNA until day 28, a time point when the MLM3 model consistently develops lung metastases close to 100% penetrance. **(B)** Tumor diameter in treatment and control groups. **(C)** Massed of the resected tumors. **(D)** Serum levels of ActA. **(E)** Body weight and **(F)** cumulative food intake. **(G)** Representative histological image of murine lungs from *Fst* mRNA LNP treatment group. **(H)** and **(I)** represent histological images of lungs from the control (PBS) group, showcasing a spectrum of MLM3 metastases, ranging from small spherical formations to large tissue infiltrates. **(J)** Metastatic area normalized to total cross-section area of lung lobe. (B, E, F) expressed as mean ± SEM, *n*=7 analyzed by one-way repeated measures ANOVA. (C, D, J) expressed as mean ± SEM, *n*=7, analyzed by unpaired t-test, * $p<0.05$.

One of the most striking findings was the suppression of subcutaneous tumor growth in *Fst* mRNA LNP-treated mice compared to the control (PBS) group (**Figure 64 B**). In the initial 7 days of therapy, MLM3 tumor sizes remained unchanged by caliper measurements. However, a notable change in tumor stiffness was observed, with *Fst* mRNA LNP-treated tumors appearing softer. After 7 days, the *Fst* mRNA LNP administration resulted in reduced tumor growth. Although the final mass of dissected tumors at study completion did not reach statistical significance, a trend towards lower tumor masses was evident (**Figure 64 C**). Mirroring tumor size, the concentration of ActA was decreased in the treated mice (**Figure 64 D**). Additionally, the treated mice exhibited an ability to sustain their overall body mass, in contrast to PBS-treated mice bearing MLM3 tumors (**Figure 64 E**). While there was a modest increase in food intake in the control group in comparison to the treatment group (**Figure 64 F**), we believe this was due to inherent reactogenicity of LNP formulation decreasing food intake around day 7 of the model progression that then parallels with control group without further decrease.

Importantly, our therapeutic approach demonstrated remarkable efficacy in preventing metastatic spread from primary MLM3 tumors to the lungs. Lung tissue analysis revealed minimal metastatic dissemination in *Fst* mRNA LNP-treated mice (**Figure 64 G**), marking a potential milestone in HNSCC management. In contrast, the control group exhibited varying levels of metastatic infiltration in the lungs, ranging from small spherical metastases in subpleural regions (**Figure 64 H**) to large cancer infiltrates occupying up to 16% of the lung lobe (**Figure 64 I**). Notably, only one mouse in the treatment group developed metastases, compared to all mice (n=7) in the control group, as indicated by the calculation of metastases area normalized to lung lobe area (**Figure 64 I**).

7.6 Impact of *Fst* mRNA LNP therapy on body composition and autophagy-related genes in cachexia-induced changes

Evaluation of body composition of the live mice using magnetic resonance imaging (MRI) provided insights into the physiological changes induced by our therapy. Mice subjected to a 14-day SubQ administration of the *Fst* mRNA LNP formulation exhibited a notable increase in fat content, suggesting a protective effect on adipose tissue (**Figure 65**).

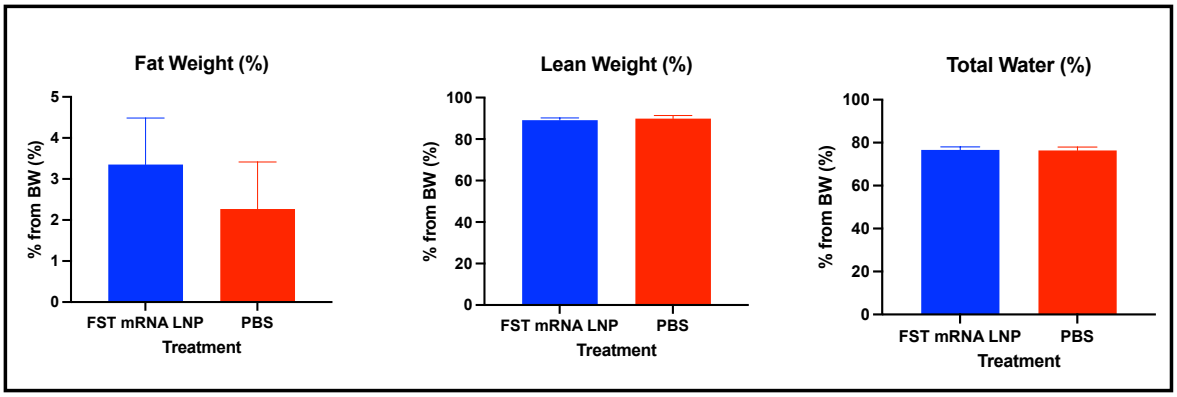

Figure 65. Magnetic resonance imaging results show increased adiposity in the mice receiving *Fst* mRNA LNP formulation. Fat, lean and total water percent from the total weight were determined using MRI; expressed as mean ± SEM, *n*=7, analyzed by unpaired t-test, * p<0.05.

While lean weight and total water content remained consistent across both treatment and control groups, the unexpected similarity in lean weight between the treatment and control groups may be attributed to the control group's elevated tumor burden, potentially influencing MRI detection as lean tissue (**Figure 66 A**).

Post-mortem examination of the organs indicated unaltered liver and kidney masses in both groups (**Figure 66 B**), while spleen sizes were increased in the treatment group. In addition, inguinal and gonadal fat pad masses showed an increase in mice subjected to *Fst* mRNA LNP therapy (**Figure 66 C**), aligning with MRI findings that demonstrated heightened adiposity in the treatment group. This observation holds significance, as during cachexia, the depletion of fat stores becomes a critical issue due to its association with muscle wasting and compromised overall health, emphasizing the importance of preserving adipose tissue for maintaining physiological balance. Regarding muscle mass alterations, no significant change was noted in heart masses (cardiac muscle) between the groups, while a positive trend toward increased skeletal muscle masses was observed in the gastrocnemius (GA) and flexor digitorum longus (FDL) muscles (**Figure 66 D**).

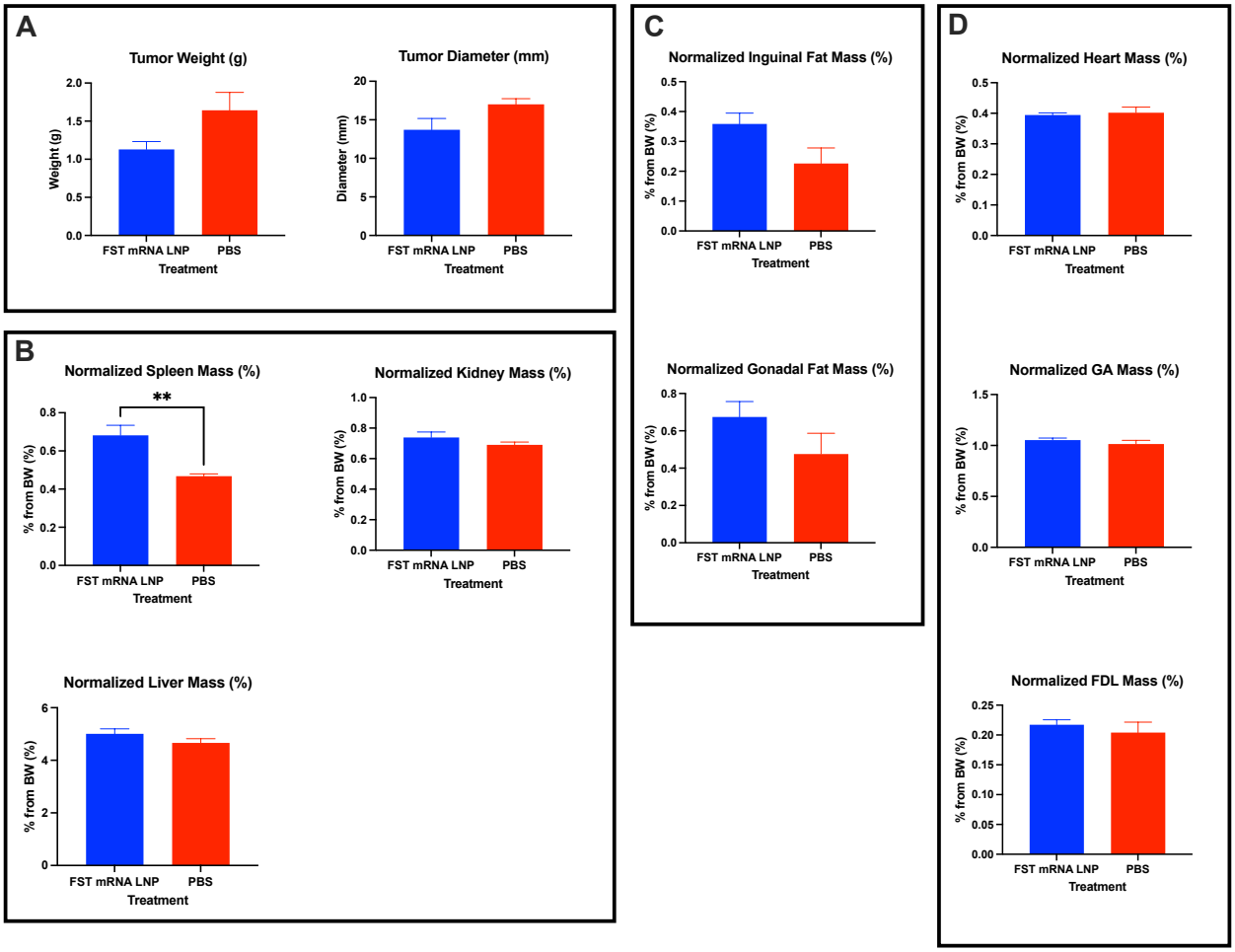

Figure 66. Post-therapy organ mass analysis reveals a noteworthy increase in fat mass. (A) Tumor weight and tumor diameter. **(B)** Spleen, kidney, and lvie masses normalized to pre-tumor inoculation mouse body weight (C) Normalized inguinal and gonadal fat pad masses normalized to pre-tumor inoculation mouse body weight. **(D)** Heart, gastrocnemius (GA), and flexor digitorum longus masses normalized to pre-tumor inoculation mouse body weight. All were expressed as mean ± SEM, *n*=7, analyzed by unpaired t-test, ** p<0.01.

Although the gross composition of lean muscle weight was comparable between the two groups, a negative trend in the expression of autophagy-related genes was observed in therapy-treated mice, specifically transcription factor Forkhead box O1 (*Foxo1*) in both GA and FDL muscle (**Figure 67 A and B**). In cachexia, muscle cells often show an increase in autophagy, which is a cellular response to heightened stress and energy requirements. [586] The heightened autophagic activity serves as a survival

mechanism for cells, aiming to break down and recycle proteins to meet increased energy demands. [587] While it aids cellular survival, persistent and excessive autophagy can contribute to muscle wasting by breaking down essential proteins and organelles crucial for muscle function. [588] The observed decrease in *Foxo1*, a key regulator of autophagy, in the treated mice suggests a potential downregulation of cachexia-related protein recycling leading to muscle wasting.

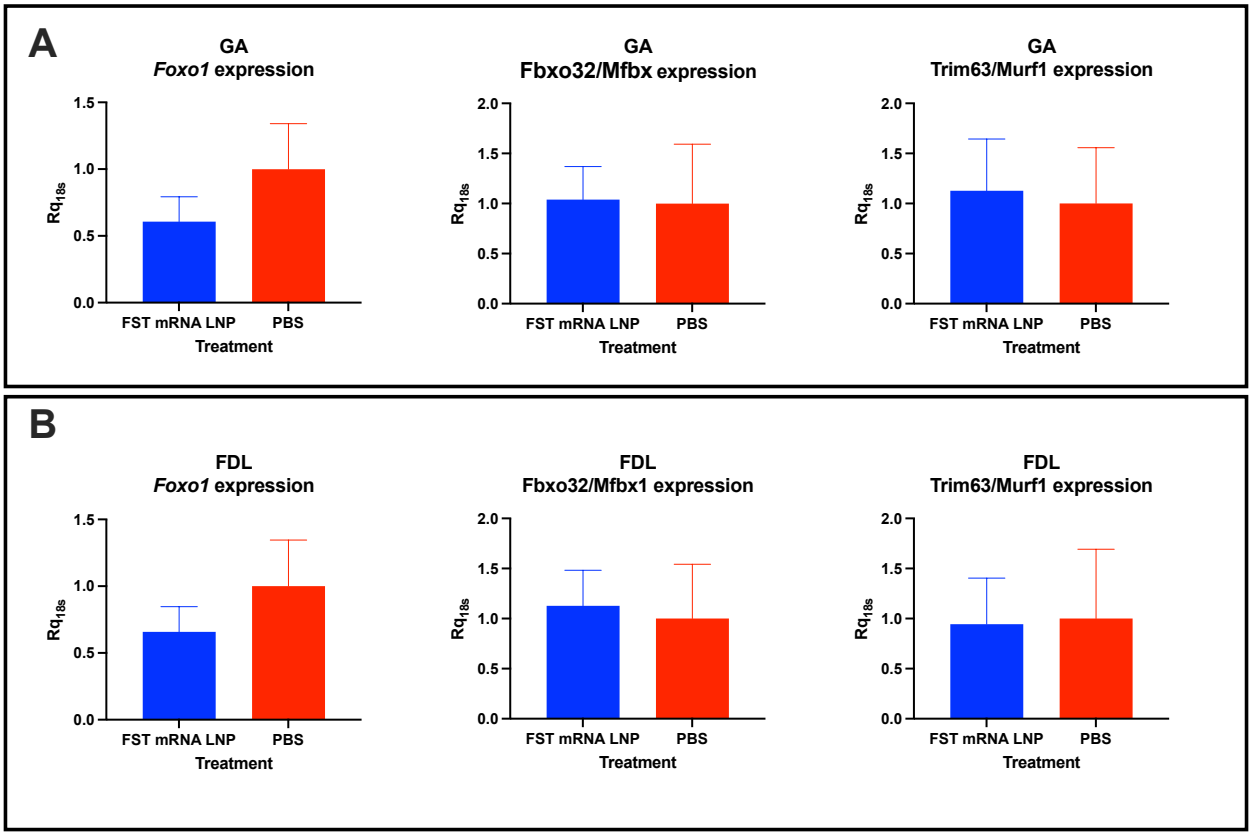

Figure 67. Assessment of autophagy gene expression in murine muscles shows *Foxo1* downregulation in *Fst* mRNA LNP-treated mice. *Foxo1, Fbxo32/Mfbx1, Trim63/Murf1* expression in gastrocnemius **(A)** and flexor digitorum longus **(B)** muscles; expressed as mean ± SEM, *n*=7, analyzed by unpaired t-test, * p<0.05.

Finally, the administration of *Fst* mRNA LNP therapy proved highly effective in mitigating cachexia, specifically evidenced by a notable rescue in muscle fiber cross-sectional area (CSA). The *Fst* mRNA LNP-treated mice displayed a modest 11.33% reduction in CSA in comparison to healthy mice, while the control group treated with

PBS exhibited a significant 50% decrease (**Figure 68 A, B**). Notably, this muscle-sparing effect aligns with our previous observations in the ES2 clear cell carcinoma model in nude mice (refer to Chapter 4). These consistent findings underscore the potential of *Fst* mRNA LNP as a robust intervention for preserving muscle integrity and combating cachexia across different experimental models, emphasizing its promising translational implications.

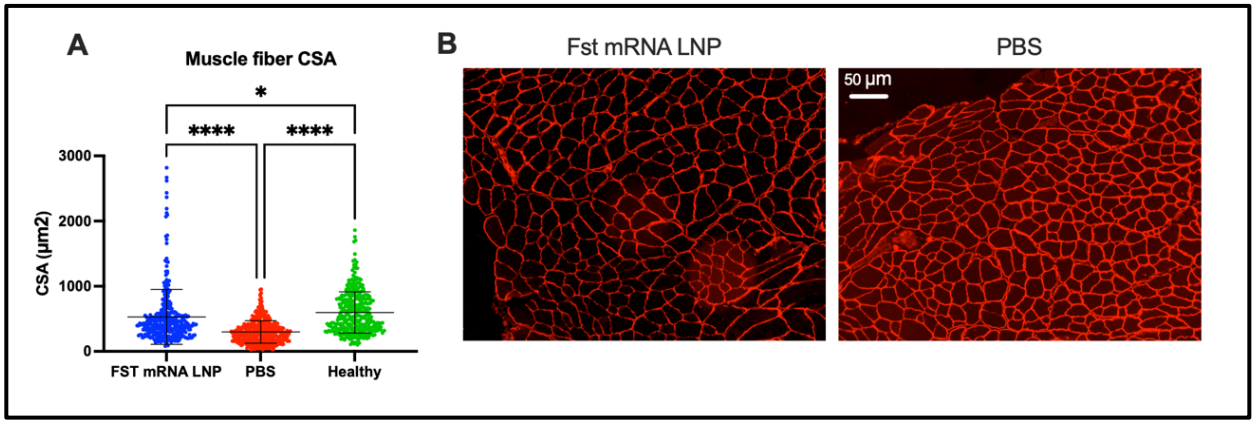

Figure 68. *Fst* mRNA LNP therapy administration prevents cachexia-induced decrease in muscle fiber cross-sectional area. (A) Muscle fiber cross-sectional area (CSA) in MLM3 cancer-bearing mice treated with *Fst* mRNA LNP or PBS in comparison to muscle fiber CSA of healthy mice. **(B)** Illustrative laminin immunohistochemistry, emphasizing the boundaries of muscle fibers in *Fst* mRNA LNP treatment group and control. (A) expressed as mean ± SEM, n=7, analyzed by one-way ANOVA, * p<0.05, ****p<0.001

7.7 Methods

Materials

LNP components included ALC-0315 ionizable lipid, cholesterol, DSPC, and DMG-PEG2k, and were sourced from BroadPharm Inc. (San Diego, CA), BioFine International (Vancouver, BC, Canada), and Avanti Polar Lipids (Alabaster, AL, USA). For the synthesis of mRNA LNPs, luciferase (*Luc*) mRNA, erythropoietin (*Epo)* mRNA and N1-methyl-Ψ *Fst* mRNA (open reading frame sequence published in [64]) were

obtained from TriLink Biotechnologies Inc. (San Diego, CA, USA). NanoAssemblr cartridges were purchased from Precision NanoSystems (Vancouver, Canada). The concentration of LNPs post-synthesis utilized Amicon ultra centrifugal filters from MilliporeSigma (Burlington, MA, USA). The cell culture reagents, including DMEM and F-12 media, fetal bovine serum (FBS), phosphate-buffered saline (PBS), and penicillin-streptomycin, were supplied by Gibco (Gaithersburg, MD, USA). Nuclease-free water was obtained from Cytiva (Hyclone Laboratories, South Logan, UT, USA). The assortment of reagents, including d-luciferin for bioluminescence assays, Halt Protease Inhibitor Cocktail, Pierce BCA protein assay kit, insulin-transferrin-selenium, Pen-Strep, Quant-iT RiboGreen RNA kit, and RNA standards, was provided by Thermo Fisher Scientific (Waltham, MA, USA). Further molecular biology reagents, including the DNA-free Kit and TRIzol reagent for RNA isolation, were sourced from Ambion (Carlsbad, CA, USA). The RNeasy Mini kit and Proteinase K reagent, used for RNA purification and DNA digestion respectively, were purchased from Qiagen Corporation (Hilden, Germany). Applied Biosystems (Foster City, CA, USA) supplied components for gene expression analysis, such as the TaqMan Reverse Transcription Reagents Kit, TaqMan Gene Expression Master Mix, and other TaqMan assay reagents. Protein extraction buffer was sourced from Invitrogen (Carlsbad, CA, USA). The protease inhibitor cocktail (Roche cOmplete) and PVDF membranes for protein transfer were obtained from MilliporeSigma (Burlington, MA, USA). Primary antibodies against E6, beta actin, and laminin, in addition to secondary Alexa Fluor-conjugated antibodies, all were purchased from Invitrogen (Carlsbad, CA, USA).

Lipid Nanoparticle Formulation and Characterization

Fst mRNA LNPs were assembled as described elsewhere [65], and included ALC-0315 ionizable lipid, cholesterol, DSPC, and DMG-PEG-2k in proportions of 50:38.5:10:1.5. N1-methyl-Ψ *Fst* mRNA (obtained from TriLink Biotechnologies Inc., San Diego, CA, USA) was incorporated with N:P ratio of 5.67 between ionizable lipids and nucleic acids. Formulations were prepared using NanoAssemblr Ignite or Benchtop (Precision Nanosystems Inc., Vancouver, Canada). LNPs were concentrated via dialysis using saline buffer exchange approach (pH 7.4), and then characterized for hydrodynamic size, PDI, and ζ potential, using Zetasizer Nano ZS (Malvern Analytical, Malvern, UK) and nanoparticle-tracking analysis (NanoSight, Malvern Instruments, Worcestershire, UK) diluted in PBS for analysis. LNPs had high mRNA encapsulation efficiency exceeding 90%, determined by Quant-iT RiboGreen assay. For biodistribution and control experiments, luciferase (*Luc*) mRNA LNPs, empty (eLNP) and erythropoietin (*Epo*) mRNA LNPs were synthesized using the aforementioned methodology. For the morphological assessment of *Fst* mRNA LNPs, cryo-electron microscopy (CryoEM) was employed using the Thermo Scientific Glacios 2 Cryo-Transmission Electron Microscope (Thermo Fisher Scientific, Waltham, MA, USA). A 2 µL - sample was distributed over two standard 300 mesh copper grids with Lacey carbon (Cu/Lacey), which were plasma cleaned at 15 mA for 60 seconds. The sample was applied to the carbon side, allowed to settle for 15 seconds, then blotted with a -15 force for 2 seconds, preparing it for imaging.

In Vitro Evaluation

The MLM3 cell line, provided by Paola D. Vermeer, and the C2C12 and AML12 cell lines, supplied by Aaron Grossberg's laboratory, were cultured according to the protocols outlined below and routinely tested for mycoplasma. C2C12 were grown in

DMEM with 10% FBS and 1% Pen-Strep for proliferation at 37°C and 5% CO2. For differentiation into myotubes, the medium was switched to DMEM supplemented with 5% horse serum. MLM3 cells were cultured in DMEM medium plus 10% FBS and 1% Pen-Strep maintained at 37°C in 5% CO2 and passaged at 80-90% confluence. AML12 cells were cultured in DMEM/F-12 media supplemented with 10% FBS, 1% Pen-Strep, 1% insulin-transferrin-selenium, and dexamethasone (40 ng/ml), at 37°C and 5% CO2 atmosphere, and passaged at 80-90% confluence. All cell lines were grown in 6 well plates, seeded with 100,000 cells/well.

Fst mRNA LNP transfection efficiency and FST protein expression in the cell lines were studied using quantitative rt-PCR on the cells and FST ELISA assays on conditioned media. The cells were seeded in 6-well plates and allowed to grow to 70% confluence before treatment. *Fst* mRNA LNP were added to the media in concentration 400 ng/mL and cells and conditioned media collected 8 horus after treatment.

For *rt-PCR analyses*, to obtain total RNA, we used the combination of TRIzol and Chloroform, supplied by Ambion Co. (Carlsbad, USA) and Sigma-Aldrich (Merck KGaA, Darmstadt, Germany), respectively. Following this, the RNeasy Mini kit from Qiagen Corporation (Hilden, Germany) was utilized for RNA purification. Genomic DNA contamination was removed using Ambion's DNA-free Kit (Invitrogen, Carlsbad, CA, USA). The synthesis of cDNA was facilitated using the TaqMan Reverse Transcription Reagents Kit from Applied Biosystems (Foster City, CA, USA). For the relative quantification of *Fst*, we employed the TaqMan Gene Expression Master Mix along with TaqMan assay reagent (Mm00514982_m1), both sourced from Applied Biosystems (Foster City, CA, USA). Relative counts were normalized to non-primer limited 18S

endogenous control Applied Biosystems, Foster City, CA, USA). Data acquisition and analysis was performed using a QuantStudio 3 real-time PCR system (Applied Biosystems, Foster City, CA. USA) and Applied Biosystems qPCR Analysis Modules via ThermoFisher cloud.

Ray Biotech (Peachtree Corners, GA) mouse FST and mouse ActA ELISA kits were used for FST and ActA quantification in the conditioned media of MLM3, C2C12 and AML12 cells grown. The assay was performed according to the manufacturer's protocol. Colorimetric data was acquired on BioTek Gen5 (Santa Clara, CA). FST and ActA protein concentrations were normalized to total protein determined by Pierce BCA protein assay (ThermoFisher Scientific, Waltham, MA, USA).

The capability of FST to inhibit MLM3 cell migration was assessed using a scratch assay. A scratch was made in a confluent layer of MLM3 cells growing in 6-well plates, followed by treatment with *Fst* mRNA LNP (400 ng/mL). Cell migration into the scratch was observed after 24 hours using a Biozero BZ-8000 fluorescence microscope (KEYENCE, Itasca, IL, USA). Analysis was conducted with BZ Viewer 2.5 software (KEYENCE, Itasca, IL, USA) and QuPath software. [66]

Animal studies

Mouse studies adhered to the National Institutes of Health's Guide for the Care and Use of Laboratory Animals. Approval for all animal experiments was granted by the Institutional Animal Care at both Oregon Health & Science University and Oregon State University (Approval ID: IP00000690). Wild-type C57BL/6J male mice (IMSR_JAX:000664) from The Jackson Laboratory were utilized for the study, with ages ranging from 8 to 10 weeks. The decision to use male mice for examining the impact of tumor-derived ActA on cancer progression and the effectiveness of *Fst* mRNA LNPs

was informed by research showing that female mice exhibit a quicker endogenous FST response to increases in tumor-derived ActA compared to male mice. This difference leads to less severe cachexia symptoms in female mice. [67] Using male mice therefore offers us a clearer baseline for assessing tumor-derived ActA effects and therapeutic efficacy of FST upregulation. This approach was also guided by the ethical imperative to minimize animal use, ensuring that our research questions could be answered while still obtaining meaningful and interpretable results. For all studies, the mice were kept in a controlled environment within a specialized mouse facility, maintaining a temperature of 26°C to mimic the murine body temperature and prevent stress from cold exposure. A consistent 12-hour light/dark cycle was ensured for all animals. Mice had free access to water and were fed a standard Purina rodent diet 5001 (Purina Mills, St. Louis, MO, USA).

The MLM3 model was established through the subcutaneous administration of 1 million MLM3 cells into the lower flank region. The levels of ActA in serum were evaluated using an ELISA that had been described in the prior section. For the examination of lung metastases in the MLM3 model, Hematoxylin and Eosin (H&E) stained paraformaldehyde-preserved tissue samples were analyzed using the Zeiss Axioscan Slide Scanner (Zeiss, Oberkochen, Germany).

Procedures for evaluating the safety profile of *Fst* mRNA LNP therapy delivered to healthy, non-tumor-bearing mice via intraperitoneal (IP) injection included food intake measurements, weight monitoring, and analysis of liver samples for pro-inflammatory cytokines, and assessment of complete blood cell count (CBC) with differential, and blood chemistry. Food was pre-dried to standardize water content, thereby eliminating

variations that could introduce errors into food intake measurements. CBC and blood chemistry were outsourced to IDEXX (Westbrook, ME, USA). ActA and FST levels, encompassing both mRNA expression in the liver and protein concentration in serum, were assessed following both a single administration and chronic treatment involving three daily injections of *Fst* mRNA LNP. Similar evaluations were conducted for two control groups, one receiving PBS and the other eLNP, each subjected to three daily injections. rt-PCR was performed on the liver samples using the approach described above with the following TaqMan assays *Cxcl1* (Mm04207460_m1), *Cxcl2* (Mm00436450_m1), *Il1b* (Mm00434228_m1), *Il6* (Mm00446190_m1), *Tnf* (Mm00443258_m1). *Fst* expression was assessed with rt-PCR using TaqMan assay Mm00514982_m1. The levels of ActA and FST in serum of healthy mice as part of *Fst* mRNA LNP therapy efficacy evaluation were determined using ELISA kits that had been described in prior section.

***Therapeutic assessmen*t**

To investigate the biodistribution patterns of LNPs in MLM3-bearing mice, 5 μg of *Luc* mRNA LNP were injected subQ (peritumorally) or IP in 100 μL of PBS for biodistribution studies. Six hours following the injections, the mice were administered with d-luciferin (150 mg/kg b.w.) and the analysis of whole-body and organ-specific bioluminescence was performed using the IVIS Lumina XRMS system (Perkin Elmer, Hopkinton, MA, USA). The bioluminescence data processed via Living Image software (Perkin Elmer, Hopkinton, MA, USA).

In evaluating the efficacy of *Fst* mRNA LNPs in the MLM3 tumor model, mice received seven daily injections of *Fst* mRNA LNPs (5 μg/dose) through either IP or

subcutaneous (subQ) injections, with each dose delivered in 100 µL of PBS. The concentrations of FST and ActA proteins in tumor lysates prepared with cell extraction buffer (Invitrogen, Carlsbad, CA, USA) and serum samples were quantified using ELISA kits specific for murine FST and ActA, as described in the previous sections, and normalized to total protein.

Gene expression linked to metastasis was evaluated using tumor-derived cDNA, prepared as outlined in earlier sections of methodology. The analysis was conducted using the TaqMan® Array Mouse Tumor Metastasis panel (array ID RA7DPDR) from ThermoFisher Scientific (Waltham, MA, USA), targeting genes implicated in tumor metastasis and proliferation.

For western blot analysis, protein extracts from tumors were prepared using cell extraction buffer (Invitrogen, Carlsbad, CA, USA) with addition of protease inhibitor cocktail (Roche cOmplete™ Protease Inhibitor Cocktail, MilliporeSigma, Burlington, MA, USA), and quantified with the BCA Protein Assay Kit (Pierce, Thermo Fisher Scientific, Waltham, MA, USA). A 20-µg aliquot of total protein was subjected to electrophoresis on a 8-20% SDS-PAGE gradient gels, followed by transfer to PVDF membranes (0.45 um, Millipore Sigma, Burlington, MA, USA). Membranes were blocked in 5% bovine serum albumin in tris-buffered saline with addition of Tween20 (TBST). Membranes were incubated overnight at 4°C with primary antibodies against E6 (PA5-117355, Invitrogen, Carlsbad, CA, USA, 1:500 dilution) and beta Actin (BA3R, Invitrogen, Carlsbad, CA, USA, 1:2500 dilution). After washing, membranes were treated with Alexa Fluor-conjugated secondary antibodies for 1 hour at room temperature. Bands were visualized using a Li-Cor Odyssey imager (Lincoln, NE, USA), and assessed with

ImageJ software (Bethesda, MD, USA) for intensity analysis, normalizing E6 levels to beta Actin.

Longitudinal study for evaluation of metastasis progression

MLM3-bearing mice were treated with *Fst* mRNA LNPs for 14 days starting day 7 post-tumor inoculation. Tumor growth was monitored daily after MLM3 cells injections by measuring the longest dimension using calipers, a method chosen due to the non-spherical, irregular shape of the tumors. At the conclusion of the study, tumors were excised to measure their weight directly. Lungs were harvested, preserved in paraformaldehyde, embedded in paraphing and sectioned for histological evaluation using H&E staining to identify areas of metastasis. For detailed microscopic analysis, sections were scanned using the Zeiss Axioscan Slide Scanner (Zeiss, Oberkochen, Germany). The resulting high-resolution images were assembled into full tissue scans and analyzed with Zeiss ZEN Light software (Zeiss, Oberkochen, Germany). The extent of metastatic involvement was quantified by measuring the metastatic area relative to the total lung area using QuPath software. [66]

Evaluation of cachexia manifestations

Body composition, including fat, lean mass, and water content, was analyzed via magnetic resonance using an EchoMRI system following the manufacturer's guidelines (EchoMRI LLC, Houston, TX). The EchoMRI system was calibrated in accordance with the manufacturer's instructions to ensure accurate measurements. Calibration involved the use of standard oil phantoms provided by EchoMRI, LLC. Mice were placed in a specialized tube, which was then inserted into the EchoMRI system to measure lean mass, fat mass and water content. After the measurements, the mice were removed

from the tube and returned to their home cage, where they were briefly monitored for any signs of distress.

The expression of autophagy-related genes (Foxo1, Fbxo32/Mfbx1, Trim63/Murf1) in muscle tissues (gastrocnemius and flexor digitorum longus) was performed using the method described in the previous section with the following TaqMan assays (Foxo1 Mm00490672_m1, Fbxo32/Mafbx1 Mm00399518_m1, Trim63/Murf1 Mm01185221_m1).

OCT-embedded frozen muscle sections of gastrocnemius muscles were prepared using a Leica cryostat (Wetzlar, Germany; 15 μm sections). Laminin immunohistostaining involved fixing, incubating with laminin primary antibody (PA5-115490, Invitrogen, Carlsbad, CA, USA, 1:200) overnight at 4°C, followed by a 1-hour room temperature incubation with an Alexa Fluor-conjugated secondary antibody. Muscle fiber cross-sectional area was determined by capturing images with a Biozero BZ-8000 fluorescence microscope (KEYENCE, Itasca, IL, USA) and analyzing the CSA using QuPath software and muscle fiber outlines.

Statistical Analysis

Data are presented as mean ± SEM and analyzed using GraphPad Prism (La Jolla, CA, United States). Tests included t-tests, one-way ANOVA, repeated measures ANOVA, and multiple t-tests. Significance levels were set at *$p<0.05$, **$p<0.01$, ***<0.001. G*power [68] was used for power analysis, targeting a power of $1-\beta = 0.8$, alpha = 0.05, and an effect size determined by preliminary studies, to establish group sizes of 5 or 7 animals.

7.8 Chapter summary

In **Chapter 7** of my dissertation, I introduce an improved *Fst* mRNA LNP formulation designed for addressing metastatic epithelial carcinomas characterized by an overexpression of ActA. My work also incorporates the findings from **Chapter 6**, allowing me to refine the LNP carriers by selecting ALC-0315, the least reactogenic ionizable lipid, and incorporating pseudouridine-substituted mRNA to mitigate the reactogenicity of both LNP carriers and mRNA cargo. Consequently, the findings from **Chapters 6** and 7 of my dissertation lead to the development of an optimized *Fst* mRNA LNP formulation. This formulation is distinguished by its notable ability to attenuate ActA's influence on cancer proliferation, migration, and muscle wasting seen in cancer-associated cachexia, all while maintaining minimal reactogenicity. This balance enhances its potential for application in immunocompetent mice, paving the way for its translational relevance.

The key theses of this chapter are summarized as follows:

1) Achieving a minimized reactogenic profile in the formulation marks a critical success, enhancing safety and tolerability in immunocompetent C57Bl/6 mice.
2) Therapeutic efficacy assessment in a metastatic epithelial carcinoma model shifted to the syngeneic MLM3 head and neck carcinoma model in immunocompetent C57Bl/6 mice, prompted by the lack of a suitable ovarian cancer model with characteristics of overactive ActA pathway, cachexia, and distant metastasis.

3) *Fst* mRNA LNP treatment achieved a reduction in tumor size and substantially decreased distant metastasis to the lungs, highlighting its effectiveness in suppressing ActA-mediated tumorigenesis and migration.
4) Gene expression analysis of tumors treated with *Fst* mRNA LNP showed alterations in the TGF-beta regulation of the extracellular matrix pathway, a finding consistent with results from the ES2 epithelial ovarian cancer model in nude mice discussed in Chapter 4.
5) *Fst* mRNA LNP treatment significantly mitigated the progression of refractory cancer-associated cachexia by increasing adiposity and muscle fiber cross-sectional area, yet, notably, it did not induce changes in the lean mass of MLM3 tumor-bearing mice.

In conclusion, **Chapter 7** is dedicated to achieving **Specific Aim 3**, which focuses on establishing the improved mRNA LNP formulation as a proof of concept in treating metastatic epithelial carcinoma and lay the foundation for future ovarian cancer therapeutics. It addresses **Objectives 3.1** and **3.2** by delineating the development of an improved mRNA LNP formulation and its successful application in treating metastatic epithelial carcinoma.

Chapter 8: Perspectives and conclusions

8.1 Summary of findings

In my dissertation, I embark on a comprehensive exploration of novel nucleic acid formulations aimed at treating metastatic epithelial ovarian carcinoma (EOC) and cancer-associated cachexia (CAC). This exploration is motivated by the urgent need to address both the direct impacts of cancer and its debilitating comorbidities, with CAC being a significant factor that worsens patient outcomes and complicates treatment (**Chapter 1**). The importance of addressing *both* cancer and CAC is underscored by the fact that CAC, characterized by weight loss, muscle and fat depletion, and systemic inflammation, is highly associated with decreased quality of life, poor responses to life-saving treatments, and reduced survival rates. This multifactorial syndrome requires a complex treatment approach, combining nutritional, pharmacological, and physical exercise interventions to alleviate its effects. [589] Although progress in cancer treatment is paramount, we should give equal attention to the formulation of specific therapies for CAC. As a condition that is largely neglected and remains untreated, its profound impact on patient quality of life and survival outcomes cannot be understated. [590]

Chapter 2 of my dissertation explores the complex field of gynecological oncology, evaluating the standard treatments, including surgery, chemotherapy, and

radiation therapy. This chapter identifies critical therapeutic gaps, such as cancer recurrence, resistance to treatments, and significant side effects that negatively impact patient quality of life. By pointing out these challenges, I set a foundation for the rest of my dissertation, which shifts focus to nucleic acid therapeutics as promising alternatives. In this chapter, I emphasize the synergy between lipid nanoparticles (LNPs) and nucleic acid-based treatments, showcasing their potential to significantly advance the field of cancer therapy.

Progressing to **Chapter 3**, my dissertation explores the historical context and evolving landscape of nucleic acid therapeutics. This chapter examines the challenges and breakthroughs in delivering these therapies, focusing on the critical role of LNPs in enhancing the stability and bioavailability of nucleic acids. The detailed review establishes a strong rationale for the subsequent experimental investigations, emphasizing the potential of these therapies in treating complex diseases like cancer and CAC.

Chapter 4 of my dissertation delineates the development of a novel therapeutic approach targeting metastatic EOC and the CAC syndrome. The conceptual advancement introduced by this research pivots on the *in situ* mRNA-guided reprogramming of cancer cells, transitioning from mesenchymal to epithelial phenotypes. This reprogramming enhances chemotherapy sensitivity, mitigating the iatrogenic burden of chemotherapy while concurrently addressing CAC manifestations. This chapter unveils an LNP-based system engineered to deliver *Fst* mRNA, focusing primarily on cancer cells to prevent malignant ascites, delay cancer progression, and reverse muscle loss in cancer-bearing mice. When combined with cisplatin, the *Fst*

mRNA LNP therapy not only augments mouse survival rates but also counteracts chemotherapy-induced muscle atrophy and cancer-associated cachexia. Remarkably, this combination therapy facilitates the surgical removal of solid tumors that were non-adherent, highlighting a synergistic effect that limits cancer progression while reinforcing resilience against aggressive chemotherapeutic regimens. This chapter's findings highlight the translational promise of *Fst* mRNA LNP therapy as a new approach for treating unresectable EOC with widespread peritoneal metastases. It demonstrates how this therapy can improve overall survival by allowing complete cytoreduction and bolstering resilience against aggressive chemotherapy in the EOC model in nude mice. However, when attempting to apply the developed *Fst* mRNA LNP therapy to immunocompetent mice, I faced the challenge of reactogenicity linked to LNP administration, which hindered the use of the treatment in the necessary chronic injection regimen. Therefore, I delved into understanding the reactogenicity of LNP formulations in Chapters 5 and 6, concentrating on the roles of toll-like receptors and their adaptor proteins. This exploration into the molecular mechanisms underlying these side effects illustrates the intricate balance required in developing practical *and* safe nanoparticle formulations for delivering therapeutic mRNAs.

Building upon the outlined challenge, **Chapter 5** transitions smoothly into a detailed examination of the reactogenicity associated with LNP formulations. This section focuses on the role of empty LNPs (eLNPs) in triggering reactogenic and immunogenic responses, further expanding our understanding of the complexities involved in nanoparticle-based therapeutic delivery. Here, I conduct an extensive literature review to understand how the structural components of LNPs trigger adverse

effects such as headaches, fevers, fatigue, and inflammation at the injection site in humans, which is also observed in the form of sickness behavior in mice. I also identify innate immune cells, especially macrophages and neutrophils, as central to the molecular interactions leading to reactogenic manifestations. On a molecular level, TLR signaling pathways and complement cascade activation are crucial in modulating these responses, leading to the overexpression of pro-inflammatory chemokines and cytokines. One of the significant contributions of this chapter is the in-depth exploration of the role of toll-like receptors (TLRs) and their associated adaptor proteins in recognizing LNPs, a topic previously not thoroughly investigated. This exploration set the stage for Chapter 6, which delves into the formal investigation of TLR4 and TRIF/MyD88 adaptors in initiating and amplifying reactogenic responses.

Transitioning from the review of LNP reactogenicity in Chapter 5, I present my research in **Chapter 6**, focusing on the molecular mechanisms behind LNP-induced reactogenicity. Here, I examine the roles of TLR4 and TRIF/MyD88 adaptors, aiming to identify their specific contributions to initiating and propagating reactogenic responses following LNP administration. A key finding from this chapter includes the characterization of LNPs with different ionizable lipids (MC3, ALC-0315, SM-102) based on their reactogenicity and biodistribution profiles using luciferase mRNA LNPs. Moreover, the chapter advances our understanding of TLR4 receptor and its adaptors, specifically MyD88 and TRIF, in eLNP-induced reactogenicity, particularly concerning the sickness response in mice. I show that TLR4- and MyD88-deficient mice display reduced sensitivity to eLNP-induced behavioral changes, underscoring TLR4-Myd88 tandem involvement in reactogenic responses. The application of the TLR4 inhibitor

TAK-242 validates the TLR4's role in eLNP reactogenicity, offering insights into therapeutic avenues to mitigate such effects. Finally, Chapter 6 evaluates the optimal dosing strategies, eLNP formulations, and administration routes necessary to identify the least reactogenic methods critical for the research continuation described in Chapter 7.

These efforts resulting in improved *Fst* mRNA LNP formulation, that minimized reactogenicity required for chronic administration regiments, helped me overcome a significant obstacle in my research. However, as I progressed, I encountered another challenge: the absence of a suitable syngeneic model for EOC to test the efficacy of the *Fst* mRNA LNP formulation in immunocompetent mice. Therefore, a pivotal part of my dissertation involved the transition from focusing on EOC to head and neck squamous cell carcinoma (HNSCC).

In **Chapter 7** of my dissertation, the therapeutic efficacy of the improved *Fst* mRNA LNP formulation was assessed using the syngeneic MLM3 model of HNSCC, exhibiting characteristics analogous to the desired overactive *ActA pathway*, *CAC*, and *distant metastasis*. This pivot underscores the complexities and challenges inherent in cancer research, particularly in the development of effective treatments for cancer cachexia, which are further complicated by the limited number of experimental murine models. Effective therapy development for cancer cachexia depends on animal models that accurately reflect human conditions. This need highlights the challenges of current model limitations and underscores the importance of advanced preclinical approaches for understanding mechanisms and creating targeted treatments. [591, 592] Therefore, the exploration into HNSCC allowed me to apply a unique experimental model,

providing valuable insights into the potential of *Fst* mRNA LNP therapy not only for cachexia but also for directly targeting the ActA-overexpressing cancer itself. After identifying a new model of epithelial cancer overexpressing ActA, Chapter 7 progresses with the optimization of LNP formulation, involving the integration of ALC-0315, the ionizable lipid with the lowest reactogenic profile, and the incorporation of pseudouridine-substituted mRNA. Achieving a formulation with reduced reactogenicity marks a significant success, improving safety and tolerability in immunocompetent C57Bl/6 mice. Treatment with *Fst* mRNA LNP formulation led to significant decreases in both tumor size and lung metastasis, demonstrating its capacity to inhibit ActA-driven tumor development and spread. Furthermore, this therapy effectively mitigated refractory CAC, as evidenced by an increase in muscle fiber cross-sectional area and enhanced fat accumulation.

8.2 Translational prospects for *Fst* mRNA LNP therapy

Aberrant activation of the ActA pathway contributes to increased tumor proliferation, metastatic potential, and CAC, highlighting the need for therapeutic intervention. *Fst* mRNA LNP therapy represents a strategic pivot from traditional receptor blockade strategies, especially those targeting the Activin type II receptors (ActRII) involved in the ActA signaling spectrum. The methods of targeting the ActA pathway involve the direct inhibition of receptors activated by ActA or sequestration of TGF-beta ligands preventing activation of these receptors. Bimagrumab, a monoclonal antibody-blocker of ActRII currently undergoing clinical trials, contrasts with the proposed approach in my dissertation using FST as an ActA-binding trap. While Bimagrumab has shown promise in enhancing muscle mass, its practical application is

constrained due to various side effects and the lack of clear evidence for its effectiveness in improving mobility, a key functional benefit expected from increased muscle mass. [593] This raises questions about its suitability for long-term treatment of muscle-related diseases and syndromes characterized by muscle loss, including CAC. The occurrence of bleeding events following Bimagrumab treatment [594], potentially influenced by its interaction with the bone morphogenic protein pathway, underscores the therapeutic navigation complexity using this approach. Bimagrumab's inhibition of ActRII signaling, involved in regulating the bone morphogenic protein (BMP) pathway, particularly BMP2, BMP4, and BMP6, potentially modulates the vascular integrity, endothelial function, and angiogenesis. This inhibition could disrupt BMP-mediated vascular homeostasis, elevating bleeding risk, and further contributing to Bimagrumab's associated bleeding outcomes. More importantly, Bimagrumab, a monoclonal antibody of ActRII, addresses only one of the receptors that is activated by ActA. ActA activates a complex signaling network by binding to type II receptors, ActRIIA and ActRIIB, and type I receptors, ALK4 and ALK5 (Activin Receptor-Like Kinase 4 and 5). [595] This activation initiates the phosphorylation of SMAD proteins, crucial for transducing signals to the nucleus to regulate gene expression, impacting cellular processes like growth, differentiation, and apoptosis. [595] Given the multifaceted signaling activated by ActA through multiple receptors, targeting ActA as a ligand upstream of these receptors presents a more comprehensive therapeutic approach.

In addition to addressing the issue with variety of ActA receptors, FST mediates its therapeutic effects by interacting not only with ActA but also with other members of the TGF-beta family, such as inhibin and myostatin, although with lower affinity. [596]

These interactions underline FST's expansive therapeutic potential, achieved through its antagonistic effects on various pathways activated by TGF-beta family ligands. The strategy of employing FST's wide-ranging activity enables the development of comprehensive anti-cancer approaches that address the complex nature of tumor biology. [597] Specifically, my work describing *Fst* mRNA LNP introduces a novel method to enhance FST expression in cancer cells, particularly those overexpressing ActA, thereby sequestering ActA produced by these cells and preventing ActA release to systemic circulation. This approach not only confronts ActA-mediated pathological signaling but also advances a more integrated treatment strategy, setting a new direction for nucleic acid-based therapeutics in oncology and beyond.

8.3 Future therapeutic perspectives for nucleic acid nanomedicines

Moving from my focused study on the *Fst* mRNA LNP formulation to the wider context, I want to reiterate the critical role of nucleic acid therapeutics in treating gynecological cancers. The potential of nucleic acid nanomedicines is increasingly recognized for their innovative approaches in medicine. Progress in nanotechnology and nucleic acid delivery systems aims to overcome current treatment limits, allowing for targeted therapies, personalized medicine, and solutions for previously untreatable conditions. [598]

The unique capability of mRNA therapies to harness cellular machinery for synthesizing therapeutic peptides presents a distinct advantage, potentially addressing the limitations inherent in conventional peptide-based treatments. Despite an extensive clinical history demonstrating the efficacy of peptide drugs since the development of

insulin therapy in 1921, peptide-based treatments are limited in applications inherent to their extracellular mode of action. [599] For instance, the systemic administration of peptide drugs restricts their effectiveness through autocrine and paracrine pathways, as these modes of action require precise and localized delivery to the cells under therapeutic intervention. Furthermore, systemic administration of therapeutic peptides cannot effectively replace intracellular and membrane proteins due to challenges related to their cellular uptake, intracellular localization, and integration into complex intracellular processes. Despite these challenges, gynecological cancers could be treated more effectively with peptides produced from delivered mRNA. These peptides then can act through paracrine and autocrine mechanisms, targeting specific signaling pathways that play a role in the growth and progression of tumors.

mRNA transcribed in vitro and delivered via LNPs can direct the expression of therapeutic peptides within the tumor's immediate environment. These expressed therapeutic agents could include inhibitors targeting Transforming Growth Factor-beta (TGF-β), Epidermal Growth Factor Receptor (EGFR), and Insulin-Like Growth Factor-1 Receptor (IGF-1R), as well as peptides aimed at angiogenic factors like VEGF. [600-603] Expanding on this potential, cancers characterized by loss-of-function mutations, which lead to defective proteins typically found within cells or on the cell membrane, stand to gain particularly from this technology. The mRNA-guided restoration of these malfunctioning proteins offers a promising avenue for correcting such genetic errors at the source, highlighting the versatility and targeted nature of mRNA therapies in addressing complex molecular dysfunctions in cancer. Additionally, supplementing oncolytic or oncostatic protein modulators can further enhance the advantages of

treating such cancers. Therefore, by selectively modulating these pathways, mRNA-guided expression of these therapeutic peptides can inhibit tumor cell proliferation, promote apoptosis, or suppress angiogenesis, offering a targeted and effective approach to the treatment of gynecological cancers. Furthermore, the localized action of these peptides expressed in the targeted cells within the tumor microenvironment may reduce off-target effects and minimize systemic toxicity while avoiding permanent genomic changes, the immunogenicity of exogenous proteins, and dose-dependent toxic effects, collectively enhancing the safety and tolerability of the therapeutic intervention. [604-606] Therefore, the development of mRNA-based cancer therapies, which direct the expression of autocrine and paracrine-acting therapeutic peptides, as well as intracellular and membrane therapeutic proteins, is of paramount importance. [607, 608] Looking ahead, further advancements in mRNA-based therapies, including improvements in delivery, stability, and reactogenicity, may enable more widespread clinical translation of these approaches, potentially offering new solutions for a broad range of diseases that rely on peptide-based signaling pathways.

8.4 Final remarks

In exploring the *Fst* mRNA LNP formulation, my dissertation contributes to the ongoing efforts in treating metastatic epithelial carcinomas and broadens our understanding of the role of nucleic acid therapeutics in oncology. However, my research is a modest contribution that builds upon the groundbreaking work of pioneers in mRNA therapeutics and LNP technology. Key figures include Pieter Cullis, whose innovations in LNP systems have been crucial for drug delivery [609], Katalin Karikó and Drew Weissman, whose work on modified nucleosides paved the way for the

development of mRNA vaccines [393]; Derrick Rossi, for his foundational work in the application of mRNA technology in reprogramming and regenerative medicine [610, 611]; and Mark E. Davis, who demonstrated the potential of targeted nanoparticles for RNAi therapy in humans [612] Contributions from Kevin J. Kauffman and J.R. Dorkin in optimizing LNP formulations for mRNA delivery [613], Bin Li and Xiao Luo in advancing lipid-like nanoparticles [614], and Nathan M. Belliveau's development of microfluidic synthesis for potent LNPs [615] have been instrumental. Further, the work by M. Maier and S. Matsuda on biodegradable lipids [616] and advancements by Akin Akinc and Daniel Anderson on lipid-based formulations for improved in vivo delivery of RNA through the development of combinatorial libraries of lipid-like materials [617] paved the way for more effective and targeted delivery mechanisms. These combined efforts have significantly advanced our understanding and application of nucleic acid therapeutics. They provide a solid foundation for my research to improve mRNA LNP therapies by focusing on lowering reactogenicity and enhancing the effectiveness of treatments that require multiple administrations.

Appendix: Supporting first-author manuscripts

Korzun, T., et al., Development and Perspectives: Multifunctional Nucleic Acid Nanomedicines for Treatment of Gynecological Cancers. *Small*, 2023: p. e2301776.

Korzun, T., et al., From Bench to Bedside: Implications of Lipid Nanoparticle Carrier Reactogenicity for Advancing Nucleic Acid Therapeutics. *Pharmaceuticals* (Basel), 2023. 16(8).

Korzun, T., et al., Nanoparticle-Based Follistatin Messenger RNA Therapy for Reprogramming Metastatic Ovarian Cancer and Ameliorating Cancer-Associated Cachexia. *Small*, 2022. 18(44): p. e2204436.

References

1. Keyvani, V., et al., Epidemiological trends and risk factors of gynecological cancers: an update. *Med Oncol*, 2023. **40**(3): p. 93.
2. Lee, J.Y., et al., Major clinical research advances in gynecologic cancer in 2022: highlight on late-line PARP inhibitor withdrawal in ovarian cancer, the impact of ARIEL-4, and SOLO-3. *J Gynecol Oncol*, 2023. **34**(2): p. e51.
3. Park, J.Y., et al., Major clinical research advances in gynecologic cancer in 2021. *J Gynecol Oncol*, 2022. **33**(2): p. e43.
4. Roett, M.A. and P. Evans, Ovarian cancer: an overview. *Am Fam Physician*, 2009. **80**(6): p. 609-16.
5. Park, H.K., J.J. Ruterbusch, and M.L. Cote, Recent Trends in Ovarian Cancer Incidence and Relative Survival in the United States by Race/Ethnicity and Histologic Subtypes. *Cancer Epidemiology Biomarkers and Prevention*, 2017. **26**(10): p. 1511.
6. Lengyel, E., Ovarian cancer development and metastasis. *Am J Pathol*, 2010. **177**(3): p. 1053-64.
7. Vermeulen, C.K.M., et al., Only complete tumour resection after neoadjuvant chemotherapy offers benefit over suboptimal debulking in advanced ovarian cancer. *European Journal of Obstetrics & Gynecology and Reproductive Biology*, 2017. **219**: p. 100-105.
8. Rauh-Hain, J.A., et al., Platinum resistance after neoadjuvant chemotherapy compared to primary surgery in patients with advanced epithelial ovarian carcinoma. *Gynecologic Oncology*, 2013. **129**(1): p. 63-68.
9. Gadducci, A., et al., Malnutrition and cachexia in ovarian cancer patients: pathophysiology and management. *Anticancer Res*, 2001. **21**(4b): p. 2941-7.
10. Mantzorou, M., et al., Clinical Value of Nutritional Status in Cancer: What is its Impact and how it Affects Disease Progression and Prognosis? *Nutrition and Cancer*, 2017. **69**(8): p. 1151-1176.
11. Mikuła-Pietrasik, J., et al., Comprehensive review on how platinum- and taxane-based chemotherapy of ovarian cancer affects biology of normal cells. *Cellular and Molecular Life Sciences*, 2019. **76**(4): p. 681-697.
12. Braun, T.P., et al., Muscle atrophy in response to cytotoxic chemotherapy is dependent on intact glucocorticoid signaling in skeletal muscle. *PLoS One*, 2014. **9**(9): p. e106489.
13. Kulkarni, J.A., et al., The current landscape of nucleic acid therapeutics. *Nat Nanotechnol*, 2021. **16**(6): p. 630-643.
14. Babu, A., A. Munshi, and R. Ramesh, Combinatorial therapeutic approaches with RNAi and anticancer drugs using nanodrug delivery systems. *Drug Dev Ind Pharm*, 2017. **43**(9): p. 1391-1401.
15. Sahin, U. and Ö. Türeci, Personalized vaccines for cancer immunotherapy. *Science*, 2018. **359**(6382): p. 1355-1360.
16. Buschmann, M.D., et al., Nanomaterial Delivery Systems for mRNA Vaccines. *Vaccines*, 2021. **9**(1): p. 65.
17. Aldosari, B.N., I.M. Alfagih, and A.S. Almurshedi, Lipid Nanoparticles as Delivery Systems for RNA-Based Vaccines. *Pharmaceutics*, 2021. **13**(2).

18. Chen, D., et al., Nanoparticle drug delivery systems for synergistic delivery of tumor therapy. *Front Pharmacol*, 2023. **14**: p. 1111991.
19. Barbier, A.J., et al., The clinical progress of mRNA vaccines and immunotherapies. *Nature Biotechnology*, 2022. **40**(6): p. 840-854.
20. Adhikari, P., P. Vietje, and S. Mount, Premalignant and malignant lesions of the vagina. *Diagnostic Histopathology*, 2017. **23**(1): p. 28-34.
21. Rajaram, S., A. Maheshwari, and A. Srivastava, Staging for vaginal cancer. *Best Practice & Research Clinical Obstetrics & Gynaecology*, 2015. **29**(6): p. 822-832.
22. Mitra, S., et al., Vulvar carcinoma: dilemma, debates, and decisions. *Cancer Manag Res*, 2018. **10**: p. 61-68.
23. Chokoeva, A.A., et al., Vulvar sarcomas: Short guideline for histopathological recognition and clinical management. Part 1. *Int J Immunopathol Pharmacol*, 2015. **28**(2): p. 168-77.
24. Chow, L., et al., Gynecologic tumor board: a radiologist's guide to vulvar and vaginal malignancies. *Abdom Radiol (NY)*, 2021. **46**(12): p. 5669-5686.
25. Bray, F., et al., Global cancer statistics 2018: GLOBOCAN estimates of incidence and mortality worldwide for 36 cancers in 185 countries. *CA Cancer J Clin*, 2018. **68**(6): p. 394-424.
26. Devine, C., et al., Imaging and Staging of Cervical Cancer. *Seminars in Ultrasound, CT and MRI*, 2019. **40**(4): p. 280-286.
27. Huang, J., et al., Global distribution, risk factors, and recent trends for cervical cancer: A worldwide country-level analysis. *Gynecologic Oncology*, 2022. **164**(1): p. 85-92.
28. Cohen, P.A., et al., Cervical cancer. *The Lancet*, 2019. **393**(10167): p. 169-182.
29. Organization, W.H., Human papillomavirus vaccines: WHO position paper, October 2014. *Vaccines*, 2014. **89**(43): p. 465-491.
30. Sherris, J., C. Herdman, and C. Elias, Cervical cancer in the developing world. *West J Med*, 2001. **175**(4): p. 231-3.
31. Hull, R., et al., Cervical cancer in low and middle-income countries. *Oncol Lett*, 2020. **20**(3): p. 2058-2074.
32. Mahdy, H., M.J. Casey, and D. Crotzer, Endometrial Cancer, in *StatPearls*. 2023, StatPearls Publishing

33. Creasman, W.T., et al., Carcinoma of the Corpus Uteri. *Int J Gynaecol Obstet*, 2006. **95 Suppl 1**: p. S105-s143.
34. Altman, A.D., et al., Canadian high risk endometrial cancer (CHREC) consortium: analyzing the clinical behavior of high risk endometrial cancers. *Gynecol Oncol*, 2015. **139**(2): p. 268-74.
35. Hendrickson, M., et al., Uterine papillary serous carcinoma: a highly malignant form of endometrial adenocarcinoma. *Am J Surg Pathol*, 1982. **6**(2): p. 93-108.
36. Abeler, V.M., et al., Clear cell carcinoma of the endometrium. Prognosis and metastatic pattern. *Cancer*, 1996. **78**(8): p. 1740-7.
37. Russo, A., et al., Hereditary ovarian cancer. *Crit Rev Oncol Hematol*, 2009. **69**(1): p. 28-44.
38. Jelovac, D. and D.K. Armstrong, Recent progress in the diagnosis and treatment of ovarian cancer. *CA: A Cancer Journal for Clinicians*, 2011. **61**(3): p. 183-203.

39. Kurman, R.J. and I.-M. Shih, The Dualistic Model of Ovarian Carcinogenesis: Revisited, Revised, and Expanded. *The American Journal of Pathology*, 2016. **186**(4): p. 733-747.
40. Bowtell, D.D., et al., Rethinking ovarian cancer II: reducing mortality from high-grade serous ovarian cancer. *Nat Rev Cancer*, 2015. **15**(11): p. 668-79.
41. Lisio, M.A., et al., High-Grade Serous Ovarian Cancer: Basic Sciences, Clinical and Therapeutic Standpoints. *Int J Mol Sci*, 2019. **20**(4).
42. Pectasides, D., E. Pectasides, and D. Kassanos, Germ cell tumors of the ovary. *Cancer treatment reviews*, 2008. **34**(5): p. 427-441.
43. Tewari, K., et al., Malignant germ cell tumors of the ovary. *Obstetrics & Gynecology*, 2000. **95**(1): p. 128-133.
44. Levin, G., et al., Granulosa cell tumor of ovary: A systematic review of recent evidence. *European Journal of Obstetrics and Gynecology and Reproductive Biology*, 2018. **225**: p. 57-61.
45. Di Donato, V., et al., Vaginal cancer. *Critical Reviews in Oncology/Hematology*, 2012. **81**(3): p. 286-295.
46. Rogers, L.J. and M.A. Cuello, Cancer of the vulva. *International Journal of Gynecology & Obstetrics*, 2018. **143**(S2): p. 4-13.
47. Olawaiye, A.B., M.A. Cuello, and L.J. Rogers, Cancer of the vulva: 2021 update. *International Journal of Gynecology & Obstetrics*, 2021. **155**(S1): p. 7-18.
48. Group, G.M.-a.T.G., Chemotherapy in adult high-grade glioma: a systematic review and meta-analysis of individual patient data from 12 randomised trials. *The Lancet*, 2002. **359**(9311): p. 1011-1018.
49. Coleridge, S.L., et al., Neoadjuvant chemotherapy before surgery versus surgery followed by chemotherapy for initial treatment in advanced ovarian epithelial cancer. *Cochrane Database of Systematic Reviews*, 2021(7).
50. Hu, Y., et al., Neoadjuvant chemotherapy for patients with international federation of gynecology and obstetrics stages IB3 and IIA2 cervical cancer: a multicenter prospective trial. *BMC cancer*, 2022. **22**(1): p. 1-16.
51. Holschneider, C.H., et al., Brachytherapy: A critical component of primary radiation therapy for cervical cancer: From the Society of Gynecologic Oncology (SGO) and the American Brachytherapy Society (ABS). *Brachytherapy*, 2019. **18**(2): p. 123-132.
52. Gopu, P., et al., Updates on systemic therapy for cervical cancer. *Indian Journal of Medical Research*, 2021. **154**(2): p. 293-302.
53. Johnson, C.A., et al., Cervical Cancer: An Overview of Pathophysiology and Management. *Seminars in Oncology Nursing*, 2019. **35**(2): p. 166-174.
54. Marth, C., et al., Cervical cancer: ESMO Clinical Practice Guidelines for diagnosis, treatment and follow-up. *Annals of Oncology*, 2017. **28**: p. iv72-iv83.
55. Colombo, N., et al., Pembrolizumab for Persistent, Recurrent, or Metastatic Cervical Cancer. *New England Journal of Medicine*, 2021. **385**(20): p. 1856-1867.
56. Passarello, K., S. Kurian, and V. Villanueva, Endometrial Cancer: An Overview of Pathophysiology, Management, and Care. *Seminars in Oncology Nursing*, 2019. **35**(2): p. 157-165.

57. Rauh-Hain, J.A. and M.G. Del Carmen, Treatment for advanced and recurrent endometrial carcinoma: combined modalities. *Oncologist*, 2010. **15**(8): p. 852-61.
58. Gómez-Raposo, C., et al., Adjuvant chemotherapy in endometrial cancer. *Cancer Chemother Pharmacol*, 2020. **85**(3): p. 477-486.
59. Mahmood, R.D., et al., First-Line Management of Advanced High-Grade Serous Ovarian Cancer. *Current Oncology Reports*, 2020. **22**(6): p. 64.
60. Vanderpuye, V.D., et al., Assessment of adult women with ovarian masses and treatment of epithelial ovarian cancer: ASCO Resource-Stratified Guideline. *JCO Global Oncology*, 2021. **7**: p. 1032-1066.
61. Jaaback, K., N. Johnson, and T.A. Lawrie, Intraperitoneal chemotherapy for the initial management of primary epithelial ovarian cancer. *Cochrane database of systematic reviews*, 2016(1).
62. Muggia, F. and A. Bonetti, History of intraperitoneal platinum drug delivery for ovarian cancer and its future applications. *Cancer Drug Resist*, 2021. **4**(2): p. 453-462.
63. Blagden, S.P., et al., Weekly platinum-based chemotherapy versus 3-weekly platinum-based chemotherapy for newly diagnosed ovarian cancer (ICON8): quality-of-life results of a phase 3, randomised, controlled trial. *Lancet Oncol*, 2020. **21**(7): p. 969-977.
64. Chan, J.K., et al., Weekly vs. Every-3-Week Paclitaxel and Carboplatin for Ovarian Cancer. *N Engl J Med*, 2016. **374**(8): p. 738-48.
65. Pignata, S., et al., Carboplatin plus paclitaxel once a week versus every 3 weeks in patients with advanced ovarian cancer (MITO-7): a randomised, multicentre, open-label, phase 3 trial. *Lancet Oncol*, 2014. **15**(4): p. 396-405.
66. Katsumata, N., et al., Long-term results of dose-dense paclitaxel and carboplatin versus conventional paclitaxel and carboplatin for treatment of advanced epithelial ovarian, fallopian tube, or primary peritoneal cancer (JGOG 3016): a randomised, controlled, open-label trial. *Lancet Oncol*, 2013. **14**(10): p. 1020-6.
67. Katsumata, N., et al., Dose-dense paclitaxel once a week in combination with carboplatin every 3 weeks for advanced ovarian cancer: a phase 3, open-label, randomised controlled trial. *Lancet*, 2009. **374**(9698): p. 1331-8.
68. Clamp, A.R., et al., Weekly dose-dense chemotherapy in first-line epithelial ovarian, fallopian tube, or primary peritoneal carcinoma treatment (ICON8): primary progression free survival analysis results from a GCIG phase 3 randomised controlled trial. *Lancet*, 2019. **394**(10214): p. 2084-2095.
69. González-Martín, A., et al., Niraparib in Patients with Newly Diagnosed Advanced Ovarian Cancer. *N Engl J Med*, 2019. **381**(25): p. 2391-2402.
70. Ray-Coquard, I., et al., Olaparib plus Bevacizumab as First-Line Maintenance in Ovarian Cancer. *N Engl J Med*, 2019. **381**(25): p. 2416-2428.
71. Morice, P.M., et al., Myelodysplastic syndrome and acute myeloid leukaemia in patients treated with PARP inhibitors: a safety meta-analysis of randomised controlled trials and a retrospective study of the WHO pharmacovigilance database. *Lancet Haematol*, 2021. **8**(2): p. e122-e134.
72. Nitecki, R., et al., Incidence of myelodysplastic syndrome and acute myeloid leukemia in patients receiving poly-ADP ribose polymerase inhibitors for the

treatment of solid tumors: A meta-analysis of randomized trials. *Gynecol Oncol*, 2021. **161**(3): p. 653-659.
73. Burger, R.A., et al., Incorporation of bevacizumab in the primary treatment of ovarian cancer. *N Engl J Med*, 2011. **365**(26): p. 2473-83.
74. Oza, A.M., et al., Standard chemotherapy with or without bevacizumab for women with newly diagnosed ovarian cancer (ICON7): overall survival results of a phase 3 randomised trial. *Lancet Oncol*, 2015. **16**(8): p. 928-36.
75. Perren, T.J., et al., A phase 3 trial of bevacizumab in ovarian cancer. *N Engl J Med*, 2011. **365**(26): p. 2484-96.
76. Ferriss, J.S., et al., Ascites predicts treatment benefit of bevacizumab in front-line therapy of advanced epithelial ovarian, fallopian tube and peritoneal cancers: an NRG Oncology/GOG study. *Gynecol Oncol*, 2015. **139**(1): p. 17-22.
77. du Bois, A., et al., Incorporation of pazopanib in maintenance therapy of ovarian cancer. *J Clin Oncol*, 2014. **32**(30): p. 3374-82.
78. Conte, C., et al., Update on the secondary cytoreduction in platinum-sensitive recurrent ovarian cancer: a narrative review. *Ann Transl Med*, 2021. **9**(6): p. 510.
79. Oza, A.M., et al., Olaparib combined with chemotherapy for recurrent platinum-sensitive ovarian cancer: a randomised phase 2 trial. *The lancet oncology*, 2015. **16**(1): p. 87-97.
80. Coleman, R.L., et al., Rucaparib maintenance treatment for recurrent ovarian carcinoma after response to platinum therapy (ARIEL3): a randomised, double-blind, placebo-controlled, phase 3 trial. *The Lancet*, 2017. **390**(10106): p. 1949-1961.
81. Moore, K., et al., Maintenance olaparib in patients with newly diagnosed advanced ovarian cancer. *New England Journal of Medicine*, 2018. **379**(26): p. 2495-2505.
82. González-Martín, A., et al., Niraparib in patients with newly diagnosed advanced ovarian cancer. *New England Journal of Medicine*, 2019. **381**(25): p. 2391-2402.
83. Uccello, M., et al., Systemic anti-cancer treatment in malignant ovarian germ cell tumours (MOGCTs): current management and promising approaches. *Ann Transl Med*, 2020. **8**(24): p. 1713.
84. Li, J., J. Li, and W. Jiang, Oncological Prognosis and Fertility Outcomes of Different Surgical Extents for Malignant Ovarian Sex-Cord Stromal Tumors: A Narrative Review. *Cancer Manag Res*, 2022. **14**: p. 697-717.
85. Chuang, Y.-T. and C.-L. Chang, Extending platinum-free interval in partially platinum-sensitive recurrent ovarian cancer by a non-platinum regimen: its possible clinical significance. *Taiwanese Journal of Obstetrics and Gynecology*, 2012. **51**(3): p. 336-341.
86. Hogberg, T., et al., Sequential adjuvant chemotherapy and radiotherapy in endometrial cancer–results from two randomised studies. *European journal of cancer*, 2010. **46**(13): p. 2422-2431.
87. de Boer, S.M., et al., Adjuvant chemoradiotherapy versus radiotherapy alone for women with high-risk endometrial cancer (PORTEC-3): final results of an international, open-label, multicentre, randomised, phase 3 trial. *The lancet oncology*, 2018. **19**(3): p. 295-309.

88. Chino, J. and S. Beriwal, Advanced treatment technique for locally advanced cervical cancer: time for a standard of care Shift? *International Journal of Radiation Oncology, Biology, Physics*, 2019. **103**(5): p. 1098-1099.
89. Hanker, L., et al., The impact of second to sixth line therapy on survival of relapsed ovarian cancer after primary taxane/platinum-based therapy. *Annals of oncology*, 2012. **23**(10): p. 2605-2612.
90. Sabbatini, P., et al., Abagovomab as maintenance therapy in patients with epithelial ovarian cancer: a phase III trial of the AGO OVAR, COGI, GINECO, and GEICO--the MIMOSA study. *J Clin Oncol*, 2013. **31**(12): p. 1554-61.
91. Berek, J., et al., Oregovomab maintenance monoimmunotherapy does not improve outcomes in advanced ovarian cancer. *J Clin Oncol*, 2009. **27**(3): p. 418-25.
92. Mei, L., et al., Maintenance chemotherapy for ovarian cancer. *Cochrane Database Syst Rev*, 2013. **2013**(6): p. Cd007414.
93. Fotopoulou, C., et al., Clinical outcome of tertiary surgical cytoreduction in patients with recurrent epithelial ovarian cancer. *Ann Surg Oncol*, 2011. **18**(1): p. 49-57.
94. Shih, K.K., et al., Beyond tertiary cytoreduction in patients with recurrent epithelial ovarian, fallopian tube, or primary peritoneal cancer. *Gynecol Oncol*, 2010. **116**(3): p. 364-9.
95. Fotopoulou, C., et al., Quaternary cytoreductive surgery in ovarian cancer: does surgical effort still matter? *Br J Cancer*, 2013. **108**(1): p. 32-8.
96. Shih, K.K., et al., Tertiary cytoreduction in patients with recurrent epithelial ovarian, fallopian tube, or primary peritoneal cancer: an updated series. *Gynecol Oncol*, 2010. **117**(2): p. 330-5.
97. Harter, P., et al., Surgery for recurrent ovarian cancer: role of peritoneal carcinomatosis: exploratory analysis of the DESKTOP I Trial about risk factors, surgical implications, and prognostic value of peritoneal carcinomatosis. *Annals of Surgical Oncology*, 2009. **16**(5): p. 1324-1330.
98. Aletti, G.D., et al., Quality improvement in the surgical approach to advanced ovarian cancer: the Mayo Clinic experience. *Journal of the American College of Surgeons*, 2009. **208**(4): p. 614-620.
99. Wimberger, P., et al., Influence of residual tumor on outcome in ovarian cancer patients with FIGO stage IV disease. *Annals of surgical oncology*, 2010. **17**(6): p. 1642-1648.
100. Nunns, D., P. Symonds, and D. Ireland, Surgical Management of Advanced Ovarian Cancer. *Obstetrical & Gynecological Survey*, 2000. **55**(12).
101. Pothuri, B., et al., Palliative surgery for bowel obstruction in recurrent ovarian cancer:an updated series. *Gynecol Oncol*, 2003. **89**(2): p. 306-13.
102. Pothuri, B., et al., Reoperation for palliation of recurrent malignant bowel obstruction in ovarian carcinoma. *Gynecol Oncol*, 2004. **95**(1): p. 193-5.
103. Kolomainen, D.F., et al., Outcomes of surgical management of bowel obstruction in relapsed epithelial ovarian cancer (EOC). *Gynecol Oncol*, 2012. **125**(1): p. 31-6.

104. Chi, D.S., et al., A prospective outcomes analysis of palliative procedures performed for malignant intestinal obstruction due to recurrent ovarian cancer. *Oncologist*, 2009. **14**(8): p. 835-9.
105. Katsumata, N., Dose-Dense Approaches to Ovarian Cancer Treatment. *Current Treatment Options in Oncology*, 2015. **16**(5): p. 21.
106. Matanes, E. and W.H. Gotlieb, Immunotherapy of gynecological cancers. *Best Practice & Research Clinical Obstetrics & Gynaecology*, 2019. **60**: p. 97-110.
107. Chow, S., J.S. Berek, and O. Dorigo, Development of therapeutic vaccines for ovarian cancer. *Vaccines*, 2020. **8**(4): p. 657.
108. Liu, J., et al., Cancer vaccines as promising immuno-therapeutics: platforms and current progress. *J Hematol Oncol*, 2022. **15**(1): p. 28.
109. Katsumata, N., Dose-dense approaches to ovarian cancer treatment. *Curr Treat Options Oncol*, 2015. **16**(5): p. 21.
110. Clamp, A.R., et al., Weekly dose-dense chemotherapy in first-line epithelial ovarian, fallopian tube, or primary peritoneal carcinoma treatment (ICON8): primary progression free survival analysis results from a GCIG phase 3 randomised controlled trial. *The Lancet*, 2019. **394**(10214): p. 2084-2095.
111. Wang, R., et al., Human papillomavirus vaccine against cervical cancer: Opportunity and challenge. *Cancer Letters*, 2020. **471**: p. 88-102.
112. Pirolli, R., et al., Comparison of dose-dense vs. 3-weekly paclitaxel and carboplatin in the first-line treatment of ovarian cancer in a propensity score-matched cohort. *BMC Cancer*, 2021. **21**(1): p. 525.
113. Gabizon, A.A., Pegylated liposomal doxorubicin: metamorphosis of an old drug into a new form of chemotherapy. *Cancer investigation*, 2001. **19**(4): p. 424-436.
114. Zielińska, A., et al., Polymeric Nanoparticles: Production, Characterization, Toxicology and Ecotoxicology. *Molecules*, 2020. **25**(16).
115. Shaffer, S.A., et al., In vitro and in vivo metabolism of paclitaxel poliglumex: identification of metabolites and active proteases. *Cancer Chemother Pharmacol*, 2007. **59**(4): p. 537-48.
116. Galic, V.L., et al., Paclitaxel poliglumex for ovarian cancer. *Expert opinion on investigational drugs*, 2011. **20**(6): p. 813-821.
117. Singer, J.W., Paclitaxel poliglumex (XYOTAX, CT-2103): a macromolecular taxane. *J Control Release*, 2005. **109**(1-3): p. 120-6.
118. Huang, X., et al., Gold nanoparticles: interesting optical properties and recent applications in cancer diagnostics and therapy. *Nanomedicine (Lond)*, 2007. **2**(5): p. 681-93.
119. Albarqi, H.A., et al., Biocompatible Nanoclusters with High Heating Efficiency for Systemically Delivered Magnetic Hyperthermia. *ACS Nano*, 2019. **13**(6): p. 6383-6395.
120. Demessie, A.A., et al., An Advanced Thermal Decomposition Method to Produce Magnetic Nanoparticles with Ultrahigh Heating Efficiency for Systemic Magnetic Hyperthermia. *Small Methods*, 2022. **6**(12): p. e2200916.
121. Talluri, S. and R.R. Malla, Superparamagnetic Iron Oxide Nanoparticles (SPIONs) for Diagnosis and Treatment of Breast, Ovarian and Cervical Cancers. *Curr Drug Metab*, 2019. **20**(12): p. 942-945.

122. Barenholz, Y., Doxil® — The first FDA-approved nano-drug: Lessons learned. *Journal of Controlled Release*, 2012. **160**(2): p. 117-134.
123. Perez, A.T., et al., Pegylated liposomal doxorubicin (Doxil) for metastatic breast cancer: the Cancer Research Network, Inc., experience. *Cancer Invest*, 2002. **20 Suppl 2**: p. 22-9.
124. Makwana, V., et al., Liposomal doxorubicin as targeted delivery platform: Current trends in surface functionalization. *International Journal of Pharmaceutics*, 2021. **593**: p. 120117.
125. Tereshkina, Y.A., et al., Nanoliposomes as drug delivery systems: safety concerns. *J Drug Target*, 2022. **30**(3): p. 313-325.
126. Gabizon, A. and F. Martin, Polyethylene Glycol-Coated (Pegylated) Liposomal Doxorubicin. *Drugs*, 1997. **54**(4): p. 15-21.
127. Gabizon, A., H. Shmeeda, and Y. Barenholz, Pharmacokinetics of pegylated liposomal doxorubicin. *Clinical pharmacokinetics*, 2003. **42**(5): p. 419-436.
128. Bulbake, U., et al., Liposomal Formulations in Clinical Use: An Updated Review. *Pharmaceutics*, 2017. **9**(2).
129. Working, P. and A. Dayan, Pharmacological-toxicological expert report CAELYXTM:(stealth® liposomal doxorubicin HCl). *Human & experimental toxicology*, 1996. **15**(9): p. 751-785.
130. Gordon, A.N., et al., Recurrent epithelial ovarian carcinoma: a randomized phase III study of pegylated liposomal doxorubicin versus topotecan. *J Clin Oncol*, 2001. **19**(14): p. 3312-22.
131. Gordon, A.N., et al., Long-term survival advantage for women treated with pegylated liposomal doxorubicin compared with topotecan in a phase 3 randomized study of recurrent and refractory epithelial ovarian cancer. *Gynecol Oncol*, 2004. **95**(1): p. 1-8.
132. Mahtani, R.L., et al., Comparative effectiveness of early-line nab-paclitaxel vs. paclitaxel in patients with metastatic breast cancer: a US community-based real-world analysis. *Cancer Manag Res*, 2018. **10**: p. 249-256.
133. Parisi, A., et al., First-line carboplatin/nab-paclitaxel in advanced ovarian cancer patients, after hypersensitivity reaction to solvent-based taxanes: a single-institution experience. *Clin Transl Oncol*, 2020. **22**(1): p. 158-162.
134. Micha, J.P., et al., Abraxane in the treatment of ovarian cancer: the absence of hypersensitivity reactions. *Gynecol Oncol*, 2006. **100**(2): p. 437-8.
135. Maurer, K., et al., Universal tolerance of nab-paclitaxel for gynecologic malignancies in patients with prior taxane hypersensitivity reactions. *J Gynecol Oncol*, 2017. **28**(4): p. e38.
136. Srinivasan, K., A. Rauthan, and R. Gopal, Combination therapy of albumin-bound Paclitaxel and Carboplatin as first line therapy in a patient with ovarian cancer. *Case Reports in Oncological Medicine*, 2014. **2014**.
137. Teneriello, M.G., et al., Phase II evaluation of nanoparticle albumin–bound paclitaxel in platinum-sensitive patients with recurrent ovarian, peritoneal, or fallopian tube cancer. *Journal of Clinical Oncology*, 2009. **27**(9): p. 1426-1431.
138. Benigno, B., et al., A phase II nonrandomized study of nab-paclitaxel plus carboplatin in patients with recurrent platinum-sensitive ovarian or primary

peritoneal cancer. *Journal of Clinical Oncology*, 2010. **28**(15_suppl): p. 5011-5011.
139. Barenholz, Y.C., Doxil®—The first FDA-approved nano-drug: Lessons learned. *Journal of controlled release*, 2012. **160**(2): p. 117-134.
140. O'Brien, M.E., et al., Reduced cardiotoxicity and comparable efficacy in a phase IIItrial of pegylated liposomal doxorubicin HCl (CAELYX™/Doxil®) versus conventional doxorubicin forfirst-line treatment of metastatic breast cancer. *Annals of oncology*, 2004. **15**(3): p. 440-449.
141. Green, A.E. and P.G. Rose, Pegylated liposomal doxorubicin in ovarian cancer. *International journal of nanomedicine*, 2006. **1**(3): p. 229.
142. Dupont, J., et al., Topotecan and liposomal doxorubicin in recurrent ovarian cancer: is sequence important? *Int J Gynecol Cancer*, 2006. **16 Suppl 1**: p. 68-73.
143. Zhang, J.A., et al., Development and characterization of a novel Cremophor® EL free liposome-based paclitaxel (LEP-ETU) formulation. *European journal of pharmaceutics and biopharmaceutics*, 2005. **59**(1): p. 177-187.
144. Seiden, M.V., et al., A phase II study of liposomal lurtotecan (OSI-211) in patients with topotecan resistant ovarian cancer. *Gynecol Oncol*, 2004. **93**(1): p. 229-32.
145. Landen, C.N., et al., Intraperitoneal delivery of liposomal siRNA for therapy of advanced ovarian cancer. *Cancer biology & therapy*, 2006. **5**(12): p. 1708-1713.
146. Ozcan, G., et al., Preclinical and clinical development of siRNA-based therapeutics. *Advanced drug delivery reviews*, 2015. **87**: p. 108-119.
147. Landen Jr, C.N., et al., Therapeutic EphA2 gene targeting in vivo using neutral liposomal small interfering RNA delivery. *Cancer research*, 2005. **65**(15): p. 6910-6918.
148. Coleman, R.L., et al., A phase II evaluation of nanoparticle, albumin-bound (nab) paclitaxel in the treatment of recurrent or persistent platinum-resistant ovarian, fallopian tube, or primary peritoneal cancer: a Gynecologic Oncology Group study. *Gynecol Oncol*, 2011. **122**(1): p. 111-5.
149. Micha, J.P., et al., Abraxane in the treatment of ovarian cancer: the absence of hypersensitivity reactions. *Gynecologic oncology*, 2006. **100**(2): p. 437-438.
150. Ibrahim, N.K., et al., Phase I and pharmacokinetic study of ABI-007, a Cremophor-free, protein-stabilized, nanoparticle formulation of paclitaxel. *Clinical cancer research*, 2002. **8**(5): p. 1038-1044.
151. Lee, S.-W., et al., An open-label, randomized, parallel, phase II trial to evaluate the efficacy and safety of a cremophor-free polymeric micelle formulation of paclitaxel as first-line treatment for ovarian cancer: a Korean Gynecologic Oncology Group study (KGOG-3021). *Cancer Research and Treatment: official Journal of Korean Cancer Association*, 2018. **50**(1): p. 195-203.
152. Kim, T.-Y., et al., Phase I and pharmacokinetic study of Genexol-PM, a cremophor-free, polymeric micelle-formulated paclitaxel, in patients with advanced malignancies. *Clinical cancer research*, 2004. **10**(11): p. 3708-3716.
153. Atrafi, F., et al., A phase I dose-finding and pharmacokinetics study of CPC634 (nanoparticle entrapped docetaxel) in patients with advanced solid tumors. *Journal of Clinical Oncology*, 2019. **37**(15_suppl): p. 3026-3026.

154. Tabernero, J., et al., First-in-humans trial of an RNA interference therapeutic targeting VEGF and KSP in cancer patients with liver involvement. *Cancer discovery*, 2013. **3**(4): p. 406-417.
155. Jain, N., et al., Current ADC linker chemistry. *Pharmaceutical research*, 2015. **32**(11): p. 3526-3540.
156. Langdon, S.P. and A.H. Sims, HER2-targeted antibody treatment for ovarian cancer future opportunities. *Journal of Molecular Pharmaceutics & Organic Process Research*, 2016.
157. Xu, L. and T. Anchordoquy, Drug delivery trends in clinical trials and translational medicine: challenges and opportunities in the delivery of nucleic acid-based therapeutics. *J Pharm Sci*, 2011. **100**(1): p. 38-52.
158. Mitchell, M.J., et al., Engineering precision nanoparticles for drug delivery. *Nat Rev Drug Discov*, 2021. **20**(2): p. 101-124.
159. Mendes, B.B., et al., Nanodelivery of nucleic acids. *Nat Rev Methods Primers*, 2022. **2**.
160. Patra, J.K., et al., Nano based drug delivery systems: recent developments and future prospects. *J Nanobiotechnology*, 2018. **16**(1): p. 71.
161. Zhou, M., et al., The role of cell-penetrating peptides in potential anti-cancer therapy. *Clin Transl Med*, 2022. **12**(5): p. e822.
162. Yu, B., et al., Receptor-targeted nanocarriers for therapeutic delivery to cancer. *Mol Membr Biol*, 2010. **27**(7): p. 286-98.
163. Yao, Y., et al., Nanoparticle-Based Drug Delivery in Cancer Therapy and Its Role in Overcoming Drug Resistance. *Front Mol Biosci*, 2020. **7**: p. 193.
164. Hou, X., et al., Lipid nanoparticles for mRNA delivery. *Nat Rev Mater*, 2021. **6**(12): p. 1078-1094.
165. Kim, J., et al., Self-assembled mRNA vaccines. *Adv Drug Deliv Rev*, 2021. **170**: p. 83-112.
166. Kowalski, P.S., et al., Delivering the Messenger: Advances in Technologies for Therapeutic mRNA Delivery. *Mol Ther*, 2019. **27**(4): p. 710-728.
167. Hajj, K.A. and K.A. Whitehead, Tools for translation: non-viral materials for therapeutic mRNA delivery. *Nature Reviews Materials*, 2017. **2**(10): p. 17056.
168. Wahane, A., et al., Role of Lipid-Based and Polymer-Based Non-Viral Vectors in Nucleic Acid Delivery for Next-Generation Gene Therapy. *Molecules*, 2020. **25**(12).
169. Bulcha, J.T., et al., Viral vector platforms within the gene therapy landscape. *Signal Transduction and Targeted Therapy*, 2021. **6**(1): p. 53.
170. Sung, Y.K. and S.W. Kim, Recent advances in the development of gene delivery systems. *Biomaterials Research*, 2019. **23**(1): p. 8.
171. Broderick, K.E. and L.M. Humeau, Enhanced Delivery of DNA or RNA Vaccines by Electroporation. *Methods Mol Biol*, 2017. **1499**: p. 193-200.
172. Rychak, J.J. and A.L. Klibanov, Nucleic acid delivery with microbubbles and ultrasound. *Adv Drug Deliv Rev*, 2014. **72**: p. 82-93.
173. Helfield, B., et al., Biophysical insight into mechanisms of sonoporation. *Proceedings of the National Academy of Sciences*, 2016. **113**(36): p. 9983-9988.
174. Guevara, M.L., F. Persano, and S. Persano, Advances in Lipid Nanoparticles for mRNA-Based Cancer Immunotherapy. *Front Chem*, 2020. **8**: p. 589959.

175. Benmebarek, M.R., et al., Killing Mechanisms of Chimeric Antigen Receptor (CAR) T Cells. *Int J Mol Sci*, 2019. **20**(6).
176. Hung, C.F., et al., Development of Anti-Human Mesothelin-Targeted Chimeric Antigen Receptor Messenger RNA-Transfected Peripheral Blood Lymphocytes for Ovarian Cancer Therapy. *Hum Gene Ther*, 2018. **29**(5): p. 614-625.
177. Beatty, G.L., et al., Safety and antitumor activity of chimeric antigen receptor modified T cells in patients with chemotherapy refractory metastatic pancreatic cancer. *Journal of Clinical Oncology*, 2015. **33**(15_suppl): p. 3007-3007.
178. Beatty, G.L., et al., Mesothelin-specific chimeric antigen receptor mRNA-engineered T cells induce anti-tumor activity in solid malignancies. *Cancer Immunol Res*, 2014. **2**(2): p. 112-20.
179. Esprit, A., et al., Neo-Antigen mRNA Vaccines. *Vaccines (Basel)*, 2020. **8**(4).
180. Coosemans, A., et al., Immunological response after WT1 mRNA-loaded dendritic cell immunotherapy in ovarian carcinoma and carcinosarcoma. *Anticancer Res*, 2013. **33**(9): p. 3855-9.
181. Hernando, J.J., et al., Vaccination with dendritic cells transfected with mRNA-encoded folate-receptor-alpha for relapsed metastatic ovarian cancer. *Lancet Oncol*, 2007. **8**(5): p. 451-4.
182. Gildiz, S. and T. Minko, Nanotechnology-Based Nucleic Acid Vaccines for Treatment of Ovarian Cancer. *Pharm Res*, 2023. **40**(1): p. 123-144.
183. Chen, X., et al., RNA interference-based therapy and its delivery systems. *Cancer Metastasis Rev*, 2018. **37**(1): p. 107-124.
184. Subhan, M.A. and V. Torchilin, siRNA based drug design, quality, delivery and clinical translation. *Nanomedicine: Nanotechnology, Biology and Medicine*, 2020. **29**: p. 102239.
185. Courtête, J.r.m., et al., Suppression of cervical carcinoma cell growth by intracytoplasmic codelivery of anti-oncoprotein E6 antibody and small interfering RNA. *Molecular Cancer Therapeutics*, 2007. **6**(6): p. 1728-1735.
186. Saengkrit, N., et al., The PEI-introduced CS shell/PMMA core nanoparticle for silencing the expression of E6/E7 oncogenes in human cervical cells. *Carbohydr Polym*, 2012. **90**(3): p. 1323-9.
187. Yi, Y., et al., Targeted systemic delivery of siRNA to cervical cancer model using cyclic RGD-installed unimer polyion complex-assembled gold nanoparticles. *J Control Release*, 2016. **244**(Pt B): p. 247-256.
188. Kim, H.J., et al., Precise engineering of siRNA delivery vehicles to tumors using polyion complexes and gold nanoparticles. *ACS Nano*, 2014. **8**(9): p. 8979-91.
189. Chapoy-Villanueva, H., et al., Therapeutic silencing of HPV 16 E7 by systemic administration of siRNA-neutral DOPC nanoliposome in a murine cervical cancer model with obesity. *Journal of BU ON.: Official Journal of the Balkan Union of Oncology*, 2015. **20**(6): p. 1471-1479.
190. Wang, X., et al., Efficient down-regulation of CDK4 by novel lipid nanoparticle-mediated siRNA delivery. *Anticancer Res*, 2011. **31**(5): p. 1619-26.
191. Khairuddin, N., et al., siRNA-induced immunostimulation through TLR7 promotes antitumoral activity against HPV-driven tumors in vivo. *Immunology & Cell Biology*, 2012. **90**(2): p. 187-196.

192. Niu, X.Y., et al., Inhibition of HPV 16 E6 oncogene expression by RNA interference in vitro and in vivo. *Int J Gynecol Cancer*, 2006. **16**(2): p. 743-51.
193. Lechanteur, A., et al., Development of anti-E6 pegylated lipoplexes for mucosal application in the context of cervical preneoplastic lesions. *International Journal of Pharmaceutics*, 2015. **483**(1): p. 268-277.
194. Nishida, H., et al., Systemic delivery of siRNA by actively targeted polyion complex micelles for silencing the E6 and E7 human papillomavirus oncogenes. *Journal of Controlled Release*, 2016. **231**: p. 29-37.
195. Kumar, K., et al., Efficacious cellular codelivery of doxorubicin and EGFP siRNA mediated by the composition of PLGA and PEI protected gold nanoparticles. *Bioorganic & Medicinal Chemistry Letters*, 2017. **27**(18): p. 4288-4293.
196. Nagapoosanam, A.L., et al., Knockdown of human telomerase reverse transcriptase induces apoptosis in cervical cancer cell line. *Indian J Med Res*, 2019. **149**(3): p. 345-353.
197. Xia, Y., et al., Functionalized selenium nanoparticles for targeted siRNA delivery silence Derlin1 and promote antitumor efficacy against cervical cancer. *Drug Deliv*, 2020. **27**(1): p. 15-25.
198. Roh, J.W., et al., Clinical and biological significance of EZH2 expression in endometrial cancer. *Cancer Biol Ther*, 2020. **21**(2): p. 147-156.
199. Mills, K.A., et al., p5RHH nanoparticle-mediated delivery of AXL siRNA inhibits metastasis of ovarian and uterine cancer cells in mouse xenografts. *Scientific Reports*, 2019. **9**(1): p. 4762.
200. Sengupta, A., et al., Delivery of siRNA to ovarian cancer cells using laser-activated carbon nanoparticles. *Nanomedicine*, 2015. **10**(11): p. 1775-1784.
201. Li, T.S., T. Yawata, and K. Honke, Efficient siRNA delivery and tumor accumulation mediated by ionically cross-linked folic acid-poly(ethylene glycol)-chitosan oligosaccharide lactate nanoparticles: for the potential targeted ovarian cancer gene therapy. *Eur J Pharm Sci*, 2014. **52**: p. 48-61.
202. Han, H.D., et al., Targeted gene silencing using RGD-labeled chitosan nanoparticles. *Clin Cancer Res*, 2010. **16**(15): p. 3910-22.
203. Kim, G.H., et al., Selective delivery of PLXDC1 small interfering RNA to endothelial cells for anti-angiogenesis tumor therapy using CD44-targeted chitosan nanoparticles for epithelial ovarian cancer. *Drug Deliv*, 2018. **25**(1): p. 1394-1402.
204. Kim, H.-S., et al., Functional Roles of Src and Fgr in Ovarian CarcinomaFunctional Roles of Src and Fgr in Ovarian Carcinoma. *Clinical Cancer Research*, 2011. **17**(7): p. 1713-1721.
205. Steg, A.D., et al., Targeting the Notch Ligand Jagged1 in Both Tumor Cells and Stroma in Ovarian CancerTargeting Jagged1 in Ovarian Cancer. *Clinical cancer research*, 2011. **17**(17): p. 5674-5685.
206. Ma, J., et al., Blocking Stemness and Metastatic Properties of Ovarian Cancer Cells by Targeting p70(S6K) with Dendrimer Nanovector-Based siRNA Delivery. *Mol Ther*, 2018. **26**(1): p. 70-83.
207. Kala, S., et al., Combination of Dendrimer-Nanovector-Mediated Small Interfering RNA Delivery to Target Akt with the Clinical Anticancer Drug Paclitaxel for

Effective and Potent Anticancer Activity in Treating Ovarian Cancer. *Journal of Medicinal Chemistry*, 2014. **57**(6): p. 2634-2642.
208. Shah, V., et al., Targeted nanomedicine for suppression of CD44 and simultaneous cell death induction in ovarian cancer: an optimal delivery of siRNA and anticancer drug. *Clin Cancer Res*, 2013. **19**(22): p. 6193-204.
209. Schumann, C., et al., ROS-induced nanotherapeutic approach for ovarian cancer treatment based on the combinatorial effect of photodynamic therapy and DJ-1 gene suppression. *Nanomedicine: Nanotechnology, Biology and Medicine*, 2015. **11**(8): p. 1961-1970.
210. Kotcherlakota, R., et al., Engineered fusion protein-loaded gold nanocarriers for targeted co-delivery of doxorubicin and erbB2-siRNA in human epidermal growth factor receptor-2+ ovarian cancer. *Journal of Materials Chemistry B*, 2017. **5**(34): p. 7082-7098.
211. Arvizo, R.R., et al., Probing Novel Roles of the Mitochondrial Uniporter in Ovarian Cancer Cells Using Nanoparticles. *Journal of Biological Chemistry*, 2013. **288**(24): p. 17610-17618.
212. Yang, X., et al., MDR1 siRNA loaded hyaluronic acid-based CD44 targeted nanoparticle systems circumvent paclitaxel resistance in ovarian cancer. *Scientific Reports*, 2015. **5**(1): p. 8509.
213. Byeon, Y., et al., CD44-Targeting PLGA Nanoparticles Incorporating Paclitaxel and FAK siRNA Overcome Chemoresistance in Epithelial Ovarian Cancer. *Cancer Res*, 2018. **78**(21): p. 6247-6256.
214. Dickerson, E.B., et al., Chemosensitization of cancer cells by siRNA using targeted nanogel delivery. *BMC Cancer*, 2010. **10**(1): p. 10.
215. Sakurai, Y., et al., Improved Stability of siRNA-Loaded Lipid Nanoparticles Prepared with a PEG-Monoacyl Fatty Acid Facilitates Ligand-Mediated siRNA Delivery. *Molecular Pharmaceutics*, 2020. **17**(4): p. 1397-1404.
216. Armaiz-Pena, G.N., et al., Adrenergic regulation of monocyte chemotactic protein 1 leads to enhanced macrophage recruitment and ovarian carcinoma growth. *Oncotarget*, 2015. **6**(6): p. 4266.
217. Huang, Y.-H., et al., Claudin-3 gene silencing with siRNA suppresses ovarian tumor growth and metastasis. *Proceedings of the National Academy of Sciences*, 2009. **106**(9): p. 3426-3430.
218. Goldberg, M.S., et al., Nanoparticle-mediated delivery of siRNA targeting Parp1 extends survival of mice bearing tumors derived from Brca1-deficient ovarian cancer cells. *Proceedings of the National Academy of Sciences*, 2011. **108**(2): p. 745-750.
219. Murmann, A.E., et al., Induction of DISE in ovarian cancer cells in vivo. *Oncotarget*, 2017. **8**(49): p. 84643.
220. Zhao, Y.-C., et al., Efficient delivery of Notch1 siRNA to SKOV3 cells by cationic cholesterol derivative-based liposome. *International journal of nanomedicine*, 2016. **11**: p. 5485.
221. Lee, J. and H.J. Ahn, PEGylated DC-Chol/DOPE cationic liposomes containing KSP siRNA as a systemic siRNA delivery Carrier for ovarian cancer therapy. *Biochem Biophys Res Commun*, 2018. **503**(3): p. 1716-1722.

222. Tanaka, T., et al., Sustained small interfering RNA delivery by mesoporous silicon particles. *Cancer research*, 2010. **70**(9): p. 3687-3696.
223. Salzano, G., et al., Polymeric micelles containing reversibly phospholipid-modified anti-survivin siRNA: A promising strategy to overcome drug resistance in cancer. *Cancer Letters*, 2014. **343**(2): p. 224-231.
224. Gharpure, K.M., et al., Metronomic Docetaxel in PRINT Nanoparticles and EZH2 Silencing Have Synergistic Antitumor Effect in Ovarian CancerEffect of Metronomic Docetaxel in PRINT Particles and siEZH2. *Molecular cancer therapeutics*, 2014. **13**(7): p. 1750-1757.
225. Jones, S.K., V. Lizzio, and O.M. Merkel, Folate receptor targeted delivery of siRNA and paclitaxel to ovarian cancer cells via folate conjugated triblock copolymer to overcome TLR4 driven chemotherapy resistance. *Biomacromolecules*, 2016. **17**(1): p. 76-87.
226. Florinas, S., H.Y. Nam, and S.W. Kim, Enhanced siRNA delivery using a combination of an arginine-grafted bioreducible polymer, ultrasound, and microbubbles in cancer cells. *Mol Pharm*, 2013. **10**(5): p. 2021-30.
227. Florinas, S., et al., Ultrasound-assisted siRNA delivery via arginine-grafted bioreducible polymer and microbubbles targeting VEGF for ovarian cancer treatment. *J Control Release*, 2014. **183**: p. 1-8.
228. Teo, P.Y., et al., Ovarian cancer immunotherapy using PD-L1 siRNA targeted delivery from folic acid-functionalized polyethylenimine: strategies to enhance T cell killing. *Adv Healthc Mater*, 2015. **4**(8): p. 1180-9.
229. Hong, S., et al., Targeted gene silencing using a follicle-stimulating hormone peptide-conjugated nanoparticle system improves its specificity and efficacy in ovarian clear cell carcinoma in vitro. *J Ovarian Res*, 2013. **6**(1): p. 80.
230. Palanca-Wessels, M.C., et al., Antibody targeting facilitates effective intratumoral siRNA nanoparticle delivery to HER2-overexpressing cancer cells. *Oncotarget*, 2016. **7**(8): p. 9561-75.
231. Wang, H., et al., The Epithelial-Mesenchymal Transcription Factor SNAI1 Represses Transcription of the Tumor Suppressor miRNA let-7 in Cancer. *Cancers (Basel)*, 2021. **13**(6).
232. Babu, A., et al., Chitosan coated polylactic acid nanoparticle-mediated combinatorial delivery of cisplatin and siRNA/Plasmid DNA chemosensitizes cisplatin-resistant human ovarian cancer cells. *Mol Pharm*, 2014. **11**(8): p. 2720-33.
233. Zou, S., et al., Enhanced apoptosis of ovarian cancer cells via nanocarrier-mediated codelivery of siRNA and doxorubicin. *International journal of nanomedicine*, 2012. **7**: p. 3823.
234. Chen, Y., et al., Targeted chimera delivery to ovarian cancer cells by heterogeneous gold magnetic nanoparticle. *Nanotechnology*, 2016. **28**(2): p. 025101.
235. Roberts, C.M., et al., Nanoparticle delivery of siRNA against TWIST to reduce drug resistance and tumor growth in ovarian cancer models. *Nanomedicine: Nanotechnology, Biology and Medicine*, 2017. **13**(3): p. 965-976.
236. Talekar, M., et al., Cosilencing of PKM-2 and MDR-1 Sensitizes Multidrug-Resistant Ovarian Cancer Cells to Paclitaxel in a Murine Model of Ovarian

CancerCosilencing PKM-2 and MDR-1 in Ovarian Cancer. *Molecular cancer therapeutics*, 2015. **14**(7): p. 1521-1531.
237. He, C., D. Liu, and W. Lin, Self-assembled nanoscale coordination polymers carrying siRNAs and cisplatin for effective treatment of resistant ovarian cancer. *Biomaterials*, 2015. **36**: p. 124-133.
238. Yang, L., et al., Molecular mechanisms of platinum-based chemotherapy resistance in ovarian cancer (Review). *Oncol Rep*, 2022. **47**(4): p. 82.
239. Gottesman, M.M., T. Fojo, and S.E. Bates, Multidrug resistance in cancer: role of ATP–dependent transporters. *Nature reviews cancer*, 2002. **2**(1): p. 48-58.
240. Subhan, M.A. and V.P. Torchilin, Efficient nanocarriers of siRNA therapeutics for cancer treatment. *Translational Research*, 2019. **214**: p. 62-91.
241. Jain, S., K. Pathak, and A. Vaidya, Molecular therapy using siRNA: Recent trends and advances of multi target inhibition of cancer growth. *International Journal of Biological Macromolecules*, 2018. **116**: p. 880-892.
242. Wang, Z., et al., The circadian rhythm and core gene Period2 regulate the chemotherapy effect and multidrug resistance of ovarian cancer through the PI3K signaling pathway. *Bioscience Reports*, 2020. **40**(11): p. BSR20202683.
243. Wei, L., et al., Expression of integrin α-6 is associated with multi drug resistance and prognosis in ovarian cancer. *Oncol Lett*, 2019. **17**(4): p. 3974-3980.
244. Gao, B., et al., Multidrug resistance affects the prognosis of primary epithelial ovarian cancer. *Oncology letters*, 2019. **18**(4): p. 4262-4269.
245. Diaz Osterman, C.J., et al., FAK activity sustains intrinsic and acquired ovarian cancer resistance to platinum chemotherapy. *eLife*, 2019. **8**: p. e47327.
246. Abraham, E.H., et al., The multidrug resistance (mdr1) gene product functions as an ATP channel. *Proceedings of the National Academy of Sciences*, 1993. **90**(1): p. 312-316.
247. Mendes, L.P., et al., Surface-engineered polyethyleneimine-modified liposomes as novel carrier of siRNA and chemotherapeutics for combination treatment of drug-resistant cancers. *Drug delivery*, 2019. **26**(1): p. 443-458.
248. Chen, L., et al., Survivin status affects prognosis and chemosensitivity in epithelial ovarian cancer. *International Journal of Gynecologic Cancer*, 2013. **23**(2).
249. Liguang, Z., et al., Survivin expression in ovarian cancer. *Experimental oncology*, 2007.
250. Jin, W., Novel Insights into PARK7 (DJ-1), a Potential Anti-Cancer Therapeutic Target, and Implications for Cancer Progression. *J Clin Med*, 2020. **9**(5).
251. Schumann, C., et al., Intraperitoneal nanotherapy for metastatic ovarian cancer based on siRNA-mediated suppression of DJ-1 protein combined with a low dose of cisplatin. *Nanomedicine*, 2018. **14**(4): p. 1395-1405.
252. Court, K.A., et al., HSP70 Inhibition Synergistically Enhances the Effects of Magnetic Fluid Hyperthermia in Ovarian Cancer. *Molecular Cancer Therapeutics*, 2017. **16**(5): p. 966-976.
253. Hatakeyama, H., et al., Role of CTGF in sensitivity to hyperthermia in ovarian and uterine cancers. *Cell reports*, 2016. **17**(6): p. 1621-1631.
254. Raemdonck, K., et al., Maintaining the silence: reflections on long-term RNAi. *Drug Discov Today*, 2008. **13**(21-22): p. 917-31.

255. Narisawa-Saito, M. and T. Kiyono, Basic mechanisms of high-risk human papillomavirus-induced carcinogenesis: roles of E6 and E7 proteins. *Cancer science*, 2007. **98**(10): p. 1505-1511.
256. Estêvão, D., et al., Hallmarks of HPV carcinogenesis: The role of E6, E7 and E5 oncoproteins in cellular malignancy. *Biochimica et Biophysica Acta (BBA) - Gene Regulatory Mechanisms*, 2019. **1862**(2): p. 153-162.
257. Perez-Fidalgo, J.A., et al., NOTCH signalling in ovarian cancer angiogenesis. *Ann Transl Med*, 2020. **8**(24): p. 1705.
258. Yang, X., et al., New ways to successfully target tumor vasculature in ovarian cancer. *Curr Opin Obstet Gynecol*, 2015. **27**(1): p. 58-65.
259. Charbe, N.B., et al., Small interfering RNA for cancer treatment: overcoming hurdles in delivery. *Acta Pharmaceutica Sinica B*, 2020. **10**(11): p. 2075-2109.
260. Shao, L., et al., Delivery of MicroRNA-let-7c-5p by Biodegradable Silica Nanoparticles Suppresses Human Cervical Carcinoma Cell Proliferation and Migration. *J Biomed Nanotechnol*, 2020. **16**(11): p. 1600-1611.
261. Jing, L., et al., Exosomal miR-499a-5p Inhibits Endometrial Cancer Growth and Metastasis via Targeting VAV3. *Cancer Manag Res*, 2020. **12**: p. 13541-13552.
262. van der Koog, L., T.B. Gandek, and A. Nagelkerke, Liposomes and Extracellular Vesicles as Drug Delivery Systems: A Comparison of Composition, Pharmacokinetics, and Functionalization. *Advanced Healthcare Materials*, 2022. **11**(5): p. 2100639.
263. Gandham, S.K., et al., Combination microRNA-based cellular reprogramming with paclitaxel enhances therapeutic efficacy in a relapsed and multidrug-resistant model of epithelial ovarian cancer. *Mol Ther Oncolytics*, 2022. **25**: p. 57-68.
264. Ysrafil, Y. and I. Astuti, Chitosan nanoparticle-mediated effect of antimiRNA-324-5p on decreasing the ovarian cancer cell proliferation by regulation of GLI1 expression. *Bioimpacts*, 2022. **12**(3): p. 195-202.
265. Nishimura, M., et al., Therapeutic Synergy between microRNA and siRNA in Ovarian Cancer Treatment. *Cancer Discovery*, 2013. **3**(11): p. 1302-1315.
266. Rickard, B.P., et al., Malignant Ascites in Ovarian Cancer: Cellular, Acellular, and Biophysical Determinants of Molecular Characteristics and Therapy Response. *Cancers (Basel)*, 2021. **13**(17).
267. Latifi, A., et al., Isolation and characterization of tumor cells from the ascites of ovarian cancer patients: molecular phenotype of chemoresistant ovarian tumors. 2012.
268. Ayhan, A., et al., Ascites and epithelial ovarian cancers: a reappraisal with respect to different aspects. *International Journal of Gynecologic Cancer*, 2007. **17**(1).
269. Huang, H., et al., Clinical significance of ascites in epithelial ovarian cancer. *Neoplasma*, 2013. **60**(5): p. 546-552.
270. Ayantunde, A. and S. Parsons, Pattern and prognostic factors in patients with malignant ascites: a retrospective study. *Annals of oncology*, 2007. **18**(5): p. 945-949.
271. Becker, G., D. Galandi, and H.E. Blum, Malignant ascites: systematic review and guideline for treatment. *European Journal of Cancer*, 2006. **42**(5): p. 589-597.

272. Nagy, J.A., et al., Pathogenesis of ascites tumor growth: vascular permeability factor, vascular hyperpermeability, and ascites fluid accumulation. *Cancer research*, 1995. **55**(2): p. 360-368.
273. Loh, C.Y., et al., The E-Cadherin and N-Cadherin Switch in Epithelial-to-Mesenchymal Transition: Signaling, Therapeutic Implications, and Challenges. *Cells*, 2019. **8**(10).
274. Yang, D., et al., Integrated analyses identify a master microRNA regulatory network for the mesenchymal subtype in serous ovarian cancer. *Cancer Cell*, 2013. **23**(2): p. 186-99.
275. Sun, Y., et al., MiR-506 inhibits multiple targets in the epithelial-to-mesenchymal transition network and is associated with good prognosis in epithelial ovarian cancer. *J Pathol*, 2015. **235**(1): p. 25-36.
276. Liang, B., et al., Elevated VEGF concentrations in ascites and serum predict adverse prognosis in ovarian cancer. *Scandinavian journal of clinical and laboratory investigation*, 2013. **73**(4): p. 309-314.
277. Matte, I., et al., Profiling of cytokines in human epithelial ovarian cancer ascites. *American journal of cancer research*, 2012. **2**(5): p. 566.
278. Ahmed, N. and K.L. Stenvers, Getting to know ovarian cancer ascites: opportunities for targeted therapy-based translational research. *Front Oncol*, 2013. **3**: p. 256.
279. Massagué, J., TGFbeta in Cancer. *Cell*, 2008. **134**(2): p. 215-230.
280. Chen, J.L., et al., Elevated expression of activins promotes muscle wasting and cachexia. *The FASEB Journal*, 2014. **28**(4): p. 1711-1723.
281. Cobellis, L., et al., High concentrations of activin A in the peritoneal fluid of women with epithelial ovarian cancer. *J Soc Gynecol Investig*, 2004. **11**(4): p. 203-6.
282. Lambert-Messerlian, G.M., et al., Secretion of activin A in recurrent epithelial ovarian carcinoma. *Gynecol Oncol*, 1999. **74**(1): p. 93-7.
283. Di Simone, N., et al., Characterization of inhibin/activin subunit, follistatin, and activin type II receptors in human ovarian cancer cell lines: a potential role in autocrine growth regulation. *Endocrinology*, 1996. **137**(2): p. 486-494.
284. Steller, M.D., et al., Inhibin resistance is associated with aggressive tumorigenicity of ovarian cancer cells. *Mol Cancer Res*, 2005. **3**(1): p. 50-61.
285. Welt, C.K., et al., Presence of activin, inhibin, and follistatin in epithelial ovarian carcinoma. *J Clin Endocrinol Metab*, 1997. **82**(11): p. 3720-7.
286. Ries, A., et al., Activin A: an emerging target for improving cancer treatment? *Expert Opin Ther Targets*, 2020. **24**(10): p. 985-996.
287. Olson, B., D.L. Marks, and A.J. Grossberg, Diverging metabolic programmes and behaviours during states of starvation, protein malnutrition, and cachexia. *J Cachexia Sarcopenia Muscle*, 2020. **11**(6): p. 1429-1446.
288. Zhou, X., et al., Reversal of cancer cachexia and muscle wasting by ActRIIB antagonism leads to prolonged survival. *Cell*, 2010. **142**(4): p. 531-43.
289. Latres, E., et al., Activin A more prominently regulates muscle mass in primates than does GDF8. *Nat Commun*, 2017. **8**: p. 15153.

290. Pearsall, R.S., et al., Follistatin-based ligand trap ACE-083 induces localized hypertrophy of skeletal muscle with functional improvement in models of neuromuscular disease. *Scientific Reports*, 2019. **9**(1): p. 11392.
291. Ozawa, T., et al., Systemic administration of monovalent follistatin-like 3-Fc-fusion protein increases muscle mass in mice. *iScience*, 2021. **24**(5): p. 102488.
292. Tao, J.J., et al., First-in-Human Phase I Study of the Activin A Inhibitor, STM 434, in Patients with Granulosa Cell Ovarian Cancer and Other Advanced Solid Tumors. *Clinical Cancer Research*, 2019. **25**(18): p. 5458.
293. Lee, S.J., et al., Regulation of muscle mass by follistatin and activins. *Mol Endocrinol*, 2010. **24**(10): p. 1998-2008.
294. Yaden, B.C., et al., Follistatin: a novel therapeutic for the improvement of muscle regeneration. *J Pharmacol Exp Ther*, 2014. **349**(2): p. 355-71.
295. Lee, S.J. and A.C. McPherron, Regulation of myostatin activity and muscle growth. *Proc Natl Acad Sci U S A*, 2001. **98**(16): p. 9306-11.
296. Xia, Y. and A.L. Schneyer, The biology of activin: recent advances in structure, regulation and function. *J Endocrinol*, 2009. **202**(1): p. 1-12.
297. Choi, K.C., et al., Differential expression of activin/inhibin subunit and activin receptor mRNAs in normal and neoplastic ovarian surface epithelium (OSE). *Mol Cell Endocrinol*, 2001. **174**(1-2): p. 99-110.
298. Mabuchi, Y., et al., The autocrine effect of activin A on human ovarian clear cell adenocarcinoma cells. *Oncol Rep*, 2006. **16**(2): p. 373-9.
299. Dean, M., D.A. Davis, and J.E. Burdette, Activin A stimulates migration of the fallopian tube epithelium, an origin of high-grade serous ovarian cancer, through non-canonical signaling. *Cancer Lett*, 2017. **391**: p. 114-124.
300. Valencia-Sanchez, M.A., et al., Control of translation and mRNA degradation by miRNAs and siRNAs. *Genes & development*, 2006. **20**(5): p. 515-524.
301. Patel, S., et al., Naturally-occurring cholesterol analogues in lipid nanoparticles induce polymorphic shape and enhance intracellular delivery of mRNA. *Nature Communications*, 2020. **11**(1): p. 983.
302. Ogasawara, A., S. Sato, and K. Hasegawa, Current and future strategies for treatment of ovarian clear cell carcinoma. *J Obstet Gynaecol Res*, 2020. **46**(9): p. 1678-1689.
303. Pectasides, D., et al., Treatment issues in clear cell carcinoma of the ovary: a different entity? *Oncologist*, 2006. **11**(10): p. 1089-94.
304. Mellman, I. and Y. Yarden, Endocytosis and cancer. *Cold Spring Harbor perspectives in biology*, 2013. **5**(12): p. a016949-a016949.
305. Colotta, F., et al., Cancer-related inflammation, the seventh hallmark of cancer: links to genetic instability. *Carcinogenesis*, 2009. **30**(7): p. 1073-1081.
306. Tanaka, T., M. Narazaki, and T. Kishimoto, IL-6 in inflammation, immunity, and disease. *Cold Spring Harb Perspect Biol*, 2014. **6**(10): p. a016295.
307. Lopez-Castejon, G. and D. Brough, Understanding the mechanism of IL-1β secretion. *Cytokine Growth Factor Rev*, 2011. **22**(4): p. 189-95.
308. Jang, D.I., et al., The Role of Tumor Necrosis Factor Alpha (TNF-α) in Autoimmune Disease and Current TNF-α Inhibitors in Therapeutics. *Int J Mol Sci*, 2021. **22**(5).

309. Do, T.-V., et al., The Role of Activin A and Akt/GSK Signaling in Ovarian Tumor Biology. *Endocrinology*, 2008. **149**(8): p. 3809-3816.
310. Menon, U., et al., Serum inhibin, activin and follistatin in postmenopausal women with epithelial ovarian carcinoma. *BJOG*, 2000. **107**(9): p. 1069-74.
311. Ren, P., et al., High serum levels of follistatin in patients with ovarian cancer. *J Int Med Res*, 2012. **40**(3): p. 877-86.
312. Khoury, R.H., et al., Serum follistatin levels in women: evidence against an endocrine function of ovarian follistatin. *The Journal of Clinical Endocrinology & Metabolism*, 1995. **80**(4): p. 1361-1368.
313. Nakamura, T., et al., Follistatin, an activin-binding protein, associates with heparan sulfate chains of proteoglycans on follicular granulosa cells. *J Biol Chem*, 1991. **266**(29): p. 19432-7.
314. Mather, J.P., P.E. Roberts, and L.A. Krummen, Follistatin modulates activin activity in a cell- and tissue-specific manner. *Endocrinology*, 1993. **132**(6): p. 2732-2734.
315. Harrison, C.A., K.L. Chan, and D.M. Robertson, Activin-A Binds Follistatin and Type II Receptors through Overlapping Binding Sites: Generation of Mutants with Isolated Binding Activities. *Endocrinology*, 2006. **147**(6): p. 2744-2753.
316. Lamouille, S., J. Xu, and R. Derynck, Molecular mechanisms of epithelial-mesenchymal transition. *Nature reviews. Molecular cell biology*, 2014. **15**(3): p. 178-196.
317. Singh, A. and J. Settleman, EMT, cancer stem cells and drug resistance: an emerging axis of evil in the war on cancer. *Oncogene*, 2010. **29**(34): p. 4741-4751.
318. Yi, Y., et al., Activin A promotes ovarian cancer cell migration by suppressing E-cadherin expression. *Exp Cell Res*, 2019. **382**(2): p. 111471.
319. Scott, L.E., S.H. Weinberg, and C.A. Lemmon, Mechanochemical Signaling of the Extracellular Matrix in Epithelial-Mesenchymal Transition. *Front Cell Dev Biol*, 2019. **7**: p. 135.
320. Lamouille, S., J. Xu, and R. Derynck, Molecular mechanisms of epithelial-mesenchymal transition. *Nat Rev Mol Cell Biol*, 2014. **15**(3): p. 178-96.
321. Li, L.T., et al., Ki67 is a promising molecular target in the diagnosis of cancer (review). *Mol Med Rep*, 2015. **11**(3): p. 1566-72.
322. Uusküla-Reimand, L. and M.D. Wilson, Untangling the roles of TOP2A and TOP2B in transcription and cancer. *Sci Adv*, 2022. **8**(44): p. eadd4920.
323. Shao, T., et al., Comprehensive Analysis of the Oncogenic Role of Targeting Protein for Xklp2 (TPX2) in Human Malignancies. *Dis Markers*, 2022. **2022**: p. 7571066.
324. Kalfusova, A., et al., Gastrointestinal stromal tumors - quantitative detection of the Ki-67, TPX2, TOP2A, and hTERT telomerase subunit mRNA levels to determine proliferation activity and a potential for aggressive biological behavior. *Neoplasma*, 2016. **63**(3): p. 484-92.
325. Ye, T., et al., Cdh1 functions as an oncogene by inducing self-renewal of lung cancer stem-like cells via oncogenic pathways. *Int J Biol Sci*, 2020. **16**(3): p. 447-459.

326. Taha, E.A., et al., Knockout of MMP3 Weakens Solid Tumor Organoids and Cancer Extracellular Vesicles. *Cancers (Basel)*, 2020. **12**(5).
327. Upadhyay, P., et al., Genomic characterization of tobacco/nut chewing HPV-negative early stage tongue tumors identify MMP10 asa candidate to predict metastases. *Oral Oncol*, 2017. **73**: p. 56-64.
328. Shen, C.J., et al., MMP1 expression is activated by Slug and enhances multi-drug resistance (MDR) in breast cancer. *PLoS One*, 2017. **12**(3): p. e0174487.
329. Li, J., et al., Young Bone Marrow Sca-1 Cells Rejuvenate the Aged Heart by Promoting Epithelial-to-Mesenchymal Transition. *Theranostics*, 2018. **8**(7): p. 1766-1781.
330. Wafai, R., et al., Integrin alpha-2 and beta-1 expression increases through multiple generations of the EDW01 patient-derived xenograft model of breast cancer—insight into their role in epithelial mesenchymal transition in vivo gained from an in vitro model system. *Breast Cancer Research*, 2020. **22**(1): p. 136.
331. Zhang, D., et al., VCAM1 Promotes Tumor Cell Invasion and Metastasis by Inducing EMT and Transendothelial Migration in Colorectal Cancer. *Front Oncol*, 2020. **10**: p. 1066.
332. Donaldson, K.L., G.L. Goolsby, and A.F. Wahl, Cytotoxicity of the anticancer agents cisplatin and taxol during cell proliferation and the cell cycle. *Int J Cancer*, 1994. **57**(6): p. 847-55.
333. Sandri, M., et al., Foxo transcription factors induce the atrophy-related ubiquitin ligase atrogin-1 and cause skeletal muscle atrophy. *Cell*, 2004. **117**(3): p. 399-412.
334. Singh, R., et al., Follistatin Targets Distinct Pathways To Promote Brown Adipocyte Characteristics in Brown and White Adipose Tissues. *Endocrinology*, 2017. **158**(5): p. 1217-1230.
335. Aust, S., et al., Skeletal Muscle Depletion and Markers for Cancer Cachexia Are Strong Prognostic Factors in Epithelial Ovarian Cancer. *PLoS One*, 2015. **10**(10): p. e0140403.
336. Barreto, R., et al., Chemotherapy-related cachexia is associated with mitochondrial depletion and the activation of ERK1/2 and p38 MAPKs. *Oncotarget*, 2016. **7**(28): p. 43442-43460.
337. Duong, T., et al., Phototheranostic nanoplatform based on a single cyanine dye for image-guided combinatorial phototherapy. *Nanomedicine*, 2017. **13**(3): p. 955-963.
338. Guo, J., et al., Establishment of two ovarian cancer orthotopic xenograft mouse models for in vivo imaging: A comparative study. *Int J Oncol*, 2017. **51**(4): p. 1199-1208.
339. Pin, F., et al., Growth of ovarian cancer xenografts causes loss of muscle and bone mass: a new model for the study of cancer cachexia. *J. Cachexia Sarcopenia Muscle*, 2018. **9**(4): p. 685-700.
340. Chan, J.K., et al., Do clear cell ovarian carcinomas have poorer prognosis compared to other epithelial cell types? A study of 1411 clear cell ovarian cancers. *Gynecol Oncol*, 2008. **109**(3): p. 370-6.

341. Tudrej, P., et al., Establishment and Characterization of the Novel High-Grade Serous Ovarian Cancer Cell Line OVPA8. *International journal of molecular sciences*, 2018. **19**(7): p. 2080.
342. Kwok, A.L.M., et al., Caution over use of ES2 as a model of ovarian clear cell carcinoma. *J. Clin. Pathol.*, 2014. **67**(10): p. 921.
343. Han, G., et al., Mixed Ovarian Epithelial Carcinomas With Clear Cell and Serous Components are Variants of High-grade Serous Carcinoma: An Interobserver Correlative and Immunohistochemical Study of 32 Cases. *Am. J. Surg. Pathol.*, 2008. **32**(7).
344. Ye, S., et al., Comparison of pure and mixed-type clear cell carcinoma of the ovary: a clinicopathological analysis of 341 Chinese patients. *Int J Gynecol Cancer*, 2014. **24**(9): p. 1590-6.
345. Shaw, T.J., et al., Characterization of intraperitoneal, orthotopic, and metastatic xenograft models of human ovarian cancer. *Mol Ther*, 2004. **10**(6): p. 1032-42.
346. Sugiyama, T., et al., Clinical characteristics of clear cell carcinoma of the ovary. *Cancer*, 2000. **88**(11): p. 2584-2589.
347. Lee, W., et al., Neutrophils facilitate ovarian cancer premetastatic niche formation in the omentum. *The Journal of experimental medicine*, 2019. **216**(1): p. 176-194.
348. Forootan, A., et al., Methods to determine limit of detection and limit of quantification in quantitative real-time PCR (qPCR). *Biomolecular detection and quantification*, 2017. **12**: p. 1-6.
349. Korzun, T., et al., Nanoparticle-Based Follistatin Messenger RNA Therapy for Reprogramming Metastatic Ovarian Cancer and Ameliorating Cancer-Associated Cachexia. *Small*, 2022. **18**(44): p. e2204436.
350. Pelaz, B., et al., Diverse Applications of Nanomedicine. *ACS Nano*, 2017. **11**(3): p. 2313-2381.
351. Polack, F.P., et al., Safety and Efficacy of the BNT162b2 mRNA Covid-19 Vaccine. *N Engl J Med*, 2020. **383**(27): p. 2603-2615.
352. Walsh, E.E., et al., Safety and Immunogenicity of Two RNA-Based Covid-19 Vaccine Candidates. *N Engl J Med*, 2020. **383**(25): p. 2439-2450.
353. Verbeke, R., et al., Three decades of messenger RNA vaccine development. *Nano Today*, 2019. **28**: p. 100766.
354. Baden, L.R., et al., Efficacy and safety of the mRNA-1273 SARS-CoV-2 vaccine. *NEJM*, 2021. **384**(5): p. 403-416.
355. Sahin, U., et al., COVID-19 vaccine BNT162b1 elicits human antibody and T(H)1 T cell responses. *Nature*, 2020. **586**(7830): p. 594-599.
356. Sasso, J.M., et al., The Progress and Promise of RNA Medicine─An Arsenal of Targeted Treatments. *J Med Chem*, 2022. **65**(10): p. 6975-7015.
357. Jackson, L.A., et al., An mRNA vaccine against SARS-CoV-2—preliminary report. *New England journal of medicine*, 2020. **383**(20): p. 1920-1931.
358. Matsumura, T., T. Takano, and Y. Takahashi, Immune responses related to the immunogenicity and reactogenicity of COVID-19 mRNA vaccines. *Int. Immunol.*, 2022.
359. Watad, A., et al., Immune-Mediated Disease Flares or New-Onset Disease in 27 Subjects Following mRNA/DNA SARS-CoV-2 Vaccination. *Vaccines*, 2021. **9**(5): p. 435.

360. Chen, Y., et al., New-onset autoimmune phenomena post-COVID-19 vaccination. *Immunology*, 2022. **165**(4): p. 386-401.
361. Ouldali, N., et al., Hyper inflammatory syndrome following COVID-19 mRNA vaccine in children: A national post-authorization pharmacovigilance study. *Lancet Reg Health Eur*, 2022. **17**: p. 100393.
362. Hermann, E.A., et al., Association of Symptoms After COVID-19 Vaccination With Anti–SARS-CoV-2 Antibody Response in the Framingham Heart Study. *JAMA Netw. Open*, 2022. **5**(10): p. e2237908-e2237908.
363. Sprent, J. and C. King, COVID-19 vaccine side effects: The positives about feeling bad. *Science Immunology*, 2021. **6**(60): p. eabj9256.
364. Anderson, B.R., et al., Incorporation of pseudouridine into mRNA enhances translation by diminishing PKR activation. *Nucleic Acids Res*, 2010. **38**(17): p. 5884-92.
365. Karikó, K., et al., Suppression of RNA recognition by Toll-like receptors: the impact of nucleoside modification and the evolutionary origin of RNA. *Immunity*, 2005. **23**(2): p. 165-175.
366. Karikó, K., et al., mRNA is an endogenous ligand for Toll-like receptor 3. *Journal of Biological Chemistry*, 2004. **279**(13): p. 12542-12550.
367. Ju, Y., et al., Impact of anti-PEG antibodies induced by SARS-CoV-2 mRNA vaccines. *Nat Rev Immunol*, 2022: p. 1-2.
368. Hause, A.M., et al., Safety monitoring of COVID-19 mRNA vaccine second booster doses among adults aged≥ 50 years—United States, March 29, 2022–July 10, 2022. *Morbidity and Mortality Weekly Report*, 2022. **71**(30): p. 971.
369. Mulligan, M.J., et al., Phase I/II study of COVID-19 RNA vaccine BNT162b1 in adults. *Nature*, 2020. **586**(7830): p. 589-593.
370. Ndeupen, S., et al., The mRNA-LNP platform's lipid nanoparticle component used in preclinical vaccine studies is highly inflammatory. *iScience*, 2021. **24**(12): p. 103479.
371. Cafri, G., et al., mRNA vaccine-induced neoantigen-specific T cell immunity in patients with gastrointestinal cancer. *JCI*, 2020. **130**(11): p. 5976-5988.
372. Samaridou, E., J. Heyes, and P. Lutwyche, Lipid nanoparticles for nucleic acid delivery: Current perspectives. *Adv Drug Deliv Rev*, 2020. **154-155**: p. 37-63.
373. Cheng, X. and R.J. Lee, The role of helper lipids in lipid nanoparticles (LNPs) designed for oligonucleotide delivery. *Adv Drug Deliv Rev*, 2016. **99**(Pt A): p. 129-137.
374. Patel, S., et al., Naturally-occurring cholesterol analogues in lipid nanoparticles induce polymorphic shape and enhance intracellular delivery of mRNA. *Nat Commun*, 2020. **11**(1): p. 983.
375. Holland, J.W., et al., Poly (ethylene glycol)− lipid conjugates regulate the calcium-induced fusion of liposomes composed of phosphatidylethanolamine and phosphatidylserine. *Biochemistry*, 1996. **35**(8): p. 2618-2624.
376. Kalyanram, P., A. Puri, and A. Gupta, Thermotropic effects of PEGylated lipids on the stability of HPPH-encapsulated lipid nanoparticles (LNP). *J Therm Anal Calorim*, 2022. **147**(11): p. 6337-6348.
377. Judge, A., et al., Hypersensitivity and loss of disease site targeting caused by antibody responses to PEGylated liposomes. *Mol Ther*, 2006. **13**(2): p. 328-37.

378. Hald Albertsen, C., et al., The role of lipid components in lipid nanoparticles for vaccines and gene therapy. *Adv Drug Deliv Rev*, 2022. **188**: p. 114416.
379. Akinc, A., et al., The Onpattro story and the clinical translation of nanomedicines containing nucleic acid-based drugs. *Nat Nanotechnol*, 2019. **14**(12): p. 1084-1087.
380. Suzuki, Y. and H. Ishihara, Difference in the lipid nanoparticle technology employed in three approved siRNA (Patisiran) and mRNA (COVID-19 vaccine) drugs. *Drug Metab Pharmacokinet*, 2021. **41**: p. 100424.
381. Paloncýová, M., et al., Role of Ionizable Lipids in SARS-CoV-2 Vaccines As Revealed by Molecular Dynamics Simulations: From Membrane Structure to Interaction with mRNA Fragments. *J Phys Chem Lett*, 2021. **12**(45): p. 11199-11205.
382. Suzuki, T., et al., PEG shedding-rate-dependent blood clearance of PEGylated lipid nanoparticles in mice: Faster PEG shedding attenuates anti-PEG IgM production. *Int J Pharm*, 2020. **588**: p. 119792.
383. McSweeney, M.D., et al., Pre-treatment with high molecular weight free PEG effectively suppresses anti-PEG antibody induction by PEG-liposomes in mice. *J Control Release*, 2021. **329**: p. 774-781.
384. Chen, B.-M., T.-L. Cheng, and S.R. Roffler, Polyethylene glycol immunogenicity: theoretical, clinical, and practical aspects of anti-polyethylene glycol antibodies. *ACS nano*, 2021. **15**(9): p. 14022-14048.
385. Lutz, J., et al., Unmodified mRNA in LNPs constitutes a competitive technology for prophylactic vaccines. *npj Vaccines*, 2017. **2**(1): p. 29.
386. Richner, J.M., et al., Modified mRNA Vaccines Protect against Zika Virus Infection. *Cell*, 2017. **168**(6): p. 1114-1125.e10.
387. Freyn, A.W., et al., A Multi-Targeting, Nucleoside-Modified mRNA Influenza Virus Vaccine Provides Broad Protection in Mice. *Molecular Therapy*, 2020. **28**(7): p. 1569-1584.
388. Corbett, K.S., et al., Evaluation of the mRNA-1273 Vaccine against SARS-CoV-2 in Nonhuman Primates. *New England Journal of Medicine*, 2020. **383**(16): p. 1544-1555.
389. Rauch, S., et al., mRNA-based SARS-CoV-2 vaccine candidate CVnCoV induces high levels of virus-neutralising antibodies and mediates protection in rodents. *npj Vaccines*, 2021. **6**(1): p. 57.
390. Kalnin, K.V., et al., Immunogenicity and efficacy of mRNA COVID-19 vaccine MRT5500 in preclinical animal models. *npj Vaccines*, 2021. **6**(1): p. 61.
391. Li, S., et al., Payload distribution and capacity of mRNA lipid nanoparticles. *Nature Communications*, 2022. **13**(1): p. 5561.
392. Long, J., et al., Novel Ionizable Lipid Nanoparticles for SARS-CoV-2 Omicron mRNA Delivery. *Advanced Healthcare Materials*. **n/a**(n/a): p. 2202590.
393. Pardi, N., et al., Expression kinetics of nucleoside-modified mRNA delivered in lipid nanoparticles to mice by various routes. *Journal of Controlled Release*, 2015. **217**: p. 345-351.
394. Liang, F., et al., Efficient Targeting and Activation of Antigen-Presenting Cells In Vivo after Modified mRNA Vaccine Administration in Rhesus Macaques. *Mol Ther*, 2017. **25**(12): p. 2635-2647.

395. Sedic, M., et al., Safety Evaluation of Lipid Nanoparticle-Formulated Modified mRNA in the Sprague-Dawley Rat and Cynomolgus Monkey. *Vet Pathol*, 2018. **55**(2): p. 341-354.
396. Connors, J., et al., Lipid nanoparticles (LNP) induce activation and maturation of antigen presenting cells in young and aged individuals. *Commun Biol*, 2023. **6**(1): p. 188.
397. Maier, M.A., et al., Biodegradable Lipids Enabling Rapidly Eliminated Lipid Nanoparticles for Systemic Delivery of RNAi Therapeutics. *Molecular Therapy*, 2013. **21**(8): p. 1570-1578.
398. Alameh, M.G., et al., Lipid nanoparticles enhance the efficacy of mRNA and protein subunit vaccines by inducing robust T follicular helper cell and humoral responses. *Immunity*, 2021. **54**(12): p. 2877-2892.e7.
399. Tahtinen, S., et al., IL-1 and IL-1ra are key regulators of the inflammatory response to RNA vaccines. *Nature Immunology*, 2022. **23**(4): p. 532-542.
400. Qin, Z., et al., Pre-exposure to mRNA-LNP inhibits adaptive immune responses and alters innate immune fitness in an inheritable fashion. *PLoS Pathog*, 2022. **18**(9): p. e1010830.
401. Pardi, N., et al., Nucleoside-modified mRNA vaccines induce potent T follicular helper and germinal center B cell responses. *Journal of Experimental Medicine*, 2018. **215**(6): p. 1571-1588.
402. Parhiz, H., et al., Added to pre-existing inflammation, mRNA-lipid nanoparticles induce inflammation exacerbation (IE). *Journal of Control Release*, 2022. **344**: p. 50-61.
403. Bradley, A.J., et al., C1q binding to liposomes is surface charge dependent and is inhibited by peptides consisting of residues 14-26 of the human C1qA chain in a sequence independent manner. *Biochim Biophys Acta*, 1999. **1418**(1): p. 19-30.
404. Moghimi, S.M. and I. Hamad, Liposome-mediated triggering of complement cascade. *J Liposome Res*, 2008. **18**(3): p. 195-209.
405. Szebeni, J., et al., The interaction of liposomes with the complement system: in vitro and in vivo assays. *Methods Enzymol*, 2003. **373**: p. 136-54.
406. Szebeni, J., et al., Complement activation in vitro by the red cell substitute, liposome-encapsulated hemoglobin: mechanism of activation and inhibition by soluble complement receptor type 1. *Transfusion*, 1997. **37**(2): p. 150-9.
407. Neun, B.W., A.N. Ilinskaya, and M.A. Dobrovolskaia, Analysis of Complement Activation by Nanoparticles. *Methods Mol Biol*, 2018. **1682**: p. 149-160.
408. Pannuzzo, M., et al., Overcoming Nanoparticle-Mediated Complement Activation by Surface PEG Pairing. *Nano Lett*, 2020. **20**(6): p. 4312-4321.
409. Alving, C.R. and G.M. Swartz, Jr., Antibodies to cholesterol, cholesterol conjugates and liposomes: implications for atherosclerosis and autoimmunity. *Crit Rev Immunol*, 1991. **10**(5): p. 441-53.
410. Alving, C.R., et al., Antibody binding and complement fixation by a liposomal model membrane. *Biochemistry*, 1969. **8**(4): p. 1582-7.
411. La-Beck, N.M., M.R. Islam, and M.M. Markiewski, Nanoparticle-Induced Complement Activation: Implications for Cancer Nanomedicine. *Front Immunol*, 2020. **11**: p. 603039.

412. Longmire, M., P.L. Choyke, and H. Kobayashi, Clearance properties of nano-sized particles and molecules as imaging agents: considerations and caveats. *Nanomedicine (Lond)*, 2008. **3**(5): p. 703-17.
413. Sturgill, M.G. and G.H. Lambert, Xenobiotic-induced hepatotoxicity: mechanisms of liver injury and methods of monitoring hepatic function. *Clin Chem*, 1997. **43**(8 Pt 2): p. 1512-26.
414. Werner, M., et al., Nephrotoxicity of xenobiotics. *Clin Chim Acta*, 1995. **237**(1-2): p. 107-54.
415. Shi, C. and E.G. Pamer, Monocyte recruitment during infection and inflammation. *Nat Rev Immunol*, 2011. **11**(11): p. 762-74.
416. Kolaczkowska, E. and P. Kubes, Neutrophil recruitment and function in health and inflammation. *Nature reviews immunology*, 2013. **13**(3): p. 159-175.
417. Beyrau, M., J.V. Bodkin, and S. Nourshargh, Neutrophil heterogeneity in health and disease: a revitalized avenue in inflammation and immunity. *Open Biol*, 2012. **2**(11): p. 120134.
418. Eash, K.J., et al., CXCR2 and CXCR4 antagonistically regulate neutrophil trafficking from murine bone marrow. *J Clin Invest*, 2010. **120**(7): p. 2423-31.
419. Summers, C., et al., Neutrophil kinetics in health and disease. *Trends Immunol*, 2010. **31**(8): p. 318-24.
420. Köhler, A., et al., G-CSF-mediated thrombopoietin release triggers neutrophil motility and mobilization from bone marrow via induction of Cxcr2 ligands. *Blood*, 2011. **117**(16): p. 4349-57.
421. Hwang, T.-L., et al., Cationic liposomes evoke proinflammatory mediator release and neutrophil extracellular traps (NETs) toward human neutrophils. *Colloids and Surfaces B: Biointerfaces*, 2015. **128**: p. 119-126.
422. Hwang, T.L., et al., The impact of cationic solid lipid nanoparticles on human neutrophil activation and formation of neutrophil extracellular traps (NETs). *Chem Biol Interact*, 2015. **235**: p. 106-14.
423. Lin, M.H., et al., The Interplay Between Nanoparticles and Neutrophils. *J Biomed Nanotechnol*, 2018. **14**(1): p. 66-85.
424. Liu, Y., et al., Optimization of lipid-assisted nanoparticle for disturbing neutrophils-related inflammation. *Biomaterials*, 2018. **172**: p. 92-104.
425. Wynn, T.A., A. Chawla, and J.W. Pollard, Macrophage biology in development, homeostasis and disease. *Nature*, 2013. **496**(7446): p. 445-55.
426. Serbina, N.V., et al., Monocyte-mediated defense against microbial pathogens. *Annu Rev Immunol*, 2008. **26**: p. 421-52.
427. Hughes, C.E. and R.J.B. Nibbs, A guide to chemokines and their receptors. *Febs j*, 2018. **285**(16): p. 2944-2971.
428. Gustafson, H.H., et al., Nanoparticle Uptake: The Phagocyte Problem. *Nano Today*, 2015. **10**(4): p. 487-510.
429. Owens, D.E., 3rd and N.A. Peppas, Opsonization, biodistribution, and pharmacokinetics of polymeric nanoparticles. *Int J Pharm*, 2006. **307**(1): p. 93-102.
430. Ohno, K., et al., Blood clearance and biodistribution of polymer brush-afforded silica particles prepared by surface-initiated living radical polymerization. *Biomacromolecules*, 2012. **13**(3): p. 927-36.

431. Cai, D., et al., Current Development of Nano-Drug Delivery to Target Macrophages. *Biomedicines*, 2022. **10**(5).
432. Lonez, C., et al., Cationic lipid nanocarriers activate Toll-like receptor 2 and NLRP3 inflammasome pathways. *Nanomedicine*, 2014. **10**(4): p. 775-82.
433. O'Neill, L.A. and A.G. Bowie, The family of five: TIR-domain-containing adaptors in Toll-like receptor signalling. *Nat Rev Immunol*, 2007. **7**(5): p. 353-64.
434. Murphy, J.E., et al., Endosomes: a legitimate platform for the signaling train. *PNAS*, 2009. **106**(42): p. 17615-22.
435. Yamamoto, M., et al., Role of adaptor TRIF in the MyD88-independent toll-like receptor signaling pathway. *Science*, 2003. **301**(5633): p. 640-3.
436. Huotari, J. and A. Helenius, Endosome maturation. *Embo j*, 2011. **30**(17): p. 3481-500.
437. Patel, S., et al., Brief update on endocytosis of nanomedicines. *Adv Drug Deliv Rev*, 2019. **144**: p. 90-111.
438. Herrera, M., et al., Illuminating endosomal escape of polymorphic lipid nanoparticles that boost mRNA delivery. *Biomater Sci*, 2021. **9**(12): p. 4289-4300.
439. Hui, S.W., et al., The role of helper lipids in cationic liposome-mediated gene transfer. *Biophys J*, 1996. **71**(2): p. 590-9.
440. Tregoning, J.S., et al., Formulation, inflammation, and RNA sensing impact the immunogenicity of self-amplifying RNA vaccines. *Mol Ther Nucleic Acids*, 2023. **31**: p. 29-42.
441. Kawai, T. and S. Akira, Signaling to NF-κB by Toll-like receptors. *Trends in molecular medicine*, 2007. **13**(11): p. 460-469.
442. Merle, N.S., et al., Complement System Part II: Role in Immunity. *Front Immunol*, 2015. **6**: p. 257.
443. Noris, M. and G. Remuzzi, Overview of complement activation and regulation. *Semin Nephrol*, 2013. **33**(6): p. 479-92.
444. Szebeni, J., et al., Activation of complement by therapeutic liposomes and other lipid excipient-based therapeutic products: Prediction and prevention. *Advanced Drug Delivery Reviews*, 2011. **63**(12): p. 1020-1030.
445. Aksamit, R.R., W. Falk, and E.J. Leonard, Chemotaxis by mouse macrophage cell lines. *J Immunol*, 1981. **126**(6): p. 2194-9.
446. Lett-Brown, M.A. and E.J. Leonard, Histamine-induced inhibition of normal human basophil chemotaxis to C5a. *J Immunol*, 1977. **118**(3): p. 815-8.
447. Peng, Q., et al., Dendritic cell synthesis of C3 is required for full T cell activation and development of a Th1 phenotype. *J Immunol*, 2006. **176**(6): p. 3330-41.
448. Ehrengruber, M.U., T. Geiser, and D.A. Deranleau, Activation of human neutrophils by C3a and C5A. Comparison of the effects on shape changes, chemotaxis, secretion, and respiratory burst. *FEBS Lett*, 1994. **346**(2-3): p. 181-4.
449. Lalli, P.N., et al., Decay accelerating factor can control T cell differentiation into IFN-gamma-producing effector cells via regulating local C5a-induced IL-12 production. *J Immunol*, 2007. **179**(9): p. 5793-802.
450. Markiewski, M.M., et al., Modulation of the antitumor immune response by complement. *Nat Immunol*, 2008. **9**(11): p. 1225-35.

451. Hartmann, K., et al., C3a and C5a stimulate chemotaxis of human mast cells. *Blood*, 1997. **89**(8): p. 2863-70.
452. Asgari, E., et al., C3a modulates IL-1β secretion in human monocytes by regulating ATP efflux and subsequent NLRP3 inflammasome activation. *Blood*, 2013. **122**(20): p. 3473-81.
453. Takabayashi, T., et al., A new biologic role for C3a and C3a desArg: regulation of TNF-alpha and IL-1 beta synthesis. *J Immunol*, 1996. **156**(9): p. 3455-60.
454. Kumar, S., et al., COVID-19: Clinical status of vaccine development to date. *British Journal of Clinical Pharmacology*, 2023. **89**(1): p. 114-149.
455. Hervé, C., et al., The how's and what's of vaccine reactogenicity. *NPJ Vaccines*, 2019. **4**: p. 39.
456. Hayden, M.S., A.P. West, and S. Ghosh, NF-kappaB and the immune response. *Oncogene*, 2006. **25**(51): p. 6758-80.
457. Negishi, H., T. Taniguchi, and H. Yanai, The Interferon (IFN) Class of Cytokines and the IFN Regulatory Factor (IRF) Transcription Factor Family. *Cold Spring Harb Perspect Biol*, 2018. **10**(11).
458. Tanaka, T., et al., DiC14-amidine cationic liposomes stimulate myeloid dendritic cells through Toll-like receptor 4. *Eur J Immunol*, 2008. **38**(5): p. 1351-7.
459. Verbeke, R., et al., Innate immune mechanisms of mRNA vaccines. *Immunity*, 2022. **55**(11): p. 1993-2005.
460. Kawai, T. and S. Akira, Signaling to NF-kappaB by Toll-like receptors. *Trends in molecular medicine*, 2007. **13**(11): p. 460-9.
461. Medzhitov, R., et al., MyD88 is an adaptor protein in the hToll/IL-1 receptor family signaling pathways. *Mol Cell*, 1998. **2**(2): p. 253-8.
462. Kelley, N., et al., The NLRP3 Inflammasome: An Overview of Mechanisms of Activation and Regulation. *Int J Mol Sci*, 2019. **20**(13).
463. Frenois, F., et al., Lipopolysaccharide induces delayed FosB/DeltaFosB immunostaining within the mouse extended amygdala, hippocampus and hypothalamus, that parallel the expression of depressive-like behavior. *Psychoneuroendocrinology*, 2007. **32**(5): p. 516-31.
464. Burfeind, K.G., K.A. Michaelis, and D.L. Marks, The central role of hypothalamic inflammation in the acute illness response and cachexia. *Semin Cell Dev Biol*, 2016. **54**: p. 42-52.
465. Engström, L., et al., Lipopolysaccharide-Induced Fever Depends on Prostaglandin E2 Production Specifically in Brain Endothelial Cells. *Endocrinology*, 2012. **153**(10): p. 4849-4861.
466. Timper, K., et al., IL-6 improves energy and glucose homeostasis in obesity via enhanced central IL-6 trans-signaling. *Cell reports*, 2017. **19**(2): p. 267-280.
467. Wallenius, K., et al., Intracerebroventricular interleukin-6 treatment decreases body fat in rats. *Biochemical and biophysical research communications*, 2002. **293**(1): p. 560-565.
468. Petruzzelli, M., et al., A switch from white to brown fat increases energy expenditure in cancer-associated cachexia. *Cell metabolism*, 2014. **20**(3): p. 433-447.
469. Wallenius, V., et al., Interleukin-6-deficient mice develop mature-onset obesity. *Nature medicine*, 2002. **8**(1): p. 75-79.

470. Nov, O., et al., Interleukin-1β regulates fat-liver crosstalk in obesity by auto-paracrine modulation of adipose tissue inflammation and expandability. *PLoS One*, 2013. **8**(1): p. e53626.
471. Konsman, J.P., P. Parnet, and R. Dantzer, Cytokine-induced sickness behaviour: mechanisms and implications. *Trends in neurosciences*, 2002. **25**(3): p. 154-159.
472. Han, M.S., et al., Regulation of adipose tissue inflammation by interleukin 6. *Proceedings of the National Academy of Sciences*, 2020. **117**(6): p. 2751-2760.
473. Kistner, T.M., B.K. Pedersen, and D.E. Lieberman, Interleukin 6 as an energy allocator in muscle tissue. *Nature Metabolism*, 2022. **4**(2): p. 170-179.
474. Mohamed-Ali, V., et al., Subcutaneous adipose tissue releases interleukin-6, but not tumor necrosis factor-α, in vivo. *The Journal of Clinical Endocrinology & Metabolism*, 1997. **82**(12): p. 4196-4200.
475. López-Ferreras, L., et al., Key role for hypothalamic interleukin-6 in food-motivated behavior and body weight regulation. *Psychoneuroendocrinology*, 2021. **131**: p. 105284.
476. Dinarello, C.A., Biologic basis for interleukin-1 in disease. *Blood*, 1996. **87(6):2095-147**.
477. Ren, K. and R. Torres, Role of interleukin-1beta during pain and inflammation. *Brain Res Rev*, 2009. **60**(1): p. 57-64.
478. Ahima, R.S. and D.A. Antwi, Brain regulation of appetite and satiety. *Endocrinol Metab Clin North Am*, 2008. **37**(4): p. 811-23.
479. Katahira, M., et al., Cytokine regulation of the rat proopiomelanocortin gene expression in AtT-20 cells. *Endocrinology*, 1998. **139**(5): p. 2414-2422.
480. Pereda, M.P., et al., Interleukin-6 is inhibited by glucocorticoids and stimulates ACTH secretion and POMC expression in human corticotroph pituitary adenomas. *Experimental and clinical endocrinology & diabetes*, 2000. **108**(03): p. 202-207.
481. Laddha, N.C., et al., Association of neuropeptide Y (NPY), interleukin-1B (IL1B) genetic variants and correlation of IL1B transcript levels with vitiligo susceptibility. *PLoS One*, 2014. **9**(9): p. e107020.
482. Braun, T.P., et al., Central nervous system inflammation induces muscle atrophy via activation of the hypothalamic–pituitary–adrenal axis. *Journal of Experimental Medicine*, 2011. **208**(12): p. 2449-2463.
483. Kumar, V., Toll-like receptors in sepsis-associated cytokine storm and their endogenous negative regulators as future immunomodulatory targets. *Int Immunopharmacol*, 2020. **89**(Pt B): p. 107087.
484. Yang, T., et al., The clinical value of cytokines in chronic fatigue syndrome. *Journal of translational medicine*, 2019. **17**(1): p. 1-12.
485. Trask, P.C., et al., Longitudinal course of depression, fatigue, and quality of life in patients with high risk melanoma receiving adjuvant interferon. *Psycho-Oncology: Journal of the Psychological, Social and Behavioral Dimensions of Cancer*, 2004. **13**(8): p. 526-536.
486. Kirkwood, J.M., et al., Mechanisms and management of toxicities associated with high-dose interferon alfa-2b therapy. *Journal of Clinical Oncology*, 2002. **20**(17): p. 3703-3718.

487. Malik, U.R., D.F. Makower, and S. Wadler, Interferon-mediated fatigue. *Cancer: Interdisciplinary International Journal of the American Cancer Society*, 2001. **92**(S6): p. 1664-1668.
488. Russell, A., et al., Persistent fatigue induced by interferon-alpha: a novel, inflammation-based, proxy model of chronic fatigue syndrome. *Psychoneuroendocrinology*, 2019. **100**: p. 276-285.
489. Rönnblom, L. and D. Leonard, Interferon pathway in SLE: one key to unlocking the mystery of the disease. *Lupus Science & Medicine*, 2019. **6**(1): p. e000270.
490. Dighriri, I.M., et al., Pfizer-BioNTech COVID-19 vaccine (BNT162b2) side effects: a systematic review. *Cureus*, 2022. **14**(3).
491. Rabail, R., et al., The Side Effects and Adverse Clinical Cases Reported after COVID-19 Immunization. *Vaccines (Basel)*, 2022. **10**(4).
492. Teijaro, J.R. and D.L. Farber, COVID-19 vaccines: modes of immune activation and future challenges. *Nature Reviews Immunology*, 2021. **21**(4): p. 195-197.
493. Dalpke, A. and M. Helm, RNA mediated Toll-like receptor stimulation in health and disease. *RNA Biol*, 2012. **9**(6): p. 828-42.
494. Ning, S., J.S. Pagano, and G.N. Barber, IRF7: activation, regulation, modification and function. *Genes Immun*, 2011. **12**(6): p. 399-414.
495. Ivashkiv, L.B., IFNγ: signalling, epigenetics and roles in immunity, metabolism, disease and cancer immunotherapy. *Nat Rev Immunol*, 2018. **18**(9): p. 545-558.
496. Delehedde, C., et al., Intracellular Routing and Recognition of Lipid-Based mRNA Nanoparticles. *Pharmaceutics*, 2021. **13**(7).
497. Lokugamage, M.P., et al., Mild Innate Immune Activation Overrides Efficient Nanoparticle-Mediated RNA Delivery. *Adv Mater*, 2020. **32**(1): p. e1904905.
498. Duan, L.-J., et al., Potentialities and challenges of mRNA vaccine in cancer immunotherapy. *Frontiers in Immunology*, 2022. **13**.
499. García, M.A., et al., Impact of protein kinase PKR in cell biology: from antiviral to antiproliferative action. *Microbiol Mol Biol Rev*, 2006. **70**(4): p. 1032-60.
500. Goh, K.C., M.J. deVeer, and B.R.G. Williams, The protein kinase PKR is required for p38 MAPK activation and the innate immune response to bacterial endotoxin. *The EMBO Journal*, 2000. **19**(16): p. 4292-4297.
501. Ito, T., M. Yang, and W.S. May, RAX, a cellular activator for double-stranded RNA-dependent protein kinase during stress signaling. *Journal of Biological Chemistry*, 1999. **274**(22): p. 15427-15432.
502. Nakamura, T., et al., Double-stranded RNA-dependent protein kinase links pathogen sensing with stress and metabolic homeostasis. *Cell*, 2010. **140**(3): p. 338-348.
503. Liu, Y., et al., The role of host eIF2α in viral infection. *Virology Journal*, 2020. **17**(1): p. 112.
504. Jiang, H.Y., et al., Phosphorylation of the alpha subunit of eukaryotic initiation factor 2 is required for activation of NF-kappaB in response to diverse cellular stresses. *Mol Cell Biol*, 2003. **23**(16): p. 5651-63.
505. Burke, J.M., et al., RNase L Reprograms Translation by Widespread mRNA Turnover Escaped by Antiviral mRNAs. *Mol Cell*, 2019. **75**(6): p. 1203-1217.e5.

506. Gusho, E., D. Baskar, and S. Banerjee, New advances in our understanding of the "unique" RNase L in host pathogen interaction and immune signaling. *Cytokine*, 2020. **133**: p. 153847.
507. Burke, J.M., et al., RNase L activation in the cytoplasm induces aberrant processing of mRNAs in the nucleus. *PLoS pathogens*, 2022. **18**(11): p. e1010930.
508. Green, D.R., et al., Immunogenic and tolerogenic cell death. *Nature Reviews Immunology*, 2009. **9**(5): p. 353-363.
509. Dunkelberger, J.R. and W.C. Song, Complement and its role in innate and adaptive immune responses. *Cell Res*, 2010. **20**(1): p. 34-50.
510. Szebeni, J., Complement activation-related pseudoallergy: A new class of drug-induced acute immune toxicity. *Toxicology*, 2005. **216**(2): p. 106-121.
511. Kozma, G.T., et al., Anti-PEG antibodies: Properties, formation, testing and role in adverse immune reactions to PEGylated nano-biopharmaceuticals. *Advanced Drug Delivery Reviews*, 2020. **154-155**: p. 163-175.
512. Szebeni, J., Complement activation-related pseudoallergy: a new class of drug-induced acute immune toxicity. *Toxicology*, 2005. **216**(2-3): p. 106-21.
513. Ju, Y., et al., Anti-PEG Antibodies Boosted in Humans by SARS-CoV-2 Lipid Nanoparticle mRNA Vaccine. *ACS Nano*, 2022. **16**(8): p. 11769-11780.
514. Ju, Y., et al., Impact of anti-PEG antibodies induced by SARS-CoV-2 mRNA vaccines. *Nature Reviews Immunology*, 2023. **23**(3): p. 135-136.
515. Oberli, M.A., et al., Lipid Nanoparticle Assisted mRNA Delivery for Potent Cancer Immunotherapy. *Nano Lett*, 2017. **17**(3): p. 1326-1335.
516. Bevers, S., et al., mRNA-LNP vaccines tuned for systemic immunization induce strong antitumor immunity by engaging splenic immune cells. *Mol Ther*, 2022. **30**(9): p. 3078-3094.
517. Dilliard, S.A., Q. Cheng, and D.J. Siegwart, On the mechanism of tissue-specific mRNA delivery by selective organ targeting nanoparticles. *PNAS*, 2021. **118**(52).
518. Yamaguchi, Y., et al., Consecutive BNT162b2 mRNA vaccination induces short-term epigenetic memory in innate immune cells. *JCI insight*, 2022. **7**(22).
519. Liu, C., et al., Research and development on therapeutic agents and vaccines for COVID-19 and related human coronavirus diseases. 2020, ACS Publications.
520. Polack, F.P., et al., Safety and efficacy of the BNT162b2 mRNA Covid-19 vaccine. *New England Journal of Medicine*, 2020.
521. Pardi, N., et al., In vitro transcription of long RNA containing modified nucleosides. *Methods Mol Biol*, 2013. **969**: p. 29-42.
522. Jackson, L.A., et al., An mRNA vaccine against SARS-CoV-2—preliminary report. *New England journal of medicine*, 2020.
523. Cafri, G., et al., mRNA vaccine–induced neoantigen-specific T cell immunity in patients with gastrointestinal cancer. *The Journal of clinical investigation*, 2020. **130**(11): p. 5976-5988.
524. Dror, A.A., et al., Vaccine hesitancy: the next challenge in the fight against COVID-19. *Eur J Epidemiol*, 2020. **35**(8): p. 775-779.
525. Al-Obaydi, S., et al., Hesitancy and reactogenicity to mRNA-based COVID-19 vaccines–Early experience with vaccine rollout in a multi-site healthcare system. *PloS one*, 2022. **17**(8): p. e0272691.

526. Korzun, T., et al., From Bench to Bedside: Implications of Lipid Nanoparticle Carrier Reactogenicity for Advancing Nucleic Acid Therapeutics. *Pharmaceuticals (Basel)*, 2023. **16**(8).
527. Lonez, C., et al., Cationic lipid nanocarriers activate Toll-like receptor 2 and NLRP3 inflammasome pathways. *Nanomedicine: Nanotechnology, Biology and Medicine*, 2014. **10**(4): p. 775-782.
528. Delehedde, C., et al., Intracellular Routing and Recognition of Lipid-Based mRNA Nanoparticles. *Pharmaceutics*, 2021. **13**(7): p. 945.
529. Lokugamage, M.P., et al., Mild innate immune activation overrides efficient nanoparticle-mediated RNA delivery. *Advanced Materials*, 2020. **32**(1): p. 1904905.
530. Estapé Senti, M., et al., Anti-PEG antibodies compromise the integrity of PEGylated lipid-based nanoparticles via complement. *Journal of Controlled Release*, 2022. **341**: p. 475-486.
531. Lonez, C., M. Vandenbranden, and J.-M. Ruysschaert, Cationic lipids activate intracellular signaling pathways. *Advanced drug delivery reviews*, 2012. **64**(15): p. 1749-1758.
532. Tanaka, T., et al., diC14-amidine cationic liposomes stimulate myeloid dendritic cells through Toll-like receptor 4. *European journal of immunology*, 2008. **38**(5): p. 1351-1357.
533. O'Neill, L.A.J. and A.G. Bowie, The family of five: TIR-domain-containing adaptors in Toll-like receptor signalling. *Nature Reviews Immunology*, 2007. **7**(5): p. 353-364.
534. Murphy, J.E., et al., Endosomes: a legitimate platform for the signaling train. *Proc Natl Acad Sci U S A*, 2009. **106**(42): p. 17615-22.
535. Ahmed, A.U., B.R. Williams, and G.E. Hannigan, Transcriptional Activation of Inflammatory Genes: Mechanistic Insight into Selectivity and Diversity. *Biomolecules*, 2015. **5**(4): p. 3087-111.
536. Medzhitov, R., Inflammation 2010: new adventures of an old flame. *Cell*, 2010. **140**(6): p. 771-6.
537. Sochocka, M., B.S. Diniz, and J. Leszek, Inflammatory Response in the CNS: Friend or Foe? *Mol Neurobiol*, 2017. **54**(10): p. 8071-8089.
538. Thaler, J.P., et al., Hypothalamic inflammation and energy homeostasis: Resolving the paradox. *Frontiers in Neuroendocrinology*, 2010. **31**(1): p. 79-84.
539. Kanneganti, T.D., M. Lamkanfi, and G. Núñez, Intracellular NOD-like receptors in host defense and disease. *Immunity*, 2007. **27**(4): p. 549-59.
540. Ullah, M.O., et al., TRIF-dependent TLR signaling, its functions in host defense and inflammation, and its potential as a therapeutic target. *J Leukoc Biol*, 2016. **100**(1): p. 27-45.
541. Huang, R., et al., The NCATS BioPlanet - An Integrated Platform for Exploring the Universe of Cellular Signaling Pathways for Toxicology, Systems Biology, and Chemical Genomics. *Front Pharmacol*, 2019. **10**: p. 445.
542. Rio, D.C., et al., Purification of RNA using TRIzol (TRI reagent). *Cold Spring Harbor Protocols*, 2010. **2010**(6): p. pdb. prot5439.

543. Zhang, L., et al., Generation of a syngeneic mouse model to study the effects of vascular endothelial growth factor in ovarian carcinoma. *Am J Pathol*, 2002. **161**(6): p. 2295-309.
544. Vladimir, B., et al., A Clinically Relevant, Syngeneic Model of Spontaneous, Highly Metastatic B16 Mouse Melanoma. *Anticancer Research*, 2010. **30**(12): p. 4799.
545. Bloise, E., et al., Activin A in Mammalian Physiology. *Physiol Rev*, 2019. **99**(1): p. 739-780.
546. Donovan, P., et al., Paracrine Activin-A Signaling Promotes Melanoma Growth and Metastasis through Immune Evasion. *J Invest Dermatol*, 2017. **137**(12): p. 2578-2587.
547. Kang, H.Y., et al., Activin A enhances prostate cancer cell migration through activation of androgen receptor and is overexpressed in metastatic prostate cancer. *J Bone Miner Res*, 2009. **24**(7): p. 1180-93.
548. Seder, C.W., et al., Upregulated INHBA expression may promote cell proliferation and is associated with poor survival in lung adenocarcinoma. *Neoplasia*, 2009. **11**(4): p. 388-96.
549. Wildi, S., et al., Overexpression of activin A in stage IV colorectal cancer. *Gut*, 2001. **49**(3): p. 409-17.
550. Lonardo, E., et al., Nodal/Activin signaling drives self-renewal and tumorigenicity of pancreatic cancer stem cells and provides a target for combined drug therapy. *Cell Stem Cell*, 2011. **9**(5): p. 433-46.
551. Yoshinaga, K., et al., Activin a causes cancer cell aggressiveness in esophageal squamous cell carcinoma cells. *Ann Surg Oncol*, 2008. **15**(1): p. 96-103.
552. Antsiferova, M., et al., Activin enhances skin tumourigenesis and malignant progression by inducing a pro-tumourigenic immune cell response. *Nat Commun*, 2011. **2**: p. 576.
553. Loumaye, A., et al., Circulating Activin A predicts survival in cancer patients. *J Cachexia Sarcopenia Muscle*, 2017. **8**(5): p. 768-777.
554. Loumaye, A., et al., Role of Activin A and myostatin in human cancer cachexia. *J Clin Endocrinol Metab*, 2015. **100**(5): p. 2030-8.
555. Grossberg, A.J., J.M. Scarlett, and D.L. Marks, Hypothalamic mechanisms in cachexia. *Physiol Behav*, 2010. **100**(5): p. 478-89.
556. Harrington, A.E., et al., Structural basis for the inhibition of activin signalling by follistatin. *Embo j*, 2006. **25**(5): p. 1035-45.
557. Johnson, D.E., et al., Head and neck squamous cell carcinoma. *Nat Rev Dis Primers*, 2020. **6**(1): p. 92.
558. Stein, A.P., et al., Prevalence of Human Papillomavirus in Oropharyngeal Cancer: A Systematic Review. *Cancer J*, 2015. **21**(3): p. 138-46.
559. Ferlay, J., et al., Estimating the global cancer incidence and mortality in 2018: GLOBOCAN sources and methods. *Int J Cancer*, 2019. **144**(8): p. 1941-1953.
560. Mamelle, G., et al., Lymph node prognostic factors in head and neck squamous cell carcinomas. *Am J Surg*, 1994. **168**(5): p. 494-8.
561. Baracos, V.E., et al., Cancer-associated cachexia. *Nat Rev Dis Primers*, 2018. **4**: p. 17105.

562. Olson, B., et al., Association of Sarcopenia With Oncologic Outcomes of Primary Surgery or Definitive Radiotherapy Among Patients With Localized Oropharyngeal Squamous Cell Carcinoma. *JAMA Otolaryngol Head Neck Surg*, 2020. **146**(8): p. 714-722.
563. Jager-Wittenaar, H., et al., High prevalence of cachexia in newly diagnosed head and neck cancer patients: An exploratory study. *Nutrition*, 2017. **35**: p. 114-118.
564. Tisdale, M.J., Biology of cachexia. *J Natl Cancer Inst*, 1997. **89**(23): p. 1763-73.
565. Mäkitie, A.A., et al., Managing Cachexia in Head and Neck Cancer: a Systematic Scoping Review. *Adv Ther*, 2022. **39**(4): p. 1502-1523.
566. Chang, W.M., et al., Dysregulation of RUNX2/Activin-A Axis upon miR-376c Downregulation Promotes Lymph Node Metastasis in Head and Neck Squamous Cell Carcinoma. *Cancer Res*, 2016. **76**(24): p. 7140-7150.
567. Kelner, N., et al., Activin A immunoexpression as predictor of occult lymph node metastasis and overall survival in oral tongue squamous cell carcinoma. *Head Neck*, 2015. **37**(4): p. 479-86.
568. Wang, Z., et al., Activin A expression in esophageal carcinoma and its association with tumor aggressiveness and differentiation. *Oncol Lett*, 2015. **10**(1): p. 143-148.
569. Wu, Z.H., et al., Expression and gene regulation network of INHBA in Head and neck squamous cell carcinoma based on data mining. *Sci Rep*, 2019. **9**(1): p. 14341.
570. Ervolino De Oliveira, C., et al., Activin A triggers angiogenesis via regulation of VEGFA and its overexpression is associated with poor prognosis of oral squamous cell carcinoma. *Int J Oncol*, 2020. **57**(1): p. 364-376.
571. Tenchov, R., et al., Lipid Nanoparticles─From Liposomes to mRNA Vaccine Delivery, a Landscape of Research Diversity and Advancement. *ACS Nano*, 2021. **15**(11): p. 16982-17015.
572. Cheng, M.H.Y., et al., Induction of Bleb Structures in Lipid Nanoparticle Formulations of mRNA Leads to Improved Transfection Potency. *Advanced Materials*, 2023. **35**(31): p. 2303370.
573. Mulroney, T.E., et al., N1-methylpseudouridylation of mRNA causes +1 ribosomal frameshifting. *Nature*, 2024. **625**(7993): p. 189-194.
574. Buryska, S., et al., Potential Roles of Activin in Head and Neck Squamous Cell Carcinoma Progression and Mortality. *Anticancer Res*, 2023. **43**(12): p. 5299-5310.
575. Wu, Z.-h., et al., Expression and gene regulation network of INHBA in Head and neck squamous cell carcinoma based on data mining. *Scientific Reports*, 2019. **9**(1): p. 14341.
576. Tang, Z., et al., GEPIA: a web server for cancer and normal gene expression profiling and interactive analyses. *Nucleic Acids Res*, 2017. **45**(W1): p. W98-w102.
577. Jing, S.-l., K. Afshari, and Z.-c. Guo, Inflammatory response-related genes predict prognosis in patients with HNSCC. *Immunology Letters*, 2023. **259**: p. 46-60.

578. Abou Kors, T., et al., INHBA is enriched in HPV-negative oropharyngeal squamous cell carcinoma and promotes cancer progression. *Cancer Research Communications*, 2024.
579. Michaud, D.S., et al., High-risk HPV types and head and neck cancer. *Int J Cancer*, 2014. **135**(7): p. 1653-61.
580. Bhaskar, S., S. Mony, and P. Taunk, Metastatic Head and Neck Squamous Cell Carcinoma Masquerading as Crohn's Disease. *ACG Case Reports Journal*, 2022. **9**(1).
581. Lucido, C.T., et al., β(2)-Adrenergic receptor modulates mitochondrial metabolism and disease progression in recurrent/metastatic HPV(+) HNSCC. *Oncogenesis*, 2018. **7**(10): p. 81.
582. Olson, B., et al., Physiologic and molecular characterization of a novel murine model of metastatic head and neck cancer cachexia. *J Cachexia Sarcopenia Muscle*, 2021. **12**(5): p. 1312-1332.
583. Osozawa, S., Case report: anorexia as a new type of adverse reaction caused by the COVID-19 vaccination: a case report applying detailed personal care records. *F1000Research*, 2024. **11**: p. 4.
584. He, X., B. Lee, and Y. Jiang, Extracellular matrix in cancer progression and therapy. *Med Rev (2021)*, 2022. **2**(2): p. 125-139.
585. Yeo-Teh, N.S.L., Y. Ito, and S. Jha, High-Risk Human Papillomaviral Oncogenes E6 and E7 Target Key Cellular Pathways to Achieve Oncogenesis. *Int J Mol Sci*, 2018. **19**(6).
586. Reed, S.A., et al., Inhibition of FoxO transcriptional activity prevents muscle fiber atrophy during cachexia and induces hypertrophy. *Faseb j*, 2012. **26**(3): p. 987-1000.
587. Wang, Y. and Z.-h. Qin, Coordination of autophagy with other cellular activities. *Acta Pharmacologica Sinica*, 2013. **34**(5): p. 585-594.
588. Sandri, M., Protein breakdown in muscle wasting: role of autophagy-lysosome and ubiquitin-proteasome. *Int J Biochem Cell Biol*, 2013. **45**(10): p. 2121-9.
589. Baracos, V.E., et al., Cancer-associated cachexia. *Nature Reviews Disease Primers*, 2018. **4**(1): p. 17105.
590. Marceca, G.P., P. Londhe, and F. Calore, Management of Cancer Cachexia: Attempting to Develop New Pharmacological Agents for New Effective Therapeutic Options. *Front Oncol*, 2020. **10**: p. 298.
591. Penna, F., S. Busquets, and J.M. Argilés, Experimental cancer cachexia: Evolving strategies for getting closer to the human scenario. *Seminars in Cell & Developmental Biology*, 2016. **54**: p. 20-27.
592. Ballarò, R., P. Costelli, and F. Penna, Animal models for cancer cachexia. *Curr Opin Support Palliat Care*, 2016. **10**(4): p. 281-287.
593. Rooks, D., et al., Bimagrumab vs Optimized Standard of Care for Treatment of Sarcopenia in Community-Dwelling Older Adults: A Randomized Clinical Trial. *JAMA Netw Open*, 2020. **3**(10): p. e2020836.
594. Amato, A.A., et al., Efficacy and Safety of Bimagrumab in Sporadic Inclusion Body Myositis: Long-term Extension of RESILIENT. *Neurology*, 2021. **96**(12): p. e1595-e1607.

595. Rodgers, B.D. and C.W. Ward, Myostatin/Activin Receptor Ligands in Muscle and the Development Status of Attenuating Drugs. *Endocr Rev*, 2022. **43**(2): p. 329-365.
596. Thompson, T.B., et al., The Structure of the Follistatin:Activin Complex Reveals Antagonism of Both Type I and Type II Receptor Binding. *Developmental Cell*, 2005. **9**(4): p. 535-543.
597. Shi, L., et al., Clinical and Therapeutic Implications of Follistatin in Solid Tumours. *Cancer Genomics Proteomics*, 2016. **13**(6): p. 425-435.
598. Peer, D., et al., Nanocarriers as an emerging platform for cancer therapy. *Nano-enabled medical applications*, 2020: p. 61-91.
599. Leader, B., Q.J. Baca, and D.E. Golan, Protein therapeutics: a summary and pharmacological classification. *Nat Rev Drug Discov*, 2008. **7**(1): p. 21-39.
600. Roane, B.M., R.C. Arend, and M.J. Birrer, Review: Targeting the Transforming Growth Factor-Beta Pathway in Ovarian Cancer. *Cancers (Basel)*, 2019. **11**(5).
601. Morrison, J., et al., Epidermal growth factor receptor blockers for the treatment of ovarian cancer. *Cochrane Database Syst Rev*, 2018. **10**(10): p. Cd007927.
602. Amutha, P. and T. Rajkumar, Role of Insulin-like Growth Factor, Insulin-like Growth Factor Receptors, and Insulin-like Growth Factor-binding Proteins in Ovarian Cancer. *Indian J Med Paediatr Oncol*, 2017. **38**(2): p. 198-206.
603. Zhang, C. and W. Zhao, The efficacy and safety of angiogenesis inhibitors for recurrent ovarian cancer: a meta-analysis. *J Ovarian Res*, 2022. **15**(1): p. 99.
604. Hutvágner, G. and P.D. Zamore, A microRNA in a multiple-turnover RNAi enzyme complex. *Science*, 2002. **297**(5589): p. 2056-60.
605. Stark, A., et al., Animal MicroRNAs confer robustness to gene expression and have a significant impact on 3'UTR evolution. *Cell*, 2005. **123**(6): p. 1133-46.
606. Valencia-Sanchez, M.A., et al., Control of translation and mRNA degradation by miRNAs and siRNAs. *Genes Dev*, 2006. **20**(5): p. 515-24.
607. Fosgerau, K. and T. Hoffmann, Peptide therapeutics: current status and future directions. *Drug Discov Today*, 2015. **20**(1): p. 122-8.
608. Keller, A.S., et al., Replacement Therapies in Metabolic Disease. *Curr Pharm Biotechnol*, 2018. **19**(5): p. 382-399.
609. Fenske, D.B. and P.R. Cullis, Liposomal nanomedicines. *Expert Opinion on Drug Delivery*, 2008. **5**(1): p. 25-44.
610. Riddell, J., et al., Reprogramming committed murine blood cells to induced hematopoietic stem cells with defined factors. *Cell*, 2014. **157**(3): p. 549-64.
611. Mandal, P.K. and D.J. Rossi, Reprogramming human fibroblasts to pluripotency using modified mRNA. *Nature Protocols*, 2013. **8**(3): p. 568-582.
612. Davis, M.E., et al., Evidence of RNAi in humans from systemically administered siRNA via targeted nanoparticles. *Nature*, 2010. **464**(7291): p. 1067-1070.
613. Kauffman, K.J., et al., Optimization of Lipid Nanoparticle Formulations for mRNA Delivery in Vivo with Fractional Factorial and Definitive Screening Designs. *Nano Letters*, 2015. **15**(11): p. 7300-7306.
614. Li, B., et al., An Orthogonal Array Optimization of Lipid-like Nanoparticles for mRNA Delivery in Vivo. *Nano Letters*, 2015. **15**(12): p. 8099-8107.

615. Belliveau, N.M., et al., Microfluidic Synthesis of Highly Potent Limit-size Lipid Nanoparticles for In Vivo Delivery of siRNA. *Mol Ther Nucleic Acids*, 2012. **1**(8): p. e37.
616. Maier, M.A., et al., Biodegradable lipids enabling rapidly eliminated lipid nanoparticles for systemic delivery of RNAi therapeutics. *Mol Ther*, 2013. **21**(8): p. 1570-8.
617. Akinc, A., et al., A combinatorial library of lipid-like materials for delivery of RNAi therapeutics. *Nature Biotechnology*, 2008. **26**(5): p. 561-569.